IMAGING STRUCTURAL CONNECTIONS OF THE BRAIN IN EPILEPSY

Mahinda Yogarajah BSc MBBS MRCP

DEPARTMENT OF CLINICAL AND EXPERIMENTAL EPILEPSY, INSTITUTE OF NEUROLOGY, UNIVERSITY COLLEGE LONDON

THESIS SUBMITTED TO UNIVERSITY COLLEGE LONDON FOR THE DEGREE OF DOCTOR OF PHILOSOPHY, 2013

PERSONEL CONTRIBUTION

I, Mahinda Yogarajah, confirm that the work presented in this thesis is my own. Where information has been derived from other sources, I confirm that this has been indicated in the thesis. Although the work reflects the contributions of a team of researchers, I have outlined my individual contribution below:

I was responsible for recruitment and data acquisition on all subjects studied, except those in chapter 3. I performed all data analyses described in the thesis and was responsible for archiving the data. I performed all the statistical analyses and was responsible for producing all the figures and graphical presentation of the data. All results and interpretations were presented by myself and developed following discussions at regular supervision meetings.

ABSTRACT

Imaging the Structural Connections of the Brain in Epilepsy

Introduction

Temporal lobe epilepsy (TLE) is the most common cause of medically intractable partial epilepsy in adults. For many patients, anterior temporal lobe resection (ATLR) is an effective means of treatment, but can cause a significant decline in language or memory function, and visual field deficits. Diffusion tensor imaging and tractography is an MRI technique that can be used to probe white matter structure, and delineate the white matter tracts relevant to vision, language, and memory function.

Aims

We aimed to use diffusion MRI to increase understanding of the causes and consequences of TLE, and identify patients who are at risk of language, and visual impairment after surgery.

Methods and Analysis Techniques

Healthy controls, and patients with TLE were scanned pre- and post operatively using 3T MRI. All patients in the study underwent a comprehensive pre- and post-surgical evaluation including clinical, MRI, video-EEG, and neuropsychological assessment. Whole brain analysis of both pre-, and post-operative diffusion MRI was carried out. Tractography was used to assess white matter relevant to memory, language and vision. Correlation analysis of white matter data, and neuropsychological and clinical variables was carried out using the statistical software package, SPSS.

Results and Discussion

This thesis demonstrates the widespread changes in white matter microstructure present in patients with TLE, and the relationship between medial temporal lobe connections and memory function. It demonstrates how white matter microstructure changes after anterior temporal lobe resection, and how this information can be used to aid prediction of post-operative language deficits in patients. It concludes by showing that tractography can be used to predict postoperative visual field deficits.

Conclusion

Diffusion MRI can be used to increase our understanding of the causes and consequences of TLE, and to improve pre-surgical planning.

(Word count - 80,002 words)

TABLE OF CONTENTS

1

TABLES

FIGURES

2

ABBREVIATIONS

- ADC = analogue to digital convertor or apparent diffusion coefficient
- AED = anti-epileptic drug
- ATLR = anterior temporal lobe resection
- CA = cornu ammonis
- CNS = central nervous system
- DNT = dysembryoplastic neuroepithelial tumour
- dODF = diffusion orientation density function
- EC = entorhinal cortex
- EEG = electroencephalogram
- EPI = echo planar imaging
- FA = fractional anisotropy
- FCD = focal cortical dysplasia
- FID = free induction decay
- fODF = fibre orientation density function
- FOV = field of view
- FTT = fast Fourier transform
- GCD = granule cell dispersion
- GE-EPI = gradient echo EPI
- GLM = general linear model
- GM = grey matter
- GRF = Gaussian random field theory
- GTCS = generalised tonic clonic seizure
- HC = hippocampus
- HS = hippocampal sclerosis
- IAP = Intracarotid amobarbital procedure (IAP)
- IDD = interictal dysphoric disorder
- ILAE = International League Against Epilepsy
- MCD = malformation of cortical development

- MD = mean diffusivity
- MEG = magnetoencephalography
- MFS = mossy fibre sprouting
- MRI= magnetic resonance imaging
- MRS = magnetic resonance spectroscopy
- MTLE = mesial temporal lobe epilepsy
- MTLS = mesial temporal lobe sclerosis
- NEX = number of excitations
- NMV = net magnetic vector
- NSA = number of signal averages
- PD = proton density
- PDD = principal diffusion direction
- PDF = posterior probability density function
- PET = positron emission tomography
- PHC = parahippocampal cortex
- PHG = parahippocampal gyrus
- PM = post-mortem
- PRC = perirhinal cortex
- QOL = quality of life
- RCI = reliable change index
- RF = radiofrequency
- ROI = region of interest
- SAH = selective amygdalohippocampectomy
- SE = status epilepticus
- SE-EPI = spin echo EPI
- SMR = standardised mortality ratio
- SNR = signal to noise ratio
- SPECT = single photon emission tomography
- SSRI = selective serotonin reuptake inhibitors

- SUDEP = sudden unexplained death in epilepsy
- TBSS = tract based spatial statistics
- TFCE = threshold free cluster enhancement
- TLE = temporal lobe epilepsy
- uODF = uncertainty orientation density function
- VBM = voxel based morphometry
- VFD = visual field defect

ORIGINAL ARTICLES

- *Yogarajah M*, Focke N, Bonelli S, Vollmar C, Thompson P, McEvoy A, Symms MR, Koepp MJ and Duncan JS. The Structural Plasticity of White Matter Networks Following Anterior Temporal Lobectomy. Brain 2010 Aug;133(Pt 8):2348-64.
- *Yogarajah M*, Focke N, Bonelli S, Cercignani M, Acheson J, Parker GJM, Alexander S, McEvoy A, Symms MR, Koepp MJ and Duncan JS. Defining Meyer's Loop – Temporal Lobe Resections, Visual Field Deficits and Diffusion Tensor Tractography. Brain. 2009 Jun;132(Pt 6):1656-68
- *Yogarajah M,* Powell HW, Parker GJ, Alexander DC, Thompson PJ, Symms MR, Boulby P, Wheeler-Kingshott CA, Barker GJ, Koepp MJ, Duncan JS. Tractography of the parahippocampal gyrus and material specific memory impairmenr in unilateral temporal lobe epilepsy. Neuroimage. 2008;40(4):1755-64
- Focke NK, *Yogarajah M (joint first author)*, Bonelli SB, Bartlett PA, Symms MR, Duncan JS. Voxel-based diffusion tensor imaging in patients with mesial temporal lobe epilepsy and hippocampal sclerosis. Neuroimage. 2008;40(2):728-37

REVIEW ARTICLES AND BOOK CHAPTERS

- *Yogarajah M,* Duncan JS. Diffusion-based magnetic resonance imaging and tractography in epilepsy. Epilepsia. 2008;49(2):189-200.
- *Yogarajah M,* Duncan JS, Koepp MK. Structure and Function: Imaging Connectivity Using Tractography, Encyclopaedia of Basic Epilepsy Research, Ed. P Swartzkroin, Elsevier Academic Press, May 2009

ABSTRACTS

- *Yogarajah M,* Bonelli S, Focke N Vollmar C, Thompson P, McEvoy A, Symms MR, Koepp MJ and Duncan JS. Longitudinal Changes in White Matter and Language Outcome After Anterior Temporal Lobe Resection, Human Brain Mapping Conference, Book of Abstracts, Quebec City, June 2011
- *Yogarajah M,* Focke N, Bonelli S, Vollmar C, Thompson P, McEvoy A, Symms MR, Koepp MJ and Duncan JS. The Structural Plasticity of White Matter Networks Following Anterior

Temporal Lobectomy, International Society for Magnetic Resonance in Medicine, Book of Abstracts, Stockholm, May 2010

- *Yogarajah M,* Focke N, Bonelli S, Vollmar C, Thompson P, McEvoy A, Symms MR, Koepp MJ and Duncan JS. The Structural Plasticity of White Matter Networks Following Anterior Temporal Lobectomy, Association of British Neurologists, Book of Abstracts, Bournemouth, May 2010
- *Yogarajah M,* Focke N, Bonelli S, Vollmar C, Thompson P, McEvoy A, Symms MR, Koepp MJ and Duncan JS. Hard-Wired or Soft-Wired – The Structural Plasticity of White Matter Networks Following Anterior Temporal Lobe Resection, Human Brain Mapping Conference, Book of Abstracts, Barcelona, June 2010
- *Yogarajah M*, Focke N, Bonelli S, Thompson P, Symms M, Koepp M and Duncan J. Patterns of Disconnection Associated with Memory Dysfunction in Temporal Lobe Epilepsy, American Epilepsy Society Meeting, Book of Abstracts, Boston 2009
- *Yogarajah M,* Focke N, Bonelli SB, Symms M, Koepp M, Duncan J. Tractography and the Distributed Network Damage Underlying Memory Impairment in Temporal Lobe Epilepsy. Association of British Neurologists, Book of Abstracts, Liverpool, June 2009
- *Yogarajah M,* Focke N, Bonelli SB, Symms M, Koepp M, Duncan J. Tractography and the Distributed Network Damage Underlying Memory Impairment in Temporal Lobe Epilepsy. 15th Annual Meeting, Organisation for Human Brain Mapping, San Francisco, Book of Abstracts, June 2009
- *Yogarajah M,* Focke N, Bonelli SB, Parker G, Alexander D, Symms M, Koepp M, Duncan J. Tractography and the Distributed Network Damage Underlying Memory Impairment in Temporal Lobe Epilepsy, 28th International Epilepsy Congress, Budapest, Book of Abstracts, June 2009
- *Yogarajah M,* Focke N, Bonelli SB, Parker G, Alexander D, Symms M, Koepp M, Duncan J. A disproportionate role for the fornix in recall rather than recognition memory – tractography evidence in temporal lobe epilepsy, 17th International Society for Magnetic Resonance in Medicine, Book of Abstracts, May 2009

- *Yogarjah M*, Focke N, Cercignani M, Bonelli S, Parker G, Alexander D, Symms M, Koepp M, Duncan J. Tractography of the Optic Radiation in Pre-Surgical Temporal Lobe Epilepsy Patients. ABN Meeting, Dublin, Book of Abstracts, April 2008
- *Yogarjah M*, Focke N, Cercignani M, Bonelli S, Parker G, Alexander D, Symms M, Koepp M, Duncan J. Temporal Lobe Resections, Visual Field Deficits, and Meyer's Loop. UK ILAE Chapter Annual Meeting, Dundee, Scotland, Book of Abstracts 2008
- *Yogarjah M*, Focke N, Cercignani M, Bonelli S, Parker G, Alexander D, Symms M, Koepp M, Duncan J. Tracing Meyer's loop: Temporal lobe resection, visual field deficits, and tractography. American Epilepsy Society, Seattle, Book of Abstracts 2008
- *Yogarajah M,* Powell R, Parker G, Alexander D, Symms M, Boulby P, Wheeler-Kingschott C, Barker G, Thompson P, Koepp M, Duncan JS. Tractography of the parahippocampal gyrus and material specific memory impairment in unilateral temporal lobe epilepsy. Epilepsia 48 (Suppl. 7):2-177 2007
- *Yogarajah M,* Powell R, Parker G, Alexander D, Symms M, Boulby P, Wheeler-Kingschott C, Barker G, Thompson P, Koepp M, Duncan JS. Atrophy of medial temporal lobe connections in unilateral temporal lobe epilepsy: A tractography based study. JNNP 78:1014-1038 2007
- *Yogarajah M,* Powell HWR, Parker GJM, Alexander DC, Symms MR, Boulby P, Wheeler-Kingschott CA, Barker GJ, Koepp MJ, Duncan JS. Reorganisation of medial temporal lobe connections in unilateral temporal lobe epilepsy. JNNP 78: 780-786 2007

PRIZES AND AWARDS DERIVED FROM THIS THESIS

- Longitudinal Changes in White Matter and Language Outcome After Anterior Temporal Lobe Resection, Organisation for Human Brain Mapping Meeting Trainee Abstract Award (top 113 abstracts out of 1200 abstracts), selected as platform and poster presentation, Human Brain Mapping Conference, 2011
- The Structural Plasticity of White Matter Networks Following Anterior Temporal Lobe Resection, Medical Research Society Neurosciences Section Prize, 2010
- The Structural Plasticity of White Matter Networks Following Anterior Temporal Lobe Resection, Organisation for Human Brain Mapping Meeting Trainee Abstract Award (top

86 abstracts out of 776 abstracts) and poster selected as E-poster (top ranked 246 abstracts out of 3000+), Human Brain Mapping Conference, 2010

- Brain Neurology 1-year scholarship, 2009
- Tractography and the Distributed Network Damage Underlying Memory Impairment in Temporal Lobe Epilepsy, Organisation for Human Brain Mapping Meeting Trainee Abstract Award, Human Brain Mapping Conference, 2009
- Tractography of Meyer's Loop and Temporal Lobe Resection, 8th European Congress on Epilepsy meeting abstract award (top five submitted abstracts), 2008
- Tracing Meyer's loop: Temporal lobe resection, visual field deficits, and tractography, American Epilepsy Society meeting young investigator award, 2008
- Temporal Lobe Resections, Visual Field Deficits, and Meyer's Loop., ILAE UK Chapter abstract winner, 2007

ACKNOWLEDGEMENTS

It has been a pleasure and a privilege to work as part of the Department of Clinical and Experimental Epilepsy (DCEE) during my period of research, and many need to be acknowledged. My primary supervisor Professor John Duncan has always been a patient source of guidance, support, and clarity of thought throughout this period. He is a role model I aspire to, as someone who successfully combines clinical, academic and leadership roles with good grace and humour. My co-supervisor Mark Symms has also been a great support, providing guidance in methodological issues, and teaching me about MR physics. I am also grateful to Professor Matthias Koepp for being a readily available source of insightful discussion, boundless enthusiasm and interesting ideas. Dr Pam Thompson performed all the patient neuropsychological assessments and was a source of perceptive advice when writing up the results. Thank you to the radiographers at the National Society for Epilepsy, Philippa Bartlett, Jane Burdett, and Elaine Williams, for helping me to acquire the MRI data. Joan Blissett and Peter Gilford also provided much appreciated administrative, and IT support respectively. The patients were generously referred by all the consultants in the DCEE, and expertly operated on by Mr Andrew McEvoy at the National Hospital for Neurology and Neurosurgery. It was also a pleasure to share the office with a number of research fellows over this period, many of whom, have become good friends. I am also extremely grateful to all the patients and control subjects studied in this thesis, without whom, none of this work would have been possible.

A Wellcome Trust Programme Grant, and Brain scholarship provided funding for this project.

Finally, I am grateful to my parents for all their support, and especially my father who I miss dearly. I am also thankful for my wife who was always there, offering encouragement and support when I needed it most. This thesis is dedicated to them.

1 Background

1.1 Epidemiology of epilepsy

1.1.1 Definition of epilepsy, epileptic seizures and active epilepsy

Epilepsy is defined by the International League Against Epilepsy (ILAE) as 'a disorder characterised by an enduring predisposition to generate epileptic seizures and the neurobiological, cognitive, psychological and social consequences of this condition' (1). The definition requires the occurrence of at least one epileptic seizure, but in practical terms, it is difficult to identify and define 'an enduring predisposition to seizures'. For this reason most epidemiological studies define epilepsy as 'two or more unprovoked seizures occurring at least 24 hours apart' (2). This definition permits the robust comparison of epidemiological studies from different groups, and time periods. An epileptic seizure is defined as a 'transient occurrence of signs and/or symptoms due to abnormal excessive or synchronous neuronal activity in the brain.' These signs or symptoms may include acute onset or transitory phenomena such as involuntary motor, sensory, autonomic or psychic events, or alterations in consciousness, which may be perceived by a patient or observer (1). Distinction must be made between epileptic seizures and provoked or acute symptomatic seizures which are not due to an established or 'enduring alteration in the brain'. These include solitary unprovoked epileptic seizures, or a single cluster occurring within 24 hours, febrile or neonatal seizures occurring in infants less than 28 days of age, and seizures that occur in the context of an acute systemic, metabolic or toxic insult or an acute central nervous system insult (CNS) such as infection, stroke, cranial trauma, intracerebral haemorrhage, or alcohol intoxication/withdrawal (2–4). Active epilepsy is defined as a person who is being treated for epilepsy, or whose most recent seizures occurred in the last 2 to 5 years (2).

1.1.2 Incidence and prevalence

Studies assessing the incidence and prevalence of epilepsy give variable results. Given that epilepsy is diagnosed primarily on the basis of a clinical history, and some patients with milder seizures may never seek medical attention, epidemiological studies of epilepsy are ultimately limited by diagnostic accuracy and case ascertainment bias, the latter being a particular problem in the developing world (5,6). For these reasons, depending on the study, the overall incidence of

epilepsy varies from 40 to 70 per 100,000 population per year, and this figure rises to 100 to 190 cases per 100,000 population per year in less developed regions of the world (7–11). In Europe alone the age-adjusted incidence of epilepsy ranges from 26 per 100,000 person-years in Norway (12) to 47 per 100,000 person years in England (8), while in the USA it ranges from 16 per 100,000 person-years (13) to 51 per 100,000 person-years (14). Overall, there is good evidence that people from poorer socioeconomic backgrounds are at higher risk of developing epilepsy (9), and in developed countries the incidence of epilepsy in children has declined while that in the elderly has simultaneously increased (15).

Studies assessing the age-adjusted point prevalence of active epilepsy also give variable results. Most studies report figures of 4 to 10 per 1000 persons, though this figure is slightly higher at 6 to 10 per 1000 persons in poorer regions of the world (16). Part of the reason for different prevalence rates in different regions of the world may relate to the presence (or absence) of endemic conditions such as neurocysticercosis, or malaria, and the availability of medical care, infrastructure, and preventative health programs (17). In contrast, the lifetime prevalence of epilepsy, or the risk of having a non-febrile epileptic seizure at some point in one's life does not vary markedly between richer and poorer regions of the world. In both regions, approximately 5% of the population will experience non-febrile seizures (5,6). In view of the difference between lifetime and point prevalence figures it is clear that most patients who develop epilepsy will either go into remission, or die (18). The impact of each of these factors on prevalence rates has not yet been fully appraised.

1.1.3 Mortality

People with epilepsy have a mortality rate 2 to 3 times higher than that of the general population (19). Typically mortality rates have a bimodal peak, one early in life reflecting early risk factors for epilepsy such as severe perinatal hypoxic brain damage, brain malformations and inherited metabolic disorders, and one late in life secondary to cerebrovascular disease (20). Cohort studies report standardised mortality ratios (SMR) that range from 2.1 to 5.1 (21–25), but longer prospective studies in which large populations of children are followed for 15 to 30 years report higher SMRs of 8.8 to 13.2 (26–29). Death in epilepsy can be classified into several groups (table

1.1): those deaths related directly or indirectly to the epilepsy, deaths related to the cause of the epilepsy, and deaths that are unrelated to both. Generalised convulsive status epilepticus (SE), defined as a generalised convulsion lasting 30 minutes or longer, or repeated tonic-clonic convulsions occurring over a 30 minute period without recovery of consciousness between each convulsion, accounts for up to 10% of all deaths in epilepsy, and has a standardised mortality ratio of 2.8% (30). SUDEP or sudden unexplained death in epilepsy, is defined as a sudden, unexpected, witnessed/unwitnessed, non-traumatic, and non-drowning death in patients with epilepsy, with or without evidence of seizures, and excluding status epilepticus, in which the post mortem examination does not reveal a toxicological or anatomical basis for death (31). The incidence of SUDEP ranges from 0.35 to 9.3 per 1000 person years depending on the study population assessed (32).

Table 1.1 – Causes of death in epilepsy (33)

Unrelated deaths	**Related to underlying cause of epilepsy**	**Epilepsy-related deaths**
Non-brain neoplasms	Brain tumours	Sudden unexpected death in epilepsy (SUDEP)
Ischaemic heart disease	Cerebral infections - encephalitis - abscesses	Seizure related deaths - status epilepticus - trauma - burns - drowning - asphyxiation - aspiration pneumonia post seizure
Pneumonia	Cerebrovascular disease - infarction - haemorrhage	Suicides
Others	Inherited disorders - eg metabolic disorders	Treatment related deaths - idiosyncratic drug reactions - medication side effects/adverse events

1.1.4 Prognosis

Prognostic studies of newly diagnosed and treated patients with epilepsy suggest that 60 to 90% of patients will enter long-term remission on treatment initiation, and about 50% will remain in remission after treatment withdrawal (34). However, studies from developing countries and patients with untreated epilepsy suggest that spontaneous remission rates may be high as 40%

after 10 years (35). In treated patients, the response to the first anti-epileptic drug (AED) is the most powerful predictor of prognosis (36), and failure to control seizures with the first or second AED suggests that the probability of subsequent seizure control with further AEDs is about 4% (34). The ILAE have proposed that drug-resistant epilepsy be defined as the failure of adequate trials of two tolerated, appropriately chosen and administered antiepileptic drugs (whether as monotherapy or in combination) to achieve seizure freedom (37). Overall, 10 to 20% of all incident cases of epilepsy result in intractable disease, but 5% per year of these patients become seizure free after medication changes (38).

1.2 The Classification of epilepsy

1.2.1 Seizure classification

The classification of seizures, epilepsies, and epilepsy syndromes has been a subject of considerable controversy. In 1981 the ILAE proposed an International Classification of Epileptic Seizures (table 1.2) (39). Seizures were classified as partial or generalised. In partial seizures clinical and electroencephalographic (EEG) signs indicated that initial activation was limited to one part of the cerebral hemisphere. They were further sub-classified into simple and complex partial seizures on the basis of whether awareness was impaired during an attack. Generalised seizures were dependent on the first clinical and EEG changes indicating initial involvement of both cerebral hemispheres. Described below are the main features of the differing seizure types.

Generalized onset

A) Tonic and/or clonic seizures

Tonic seizures are fast rhythmic events (1–2 Hz), often associated with impaired consciousness. Tonic seizures occur in Lennox–Gastaut syndrome and occasionally in epilepsy with myoclonic astatic (or myoclonic-atonic) seizures. Generalized tonic–clonic seizures (GTCSs) have sudden onset with immediate loss of consciousness. There is a brief tonic phase lasting 10–30 seconds with a whole body tonic contraction, associated with a loud scream and autonomic symptoms such as tachycardia, pupillary dilation, a rise in blood pressure, and depression of breathing. Tongue biting may also be present. The clonic phase lasts around 30 to 60 seconds and is characterized by bilateral clonic jerks that gradually decrease in intensity and frequency. The postictal phase can last up to several hours, is characterized by body relaxation, hypotonia, and sleep. Urinary incontinence may take place at this stage. The patient gradually recovers and may appear confused, and may have automatisms, headache, and generalised myalgia.

B) Myoclonic seizures

Myoclonic seizures are brief symmetrical muscle jerks of variable intensity, which typically affect the proximal musculature. The patient is usually conscious during a myoclonic seizure, and if severe enough they may fall over.

C) Absences

Typical absence seizures are brief lasting no more than 5 to 10 seconds, and are provoked in children by hyperventilation. They occur predominantly in children, and are characterized by sudden interruption of on-going activity and staring straight ahead or drifting upwards, with complete loss of awareness during the seizure. The offset of the seizure is as acute as its onset. Other possible associated features include eyelid myoclonus, change in muscle tone, simple gestural automatisms and, rarely, autonomic symptoms such as urinary incontinence, pupillary dilatation, pallor, flushing, tachycardia, and a change in blood pressure. Concomitant EEG abnormalities are typical generalized spike-and wave discharge at 3 Hz.

D) Atonic seizures

Atonic seizures are characterized by decreased or absent postural tone. They manifest as head nodding, dropping of the jaw or of a limb, or falls. The patient typically makes a quick recovery. Ictal EEG is usually characterized by a generalized slow spike-and-wave discharge.

Focal onset

The semiology of these seizures depends on the lobe of origin. The semiology of temporal lobe seizures is described in more detail in section 1.4.4.1. Focal onset seizures can be divided into two groups.

A) Focal sensory seizures.

Focal sensory seizures may have associated elemental sensory symptoms if the primary sensory cortex (e.g. occipital and parietal lobe seizures) is activated. These include visual, somatosensory, vestibular, olfactory, gustatory, or auditory symptoms. Alternatively if the association cortices is activated (e.g. temporo-parieto-occipital junction) the patient may experience experiential symptoms which are complex, formed, distorted, and/or multimodal sensory symptoms.

B) Focal motor seizures.

These can be sub-classified further:

- With elementary clonic motor signs.
- With asymmetric tonic motor seizures (e.g. supplementary motor seizures).
- With typical (temporal lobe) automatisms (e.g. mesial temporal lobe seizures).
- With hyperkinetic automatisms.
- With focal negative myoclonus.
- With inhibitory motor seizures.

Table 1.2 – International classification of epileptic seizures based on 1981 ILAE report (39)

Partial/Focal/Local seizures
• Simple partial seizures (consciousness not impaired) - with motor symptoms - with somatosensory or special sensory symptoms - with autonomic symptoms - with psychic symptoms • Complex (with impairment of consciousness) - beginning as simple partial seizure (progressing to complex seizure) - impairment of consciousness at onset a) impairment of consciousness only b) with automatism • Partial seizures becoming secondarily generalised
Generalised seizures
• Absence seizures - absences - atypical absences • Myoclonic seizures • Tonic seizures • Atonic seizures • Clonic seizures • Tonic-clonic seizures
Unclassified epileptic seizures

1.2.2 Syndromic classification of epilepsy

In 1989 the ILAE also proposed a Classification of Epilepsies and Epileptic Syndromes (table 1.3) (40). Due to limited knowledge about the mechanisms of epileptogenesis at that time, this was a syndromic classification. That is, it was based on groups of signs and symptoms that often occurred in association with one another. These included seizure types, clinical background, neurophysiological and neuroimaging findings and, outcome. According to this classification, epilepsies were classified as generalized and partial (or focal). Generalized epilepsies were defined as characterized by generalized seizures, bilateral motor manifestations, and generalized interictal

and ictal EEG discharges. Partial epilepsies were characterized by seizures originating from a localised brain region, and by clinical features consistent with a focal onset of the epileptic discharge, with or without subsequent spread, and by focal ictal or interictal EEG abnormalities. This classification system also divided the epilepsies by aetiology, into two categories: idiopathic and symptomatic epilepsies. Idiopathic epilepsies were defined by the absence of any brain lesions, normal background EEG activity and interictal generalized spike and wave discharges. They were presumed to be due to a genetic predisposition or cause. Symptomatic epilepsies were considered to result from focal or diffuse brain lesion as elucidated by the clinical history, structural neuroimaging, EEG findings, or biological tests. A third category, "cryptogenic epilepsies", was also used to describe those epilepsy syndromes which were presumed to be symptomatic but of unknown aetiology.

Table 1.3 – International classification of epilepsy syndromes based on 1989 ILAE report (40)

Localisation-related (focal, local) epilepsies and epileptic syndromes
• Idiopathic (with age-related onset) - Benign childhood epilepsy with centro-temporal spikes - Childhood epilepsy with occipital paroxysms - Primary reading epilepsy • Symptomatic - Chronic progressive epilepsia partialis continua of childhood (Kojewnikow's syndrome) - Syndromes characterised by seizures with specific modes of precipitation - Temporal, frontal, parietal and occipital lobe seizures – classification based on seizure types and other clinical features as well as anatomic localisation and aetiology • Cryptogenic - Temporal, frontal, parietal, and occipital lobe epilepsies – presumed to be symptomatic and aetiology unknown
Generalised epilepsies and syndromes
• Idiopathic (with age-related onset) - Benign neonatal familial convulsions - Benign neonatal convulsions - Benign myoclonic epilepsy in infancy - Childhood absence epilepsy (pyknolepsy)/Juvenile absence epilepsy - Juvenile myoclonic epilepsy - Epilepsy with generalised tonic-clonic seizures on awakening - Other generalised idiopathic epilepsies not defined above - Epilepsies with seizures precipitated by specific modes of activation • Cryptogenic or symptomatic - West syndrome - Lennox-Gastaut syndrome - Epilepsy with myoclonic-astatic seizures - Epilepsy with myoclonic absences • Symptomatic - Non-specific aetiology - Early myoclonic encephalopathy - Early infantile encephalopathy with suppression bursts - Other symptomatic generalised epilepsies not defined above - Epilepsies due to specific neurological diseases
Epilepsies and syndromes undetermined as to whether focal or generalised
• With both generalised and focal seizures - Neonatal seizures - Severe myoclonic epilepsy in infancy - Epilepsy with continuous spike-waves during slow wave sleep - Acquired epileptic aphasia (Landau-Kleffner-syndrome) - Other undetermined epilepsies not defined above • Without unequivocal generalised or focal features. All cases with generalised tonic-clonic seizures in which clinical and EEG findings do not permit classification as clearly generalised or localisation related .
Special syndromes
• Situation-related seizures - Febrile convulsions - Isolated seizures or isolated status epilepticus - Seizures occurring only when there is an acute metabolic or toxic event such as alcohol, drugs, eclampsia, non-ketotic hyperglycaemia

1.2.3 Problems with the classification system

Since 1989 a number of problems have been identified with both classification systems, and attempts have been made to revise them, most recently in 2010 (41–44). Since the original classifications in the 1980s, there have been considerable advances in our understanding of the biological basis of seizures and epilepsy, which are not incorporated into the original classification systems. The seizure classification system included nothing about any localising or lateralising features that might be important for epilepsy surgery, and nothing about the pathophysiological mechanisms, neuronal substrates, response to anticonvulsant medications, and ictal EEG findings of seizures. Similarly the classification of epileptic syndromes included nothing about seizure type, age of onset, prognosis, interictal EEG findings, pathophysiological mechanisms, anatomical substrate or aetiological or genetic basis, and associated interictal features.

In 2001 an ILAE report proposed a new classification of seizures and epilepsy based around the concept of five axes, namely, ictal phenomenology, seizure type, syndrome, aetiology and impairment (42). It was recommended that the terms "simple" and "complex" be avoided when classifying seizure types, and instead, "ictal impairment of consciousness" should be used where appropriate to describe individual seizures. Similarly, it was recommended that the terms "partial" and "cryptogenic" be replaced by "focal" and "probably symptomatic". In the latter case this recommendation was made to avoid any ambiguity between the intended meaning, and all conditions with unknown aetiology as often meant by epidemiologists. The report also highlighted that the dichotomy between 'partial' and 'generalised' abnormalities neglects a number of newly described conditions that lie between the spectrum of these two extremes such as diffuse hemispheric or multifocal abnormalities.

Further ILAE reports in 2006 (43) and 2010 (44) have attempted to redefine specific epileptic seizure types, and the epilepsies, by incorporating the advances in molecular biology and imaging that have occurred since the publication of the original classification systems. In the 2010 report generalized and focal are redefined for seizures as occurring in and rapidly engaging bilaterally distributed networks (generalized), and within networks limited to one hemisphere and either discretely localized or more widely distributed (focal). The classification of generalized seizures

has been simplified, and focal seizures should be described according to their manifestations (e.g., dyscognitive, focal motor). The concepts of generalized and focal as applied to epilepsies and electroclinical syndromes are made redundant. Genetic, structural–metabolic, and unknown represent modified concepts to replace idiopathic, symptomatic, and cryptogenic. The 2010 report also highlighted that not all epilepsies are recognized as electroclinical syndromes (defined as a complex of clinical features, signs, and symptoms that together define a distinctive, recognizable clinical disorder). The report recommends that levels of specificity should define the organization of forms of epilepsy: electroclinical syndromes, non-syndromic epilepsies with structural–metabolic causes, and epilepsies of unknown cause. The report also emphasizes that further organization within these divisions can be accomplished in a flexible manner depending on purpose. For example, natural classes (e.g., specific underlying cause, age at onset, associated seizure type), or pragmatic groupings (e.g., epileptic encephalopathies, self-limited electroclinical syndromes) can be used as a further basis for organizing knowledge about recognized forms of epilepsy. The revised 2010 classifications of seizures and electroclincial syndromes and other epilepsies is shown in tables 1.4 and 1.5.

Table 1.4 – Classification of seizures based on 2010 recommendations (44)

Generalised seizures
• Tonic –clonic (in any combination)
• Absence
- typical
- atypical
- absence with special features
  - myoclonic absence
  - eyelid myoclonia
• Myoclonic
- myoclonic
- myoclonic atonic
- myoclonic tonic
• Clonic
• Tonic
• Atonic

Focal seizures
Unknown • Epileptic spasms

Table 1.5 – Classification of electroclinical syndromes and other epilepsies based on 2010 recommendations (44)

Electroclinical syndromes arranged by age at onset • Neonatal period - Benign familial neonatal epilepsy (BFNE) - Early myoclonic encephalopathy (EME) - Ohtahara syndrome • Infancy - Epilepsy of infancy with migrating focal seizures - West syndrome - Myoclonic epilepsy in infancy (MEI) - Benign infantile epilepsy - Benign familial infantile epilepsy - Dravet syndrome - Myoclonic encephalopathy in nonprogressive disorders • Childhood - Febrile seizures plus (FS+) (can start in infancy) - Panayiotopoulos syndrome - Epilepsy with myoclonic atonic (previously astatic) seizures - Benign epilepsy with centrotemporal spikes (BECTS) - Autosomal-dominant nocturnal frontal lobe epilepsy (ADNFLE) - Late onset childhood occipital epilepsy (Gastaut type) - Epilepsy with myoclonic absences - Lennox-Gastaut syndrome - Epileptic encephalopathy with continuous spike-and-wave during sleep (CSWS) Landau-Kleffner syndrome (LKS) Childhood absence epilepsy (CAE) • Adolescence – Adult - Juvenile absence epilepsy (JAE) - Juvenile myoclonic epilepsy (JME) - Epilepsy with generalized tonic–clonic seizures alone - Progressive myoclonus epilepsies (PME) - Autosomal dominant epilepsy with auditory features (ADEAF) - Other familial temporal lobe epilepsies • Less specific age relationship - Familial focal epilepsy with variable foci (childhood to adult) - Reflex epilepsies
Distinctive constellations • Mesial temporal lobe epilepsy with hippocampal sclerosis (MTLE with HS) • Rasmussen syndrome • Gelastic seizures with hypothalamic hamartoma • Hemiconvulsion–hemiplegia–epilepsy • Epilepsies that do not fit into any of these diagnostic categories can be distinguished first on the basis of the presence or absence of a known structural or metabolic condition (presumed cause) and then on the basis of the primary mode of seizure onset (generalized vs. focal)
Epilepsies attributed to and organized by structural-metabolic causes • Malformations of cortical development (hemimegalencephaly, heterotopias, etc.) • Neurocutaneous syndromes (tuberous sclerosis complex, Sturge-Weber, etc.) • Tumor • Infection • Trauma

• Angioma - perinatal insults, stroke etc.
Epilepsies of unknown cause
Conditions with epileptic seizures that are traditionally not diagnosed as a form of epilepsy per se • Benign neonatal seizures (BNS) • Febrile seizures (FS)

The new classification of seizures and epilepsy syndromes is a work in progress and may require further revision. The older classifications were simplified and specific seizure types were added. The replacement of the term "idiopathic" by the term "genetic" may be problematic. First, genetic etiologies due to a single gene mutation are rare. Secondly, many of the epilepsies may be defined by multiple gene mutations and not due to a specific genetic defect. Additionally, some of the epilepsies don't fit into a single category in the new classification system eg. age-specific epilepsies, such as the primarily generalized epilepsies. For this reason many argue that the original 1989 classification of epilepsy syndromes and epilepsies was widely understood, and is still reliable for clinical and epidemiological purposes, and should not be discarded (45). For this reason it is used in the remainder of this thesis.

1.3 The causes of epilepsy

Epilepsy is the result of a combination of genetic, acquired and provoking factors. Despite this multifactorial aetiology, the causes of epilepsy can be classified into four groups according to the predominant cause as proposed by Shorvon et al (46). It should be noted that in using this classification system, categories do not easily map to focal or generalised groupings, and that the meaning of 'aetiology' refers to the 'underlying cause' rather than the mechanism of epileptogenesis.

Idiopathic epilepsy is caused by a complex combination of genetic and non-genetic mechanisms. There are no structural or pathological abnormalities, and it is likely to have a polygenic and complex inheritance. Symptomatic epilepsy is of an acquired or genetic cause, and is associated with structural or pathological abnormalities. It includes acquired, and developmental or congenital disorders (whether genetic, acquired or cryptogenic) where they are associated with structural and pathological changes. Provoked epilepsy is predominantly caused by specific systemic or environmental factors. It may have a genetic or acquired basis, and there are no structural or pathological changes evident. Cryptogenic epilepsy of presumed symptomatic nature is one in which a cause has not been identified, and makes up to 40% of adult onset cases of epilepsy. Table 1.6 outlines the common aetiologies of epilepsy as outlined by this classification system.

Table 1.6 – Categories of causation of epilepsy (46)

Main category	Subcategory 1	Subcategory 2	Examples
Idiopathic	• Pure epilepsies due to single gene disorders		• Benign familial neonatal convulsions, autosomal dominant nocturnal frontal lobe epilepsy, generalised epilepsy with febrile seizures plus, severe myoclonic epilepsy of childhood
	• Pure epilepsies with complex inheritance (much more common than category above)		• Idiopathic generalised epilepsies (most common variant being juvenile myoclonic epilepsy), benign partial epilepsies of childhood (most common variant being benign partial epilepsy with centrotemporal spikes)
Symptomatic	• Predominant genetic or developmental causation	• Childhood epilepsy syndromes	• West syndrome, Lennox-Gastaut syndrome
		• Progressive myoclonic epilepsies	• Unverricht-Lundborg disease, dentate-rubro-pallido-luysian atrophy (DRPLA), Lafora body disease, mitochondrial cytopathy, neuronal ceroid lipofuscinosis, sialidosis
		• Neurocutaneous syndromes	• Tuberous sclerosis, neurofibromatosis, Sturge-Weber disease
		• Single gene disorders	• Neuroacanthocytosis, Rett syndrome, Wilson's disease, Angelman syndrome, lysosomal storage or transport disorders, porphyrias, amino acid and organic acid disorders, urea cycle disorders, cobalamin and folate metabolism disorders
		• Chromosomal disorders	• Down syndrome, fragile X syndrome, ring chromosome 20
		• Developmental structural abnormalities of the brain	• Cortical dysplasias: abnormalities of gyration (agyria, polymicrogyria, schizencephaly), heterotopias, megalencephaly and hemimegalencephaly, agenesis corpus callosum, microcephaly, anencephaly, cortical dysgenesis

			associated with neoplasia (DNET, ganglioglioma, gangliocytoma), hypothalamic hamartoma, focal cortical dysplasia, microdysgenesis
	• Predominant acquired causation	• Hippocampal sclerosis	
		• Pre-/Peri-natal and infantile causes	• Neonatal seizures, cerebral palsy, post-vaccination
		• Cerebral trauma	• Head injury, neurosurgery
		• Cerebral tumour	• Primary and secondary brain tumours
		• Cerebral infection	• Viral meningitis and encephalitis, bacterial meningitis, malaria, neurocysticercosis, tuberculosis, HIV
		• Cerebrovascular disorders	• Cerebral haemorrhage/infarction, arterio-venous malformations, cavernous haemangiomas
		• Cerebral autoimmune disorders	• Rasmussen encephalitis, SLE, autoimmune and paraneoplastic limbic encephalitis, MS, ADEM, CNS vasculitis
		• Neurodegenerative disorders	• Alzheimer's disease, hydrocephalus
Provoked		• Provoking factors	• Fever, menstrual cycle and catamenial epilepsy, endocrine (eg insulinoma) and metabolic (eg renal or liver failure) factors, drug/toxin induced seizures, alcohol abuse
		• Reflex epilepsies	• Photosensitive epilepsies, startle induced epilepsies, reading epilepsy, auditory induced epilepsy, eating epilepsy

Cryptogenic			

1.4 Temporal lobe epilepsy

1.4.1 Introduction

In some community studies, the cumulative incidence of non-febrile seizures is about 20 per 1000, the prevalence of active epilepsy is about 5 per 1000, and approximately 50% of these patients have partial seizures. Of these seizures, 60-70% originate in the temporal lobe, and therefore temporal lobe epilepsies are the most frequent type of focal epilepsy (47,48). Several sub classification systems exist for partial seizures originating from the temporal lobe. The most widely accepted system distinguishes between mesio-basal and lateral neocortical types of temporal lobe epilepsy (TLE). Though the symptomatology of the two overlaps and spread from the lateral to mesial cortex (and vice versa) is common, this system provides a useful distinction (49). Seizures arise from the mesial temporal structures (amygdala, hippocampus, and parahippocampal gyrus) in over 90% of patients with TLE (49). Hippocampal sclerosis (HS) represents the pathological substrate in at least 45% of patients with mesial TLE (MTLE) (50). Ammon's horn sclerosis and mesial temporal lobe sclerosis (MTLS) are two common pathological terms that are used synonymously with HS, but strictly speaking they imply different degrees of anatomical involvement, the latter implying more widespread temporal involvement than simple HS. Other pathologies that can cause MTLE include dysembryoplastic neuroepiltheliomas and other benign tumours, cavernous angiomas, gliomas, malformations of cortical development, and gliosis as a result of encephalitis or meningitis.

1.4.2 Normal hippocampal structure and connections

1.4.2.1 Structure

The hippocampal formation is located in the medial temporal lobe, and has an inverted S shape on coronal sections (see figure 1.1a). This appearance is the reason for the name 'hippocampus', which means 'sea horse' in Greek, or 'cornu Ammonis' which means 'horn of the God Ammon' in Latin. The three components of the hippocampal formation are the dentate gyrus (named for its tooth like projections on its medial surface), the hippocampus, and the subiculum (Latin for 'support'). The gray matter of the hippocampus is essentially an extension of the subiculum of the parahippocampal gyrus. During development the medial temporal lobe folds in on itself twice, and for this reason the gray matter surfaces of the dentate gyrus and subiculum fuse, as do the white

matter surfaces of the subiculum and parahippocampal gyrus. All hippocampal components are composed of simple three layered allocortex, which differentiates them from surrounding six layered medial temporal neocortex. The primary cells of the dentate gyrus are called granule cells, and the three layers of the dentate gyrus moving inwards from the pial surface are the, molecular layer, granule cell layer, and polymorphic layer. The main cells of the hippocampus and subiculum are pyramidal cells, and the three layers of these structures are the molecular layer, pyramidal cell layer, and polymorphic layer. The molecular layers of the dentate gyrus and subiculum appose one another, forming the hippocampal sulcus. The groove in the medial temporal lobe just dorsal to the hippocampal formation is known as the choroid fissure. In the sagittal plane the hippocampus appears as a club-shaped structure divided into three parts: head, body, and tail. The more anterior head is marked by digitations and is also called the pes hippocampus. The body is more cylindrical in shape, and the tail tapers posteriorly, and finally disappears as it curves under the ventral posterior edge of the splenium of the corpus callosum.

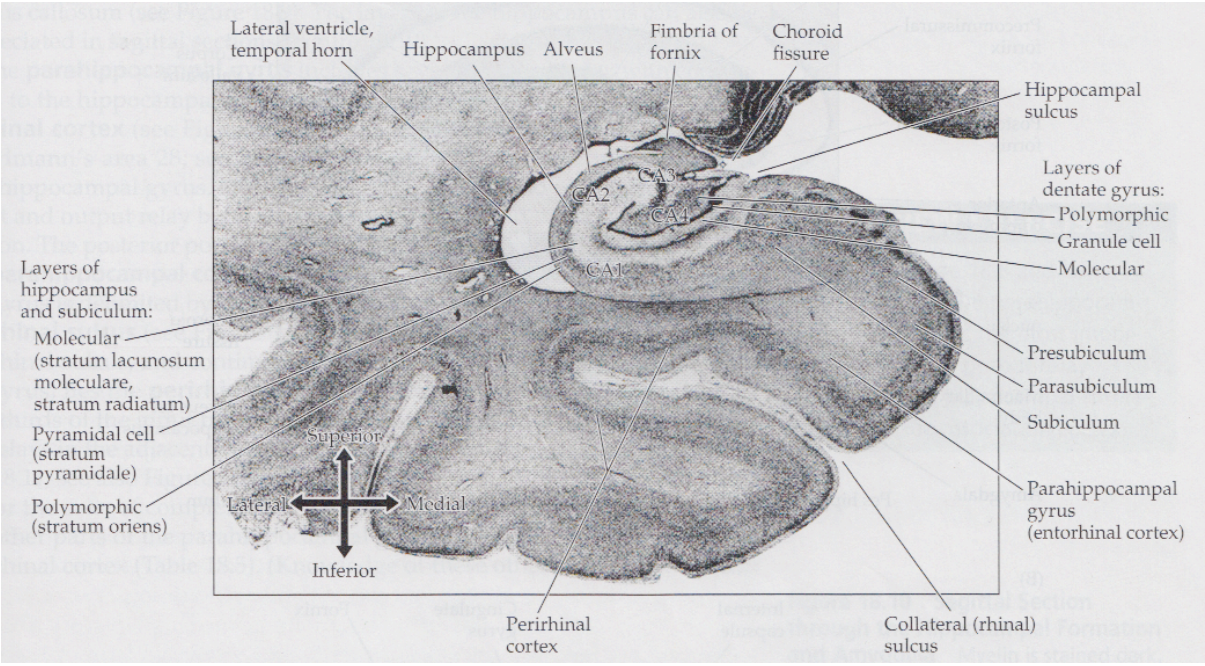

Figure 1.1a – The structure of the hippocampus (adapted from reference (51))

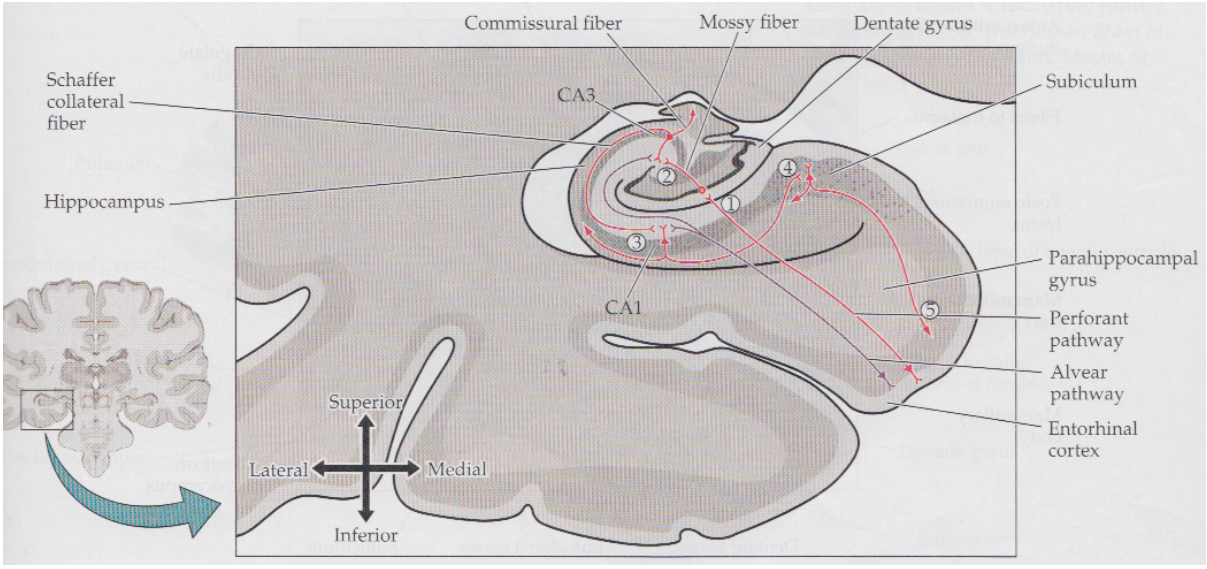

Figure 1.1b – The connections of the hippocampus (adapted from reference (51))

The parahippocampal gyrus includes several areas with connections to the hippocampal formation, the most important of which is the entorhinal cortex. This lies in the anterior part of the parahippocampal gyrus, next to the subiculum, and serves as the main input/output relay station between the association cortex and hippocampal formation. The posterior part of the parahippocampal gyrus is called the parahippocampal cortex, and it is laterally bounded by the collateral sulcus, which continues anteriorly as the rhinal sulcus. Along the medial and lateral walls of the rhinal sulcus, and continuing laterally into the adjacent occipitotemporal gyrus lies the perirhinal cortex. About seventy percent of the input from association cortex reaches the entorhinal cortex via the perirhinal and parahippocampal cortex.

1.4.2.2 Intrinsic connections of the hippocampal formation

The circuitry of the hippocampus and hippocampal formation has been the subject of considerable investigation because of its important role in human memory (see figure 1.1b) (52). The hippocampus proper or Ammon's horn is composed of the four distinct Cornu Ammonis (CA) pyramidal cell sectors, CA 1-4, whereas the hippocampal formation includes the dentate gyrus, the CA subfields and subiculum. CA4 lies within the hilus of the dentate gyrus, CA3 is adjacent to CA4, CA2 is next, and CA1 lies closest to the subiculum. Figure 1b illustrates the major circuits for information flow from the entorhinal cortex, through the hippocampal formation, and back to the entorhinal cortex. The pyramidal cells in the 2nd and

3rd layers of the entorhinal cortex project to the hippocampal formation via the perforant and alvear pathways (synapse 1 in figure 1.1b). The perforant pathway is named because of its course through the subiculum and across the space that is the hippocampal sulcus, in order to reach the granule cell layer of the dentate gyrus. The granule cells of the dentate gyrus give rise to axons called mossy fibres, which synapse on the dendrites of CA3 pyramidal cells (synapse 2 in figure 1.1b). "Mossy fibres" is a morphological description for axons with large bulbous terminals, which are located in the hilus (CA4) of the dentate gyrus. The axons of the CA3 pyramidal cells leave the hippocampal formation via the fornix, but they also give rise to Schaffer collaterals, which synapse on the dendrites of CA1 pyramidal cells (synapse 3 in figure 1.1b). The axons of the CA1 pyramidal cells leave the hippocampal formation via the fornix, and also project to the next cellular relay area, which lies in the subiculum (synapse 4 in figure 1.1b). The subiculum is the final stage in the pathway and can either send axons directly to the hypothalamus and mammillary bodies via the fornix, or it can pass along the information back to entorhinal cortex completing the loop (synapse 5 in figure 1.1b), which will relay it all back to sensory cortex. In addition to the perforant pathway described above, neurons of the entorhinal cortex project via the alvear pathway directly to the CA1 and CA3 subregions of the hippocampus. As is the case in the perforant pathway, the main outputs in the alvear pathway are from the CA1 and CA3 subregions to the subiculum.

1.4.2.3 Connections of the medial temporal lobe memory system

Figure 1.2a summarises the input and output connections to the hippocampal formation. The main input to the hippocampal formation is from the entorhinal cortex. This in turn receives input from association cortex in the frontal, parieto-occipital, and temporal lobes, via the perirhinal and parahippocampal cortex. This higher-order, sensorimotor information is processed by the medial temporal structures for memory storage. The storage process itself, takes place not in the medial temporal lobes, but the association and primary cortices. A key output therefore of the hippocampal formation is the projection from the subiculum to the entorhinal cortex, and from there to the multimodal association cortex.

Additional major outputs of the hippocampal formation (figure 1.2a and 1.2b) are the fornix and cingulum. It should be noted that the subiculum is again the main source of output fibres from the hippocampal formation to the fornix. The fornix is a prominent C-shaped fascicle of fibres that links the hippocampus

with the mammillary body of the hypothalamus. Efferent fibres converge on the ventricular surface of the hippocampus as the fimbria. This passes posteriorly and superiorly to become continuous with the crus of the fornix, which then curves forward beneath the splenium of the corpus callosum. The two crura unite in the midline, beneath the corpus callosum, to form the body of the fornix; some fibres cross to the opposite side through the small hippocampal commissure. As it passes forwards beneath the corpus callosum, the body of the fornix divides into two columns. These curve downwards, forming the anterior border of the interventricular foramen, and enter the hypothalamus, where the majority of fibres terminate in the mammillary body. The mammillary body, in turn, projects to the anterior nuclear group of the thalamus via the mammillothalamic tract and to the brain stem via the mammillotegmental tract. The anterior nuclei of the thalamus have major connections with the cingulate gyrus. In this manner, the fornix carries output to the diencephalon and septal nuclei. The fornix also carries important modulatory information to the hippocampal complex from the cholinergic neurons in the medical septal nucleus, and nucleus of the diagonal band. These cholinergic pathways may be important in modulating neuronal excitability, and synaptic plasticity.

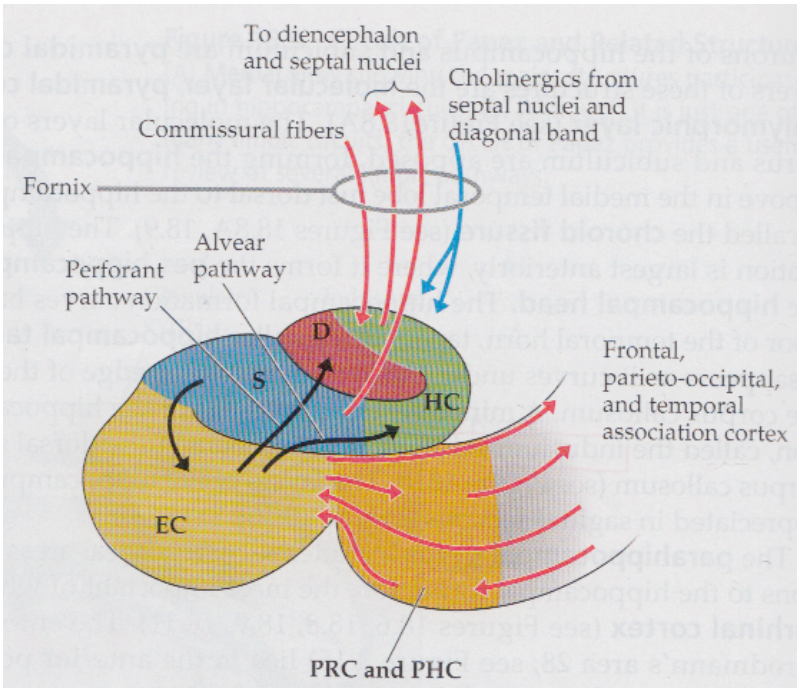

Figure 1.2a – Input and output connections of the hippocampal formation (adapted from reference (51) EC = entorhinal cortex, S = subiculum, D = dentate gyrus, HC = hippocampus, PRC = perirhinal cortex, PHC = parahippocampal cortex

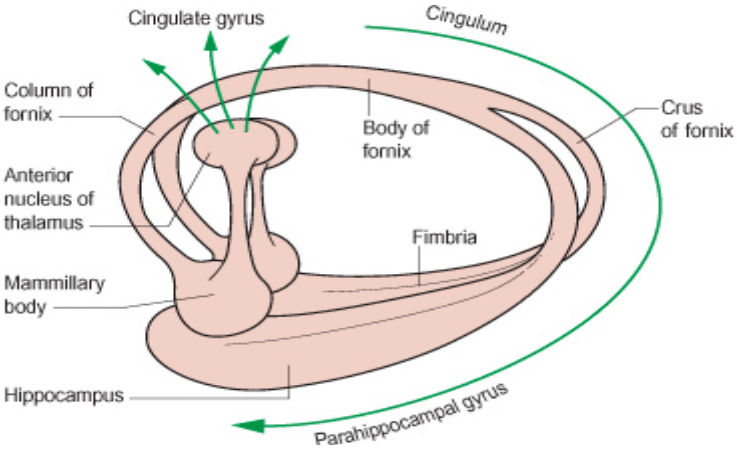

Figure 1.2b – Input and output connections of the medial temporal lobe

1.4.3 Aetiology and pathology

1.4.3.1 Histopathology of hippocampal sclerosis

Hippocampal sclerosis (HS) is the most common pathological finding in reported adult epilepsy series (53), can be detected in approximately 65% of patients with TLE (54). HS is often unilateral and diffuse (55) and can affect either hemisphere equally (56). However, numerous autopsy and surgical based pathological studies support the idea that patients with intractable TLE often have bilateral hippocampal damage. In these cases it is asymmetrical, with one side showing hippocampal sclerosis, and the other mild neuronal loss (57–59). MRI based studies corroborate these findings and have shown that some patients with TLE may have abnormal signal change contralateral to the sclerosed hippocampus and epileptogenic focus (60).

The relationship between hippocampal pathology and temporal lobe seizures has been appreciated for over 180 years. Sommer (61) and Bratz (62) were the first to provide a microscopic description of a consistent pattern of neuronal loss associated with seizures, and identified that the hippocampal pathology associated with seizures was very different to hippocampal neuronal injury associated with other cerebral diseases. Soon afterwards, studies confirmed the link between hippocampal sclerosis and the clinical description of temporal lobe seizures (63). By the mid-20th century clinicopathological studies highlighted the association between histologically confirmed hippocampal sclerosis and clinical and electrophysiological evidence of temporal lobe seizures (58). More recently epilepsy post-mortem studies and surgical series have explored the variability in the patterns and severity of neuronal loss between patients, and speculated on the pathogenesis of the disease process.

The pathologic diagnosis of HS is based on identifying neuronal loss and chronic fibrillary gliosis in the pyramidal cell layer, which leads to tissue atrophy and hardening (64). Based on qualitative or quantitative assessments of the nature of this neuronal loss, there are several patterns of hippocampal cell loss in patients with MTLE (65–67). Table 1.7 outlines one possible method of classification as suggested by Malmgren and colleagues (68). The most common type is 'classical hippocampal sclerosis', which is associated with neuronal loss of the CA1 and CA4 regions. The subiculum, and CA2 regions are well preserved, with variable amounts of loss from the CA3 subregion. Other forms of hippocampal sclerosis

together make up about 20% of cases. 'Severe or total hippocampal sclerosis', involves neuronal loss in the CA2 region as well as the granule cells of the dentate gyrus. 'Atypical or non-classical hippocampal sclerosis' includes patterns of neuronal loss restricted to the CA4 region (end-folium hippocampal sclerosis) and neuronal loss restricted to CA1 region. Atypical cases are important as they may be undetectable with neuroimaging, and they may be associated with less favourable surgical outcomes, and later onset of seizures (66,67). Most epilepsy surgical series consistently report the poorest outcomes in cases with no hippocampal sclerosis visible on MRI, with only 40–50% of patients becoming seizure-free (65,67). Significant attention has been given to the patterns of neuronal loss and the reorganization of surviving neurons in Ammon's horn, as potential contributors to epileptogenesis. In particular, alterations in the inhibitory networks in this area have been assessed, and it has been suggested that extensive synaptic reorganization takes place in the epileptic CA1 region, even in non-sclerotic tissue, before the death of significant numbers of pyramidal cells. This is thought to cause disinhibition of surviving neurons and maintenance of seizure activity (69,70). It is also hypothesized that astrocytes that predominate in sclerotic regions of the hippocampi may also contribute to the hyperexcitability of the hippocampal seizure focus (71).

A number of other pathological changes can occur in association with sclerotic hippocampi. These include granule cell dispersion, mossy fibre sprouting, changes to interneurons, sclerosis of adjacent medial temporal lobe structures, cortical dysplasia and other pathologies. These are discussed further below.

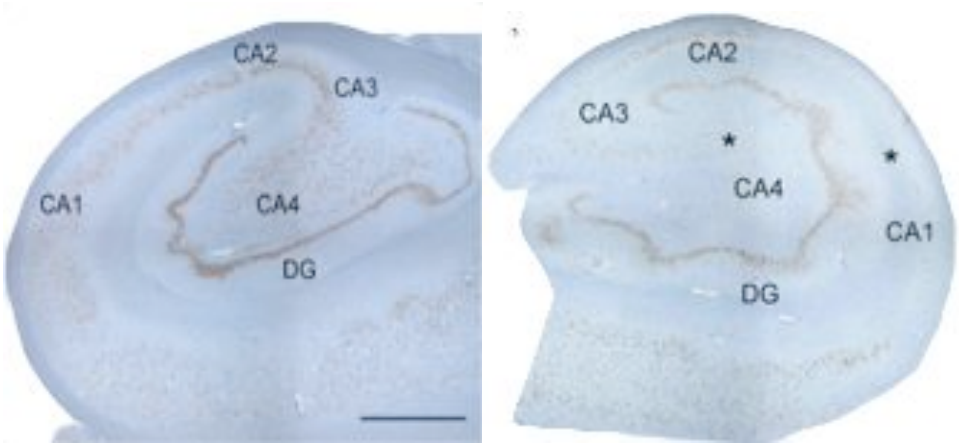

Figure 1.3 - Histopathological findings in a patient with normal hippocampus (left) and a patient with classical hippocampal sclerosis (right). Asterisks index regions with predictive cell loss patterns.

	Pathology type	Definition
Categories of hippocampal sclerosis in surgical practice	Severe hippocampal sclerosis Classical hippocampal sclerosis End folium sclerosis CA1 hippocampal sclerosis Probable hippocampal sclerosis Indeterminate hippocampal sclerosis No hippocampal sclerosis/gliosis only	Severe neuronal loss and gliosis from all subfields CA1 and CA4 neuronal loss and gliosis; variable loss in CA3 CA4 neuronal loss and gliosis CA1 neuronal loss and gliosis Not all subfields represented in specimen but neuronal loss present in CA4 or CA1 Neuronal loss and gliosis is present but does not fit one of the above defined groups (e.g., CA1 + CA3 neuronal loss) No clear qualitative evidence of significant neuronal loss. Gliosis alone does not amount to sclerosis
Mesial temporal sclerosis (MTS)/ "HS plus"	Amygdala gliosis/sclerosis Parahippocampal gyrus/entorhinal cortex Temporal neocortical sclerosis Widespread cortical atrophy Thalamic nuclei Contralateral hippocampus	Gliosis ± neuronal loss in amygdala (lateral and basal nuclear groups) Laminar neuronal loss and gliosis Neuronal loss reported in 11% of HS/TLE patients in layer II/III Subtle volume loss/cortical thinning reported both ipsilaterally and bilaterally including temporal, frontal, parietal cortical regions in MRI and PM studies Reported in MRI and postmortem studies Bilateral hippocampal sclerosis (asymmetrical/symmetrical)
Hippocampal sclerosis and dysplasia	FCD IIIa Mild malformation of cortical development type II	Temporal lobe sclerosis with layer II dysplasia Cortical dyslamination (FCD type I-like) Lentiform heterotopias An excess of single, mature neurons in the white matter of the temporal lobe
Dual pathology	Hippocampal sclerosis in the context of a second temporal/extratemporal epileptogenic pathology	Cavernoma Tumor (often low grade tumour as DNT or ganglioglioma) FCD type II (FCD IIIa and mild MCD excluded by definition)

Table 1.7 – Summary of pathologic subtypes and associated pathologies of HS in epilepsy – adapted from reference (68)

(DNT, dysembryoplastic neuroepithelial tumour; FCD, focal cortical dysplasia; MCD, malformation of cortical development; PM, postmortem; HS, hippocampal sclerosis)

Granule cell dispersion (GCD)

In the normal hippocampus, the dentate gyrus consists of a band of tightly packed small neurons called granule cells. Above the granule cell layer is a molecular layer composed of the apical dendrites of the granule cells, interneurons and the synaptic terminals of the perforant path. Below the granule cell layer and partially circumscribed by it is the hilus. This is composed of neurochemically distinct interneurons, and mossy cells, which receive inputs from granule cell axons. Granule cell dispersion (GCD) accompanies hippocampal sclerosis in 40– 50% (64,72), and is specific to epilepsy. It is not seen in other diseases causing hippocampal atrophy, such as primary neurodegenerative diseases. GCD is significantly associated with early seizure onset (73), with the extent of neuronal loss in CA4 but not CA1 (67) and with a longer duration of epilepsy (72). These features suggest that GCD may represent a consequence of the sclerosing process, or the seizures themselves, the migration of granule cells perhaps being influenced by neurotrophins or other cellular signals released during seizures. Recent evidence confirms that to be the case, showing that dispersion is promoted by a local reduction of reelin, a secreted migration guidance cue (74).

Mossy fibre sprouting (MFS)

Mossy fibre sprouting (MFS) of granule cell axons is common in hippocampal sclerosis and in experimental epilepsy models. Although this axonal sprouting is seen during brain development, it also occurs in response to seizures. In this setting the collateral axons make contact with the apical dendrites and spines of other granule cells in the molecular layer, and sets up potential recurrent excitatory circuits. For this reason, it is pro-epileptogenic, and enhances the excitability and synchronization of discharges. Studies showing that the suppression of mossy fibre sprouting does not affect seizure discharges in animal models (75), and the fact that its presence does not always give rise to seizures (76) suggests that it may represent a response to seizures, rather than actually causing them.

It is likely that the hyperexcitability seen in electrophysiological recordings from surviving granule cells in hippocampal sections from MTLE patients compared with those in non-sclerotic hippocampi (77), is in part due to morphological changes in dentate granule cells such as aberrant axonal reorganisation, and sprouting of excitatory, mossy fibre, glutamatergic axons of the dentate gyrus (78). Other factors are

likely to include changes in the neurotransmitter and receptor systems that modulate dentate granule cell activity (79).

Alterations to interneurons

Hippocampal interneurons are also affected in HS and are likely to play an important role in the genesis of epilepsy, in addition to the loss of pyramidal and excitatory neurons. They are reduced in number and are associated with the reorganization of remaining neurons, including axonal sprouting and new synaptic networks (80). These local interneuronal alterations are likely to synchronize granule cell firing, and start or promote seizures.

'Hippocampal sclerosis plus'

Hippocampal sclerosis can sometimes be accompanied by more extensive sclerosis of adjacent, connected structures in the medial temporal lobe, including the amygdala and parahippocampal gyrus (so called mesial temporal lobe sclerosis) (see table 1.7). These pathological changes manifest as atrophy in the form of neuronal loss and astrocytic gliosis (81). Quantified studies of the entorhinal cortex and parahippocampal gyrus region in patients with hippocampal sclerosis undergoing surgery show subtle and variable patterns of gliosis and neuronal loss (82,83). They may result from the spread of seizures and excitotoxic injury, and could in turn modulate seizure activity. Indeed, there is electrophysiological evidence in some cases to support an origin of temporal lobe seizures outside the hippocampus, for example, in the parahippocampal gyrus and amygdala (84,85). In other studies abnormal patterns of glutamate and GABA receptor densities and synaptic function in the amygdala in patients with TLE, have been found to correlate with observed interictal discharges from this location (85).

Studies employing advanced neuroimaging techniques have also identified more widespread extra-hippocampal atrophy accompanying HS, involving temporal and extratemporal neocortex and thalamus, in both ipsilateral and contralateral hemispheres (86–89). These findings have been corroborated by postmortem studies (58,90). Possible explanations include reciprocal atrophy via hippocampal-cortical networks, or secondary changes from generalized seizures.

HS and cortical dysplasia

In many cases, subtle, developmental, cortical neuropathologies may accompany HS, and have been labelled as ''microdysgenesis'' or focal cortical dysplasias (FCDs). In the revised classification of dysplasias in epilepsy, these findings fall within the FCD type IIIa category (91) as opposed to dysplasias found in isolation. Within the FCD IIIa spectrum are disordered cortical lamination and small ''lentiform'' neuronal heterotopias in the subcortical white matter. In addition, there is a distinct cortical abnormality associated with HS, also termed ''temporal lobe sclerosis,'' where there is neuron loss from the superficial cortex accompanied by gliosis and abnormal neuronal clustering. This is present in around 11% of HS surgical patients (92). Finally, another form of cortical dysplasia that can be found in association with HS is an excess of single, mature neurons in the white matter of the temporal lobe (93). This is not considered as a subtype of FCD IIIa but a mild malformation of cortical development (mild MCD) (91).

HS and dual pathology

Some patients with HS have a second lesion in the temporal lobe, in particular a low-grade tumour (such as a dysembryoplastic neuroepithelial tumours, gangliogliomas) or vascular and cortical malformations. The rate of dual pathology is highly variable depending on the definition of a 'second pathology' used in the study (94,95). In many cases it is possible that the HS may have been ''kindled'' by this second pathology, though the hippocampal atrophy is less severe with dual pathology than in HS alone, and end-folium sclerosis patterns may predominate (96). The coincidence of dual temporal lobe pathologies raises the issue of whether there are common predisposing malformative processes underlying both pathologies, and rendering the temporal lobe more vulnerable to seizures, neuronal injury and HS (95).

No hippocampal sclerosis

In some surgical series, up to 20% of MTLE patients do not show microscopic features of hippocampal neuronal loss, or reduction in cell density, despite electrophysiological evidence for mesial temporal lobe generation of seizures (54,97). In these cases the epileptogenic pathomechanisms remain to be determined, but a model similar to the animal kindling model may operate.

1.4.3.2 Pathogenesis of hippocampal injury in mesial temporal lobe epilepsy

The pathological origins of hippocampal sclerosis have been debated for many years now, with most contention surrounding whether hippocampal neuron loss is the cause or consequence of seizures. Studies now suggest that the answer to this question lies somewhere in the middle of both these hypotheses (98). The pathogenesis of MTLE is often associated with an initial precipitating injury such as a complex or prolonged febrile convulsion that injures the hippocampus at some time prior to habitual seizure onset. Birth trauma, head injury or meningitis, are other early childhood lesions observed in TLE. It is likely there are genetic factors which render an individual hippocampus susceptible to seizures and neuronal loss (99,100), and most of the damage to the hippocampus seems to occur with this initial precipitating injury. Following this initial injury there is typically a latent period extending into a patient's teenage years, during which a number of structural and molecular reorganisation mechanisms take place, which reduce seizure threshold levels in the hippocampus (101–103). Following onset of spontaneous seizure activity, secondary changes associated with excitotoxic cell damage lead to the full- blown picture of HS. These include changes in synaptic properties and neuronal connectivity, alterations in the intrinsic properties of neurons, and changes to glial cells which may then mediate hyperexcitability (98). There can be additional neuron loss associated with a long history of recurrent seizures, though this damage occurs throughout the hippocampus, and not in the selective pattern associated with sclerosis, as well as outside of the hippocampus (104–107). This may clearly impact the decision as to when to refer patients with temporal lobe epilepsy for surgery.

1.4.3.3 Other causes of temporal lobe epilepsy

Although hippocampal sclerosis is the most common cause of TLE, a number of other pathological substrates can also cause TLE (see table 1.6). The most common of these include malformations of cortical development (MCD), low-grade tumours such as dysembryoplastic neuroepithelial tumours (DNT), and vascular abnormalities such as cavernomas and arterio-venous malformations. Their histopathology will not be discussed in detail in this thesis because they represent a small percentage of the underlying pathology in patients with TLE.

Malformations of cortical development originate during intrauterine development as a result of a disturbance of the normal migration and differentiation of nerve cells from the germinal matrix to the

cortex and result in a wide spectrum of structural abnormalities. As imaging techniques improve, MCDs are gaining increasing recognition as an important cause of epilepsy. Hemimegalencephaly, lissencephaly, schizencephaly, and polymicrogyria results primarily from disorders of neuronal migration and cause generalised malformations. They are the most radiologically significant MCDs, and are associated both with marked epileptogenic potential and often additional physical and/or learning disabilities. Focal malformations can be divided into several groups, which include, focal cortical dysplasis, mild dysplasias (mild MCD), heterotopias and hamartomatous lesions.

Focal cortical dysplasias (FCDs) are the most common MCD, and describe a type of malformation of cortical development where the abnormality is largely restricted to a region of the cortical plate and characterized by distinctive cyto-architectural changes. These lesions are easily recognized in histological sections and subdivided into two main subgroups on the basis of histopathology. FCDs are typically characterised on MRI as focal cortical thickening with signal abnormalities in the underlying white matter, and sometimes a wedge-shaped tail extending radially into the ventricle. They may also often be associated with a number of other subtle imaging abnormalities. Mild MCD encompasses the most subtle focal cortical malformations, and previously, these lesions were referred to as microdysgenesis or microscopic dysplasias. They encompass a number of microscopic minor cyto-architectural cortical abnormalities. Currently, mild MCD are typically not visible using current neuroimaging techniques, and neuropathology remains the only method of detection.

Dysembryoplastic neuroepithelial tumours are WHO grade I glioneuronal neoplasms, typically found in the temporal or frontal lobes, and often in co-existence with cortical dysplasia. They are associated with good outcome following surgery (108). Hamartomata in epilepsy are a relatively poorly defined pathological group compared to cortical dysplasias and tumours. Glio-neuronal hamartomata have been described in various cortical locations, particularly temporal and frontal lobes. They are composed of circumscribed masses of mature, but haphazardly arranged, cell types. The imaging characteristics are variable but their lack of growth and mitotic activity help to distinguish these lesions from low-grade tumours.

Heterotopia refers to the presence of apparently normal neurons in an abnormal position, typically in the subcortical hemispheric white matter. Three main categories are recognized which include individual misplaced neurons in the white matter (neuronal heterotopia), nodules of gray matter within the white matter (nodular heterotopia) and band heterotopia (double cortex). Often heterotopias are associated with an overlying dysplastic cortex. Heterotopias are usually seen as multiple lesions, or in the company of other types of cortical abnormalities. Despite this fact, surgical treatment may be beneficial when the epileptogenic zone is carefully located before surgery (108).

1.4.4 Clinical features of temporal lobe epilepsy

1.4.4.1 Seizure characteristics

Approximately 50% of patients with MTLE have presented with an initial precipitating injury before the age of 4 years (54). Onset of seizures is typically in childhood or early adulthood. Both genders are equally affected, and a familial history of TLE is very rare indicating that monogenic hereditary factors do not play a major role in HS associated TLE. Characteristically, patients may do well for several years with anticonvulsant treatment, but seizures may return in adolescence or early adulthood and become refractory to drug treatment. Of those patients with drug refractory seizures, the majority have had complex febrile convulsions, or another initial precipitating injury (105,106).

Mesial temporal lobe seizures can take the form of simple partial seizures, that is, aura alone with clear consciousness, or complex partial seizures. Complex partial seizures typically have an indistinct onset with partial awareness initially and a gradual evolution over 1-2 minutes, in contrast to extra-temporal seizures. They also often last longer than most extra-temporal complex partial seizures (2 to 10 minutes). Overall it is difficult to clinically differentiate between mesial temporal lobe seizures due to HS from other causes. Typically there are 4 components to a complex partial seizure of mesial temporal lobe origin:

Aura:

Auras are common in MTLS and present in up to 90% of patients (106). An aura can occur in isolation as a simple partial seizure or as the initial manifestation of a complex partial seizure. It

can manifest as visceral symptoms (rising epigastric sensation, thoracic constriction, hot or cold sensation, olfactory hallucinations) or by psychic or affective symptoms (dreamy state, déjà-vu, feelings of depersonalisation), usually accompanied or followed by autonomic manifestations (pallor, flushing, heart rate changes, blood pressure changes, piloerection, mydriasis, or sweating). The abdominal aura is the most common (106,109), and is likely to be related to spreading of the epileptogenic discharge from the hippocampus to adjacent insular cortex. Fear is the second most common aura, and is likely to be caused by spread to the amygdala. The remaining aura symptoms are less common (106). Olfactory auras may reflect spread to the amygdala, gustatory auras, spread to the parietal opercula area, and déjà vu auras may represent spread to basal temporal areas. Sometimes patients may experience an aura, which cannot be described, or has no counterpart in human experience.

Blank Spell

Motor arrest or absence (commonly recognized as a 'motionless stare') together with pupillary dilation, can occur in the early stages of seizures originating in medial temporal structures, and more so than in extratemporal lobe epilepsy.

Automatisms

The automatisms of MTLE are often less violent than in frontal lobe seizures. They are usually oro-alimentary (eg. lip-smacking, chewing, swallowing) or gestural (eg. fumbling, fidgeting, repetitive motor actions, undressing, walking, running) and sometimes prolonged. Automatisms can also occur as reactions to environmental objects, or situations.

All the lateralizing signs seen with seizures arising from the mesial temporal region are also an expression of seizure spread and involvement of adjacent brain regions. The automatisms themselves are typically ipsilateral to seizure origin, and may represent spread to the cingulum. Spread to the ipsilateral basal ganglia can cause contralateral dystonia in 15 to 70% of patients (110), while spread to ipsilateral motor areas can cause late, forced, head version to the contralateral side. However, early causal head deviation can be ipsilateral to seizure origin (110). Ictal vocalisation has minimal lateralising value (111), but verbalisation of coherent speech is

associated with non-dominant temporal lobe seizure origin. Preserved consciousness and memory during a seizure with automatisms typically reflects non-dominant temporal lobe seizure origin.

Post-Ictal

Post-ictal confusion, and disorientation are more common and prolonged after a mesial temporal lobe complex partial seizure. If dysphasia occurs, this is a useful lateralizing sign indicating the seizure origin in the speech dominant hemisphere (111). Post-ictal nose rubbing is commonly seen in TLE and in approximately 90% cases it is ipsilateral to the seizure focus (112). Post-ictal lateralised weakness also localises seizure origin to the contralateral temporal lobe. Amnesia is typical for the blank spells and automatisms. Secondary generalization is much less common than in extra-temporal lobe epilepsy. Patients often complain of poor episodic memory and this can deteriorate as the epilepsy continues.

1.4.4.2 Neuropsychological features

Estimating the prevalence of memory and cognitive difficulties in patients with epilepsy, and TLE can be problematic due to the fact that self-reported measures from patient studies may represent a wide range of cognitive difficulties, and other factors such as problems with mood (113) and psychological adjustment (114). On the other hand, estimates based on clinical studies using formal neuropsychological measures may overestimate the extent of the problem, due to selection bias. Despite these difficulties, it is clear that people with epilepsy have an increased risk of cognitive impairment, and memory difficulties are the most frequently reported and assessed cognitive problem in TLE patients. There are a number of factors that may contribute to these cognitive difficulties, and they may be split into three broad categories, namely fixed factors, variable factors and factors relating to the history of the disease (see table 1.8) (115).

Table 1.8 – Factors influencing neuropsychological function in epilepsy –adapted from ref (115)

Fixed Factors	Variable factors	History of the disease
Nature of causative pathology	Interictal and subclinical EEG abnormalities	Episodes of status epilepticus
Location and lateralisation of pathology	Seizure control	Repeated generalised seizures
Age of onset of seizures and pathology	Proximity of last seizure to assessment	Head injuries
Gender	Mood	
Intellectual capacity/reserve	Quality of sleep	
	Medication	

1.4.4.2.1 Fixed factors

The hippocampus and related medial temporal lobe (MTL) structures are critical for the encoding of episodic declarative memory for subsequent long-term storage (116). Given that the most common cause of TLE is HS, it is therefore not surprising that many patients with TLEs have significant memory impairment. Studies have shown that in patients with hippocampal sclerosis the extent of hippocampal volume loss in the dominant hemisphere, as quantified by magnetic resonance imaging volumetry, correlates with scores on tests of verbal learning and recall. These findings have also been corroborated with postoperative cell density studies, which have shown significant correlations between the neuronal densities in resected hippocampi, and preoperative verbal memory scores (117). More recently, other studies have highlighted that in addition to damaged hippocampi underlying the memory impairment seen in these patients, damage to the perirhinal cortex, which is a key node in a distributed memory network, may also be important in determining the cognitive profiles of patients with TLE (118). Finally, as well as memory dysfunction, patients with MTLE in the language dominant hemisphere often also have confrontation naming problems, best exemplified by word-finding difficulties (119,120).

In addition to the nature of the underlying pathology in TLE, the laterality of the pathology or HS, also plays a significant role in memory and language impairment in these patients. The material-specific model of memory function is a well-established concept, and is based on postoperative studies of early epilepsy surgery patients (115). This model hypothesises that verbal memory functions are associated with the dominant medial structures, whilst non-verbal memory functions are associated with non-dominant mesial structures. However, recent re-evaluation of this model

suggests that the verbal/non-verbal dichotomy in mesial temporal lobe function do not represent exclusive functions, but rather specialised functions (115,118). It is clear that patients with right-sided TLE have a degree of verbal memory impairment, and similarly people with left-sided TLE may demonstrate impairments on memory tests involving both verbal and non-verbal material (121). Hermann et al. identified several cognitive profiles in a large case-control study of TLE patients (122). Nearly 50% of the patients had minimal cognitive impairment, 24% had solely memory impairment, and the remainder were impaired on wide range of cognitive tasks including measures of memory, executive function, and processing speed. In the same study, these cognitive phenotypes were shown to be associated with the presence, severity, and distribution of specific anatomic abnormalities in widely distributed cortical, subcortical, callosal, and cerebellar networks (123). Overall, the association between the dominant hemisphere and verbal memory is more consistently observed in MTLE patients than the association between the non-dominant hemisphere and non-verbal memory (124). This may be because visuospatial memory may be less localised and lateralised than verbal memory function, allowing the brain to compensate more easily when the right temporal lobe is damaged (124).

Other fixed factors that can affect the cognitive profile of patients with TLE include the gender of patients, and the nature as well as location of the underlying lesion. Early developmental lesions such as dysembryoplastic neuroepithelial tumours (DNET), and other forms of cortical dysplasia may be associated with relatively little cognitive disturbance as cognitive functions are reorganized during subsequent cognitive development (121). In contrast, lesions that occur in an adult brain that has developed normally can have a marked effect on cognitive function. Gender may also have an important role in determining the cognitive profile of patients with TLE. There is evidence to suggest that both women in the general population, and those with TLE have better verbal and non-verbal memory than men (125). However, women with left sided HS may also have more widespread cognitive deficits than men (121).

1.4.4.2.2 Variable factors

A number of variable factors, which are potentially reversible, can also have affect cognitive and memory function in TLE patients (126). Frequent or clusters of seizures may temporarily cause

reduced memory function and attention span. For this reason, a neuropsychological assessment carried out soon after seizure(s) can give misleading results. Similarly, nocturnal seizures can disrupt sleep patterns, and have a detrimental effect on cognitive efficiency the following day. Anti-epileptic medications, particularly in combination, can also sometimes adversely affect cognitive function. For example barbiturates appear to have the most severe cognitive side effects, phenytoin can slow processing speed, and topiramate can affect executive function, memory and word finding ability (127). Marked, interictal subclinical EEG discharges can also significantly impair cognitive function. Finally, both low mood and anxiety, which are common in TLE, are associated with reduced learning capacity and memory recall. Indeed, mood and quality of life measures, have been shown to be a significant determinants in self-reported memory function (128).

1.4.4.2.3 History of epilepsy

The developmental course of a patient's epilepsy can also have an important bearing on the cognitive functioning. Some studies suggest that epilepsy is over-represented in people with a low intelligence quotient (IQ), due to the extensive underlying cerebral abnormalities that lead to both limited cognitive abilities and recurrent seizures (129). For this reason cognitive difficulties may even predate the diagnosis of epilepsy (130). Studies have also shown that repeated generalised seizures can lead to an accelerated decline in in memory function (131), while longitudinal studies have shown that memory functions may never fully develop in adults who develop epilepsy in childhood (132). That is, patients with an earlier age of onset of seizures have more significant cognitive dysfunction than patients who develop seizures later in life. Although frequent partial seizures do not appear to accelerate the normal age-related decline in cognitive function, patients with epilepsy may begin this decline from a lower starting point compared to healthy peers, and may therefore become impaired at an earlier age (132). As a corollary to this, some studies also show that the duration of epilepsy is negatively correlated to cognitive performance (133), although this may be driven by age of onset of epilepsy rather than duration per se. Studies have also shown that frequent generalised seizures, and particularly status epilepticus can cause cell death, and irreversible cognitive decline. Hence patients with a history of frequent episodes of status epilepticus may have significant cognitive compromise (134).

Temporal lobe surgery, particularly if unsuccessful, may accelerate this decline, but the memory decline may also be stopped or improved if seizures are better controlled. One study showed that although approximately 30% of patients may experience a significant decline in memory function following a unilateral temporal lobe resection, memory functions for the majority of patients may remain unchanged and may improve in about 20% of patients (135). Postoperative change in memory is complex and dependent on a number of pre-, peri-, and postoperative factors (136–138). Preoperative risk factors include good preoperative memory function, and surgery on the language dominant hemisphere. If surgery fails to control or worsens seizures some patients may have a significant postoperative decline in memory function (139).

Cognitive impairment in epilepsy can have a significant impact upon the quality of life of patients (140). For this reason, early neuropsychological assessment of these patients is advisable. Furthermore, when difficulties are found it may be possible to devise cognitive rehabilitation strategies to aid patients (141).

1.4.4.3 Psychiatric features of temporal lobe epilepsy

The prevalence of psychiatric disorders is higher in patients with epilepsy, particularly refractory epilepsy, when compared to the general population. Some studies have estimated that depression occurs in 30% patients, anxiety disorders in up to 25% and psychosis in up to 7% of patients (142,143). Multiple risk factors are associated with an increased risk of psychiatric problems in epilepsy, and include psychosocial and iatrogenic (AEDs, surgery) factors (144,145). Biological factors are also important and TLE in particular, is associated with significant psychiatric co-morbidity. This co-morbidity can be classified according to how symptoms relate in time to seizure occurrence, and this classification has implications for both treatment and prognosis (see table 1.9).

Table 1.9 – Classification of psychiatric symptoms in respect of temporal relationship to seizures

Classification	Temporal relationship to seizures
Peri-ictal	Preictal Ictal Postictal
Interictal	No relation

1.4.4.3.1 Peri-ictal mood and anxiety disorders

Mood and anxiety disorders are the most common psychiatric comorbidity in patients with epilepsy, and particularly TLE. The association is underpinned by biological, and psychosocial factors (146). Patients with TLE typically have refractory seizures, which can give rise to a number of social limitations and discrimination. Furthermore, the neuroanatomical and neurobiological basis of TLE is also linked to depression (147), as are the psychotropic effects of some AEDs used to treat it (148). The consequences of mood disorders are significant. Patients with a mood disorder have a worse quality of life (149), are less likely to tolerate AEDs (150), have a worse outcome after surgery (151) and respond poorly to AED treatment (152).

Pre-ictal or prodromal mood changes usually manifest as depression, irritability or behavioural changes, usually hours to days before a secondarily generalised seizure, which relieves the symptoms (153). Ictal fear or anxiety is the most common ictal psychiatric symptom in TLE, with up to 20% patients with partial seizures reporting fear as part of their aura, particularly in patients with right temporal lobe foci (142,154). Some studies indicate that the presence of ictal anxiety is a good prognostic indicator for temporal lobe surgery in TLE (155). Ictal depression is less common than ictal anxiety, but can affect up to 1% of TLE patients (142). It can manifest as anhedonia, suicidal ideation and feelings of guilt (142). Postictal mood and anxiety disorders are less well recognised, but may be present in 18 to 45% of patients, and may be more common in those with a history of psychiatric disorders (156). Symptoms of depression or anxiety typically last less than 24 hours. Postictal (hypo)mania lasts for longer periods, and is seen in up to 20% of patients (156). It is typically seen in patients who are older and who have seizures originating from the non-dominant hemisphere, and who have other associated psychotic symptoms (156). The treatment of peri-ictal mood and anxiety disorders is based upon the adequate treatment of seizures.

1.4.4.3.2 Interictal mood and anxiety disorders

The clinical features of epilepsy related mood disorders may be similar to that of a primary mood disorders, and meet the DSM-IV diagnostic criteria for major depression, dysthymia, minor depression, bipolar disorder or cyclothymia. However a significant proportion of patients have

mood disorders that do not meet DSM-IV diagnostic criteria, and have atypical manifestations. This compounds the heterogeneity of mood related symptoms seen in these patients. The most common mood disorder is a major depressive episode. The prevalence rates for depression and anxiety in epilepsy is about 20% in community based studies (157), but is higher in patients with more severe epilepsy, and in studies based on patients attending tertiary centres rates of up to 50% are reported (158). Patients with TLE are thought to be at most risk of interictal affective disorders. Recent evidence suggests that in some patients depression may predate seizures, and actually act as a risk factor for the development of seizures (159). This suggests that common pathogenetic mechanisms may be responsible for both conditions. Symptoms of depression may include persistent low mood, anhedonia, and the biological symptoms of a change in sleep or appetite. However, a significant proportion of TLE patients have atypical depressive symptoms, referred to as interictal dysphoric disorder (IDD) (160). This is characterized by chronic intermittent dysthymia, irritability, fear and anxiety as well as lack of energy, pain, and insomnia.

Depression usually does not occur in isolation in TLE patients, but rather tends to occur in association with anxiety disorders. In study of TLE patients, over 70% who met the diagnostic criteria for a depressive episode, also met criteria for an anxiety disorder (161). Interictal anxiety disorders are therefore common in TLE patients, particularly in left TLE patients. Examples of anxiety related disorders include panic disorder, generalized anxiety disorder, phobias, agoraphobia without panic disorder, and obsessive-compulsive disorder. Psychosocial difficulties, and the social stigma, and unpredictability of seizures may also contribute to anxiety symptoms. The co-occurrence of anxiety with depression and may lead to higher suicide risk, which is particularly concerning as patients with epilepsy already have a higher risk of suicide independent of psychiatric co-morbidity (161).

The treatment options for depression include psychological interventions such as counselling, psychotherapy or cognitive behavioural therapy if appropriate. For more severe depression, antidepressants are warranted, but should be used cautiously due to the risk of lowering the seizure threshold. For this reason selective serotonin reuptake inhibitors (SSRIs) such as citalopram, which are less epileptogenic than tricylic compounds, are considered first choice agents

(162). Other classes of antidepressants can also be used, but the prescriber should be aware that any proconvulsive effect tends to occur at higher doses, often typically outside the treatment range for depression (162). Electroconvulsive treatment is also an effective treatment for severe medication resistant depression, and can be used in patients with epilepsy (163). In patients with severe mood instability related to IDD, the use of mood stabilising AEDs, and antipsychotics in selected cases may be warranted.

1.4.4.3.3 Peri-ictal psychotic symptoms

Psychoses and thought disorders are less common in epilepsy compared to depression and anxiety, but are more common than in the general population, and have serious implications for a patient's prognosis. The incidence of non-affective, non-organic, psychotic symptoms in epilepsy is about 5 to 6% (164). Risk factors for psychosis include a family history of psychoses, and epilepsy. This suggests the two conditions may share common pathogenic mechanisms (165). Ictal psychosis is typically caused by temporal lobe complex partial status epilepticus (166). Post-ictal psychosis is much more common, and makes up about 25% of the psychoses in epilepsy (166). It occurs at an older age, and older age of onset of epilepsy, than interictal psychosis, and is most often described in patients with temporal lobe epilepsy (167,168). Patients typically present 1 to 6 days after a cluster of secondarily generalised tonic-clonic seizures, and may therefore have a coherent interval prior to the onset of psychosis (166). They may have symptoms of confusion, fluctuating consciousness, abnormal mood, and paranoid delusions (166). The delusions may have elements of grandiosity, religiosity, and fear of impending death, and patients are at risk of command hallucinations, and self-harm or harm to others (169). Symptoms typically resolve spontaneously after days to weeks, though in up to 25% cases chronic psychoses may develop (170). The treatment of peri-ictal psychotic symptoms is aimed at optimising seizure control, though sometimes in acute situations short courses of benzodiazepines or antipsychotics may be needed.

1.4.4.3.4 Interictal psychotic symptoms

Interictal psychoses are less common, but tend to be more chronic, than peri-ictal psychoses. They are most prevalent in temporal lobe epilepsy, and develop after several years of active temporal lobe epilepsy (171). Risk factors for its development include, left sided seizure foci (172),

refractory seizures, and structural lesions including mesial temporal sclerosis (173,174). Psychotic symptoms are similar to those seen in schizophrenia, though personality may be better preserved, and there may be an absence of negative symptoms, or formal thought disorder (175). This form of psychosis is typically very responsive to antipsychotics. Traditional antipsychotics can lower the seizure threshold, and for this reason newer, atypical antipsychotics (with the exception of clozapine) such as risperidone, olanzapine and quetiapine are preferred.

1.4.4.3.5 Epilepsy and suicide risk

Patients with epilepsy have a risk of committing suicide that is approximately three times that of the general population (176). The reason for this increased risk is complex, and not simply related to the psychiatric comorbidity seen in epilepsy patients (176).

1.4.4.3.6 Anti-epileptic drugs and psychiatric psychopathology

Anti-convulsants can have an effect on not only seizures, but also mood and behaviour. Barbiturates, vigabatrin, tiagabine and topiramate can all cause depressive symptoms, while carbamazepine, oxcarbazepine, lamotrigine, and valproate, can have mood stabilising effects (144). Interestingly, improved seizure control has also been associated with the development of psychiatric symptoms. 'Forced normalisation' describes a reduction in epileptiform activity on EEG associated with the emergence of psychosis and/or behavioural/mood disturbances. This has been reported with most AEDs, and it is for this reason that any new drug should be started at low doses and titrated upwards slowly. The risk of occurrence may be higher in patients on multiple AEDs who become seizure free abruptly, or in those in whom there is a past psychiatric history (177).

1.4.5 EEG features of temporal lobe epilepsy

Typically both interictal and ictal EEG findings in patients with MTLE are a reflection of the localization of the epileptogenic zone to the mesial temporal region (178). Interictal surface recordings show sharp waves, spikes, and slow waves localized primarily to the anterior temporal–inferior frontal region, or sphenoidal, true temporal and earlobe electrodes. These can be bilaterally independent in up to one third of patients, but are usually more marked ipsilateral to the focus (179). Given that hippocampal spikes are typically not detectable by surface electrodes, these spikes are likely to reflect parahippocampal cortical activity. However, with depth electrodes the main spikes are limited to the hippocampus.

The localizing and lateralising value of the ictal EEG depends on the region of onset. Temporal lobe epilepsies have localized EEG findings, in 90% of mesial origin seizures and 75% of neocortical origin seizures, the latter presenting with a lateralized rather than focal/regional onset (180). A rhythmic theta pattern at onset is highly specific for temporal and exceedingly rare in extratemporal lobe epilepsies. Ictal EEG onset typically consists of unilateral 5 to 7Hz rhythmic discharges best seen in at least one basal electrode, and which appear within 30 seconds of the first ictal EEG abnormality (181). Occasionally, the scalp ictal pattern can be seen over the temporal lobe contralateral to the side with hippocampal sclerosis, and in these cases intracranial recordings reveal seizure origin in the sclerosed hippocampus, without ipsilateral cortical spread, but with contralateral spread (182). Ictal abnormalities include runs of spike discharges or fast activity, spike-wave complexes, or rhythmic slow activity, and ictal patterns can sometimes help differentiate mesial from neocortical seizures (183). Scalp EEG changes during simple partial seizures are uncommon, particularly with psychic or visceral seizures. However intracranial studies reveal that simple partial seizures are associated with hypersynchronous hippocampal discharges, and a transition to a low-voltage fast rhythm just before contralateral propagation, and clinical onset of the clinical partial seizure (179). Similarly, intracranial studies also reveal that sometimes hippocampal ictal discharges can occur without any noticeable clinical features (184). Post-ictally, the EEG may exhibit focal or generalised slow activity, or return rapidly to normal.

1.4.6 Imaging features of temporal lobe epilepsy

Magnetic resonance imaging (MRI) is the most sensitive and specific neuroimaging modality available for patients with partial epilepsy. It is non-invasive and safe, and enables the identification of structural abnormalities, that may in turn suggest the likely site of seizure onset, and represent a possible surgical target (185). Von-Oertzen et al have demonstrated that standard MRI acquisition is inadequate for patients with refractory focal epilepsy (186). They reported that the sensitivity for focal lesions of standard MRI reported by non-experts to be 39%, but this rose to 91% when a specific epilepsy MRI protocol was used for acquisition, and the images were reported by expert neuroradiologists. A typical epilepsy MR protocol might include, a T1-weighted volume acquisition that is acquired in an oblique coronal orientation, orthogonal to the long axis of the hippocampi, and covering the whole brain in 0.9 mm partitions. This sequence results in approximately cubic voxels, facilitating reformatting in any

orientation, and the subsequent measurement of hippocampal morphology and volumes, as well as three-dimensional reconstruction and surface rendering of the brain. In addition to T1-weighted volumetric acquisitions, oblique coronal spin-echo sequence, with proton density (TE = 30), heavily T2-weighted (TE = 90 or 120) and FLAIR acquisitions that are orientated perpendicular to the long axis of the hippocampus should be acquired. The FLAIR sequence allows any pathological signal change to be differentiated from physiological signal change due to cerebrospinal fluid.

1.4.6.1 Hippocampal sclerosis

The most common abnormality identified in patients with partial epilepsy is hippocampal sclerosis or mesial temporal sclerosis (185). This is demonstrated by a unilateral decrease in hippocampal volume on coronal T1 weighted images and increase in signal on T2-weighted or FLAIR MRI scans (187,188). The coronal or oblique coronal planes facilitate the assessment of asymmetry between the two hippocampi. Limitations to visual inspection include symmetrical or bilateral hippocampal pathology, head rotation, or subtle alterations in unilateral hippocampal volume or signal. In addition visual inspection of hippocampi is operator dependent.

Given these limitations, quantitative MRI measurements can increase the sensitivity of assessment of hippocampal atrophy. Absolute hippocampal volumes are obtained using a standardized protocol, and the results are compared to age-matched normal controls. The technique reliably identifies hippocampal atrophy in patients with refractory temporal lobe seizures, which correlates well with neuronal loss, particularly in the CA1 sub-region (189). The measurement of T2 relaxation time facilitates quantitative determination of T2-weighted signal changes, and may be a useful tool to identify hippocampal pathology, with marked elevations being associated with HS and intermediate values being seen in patients without qualitative MRI evidence of HS (190). Interestingly, in this latter study, contralateral abnormalities were also seen in about 30% of cases with clear-cut HS.

The identification of hippocampal sclerosis in the surgically resected temporal lobe is a good prognostic indicator for seizure control following epilepsy surgery (191). In addition hippocampal volumes on the side of the language dominant hemisphere is an important determinant of impairment of verbal memory following hippocampal resection. Some studies have shown that the more severe the atrophy pre-

operatively, the less likely it is that there will be a significant decline of verbal memory after surgery (192). Other longitudinal studies have assessed the effects of chronic epilepsy on the brain, and in particular hippocampal volume. One such study demonstrated that cortical atrophy was a common development in chronic epilepsy, and may be widespread and remote from the putative epileptic focus (193). The increased risk of cerebral atrophy in epilepsy was not related to a history of documented seizures, but instead was related to age and multiple antiepileptic drug exposure. In other similar studies, hippocampal volume loss in TLE patients over a 4 year period correlated with the number of seizures (194), and seizure free patients showed no change in hippocampal volume (195). Both results suggest seizure-associated hippocampal damage.

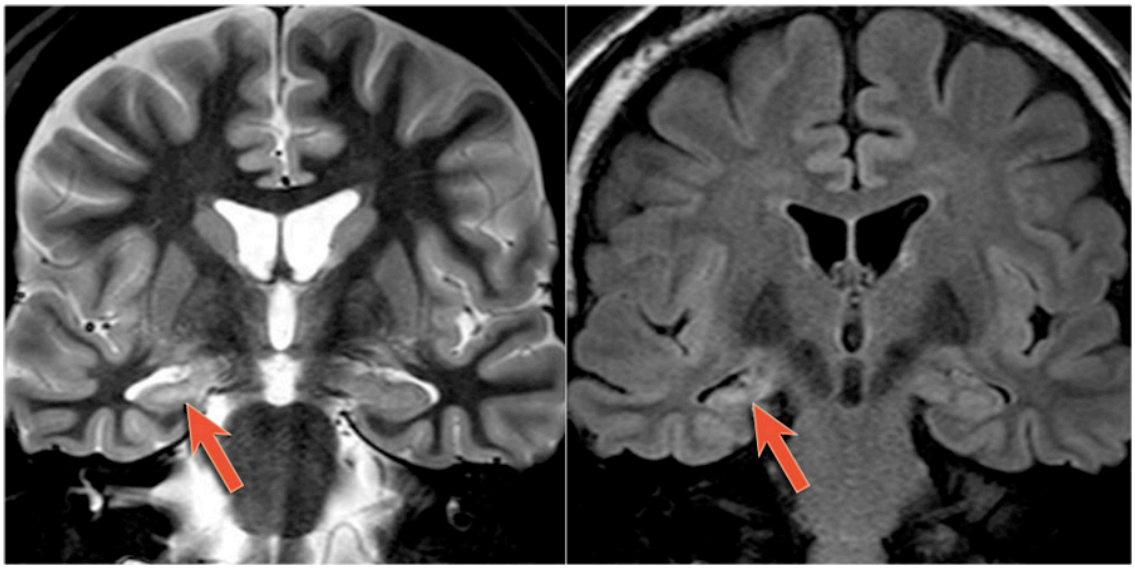

Figure 1.4 - Right sided hippocampal sclerosis (arrow).

1.4.6.2 Other structural lesions

MRI is also sensitive and specific to the detection of other structural lesions, which may underlie MTLE or neocortical TLE (196). These include primary brain tumours, vascular anomalies, and malformations of cortical development (MCD). The most common surgical pathologies are low-grade glial neoplasms such as dysembryoplastic neuroepithelial tumours (DNET), cavernous haemangiomas, and focal cortical dysplasia.

1.4.6.3 Advanced imaging techniques

In patients with partial epilepsy, and indeterminate structural MRI studies, other MRI sequences and imaging techniques may be useful. More advanced MRI techniques include whole brain T2 mapping (197), diffusion tensor imaging (198), magnetisation transfer imaging (199), and double inversion recovery imaging (200). Other imaging techniques include magnetic resonance spectroscopy (MRS), positron emission tomography (PET), and ictal single positron emission computed tomography (SPECT) all of which have a high diagnostic yield in patients with temporal lobe epilepsy, but do not confer specificity of aetiological diagnosis (185).

1.4.7 Clinical and EEG features of neocortical temporal lobe epilepsy

The clinical and EEG features of medial and lateral TLE overlap considerably. There is no association between febrile convulsions and lateral TLE and there is usually a detectable underlying structural pathology. The most common structural lesions are glioma, angioma, hamartoma, dysembryoplastic neuroepithelial tumour, other benign tumours, malformation of cortical development, cavernomas, and post-traumatic change.

If discharges arise in the superior temporal gyrus, simple auditory phenomena such as humming, buzzing, hissing, and roaring may occur. Seizures originating in the Sylvian region or entorhinal cortex can cause olfactory sensations, which are often unpleasant and difficult to define. More complex hallucinatory or illusionary states are produced with seizure discharges in the association areas (eg. structured visual hallucinations, complex visual patterns, musical sounds and speech). A cephalic aura can also occur in temporal lobe seizures, as well as frontal lobe seizures. Consciousness tends to be preserved for longer than in a typical medial temporal seizure. The automatisms can be unilateral and have more prominent motor manifestations than in MTLE. Post-ictal phenomena such as amnesia and psychiatric accompaniments are equally common in both medial and lateral TLE.

The EEG changes most commonly seen are interictal spikes over the temporal region, maximal over the lateral convexity rather than the inferomedial electrodes. MRI will reliably demonstrate any structural lesions but hippocampal volumes and T2 measurements are usually normal.

1.5 Temporal lobe epilepsy surgery

1.5.1 Introduction

As described earlier in this chapter temporal lobe epilepsy is the most common focal epilepsy syndrome, and partial seizures of mesial temporal lobe origin are the most common focal seizures. Studies demonstrate that individuals with TLE, particularly due to MTLS or HS, have the highest rates of medical intractability, of the order of 40 to 80% (201–203). Drug-resistant seizures are associated with higher rates of injury and death, psychiatric comorbidity, and psychosocial disability. Furthermore, drug resistant epilepsy is associated with a significant personal and societal economic cost (204). In these patients, randomised controlled trials have demonstrated that surgery is superior to continued medical treatment in terms of seizure freedom and quality of life measures (205). Most approaches to temporal lobe surgery are based on the technique developed by Murray Falconer in the 1960s, who was one of the first to describe mesial temporal sclerosis, and the resection of the medial temporal lobe and temporal neocortex, otherwise known as anterior temporal lobe resection (ATLR) (206). There may be variability in the amount of temporal neocortex, parahippocampal gyrus, hippocampus and amygdala that surgeons resect. Typically up to 6.5 cm of anterolateral non-dominant, and up to 4.5cm of dominant cortex may be excised, along with the entire amygdala and as much of the hippocampus as possible. The second most widely used approach to temporal lobectomy was developed by Yasargil and colleagues in the 1970s, and is known as a selective amygdalohippocampectomy (SAH) (207). Several approaches are used and include the trans-sylvian, subtemporal and transgyral approaches. This trans-sylvian approach is a method of resecting the mesial temporal lobe structures and epileptogenic foci, while minimising damage to the anterior and lateral temporal structures. The focus on the remainder of this section will be the traditional ATLR.

1.5.2 Principles of temporal lobe epilepsy pre-surgical evaluation

All patients considered for epilepsy surgery must undergo a comprehensive, multidisciplinary presurgical evaluation. The aims of this evaluation underpin the aims of temporal lobe surgery which are the resection of the epileptogenic focus, in order to maximise the reduction in seizures, while minimising damage to eloquent cortex, and subsequent neurological injury (208). The

epileptogenic zone is defined as the 'area of the cortex that is indispensible for the generation of epileptic seizures', but by definition this can only be truly identified after resection of this area and complete seizure freedom (208). Therefore preoperatively, the identification of this zone is dependent on the identification of a number of other zones that if consistently indicative of the same area, may enable localisation of the epileptogenic zone. These different zones are identified preoperatively using a number of clinical tools. The rational for surgery is weakened in patients in whom many of these zones cannot be identified. On the other hand, in patients in whom all zones can be identified and there is concordance between them, surgery is more likely to be successful.

The *symptomatogenic zone* is that part of the brain that gives rise to the semiology of the epilepsy. It may or may not be in close relation to the epileptogenic zone. For example in some seizures originating from the left hippocampus, patients may not become symptomatic until the seizure discharge reaches the left insular cortex, which causes an abdominal aura. Information about a patient's symptomatogenic zone is typically obtained from description and video of the patient's seizures. The *epileptic lesion zone* is typically identified using MRI, and is in close relation or within the epileptogenic zone. The *irritative zone* is identified by epileptiform activity on EEG or magnetoencephalography (MEG) studies. In TLE it is often in close relation to the epileptogenic zone, which is often within it. In other epilepsies there may be discordance between the epileptogenic and irritative zones. The *ictal-onset zone* is typically identified by surface, or intracranial EEG. Sometimes ictal single photon emission computed tomography (SPECT), or MEG may be used to identify it. It is usually closely related to the epileptogenic zone, and its identification is critical. The *functional deficit zone* is an area of dysfunctional brain identified in the interictal period due to structural or functional abnormalities arising from focal epilepsy. It is identified in a number of ways, which include clinical examination, positron emission tomography (PET) imaging, functional MRI (fMRI), neuropsychological testing or intracarotid amobarbital or WADA testing. The functional deficit zone is typically in close proximity to the epileptogenic zone.

1.5.3 Components of temporal lobe epilepsy pre-surgical evaluation

There are multiple components to the pre-surgical evaluation of TLE patients (209).

1.5.3.1 Seizure semiology

Careful analysis of the aura and characteristics of a seizure is an important part of the presurgical assessment. It enables identification of the symptomatogenic zone, which facilitates lateralisation, and localisation of the seizure to a specific brain region. The semiology of MTLE seizures is discussed in section 1.4.4.1.

1.5.3.2 Neuroimaging

Several neuroimaging techniques are available in epilepsy surgery, and enable the identification of several zones. The most important is structural MRI, which has revolutionised epilepsy surgery, and enables the identification of the epileptic lesion zone in as many as 50 to 60% of patients being considered for temporal lobectomy (210). Advanced imaging acquisition and analysis techniques such as diffusion tensor imaging (DTI) and tractography may aid the identification of the lesion zone, and also help prevent damage to eloquent tissue. fMRI also aids the identification of eloquent cortex, and in the context of temporal lobe surgery is important for the lateralisation and localisation of language. Finally, EEG-fMRI is a relatively new technique that combines the temporal resolution of EEG with the spatial resolution of fMRI in order to aid the localisation of the ictal-onset and irritative zones.

In patients in whom structural MRI does not identify the epileptic lesion zone, functional imaging with FDG-PET or ictal SPECT may be useful (211). In FDG-PET imaging the standard ligand is ^{18}F-fluorodeoxyglucose and imaging is carried out interictally in order to identify areas of hypometablism. Hypometabolism is seen in the epileptogenic temporal lobe in 80 to 95% of patients with drug resistant TLE, including patients with normal MRI scans (212). It therefore provides information about the functional deficit zone in which MRI shows no lesions. The area of hypometabolism is often larger than the underlying epileptogenic zone identified on intracranial EEG, and the FDG-PET scan alone should not be used to guide the extent of the temporal neocortical resection (213). A recent meta-analysis demonstrated that while PET does not add prognostic value in patients whose epileptogenic regions are localised using MRI and EEG, the presence of

unilateral temporal hypometabolism had an independent predictive value of 86% for a good surgical seizure outcome in other groups of patients. In those patients who needed intracranial EEG its predictive value was 75%, while in patients with non-localising EEG its predictive value was 73%, and in those patients with normal MRI scans its predictive value was 80% (214).

In SPECT imaging Technetium 99-m is the radiolabelled tracer used to identify areas of cerebral hyperperfusion. It is carried out during the ictal phase, and therefore provides information about the ictal onset zone. Ictal and pre-ictal SPECT images are subtracted and co-registered with the patient's MRI (SISCOM) in order to provide further anatomical information on the location of the seizure focus. Ictal SPECT is 73 to 97% sensitive for TLE, and especially specific for the epileptogenic zone, even in patients with non-localising MRI or ictal surface EEG. Interictal SPECT has a sensitivity of about 50% and is less specific (215). Ictal SPECT correctly lateralises the side of seizure onset in about 85% in patients in whom the epileptogenic zone has been identified with MRI and surface EEG (216). Although studies have shown that the predictive value of ictal SPECT for a good postoperative seizure outcome is less than that of MRI, EEG and PET (217), it still has some value as a predictive tool for seizure outcome. Atypical ictal SPECT perfusion patterns are associated with seizure freedom rates of 30% compared to rates of up to 70% after 2 years in TLE patients (218).

1.5.3.3 Surface EEG

EEG is critical to epilepsy surgery, and is necessary to identify the irritative and ictal onset zones. Typically EEG is obtained from prolonged video-EEG monitoring and the capture of habitual seizures. It provides localising information in approximately 62.2% of patients being considered for a potential temporal lobectomy (210), and concordance between structural MRI and video telemetry is reported as 58% (211). In patients with drug refractory TLE in whom there is concordance between a resectable lesion on MRI and ictal EEG, seizure outcome is likely to be good (216). Analysis of ictal EEG enables the identification of the ictal onset zone, which is closely related to the epileptogenic zone. The onset can be focal, widespread but lateralised or non-laterisable.

Sharp waves seen in the interictal record represent the irritative zone, and when highly localised are predictive of good seizure outcome following surgery. Diffuse irritative zones include posterior temporal (219), extratemporal (220) and bitemporal interictal spiking (219). Posterior and extra-temporal spiking may reflect diffuse epileptogenicity, or dual pathology and hence explain the worse postoperative seizure prognosis associated with them. However, bitemporal interictal spiking can indicate unifocal epilepsy with propagation of sharp wave discharges from a single focus in different directions at different times, or a change in the orientation of the focus that generates the sharp wave discharge, which is seen in different brain regions at different times. Alternatively, it can indicate an extratemporal focus spreading to both temporal lobes, or bi-temporal lobe epilepsy. These patients need careful analysis, potentially with intracranial EEG and other localising investigations, as the latter would be associated with poor seizure outcome after surgery, while in the former group up to 65% may become completely seizure free at 1 year (221). Discordant imaging and EEG findings may be associated with a poorer surgical outcome, and further investigation with SPECT, FDG-PET or intracranial EEG may be required (216).

MEG is used in some epilepsy centres as an additional test to localise the source of interictal epileptogenic discharges using magnetic fields, rather than electrical spikes as seen in EEG. A recent study showed that it is able to correctly lateralise the epileptogenic zone in 54 to 80% of patients (222). In 24% of cases it may provide additional localising information to EEG, and in 11% it may also change or influence the surgical decision making process (222). In other studies MEG shows concordance with video-EEG in 32%, and lateralises correctly in 59% of those with non-localising video-EEG (223). However, although it is a promising technique, it is currently not widely available.

1.5.3.4 Intracranial EEG

In some presurgical patients intracranial EEG may be necessary to make a case for surgery. Indications for intracranial EEG are listed in table 1.10. Studies report that intracranial EEG has a concordance of 47% with structural MRI, 58% with PET, and 56% with ictal SPECT (211). Intracranial EEG studies can incorporate the use of subdural grids, strip or depth electrodes. Classically depth electrodes are used to evaluate lateralisation of the epileptogenic zone, and

subdural recordings to define its extent. In all cases a clear hypothesis is needed in order to target specific brain areas, particularly as intracranial recordings carry about a 1% risk of morbidity (bleeding, infection, oedema) and mortality (224). Therefore in order to increase the yield of EEG studies, implantation should be guided by imaging findings that represent the most likely epileptogenic zones. Intracranial EEG is particularly important in patients with focal cortical dysplasias, because as described earlier in this chapter, many of these patients will have normal MRI scans. In any case, complete resection of a lesion visible on MRI is not always adequate to predict a good seizure outcome, and intracranial EEG is needed to perform a tailored resection of the ictal onset zone, as well as the lesion visible on MRI (225). The ictal onset zone may contain macroscopically normal looking tissue surrounding an obvious lesion (226). Finally, intracranial recordings can also be used to stimulate cortex and carry out brain mapping in order to delineate where eloquent regions lie in relation to the ictal onset zone. This information can be used to determine whether surgery is possible without major neurological complications, and tailor the extent of resection. For this reason, any subdural grid coverage should be extensive enough to allow mapping of both the ictal onset zone, and neighbouring eloquent cortex.

Table 1.10 – Common indications for intracranial EEG

MRI negative but other evidence suggesting single focus
MRI positive but two or more potentially epileptogenic lesions
MRI positive but large lesion without precise estimate of ictal onset zone
Discordant investigations
Identification of relationship of potential epileptogenic zone to eloquent cortex

1.5.3.5 Neuropsychology

The preoperative neuropsychological assessment is essential in order to provide information about the functional deficit zone, which in turn aids the lateralisation and localisation of the epileptogenic lesion. In the case of TLE, the typical neuropsychological profile is as outlined in section 1.4.4.2. Following a temporal lobectomy patients are at risk of memory and language impairments. The preoperative neuropsychology assessment also facilitates the identification of those patients at risk of such impairments, and may in turn enable their prevention. Please see section 1.5.6 for further discussion of this topic.

1.5.4 Seizure outcome of temporal lobe epilepsy surgery

Surgical outcome is measured in a variety of different ways in different epilepsy centres. For example, some centres classify patients with only auras, as being seizure free, while others only classify patients in whom there is no seizure activity as being seizure free. Outcome measures other than seizure freedom are also used, and include the percentage reduction in seizure frequency, and quality of life (QOL) measurements. One of the first methods of classification of postoperative seizure outcome was Engel's classification. This had a number of shortcomings, and has now been superseded by the ILAE commission on classification (227). This is shown in table 1.11.

Table 1.11- Classification of seizure outcome following surgery adapted from reference (227)

Class	Definition
I	Completely seizure free; no auras
II	Only auras; no other seizures
III	One to three seizure days per year; +/- auras
IV	Four seizure days per year to 50% reduction of baseline seizure days; +/- auras
V	Less than 50% reduction of baseline seizure days to 100% increase of baseline seizure days; +/- auras
VI	More than 100% increase of baseline seizure days; +/- auras

About 20% of patients will have seizures early in the postoperative period (<28 days) (228,229). Some argue that these seizures have little prognostic value for long term seizure outcome, due to their association with perioperative factors (228). Others take the opposite view point and report that patient who have early postoperative seizures, are less likely to be seizure free at 2 years (229).

Longer-term seizure outcome has been assessed in a number of studies. These have a number of problems associated with them. These include heterogeneous patients (with respect to demographic characteristics, epilepsy duration, and TLE pathology), and the cross-sectional (as opposed to prospective longitudinal) nature of many of them such that prognostic factors only relate to outcome at the time point of the study. Despite these issues, there are a number of key factors associated with good seizure outcome, which are described below.

In the original randomised controlled trial carried out by Wiebe et al, 58% of patients who had surgery had at least a Engel class II outcome at 1 year, compared to 8% in the medical arm, and these patients also had significantly better QOL compared to medically treated patients. 38% of patients who had surgery were completely seizure free, compared to 3% in the medical group. Residual seizure activity was similar in severity in both surgical and medical groups. Overall only two patients needed to be treated surgically for one patient to become free of disabling seizures (205). Meta-analyses and retrospective studies appear to back up these findings, with overall about 70% of patients becoming seizure free postoperatively at last follow-up, compared to 5 to 8% of patients with medical therapy. Furthermore, favourable outcomes appear to be sustained over longer periods. In patients with TLE and well-circumscribed lesions such as a tumour or vascular malformation, lesionectomies are associated with good seizure outcome, unless there is also associated hippocampal sclerosis. In these cases, it is clear that combined lesionectomy and ATLR are associated with similarly good seizure outcomes to those described above, but seizure freedom rates drop to about 10% with lesionectomy alone (230).

In a meta-analysis including 83 studies and over 3000 patients, 66% of patients achieved seizure freedom after temporal lobe resection, 14% achieved long-term medication cessation, 41% remained on one medication, and 31% remained on polytherapy (231,232). In another meta-analysis the strongest predictors of good seizure outcome were patients with a history of febrile convulsions, MTLS, low grade tumours (such as gangliogliomas or dysembryoplastic neuroepithelial tumours), MRI scans showing focal lesions which were in accord with EEG findings, and extensive resections (233).

A number of retrospective studies have also assessed seizure outcome after ATLR. McIntosh and colleagues reviewed 325 patients who underwent TLE surgery, and reported that the odds of seizure freedom at 2,5 and 10 years was 55%, 48% and 41% respectively. Patients with discrete lesions on MRI had the best chance of seizure freedom, while factors such as age of onset, duration of seizures and age at surgery had no effect (234). Other studies appear to corroborate these findings, highlighting that 60 to 85% of patients with unilateral, focal lesions such as hippocampal sclerosis, that are concordant with ictal and interictal EEG, and which can be completely excised,

have the best seizure outcome. This is in comparison to patients with normal MRI who have rates of seizure freedom of the order 30 to 50% (235,236). The exception to this is that group of patients with normal MRI but concordant video/intracranial-EEG and SPECT/PET findings, who have long-term seizure outcomes similar to those patients with lesions on MRI (237). In these patients seizure freedom may be obtained in approximately 30 to 85% (238). A significant proportion of these patients actually have hippocampal sclerosis or cortical dysplasia that is found on histological examination of resected temporal lobe specimens (238). Bilateral MRI lesions (including bilateral HS) reflect multiple potentially epileptogenic areas, and have a significantly worse surgical outcome compared to patients with unilateral lesions (239).

The most recent large retrospective study of post-operative patients appears to indicate that favourable long-term outcome many years after surgery appears to be sustained. De Tisi and colleagues assessed 497 patients who had had ATLR, and found that almost 50% remained seizure free at 10 years. Relapse was less likely the longer a patient remained seizure free. In nearly 20% of patients who achieved late remission, a medication change to a previously untried drug proved successful. Nearly 30% of seizure free patients had discontinued medications at their last follow-up (240).

Finally studies have also shown that patients, who have a good seizure outcome after surgery, also tend to have an improved QOL. Even if patients are not completely seizure free, the reduction in seizure burden is typically sufficient to give rise to improvement in QOL post-operatively (205). Other predictors of good postoperative QOL include good preoperative QOL, HS, and no preoperative psychopathology (241).

1.5.5 Non-Cognitive complications of temporal lobe epilepsy surgery

1.5.5.1 Medical complications

The medical complications of temporal lobe surgery include wound infection, intracerebral infarction or haemorrhage, and subdural haemorrhage in about 1% of cases (205). Superior quadrantic visual field deficits of varying degrees can also occur after ATLR, and occur in a

significant proportion of patients (205). Visual field defects and their prevention using diffusion tensor tractography are discussed later in detail in the results section.

1.5.5.2 Psychiatric complications

Post-surgical psychiatric complications are well recognised after ATLR, and can present in up to 30 to 50% of patients undergoing ATLR. They most typically present as a recurrence or worsening of a previous depressive or anxiety disorder, and less frequently in 10 to 15% as de novo mood disorders. A pre-surgical, lifetime history of depression has been identified as the strongest predictor of postoperative psychiatric complications, presenting in this way. Less commonly, 1 to 10% of patients can present with de novo post-surgical psychotic disorders, or psychogenic non-epileptic events. Most mood disorders occur within six months of surgery, and remit within 2 years, but up to 15% can prove refractory (158,242,243). For this reason, all patients undergoing consideration for a temporal lobectomy should undergo a formal neuropsychiatric evaluation.

In addition to its implications for post-surgical psychiatric complications, pre-surgical co-morbid psychiatric illness has a number of other implications. It can, interfere with the successful completion of the pre-surgical evaluation and consent to surgery, impact on post-surgical psychosocial adjustment, and it can also impact on post-operative seizure outcome. A number of studies suggest that a pre-surgical psychiatric history is associated with a worse post-surgical seizure outcome (244). Other studies have shown that the occurrence of post-ictal psychosis of epilepsy in potential surgical candidates or its occurrence de-novo in patients who have undergone ATLR, indicates a greater risk of bilateral independent ictal foci, and potentially poorer surgical seizure outcome. Therefore, in those surgical candidates with post-ictal psychosis, a careful evaluation should be made to ensure that seizures are originating from one hemisphere (245).

The consideration of whether patients with comorbid psychiatric disorders, and particularly psychotic disorders, should be considered for epilepsy surgery is controversial. Many would argue that surgery should not be excluded, as long as the patient is able to cooperate with the pre-surgical evaluation, and has a realistic understanding of the risks and potential benefits of the surgery. Furthermore, there is good evidence that epilepsy surgery is associated with a significant

improvement of pre-surgical psychiatric disorders, including remission of depression and anxiety disorders in approximately 50% of patients (243). In patients with epilepsy related psychosis, studies suggest that psychotic disorders vary from unchanged to improved after surgery, and therefore epilepsy related psychosis should not be an exclusion criteria for ATLR (246).

1.5.6 Cognitive complications of temporal lobe epilepsy surgery

Following anterior temporal lobectomy 25 to 40% of patients are at risk of memory and language impairments (205). Other cognitive domains and general intelligence or IQ are rarely affected after surgery (247). There is now a significant literature, which demonstrates how pre-surgical neuropsychological findings, combined with demographic variables and other neurological investigations, can be used to predict those patients at greatest risk of postoperative decline in memory or language function after ATLR.

1.5.6.1 Neuropsychological factors

1.5.6.1.1 Memory impairment

The side of surgery, and pre-operative memory performance primarily predict memory impairment after surgery. The material specific memory model posits that after a left ATLR patients are at risk of verbal memory deficits, and this is readily borne out by a number of studies (248). The verbal memory deficits are characterised by problems with encoding or retrieval, as opposed to consolidation (248). The converse of this model, namely that patients undergoing a right ATLR are at risk of non-verbal memory deficits is a less reliable finding (248). This observation may relate to the fact that the material specific model of memory is less consistently observed for non-verbal memory as discussed in section 1.4.4.2. Alternatively, it may be due to limited understanding of the role of the right temporal lobe in memory, or a lack of sensitivity of the measures used to assess visual memory.

Two models incorporate the finding that pre-surgical memory performance is an important determinant of memory outcome after surgery. The 'functional reserve' model hypothesises that post-operative memory decline is a function of the contralateral mesial temporal structures to

support memory following resection of ipsilateral structures (249). The alternative 'functional adequacy' model hypothesises that post-operative memory decline is inversely related to the functional adequacy of the resected tissue (250). That is, patients with a higher pre-operative memory performance, are at risk of the greatest declines, particularly in verbal memory for those patients undergoing dominant temporal lobe surgery. An estimated 10 to 60% of patients undergoing dominant temporal lobe resections may suffer significant declines in verbal memory (248). Currently, the latter hypothesis appears to be closer to the truth, based on neuropsychology, imaging and intracarotid amobarbital procedure (IAP) studies, some of which are described below (247).

1.5.6.1.2 Language decline

Patients undergoing surgery to the dominant temporal lobe may also suffer from post-operative naming difficulties as typically measured by tests of confrontation naming and verbal category and letter fluency (251,252). Approximately 30 to 38% of patients undergoing dominant temporal lobe resections may have a significant decline on confrontation naming tests such as the Boston Naming Test (253,254). As for memory, patients with higher preoperative language scores appear to be at greatest risk of language decline (255).

1.5.6.2 Other preoperative predictive factors

A number of other investigative techniques in addition to neuropsychology have been shown to be useful in predicting those patients at greatest risk of cognitive decline following surgery. In addition, there are several demographic and seizure variables that are also important in predicting postoperative cognitive decline.

1.5.6.2.1 Underlying pathology

A number of studies have shown that a patient's underlying pathology is important. Patients with TLE and without MTS or HS on MRI are at greater risk of both memory and language decline than those patients with MTS or HS after surgery (256). Furthermore, patients with more severe unilateral HS tend to have poorer preoperative memory and language performance, and as

postulated by the functional adequacy hypothesis, exhibit less decline in memory and language performance following dominant temporal lobe surgery (256).

1.5.6.2.2 fMRI and FDG-PET

fMRI has also recently proven itself to be a useful tool in determining the lateralisation of language and memory functions. Studies have reported a significant relationship between pre-operative hemispheric asymmetry on fMRI memory tasks and post-operative memory decline. Patients with greater ipsilateral pre-surgical activation on memory tasks had greater post-operative memory decline, whereas those patients with greater contralateral memory activation had smaller memory decline (257–259). fMRI is also useful in predicting naming decline following surgery to the dominant hemisphere. Patients with greater language lateralisation to the dominant hemisphere showed greater declines in naming after surgery (260,261). Similarly FDG-PET studies have shown that a lack of left sided hypometabolism predicts significant memory loss in patients undergoing left ATLR (262).

1.5.6.2.3 Intracarotid amobarbital procedure (IAP)

Prior to the advent of fMRI, which is non-invasive and safe, IAP was used to lateralise language, and aid prediction of those patients who may suffer the greatest memory and language declines after surgery. Less commonly it has also been used to lateralise the epileptogenic zone. In the procedure an anaesthetic agent, usually amobarbital, is injected into the internal carotid artery via a catheter in the femoral artery. This produces temporary inactivation of the ipsilateral cerebral hemisphere for about 10 minutes, thus crudely mimicking the effect of ATLR on mesial temporal lobe structures. The activity of the sodium amytal is monitored by the presence of unilateral slow wave activity on an EEG, and the presence of a contralateral hemiplegia. During this period the patient is given a number of items to name and remember.

A number of different measures of the IAP have been used to predict memory outcome, but generally its use appears to be most robust and accurately predictive of memory decline in patients undergoing dominant temporal lobe surgery (263). Some studies have reported that memory outcome is proportional to memory performance after anaesthesia of the contralateral hemisphere,

thus supporting the functional adequacy model (263). Other studies have reported that memory performance after anaesthesia of the ipsilateral hemisphere is predictive of post-operative memory impairment, thus supporting the functional reserve model (264). Finally, other studies suggest it is the IAP asymmetry of memory scores between ipsilateral and contralateral injections is useful in predicting postoperative memory impairment (265). Indeed, such asymmetries have been shown to be useful in predicting postoperative naming decline following left ATLR, in that patients with the greatest lateralisation of language to the left hemisphere tended to have the greatest decline (260). Overall, those patients at greatest risk of post-operative memory decline, are those in whom IAP testing reveals little difference between ipsilateral and contralateral scores, marked functional adequacy and limited functional reserve.

Though it is still used in places, IAP has a number of disadvantages. It is an expensive, invasive procedure with potentially serious complications. Furthermore, there are doubts about its reliability, reproducibility and validity in predicting post-operative global amnesia and memory impairment. In contrast to some of the predictive tools available, which are standardised and easily validated, the IAT differs significantly among institutions. Differences exist between centres in the testing protocol used, the patients selected for testing, the choice of behavioural stimuli, scoring methods used, dosage and administration of amytal, all of which can lead to variations in the results. The IAT is also poor at predicting verbal memory decline as deactivation of the language dominant hemisphere, may act as a confounding factor, and cause increased errors on verbal memory testing.

1.5.6.2.4 Extent of surgical resection

A number of studies have also reported that selective temporal lobe surgery may result in fewer post-operative memory complications, than standard anterior two thirds temporal lobe resections (266). However, other studies do not corroborate these finding, and instead, highlight that it is the functional adequacy of the tissue to be resected, rather than the extent of resection, that is the critical factor in predicting postoperative cognitive outcome (267).

1.5.6.2.5 Age of seizure onset

As discussed earlier in section 1.4.4.2, patients who develop seizures at an earlier age tend to have more significant cognitive impairment than patients who develop seizures later in life. In addition there may be more redistribution of function to other areas. Therefore, this latter group of patients may be at greater risk of language and memory impairment following surgery, particularly in dominant temporal lobe surgery, as more functional tissue is likely to be resected (268).

1.5.6.2.6 Age at time of surgery

Some studies have also suggested that the risk of naming and memory decline increases with advancing age, particularly in dominant temporal lobe resections (268).

1.5.6.2.7 Psychiatric history

In addition to being associated with preoperative memory performance, patients with depression may be at greater risk of verbal memory impairment following dominant temporal lobe resection.

1.5.6.2.8 Multivariate prediction of cognitive outcome

Although the aforementioned factors are useful in assessing those patients at risk of postoperative cognitive decline, many of the studies from which they are derived are group based. There has therefore been a recent trend towards studies incorporating reliable change indices (RCI), and more sophisticated statistical models, which consider predictor variables simultaneously in a multivariate fashion, and assess their importance as statistical mediators or moderators. The most recent examples of such an linear regression approach demonstrated that fMRI activation asymmetry on a verbal memory paradigm, language lateralisation, and preoperative neuropsychology performance were able predict clinically significant verbal memory decline in all patients who underwent left anterior lobe resection (269). Subsequent studies by the same group have provided further support for the use of multivariate models, and also highlighted that it is the functional adequacy of the ipsilateral hippocampus and temporal lobe, rather than the functional reserve of the contralateral hippocampus that is important for maintaining verbal memory function after anterior temporal lobe resection (270,271).

1.6 Magnetic Resonance Imaging

1.6.1 Basic principles

1.6.1.1 MR active nuclei, alignment and precession

An atom consists of several particles. Protons and neutrons are nuclear particles, and the former carry a positive charge, while the latter have no charge. Electrons orbit the nucleus and are negatively charged. The atomic number of an element is the number of protons within the nucleus and determines the identity of an element. The mass number is the sum of the protons and neutrons in the nucleus. Within the nucleus, protons and neutrons spin about their own axis. When a nucleus has an even mass number the spins cancel one another out, and the nucleus has no net spin. When a nucleus has an odd mass number, the spins do not cancel one another out, and the nucleus has a net spin. Nuclei with an odd number of protons are described as MR active. As protons have a charge, a nucleus with an odd mass number also has net charge, as well as a net spin. The classical laws of electromagnetism state that a moving charge generates a magnetic field, and the total magnetic moment of a nucleus is the vector sum of all the magnetic moments of protons in the nucleus. In MRI the isotope of hydrogen called protium, with a mass and atomic number of 1, is utilised as the active nucleus. It is abundantly present in the human body in fat and water, and its single proton gives it a large magnetic moment.

In a normal environment the magnetic moments of the hydrogen nuclei point in random directions and produce no overall magnetic effect. However, when an external magnetic field (B_0) is applied, their magnetic moments line up with the external field, a process known as alignment. Alignment can be explained in two ways. The classical theory uses the direction of the magnetic moments to illustrate alignment. The quantum theory on the other hand uses the energy level of the nuclei to illustrate alignment. According to quantum theory the magnetic moments of hydrogen nuclei align in two energy states. Spin-up nuclei have low energy and can be classically described as having magnetic moments that line up parallel to the main field. Spin-down nuclei have high energy, and can be classically described as having magnetic moments that are anti-parallel to the main field. In a state of thermal equilibrium at room temperature, at any given moment, a greater proportion of nuclei have their magnetic moment aligned with the main magnetic than against it. In classical terms therefore the net magnetism of the patient, or the net magnetization vector (NMV), is aligned parallel to the main magnetic field (in actual fact

the magnetic moments of the nuclei actually align at an angle to B_0 due to the force of repulsion between B_0 and the magnetic moments). As the external magnetic field increases in strength, more magnetic moments align themselves parallel to the main field, and the amount of energy needed to line up anti-parallel increases, and the NMV increases.

Every MR active nucleus spins on its own axis. When an external field (B_0) is applied, the nuclei precess around the B_0 axis. That is, the external field causes the nuclei to follow a circular path around B_0 such that there is constant change in the axis of spin (see figure 1.3a). When nuclei are in phase the magnetic moments of hydrogen are at the same place on the precessional path, whereas when nuclei are out of phase, the magnetic moments are at different places on the precessional path. The speed at which magnetic moments precesses about the external field is known as the precessional or Larmor frequency, and is directly proportional to the field strength B_0. The Larmor equation is used to calculate the frequency, or speed of precession for a specific nucleus in a specific magnetic field strength.

$\omega_0 = B_0 \times \lambda$

ω_0 = precessional frequency

B_0 = external field strength and is expressed in units of Tesla (T)

λ = gyromagnetic ratio or the precessional frequency of a specific nucleus at 1 T and is expressed (MHz/T)

The magnetisation that occurs when an external field is applied can be described in classical terms by using a coordinate system, with the z-axis running in the direction of the magnetic field. It can be difficult to visualise the NMV within the laboratory frame of reference. For this reason NMV can be viewed in a frame rotating with respect to the laboratory frame, known as the rotating frame; an x-y axis that rotates about z at the Larmor frequency (see figure 1.3b).

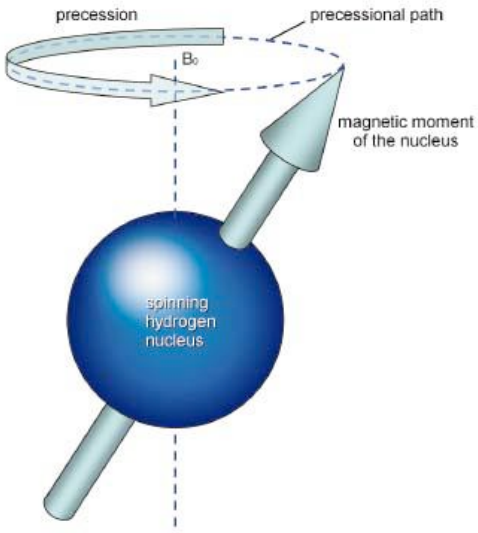

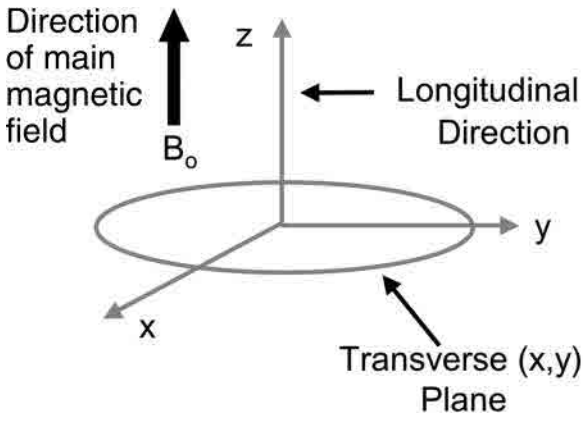

Figure 1.3a **Figure 1.3b**

Figure 1.5 - Precession and coordinate systems (adapted from (272)) a: Precession of the spinning hydrogen nucleus. b: Typical coordinate system used in MRI

1.6.1.2 Resonance and signal generation

At equilibrium the NMV lies along the direction of B_0 (the z axis). If we apply a radiofrequency (RF) pulse B_1 perpendicular to B_0, the hydrogen nuclei resonate energy from the RF pulse. That is B_1 is applied on resonance; by ensuring that B_1 has a frequency that is the same as the processional frequency of hydrogen, one can ensure that other types of MR active nuclei do not resonate. The hydrogen nuclei absorb energy from the RF pulse and this results in an increase in the number of high-energy, spin-down nuclei. This has the effect of tilting the NMV away from the z axis towards the transverse (x-y) plane. If just the right amount of energy is applied the number of nuclei in the spin-up position equals the number of nuclei in the spin-down position. This causes the NMV (which represents the balance between spin-up and spin-down nuclei) to lie in a plane 90° to the external field, or in a transverse plane (see figure 1.4a). The degree to which NMV is tilted (flip angle), is controlled by changing the duration or strength of the RF pulse. The RF pulse also typically causes the magnetic moments of all nuclei to move into phase with one another, although sometimes in other circumstances, the aim of an applied pulse may phase dispersal. The net effect of this is that the NMV precesses in the transverse plane at the Larmor frequency. As per the laws of electromagnetic induction, this oscillating magnetic field induces a voltage in a receiver coil sited in the transverse plane. It is this voltage that gives rise to the detectable MR signal (see figure 1.4b).

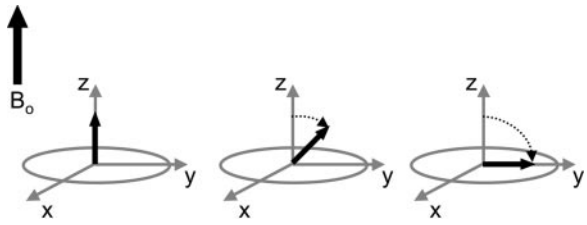

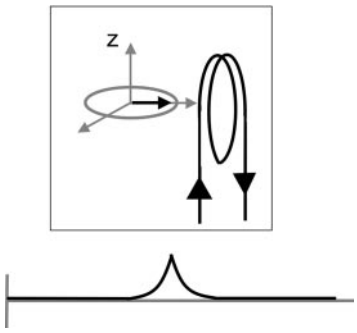

Figure 1.4a **Figure 1.4b**

Figure 1.6 - The absorption of RF energy, effect on NMV and measurement of signal (adapted from (273)). a: Prior to an RF pulse, the NMV (small black arrow) is aligned parallel to the main magnetic field. After a RF pulse at the Larmor frequency, the protons absorb energy, and this causes the NMV to rotate away from the z-axis. b: The rotating magnetic field that has an NMV perpendicular to a loop of wire or receiver coil will induce a voltage in the coil.

1.6.1.3 Relaxation mechanisms and field inhomogeneity

After the RF pulse is removed, the induced signal in the receiver coil starts to decrease, because the in-phase component of the NMV in the transverse plane decreases as the nuclear spins become out of phase with one another. This is known as free induction decay (FID). The NMV in the transverse plane decreases due to relaxation processes and field inhomogeneities. The rate of magnetization relaxation differs in different tissues, and this is one of the factors that contribute to image contrast. The longitudinal relaxation exponential time constant T1 characterises the recovery of the z-component of the magnetisation after a RF pulse (see figure 1.5a). This is called T1, or spin-lattice relaxation, as the absorbed energy is dissipated to the surrounding structure, or 'lattice'. The transverse relaxation exponential time constant T2 characterises the decay of the magnetisation in the x-y or transverse plane, and occurs at a different rate to T1 relaxation. This is called T2 decay, and represents the loss of nuclei precessional coherence, or dephasing (see figure 1.5b). This loss of coherence occurs for two reasons. Firstly, the magnetic fields of adjacent nuclei interact, a process otherwise known as spin-spin relaxation. Secondly, inhomogeneities of the external magnetic field cause exponential T2* decay. Spins that pass through the inhomogeneties experience magnetic field strengths that are different from B_0, and their

precessional frequencies therefore change. This causes a change in their phase, and results in dephasing of the NMV. Magnetic field inhomogeneities cause the NMV to diphase more quickly than would otherwise occur because of the effects of the intrinsic magnetic fields of nuceli. Overall, T2 relaxation will always be faster than T1 relaxation, and T2* dephasing occurs before T2 dephasing.

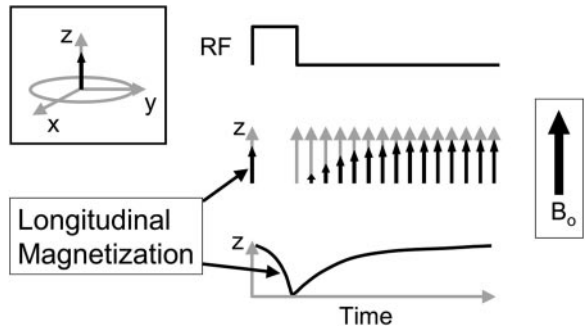

Figure1.5a

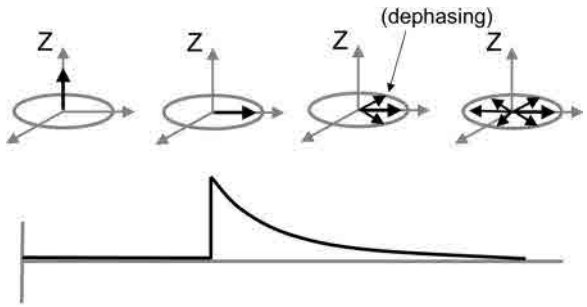

Figure 1.5b

Figure 1.7 - T1 relaxation and T2 decay – adapted from (273). a: T1 relaxation - application of a 90° RF pulse causes longitudinal NMV to become 0, but with time the longitudinal NMV grows back in a direction parallel to the main magnetic field. b: T2 decay – after the application of a 90° RF pulse the transverse NMV is maximised. This then decays for reasons described above causing a reduction in MR signal.

1.6.1.4 Image contrast

A tissue has a high signal (white on the usual grey-scale display) if it has a large transverse component of magnetization when the signal is measured. Conversely, a tissue has a low signal (black) if it has a small transverse component of magnetization when the signal is measured. A tissue has intermediate signal (grey) if it has a medium transverse component of magnetization when the signal is measured. Image contrast is controlled by extrinsic and intrinsic parameters. Extrinsic factors include the repetition time (TR), time to echo (TE) and flip angle. TR is the time measured in milliseconds from the application of one

RF pulse to the next in a particular slice. TE is the time measured in milliseconds between the application of an RF pulse, and signal collection. Intrinsic factors include T1 recovery time, T2 decay time and the proton density (PD) of a tissue.

The T1 recovery time of a tissue is defined as the time it takes for 63% of the longitudinal magnetization to recover in tissue. The period of time during which T1 recovery occurs is the time from one RF pulse to the next, and hence the TR determines how much T1 recovery occurs in a tissue. In fat the molecules are closely packed together and slow moving. This makes spin-lattice relaxation very efficient, and fat therefore has a short T1 recovery time. Conversely water has a longer T1 time as it is very inefficient at receiving energy from nuclei. A short TR, or a "T1-weighted" image, does not permit full longitudinal recovery in tissues, and so there are different longitudinal magnetization components in fat and water. These different longitudinal components are converted to different transverse components after the next RF pulse is acquired, and the NMV is pushed beyond the transverse plane by the succeeding RF pulse, causing saturation. Saturation leads to a contrast difference between fat and water due to their T1 recovery times, with fat having a higher signal. A long TR allows full recovery of longitudinal components in most tissues, which means that there is little contrast between fat and water due to differences in T1 recovery times. Any differences seen in contrast are due to differences in proton density of each tissue, and this is known as a "PD-weighted" image.

The T2 decay time of a tissue is defined as the time it takes for 63% of the transverse magnetization to be lost due to dephasing caused by spin-spin interaction. The period of time during which this occurs, is the time between the excitation pulse, and measurement of the MR signal, that is the TE. The TE therefore determines the amount of T2 decay which occurs in a given tissue. In fat the molecules are closely packed together and this makes spin-spin relaxation very efficient. For this reason, fat has a short T2 decay time compared to water. Short TEs do not allow full dephasing in either tissue, and hence their transverse components are similar, and there is little contrast difference. Long TEs facilitate dephasing of the transverse components in fat and water, so that there is a contrast difference, such that water has a higher signal compared to fat.

An image is T1-, T2-, or PD-weighted when the difference in signal intensity between tissues, or the tissue contrast, is mainly due to their differences in T1 relaxation or T2 decay times. Extrinsic contrast parameters such as TE and TR are manipulated to accentuate one intrinsic contrast parameter, and reduce the effects of others. For a T1 weighted image, the differences between the T1 times of tissues need to be exaggerated, and a short TR is used. At the same time T2 effects must be minimized, and a short TE is used. Tissues that contain mainly fat have a high signal, and tissues containing mainly water have a low signal. For a T2 weighted image, the differences between the T2 times of tissues need to be exaggerated, and a long TE is used. At the same time T1 effects must be minimized, and a long TR is used. Tissues that contain mainly fat have a low signal, and tissues containing mainly water have a high signal. In a PD weighted image, the contrast is mainly due to differences in the proton density of tissues. To achieve this both T1 and T2 effects are minimized by using a long TR and short TE. The number of protons determines the magnitude of the component of transverse magnetization, and therefore tissue with low proton density has low signal, and tissue with high proton density has a high signal.

1.6.1.5 Image formation

Magnetic field gradients in MRI imaging have several functions. They are an important part of pulse sequences described below, but are also used to spatially encode the protons. The application of a gradient magnetic field adds or subtracts from the existing field in three orthogonal directions in a linear fashion, such that the magnetic field strength at any point along the gradient is known. Including the applied gradients, the magnetic field in a scanner is given by:

$B = B_0 + G_x(t)x + G_y(t)y + G_y(t)y$

B = total magnetic field

B_0 = external field strength

$G_x(t)x$, $G_y(t)y$, and $G_y(t)y$ = applied gradients in x, y, and z directions

The slope of the gradient indicates the rate of change of the magnetic field strength along its length, and its strength or amplitude is determined by the amount of current applied to the coil producing it. The maximum amplitude determines the maximum possible resolution. At isocentre the field strength remains unchanged even when the gradient is switched on. The polarity of the gradient reflects which

end of the gradient produces a higher field strength than the isocentre (positive), and which a lower field strength than the isocentre (negative). The magnitude of the change in magnetic field strength depends on the distance from the isocentre and strength of the gradient. The speeds with which the gradients can be turned on and off are called the rise time and slew rate, and both determine the maximum speed of a system. The rise time is the time it takes the gradients to get from zero to max. The slew rate is the gradient max divided by the rise time. The Larmor equation states that the precessional frequency of the magnetic moments of nuclei is proportional to the magnetic field they experience. Therefore, the application of a gradient magnetic field changes the precessional frequency of the magnetic moments of nuclei in a linear fashion across a distance in patients. The precessional phase of magnetic moments of nuclei also changes in a linear fashion across a distance in patients, because faster magnetic moments gain phase compared to slower moments. Thus, the application of three orthogonal gradients enables the spatial encoding of an MR signal in three dimensions, that is, along the z, y and x axes. The gradient used for each dimension depends on the plane of the scan and on which gradient an operator picks for frequency or phase encoding. Slice selection locates a slice in the plane selected, and typically phase encoding locates signal along the short axis of an image (because it takes the longest to encode), and frequency encoding locates signal along the long axis of an image.

1.6.1.6 Slice selection

During slice selection the magnetic moments of nuclei within a specific slice location along a gradient have a unique precessional frequency when the gradient is switched on. Transmitting an RF pulse at that unique precessional frequency selectively excites a slice. In order to obtain slice thickness, a range of frequencies must be transmitted to produce resonance and excitation across the whole slice. This range of frequencies is known as the transmit bandwidth. Slice thickness is determined by the slope of the slice select gradient, and the transmit bandwidth. A steep slope and narrow transmit bandwidth produces thin slices and better spatial resolution. A shallow slope and broad transmit bandwidth produces thick slices and decreased spatial resolution. The slice gap is the space between slices, and if small in relation to the slice thickness, artefacts such as cross-excitation can occur. The slice select gradient is switched on during delivery of the RF excitation pulse. In spin echo sequences (see below) it is also switched on during the 180° pulse so that the RF rephasing pulse can be delivered specifically to the selected slice.

1.6.1.7 Phase encoding

After a slice has been selected and slice select gradient has been switched off, the magnetic field experienced by the nuclei within the slice is equivalent to the field strength of the system. The processional frequency of the nuclei in the slice is equal to the Larmor frequency. The phase encoding gradient is switched on briefly after the RF excitation pulse has been switched off, and by changing the phase of spinning nuclei, causes a phase shift of nuclei along the length of the gradient. Nuclei experiencing higher field strength gain phase relative to those experiencing lower field strength. When the phase-encoding gradient is switched off, nuclei return to the Larmor frequency, but the phase shift remains. This modulates the MR signal because signals from individual spins go in and out of phase with one another causing either constructive or destructive interference. The signal acquired during the echo readout therefore contains phase differences caused by the phase-encoding gradient. The system cannot measure phase directly, and for this reason the phase shift is converted into a pseudo-frequency by the system. This phase shift is used to locate nuclei and signal along one dimension. The phase encoding gradient must be applied repeatedly at different strengths to locate the source of the MR signals along the phase encoding axis. Frequency encoding by contrast maps the all points along the frequency-encoding axis based on information contained in each signal. Although each signal contains data from throughout the entire two-dimensional image slice, data from multiple signals are needed to solve for the signal location by two-dimensional Fourier transformation. The slope of the phase encoding gradient determines the degree of phase shift, and steeper gradients produce greater phase shift, increasing the phase matrix and giving rise to greater resolution of images along the phase axis.

1.6.1.8 Frequency encoding

The frequency gradient is typically switched on during the echo (see below) and is also called a readout gradient because frequencies within the signal are read by the system during its application. That is, unlike the slice select gradient, frequency is encoded by applying an imaging gradient *during* the measurement of the MR signal. In phase encoding sampling is performed *after* the gradient is applied. The echo is often centred to the middle of the gradient application. The frequency change caused by the gradient in the long axis of the image is used to locate each signal. The spin and precessional frequency of those nuclei experiencing a higher gradient speed up, while the spin and precessional frequency of nuclei experiencing a lower gradient slow down. That is, nuclei undergo a phase shift relative to their position

on the gradient, and this causes modulation of the MR signal because signals from individual spins go in and out of phase with one another, causing either constructive or destructive interference. The slope of the frequency-encoding gradient determines the size of the field of view in the frequency direction, and hence image resolution. The application of RF pulses and gradients produces a range of frequencies within the echo, which is known as the receive bandwidth. All these frequencies must be sampled by the system in order to produce an accurate image from the data. The time available to sample the frequencies in the signal is called the sampling time, and as the echo is usually centred in the middle of the sampling window, the minimum TE increases as the sampling time increases. The rate at which the frequencies are sampled is called the sampling rate. The Nyquist theorem states that the sampling rate must be at least twice the frequency of the highest frequency in the echo. If this is not the case, the data collected in K space may not accurately reflect all the frequencies present in the signal. Increasing the frequency matrix, or reducing the bandwidth increases the minimum TE for a given gradient strength.

Typically the slice select and frequency encoding gradients include dephasing and rephrasing lobes in order to ensure that the phases of the MR signal are coherent while they are being sampled in order to increase the signal measured. However no rephasing lobe is used along the phase axis before the MR signal is measured as a rephrasing lobe would eliminate phase differences, and prevent phase encoding.

1.6.1.9 K-space

The concept of k-space is essentially a formalism created to provide a useful and graphic explanation for fundamental points underpinning MRI image generation. As a result of frequency and phase encoding the MR signal is encoded spatially as it is collected. The application of superimposed, dynamically changing gradient fields introduces spatially dependent variations in frequency and phase across the region of interest, effectively interrogating the anatomy for all different spatial frequencies. The steeper the applied gradient, the greater the degree of achievable separation of spin systems, and high gradient amplitudes are needed to discern high spatial frequencies or detail, whereas less steep gradients discern lower spatial frequencies or contrast. In addition, smaller gradients generate more signal than steep gradients because precessional frequencies and phases are overall more similar across the region of interest. Using these principles individual spins can therefore in theory be discriminated depending on the number of times they pass the receiver coil (frequency) and their position as they do so (phase). However, the raw MRI

signal is complex and contains all of this frequency- and phase encoded information that is needed to construct an image. The Fourier transform is a fundamental mathematical concept that enables the decomposition of a complicated signal into the frequencies and relative amplitudes of its simple component waves. In MRI physics the MR signal is digitised, and then decomposed by the Fourier transform and entered into k-space, which is a 2D (or 3D) Fourier space that organises spatial frequency (ie information about the frequency of a signal and where it came from) and amplitude information. That is, the MR data is converted to a map of signal intensity as a function of frequency, and k-space is the 2D (or 3D) Fourier transform of that MR data. One pixel in k-space, when inverse transformed, contributes a single, specific spatial frequency (alternating light and dark lines) to the entire image. A 2D (or 3D) inverse Fourier transform of the whole of k-space combines all the spatial frequencies and results in an image. Thus, k space holds the raw MR data before it is mathematically reconstructed, and is not the MR image. Each point in k space contains information for the whole slice. The product of the gyromagnetic ratio, the gradient strength, and the time for which the gradient is left on determines the effective position in k space. The units of k space are therefore cycles/metre or phase/distance, which relates how much phase is present between two spins as a function of distance after the application of a gradient. Depending on where a pixel resides in k-space the lines will be of varying frequency and orientation. By convention, high spatial frequencies are mapped to the periphery of k-space, and low spatial frequencies are mapped near the origin. For this reason, the central portion of K space contains data that has high amplitude signal phase and frequency data and therefore good contrast and signal but poor resolution. The outer portion of K space contains data that has high spatial resolution, but low signal amplitude data, and therefore poor contrast. The relative intensity of a pixel reflects its overall contribution to an image, with brighter pixels contributing more of a particular spatial frequency. Therefore overall, the intensities of the signal at each point in k-space contain information about both contrast and location, though the location information is transformed and distorted.

By convention in common MRI sequences, each slice of an image typically has its own area of K space. The system maps each individual signal into a two dimensional grid containing pixels, which makes up the field of view (FOV) or area of anatomy to be covered. When slice thickness is considered, a three dimensional voxel is obtained. The number of pixels within the FOV depends on the number of frequency samples and phase encodings performed. The horizontal axis of K space represents the frequency axis,

while the vertical axis represents the phase axis. The number of horizontal lines in K space corresponds to the number of phase encodings performed, or phase matrix. Each horizontal line contains a number of data points, the total of which represents the number of frequency samples taken, or frequency matrix. K space has conjugate symmetry in that it is symmetrical about both axes. The field of view (FOV) is inversely proportional to the line spacing in k space, and proportional to the receiver bandwidth. A decrease in the FOV increases line spacing and resolution provided gradients are increased to encode higher spatial frequencies. Reducing the receiver bandwidth for a constant gradient decreases the FOV but also reduces pixel size, and therefore signal. In an asymmetric or rectangular FOV, the gap between the lines increases and the scan time is reduced, because fewer lines are filled. The scan time is the time needed to fill k space and depends on the TR (during which each slice is selected and phase/frequency encoded), the phase matrix (which typically determines the number of lines that must be filled to complete the scan as one line is filled per TR), and the number of excitations (which is the number of times each line is filled with data).

There are many ways in which data can be acquired, and this dictates the manner in which K space can be filled. These variations include two-dimensional volumetric, three-dimensional volumetric sequential, and three-dimensional volumetric, acquisitions. In a standard two-dimensional volumetric acquisition the same line of K space is filled in for all slices, before moving on to the next slice. Every TR, each slice is frequency encoded with the same gradient, but the amplitude and polarity of the phase encoding gradient is changed. The polarity of the frequency gradient determines whether K space is traversed in a left to right (+'ve), or right to left direction (-'ve), while the amplitude determines how far to the left or right K space is traversed. The polarity of the phase-encoding gradient determines whether a line in the top (+'ve) or bottom (-'ve) half of K space is filled in, while the slope of the line determines whether a central or outer line of K space is filled in. In three-dimensional volumetric sequential acquisitions, all the data from slice 1 is acquired before moving onto slice 2 etc. In this fashion the slices are displayed as they are acquired. In three-dimensional volumetric acquisition data is acquired from an entire volume of tissue, rather than separate slices. At the end of the acquisition, slice encoding occurs, and the volume is divided into discrete partitions by a slice select gradient that separates slices according to their phase value. The number of slices is proportional to the acquisition time. Using this method many thin slices can be obtained without a large slice gap, hence increasing resolution.

1.6.1.10 Signal to noise ratio and spatial resolution

In conventional imaging the signal to noise ratio or SNR can be affected by a number of variables that are outlined in table 1.12. Tissues with a high proton density will produce a higher signal than those with a low proton density. Small coils in a transverse plane perpendicular to the main field produce higher SNR but have lower coverage. The TR determines how much longitudinal magnetization recovers between excitation pulses and how much is available to move into the transverse plane in the next TR period. A short TR, although useful for T1 weighting, may reduce SNR. The TE is a factor in the amount of dephasing of transverse magnetization that occurs between the excitation pulse and echo. Large TEs are needed for T2 weighting, but may reduce the SNR as more transverse magnetization dephases. The larger the flip angle, the more longitudinal magnetization is converted into transverse magnetization, and the larger the signal up to 90 degrees or for shorter TR, the Ernst angle. The number of times each signal is sampled after the same slope of a phase encoding is called the number of signal averages (NSA) or number of excitations (NEX). The higher the NEX the more data is stored in each line of the MR data array, and the greater the amplitude of signal at each frequency and phase shift. However, the scan time also increases proportionally. Finally, reducing the sampling bandwidth, reduces the proportion of noise relative to signal, but also increases the minimum TE. This in turn may reduce T1 and PD weighting. The SNR is also affected by the FOV, matrix and slice thickness of an image, which are intimately linked to image spatial resolution.

Spatial resolution is defined as the ability to distinguish between two points close together in an image. The spatial resolution of an image is dependent on the voxel size. A reduction in voxel size causes a reduction in SNR, but improvement in image resolution. Each imaging volume is divided into slices, and each slice displays an area of anatomy known as a field of view (FOV). The FOV is divided into pixels, the size of which, are controlled by the matrix. The voxel is defined as the pixel area multiplied by the slice thickness. Factors that affect voxel size, and therefore resolution are slice thickness, FOV, and matrix. Increasing the matrix size, increases the number of pixels that fit into the FOV, and therefore decreases the voxel size. This increases image resolution, but decreases SNR. A reduction in the FOV gives rise to a decrease in voxel volume, increase in spatial resolution but decrease in SNR. Finally, decreasing the slice thickness also increases spatial resolution, but decreases SNR.

To optimize image	Adjusted parameter	Effect
Maximize SNR	↑ NEX	↑ Scan time
	↓ Matrix	↓ Scan time
		↓ Spatial resolution
	↑ Slice thickness	↓ Spatial resolution
	↓ Receive bandwidth	↑ Minimum TE
		↑ Chemical shift
	↑ FOV	↓ Spatial resolution
	↑ TR	↓ T1 weighting
		↑ Number of slices
	↓ TE	↓ T2 weighting
Maximize spatial resolution (assuming square FOV)	↓ Slice thickness	↓ SNR
	↑ Matrix	↓ SNR
		↑ Scan time
	↓ FOV	↓ SNR
Minimize scan time		↑ T1 weighting
	↓ TR	↓ SNR
		↓ Number of slices
	↓ Phase encodings	↓ Spatial resolution
		↑ SNR
	↓ NEX	↑ SNR
		↑ Movement artifact
	↓Slice number in volume imagin	↓ SNR

Table 1.12 – Optimising image quality – adapted from (274)

1.6.2 Pulse sequence mechanisms

A pulse sequence consists of a series of RF pulses, gradient applications and intervening time periods. They are necessary in order to refocus spins that have lost phase coherence due to spin-spin interactions and magnetic field inhomogeneity, and produce sufficient signal for an image. Manipulation of TE, TR and RF enables differing contrasts to be selected. Spins are rephrased in two ways, by either using a 180° RF pulse, or by using a gradient. MR pulse sequence diagrams show the timing of these events during MR acquisition.

1.6.2.1 Spin echo sequences

Figure 1.6 shows a spin echo sequence. After the application of a 90° RF pulse spins lose precessional coherence due to T2* decay, resulting in a decay of coherent magnetisation in the transverse plane, and reduced signal. A 180° RF pulse then causes rephasing of the spins, such that coherent signal in the receiver coil is generated and can be measured. The regenerated signal is called a spin echo. In a single spin echo sequence a single 180° pulse is applied after the excitation pulse. This refocusing RF pulse flips the spins in the plane perpendicular to B0, putting the faster precessing spins behind the slower

precessing spins. If conditions remain the same, the fast spins will catch up to the slow spins, and all spins will get back in phase. It therefore helps to overcome dephasing effects apart form those due to spin-spin interactions which cannot be reversed as it is a random process. The TR is defined as the repetition time and its length is usually the time from one 90° RF pulse to the next 90° RF pulse in a particular slice. The TE is the length of time from the 90° RF pulse to the midpoint of the signal generated after the 180° RF pulse or spin echo. Typically the refocusing RF pulse is applied TE/2 after the excitation pulse. By manipulating the TR and TE as described earlier, images can be proton, T1 or T2 weighted.

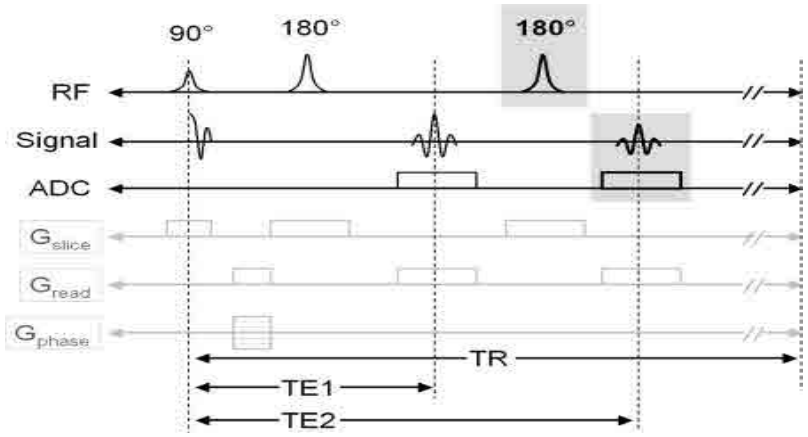

Figure 1.8 - A multi spin echo sequence (273). The gray shading highlights the difference between a multi- and single spin echo sequence (ADC = analogue to digital convertor)

A dual echo sequence (as shown in figure 1.6) consists of two 180° pulses which produces two spin echoes. That is, one obtains two images per slice location. The first echo has a short TE and a long TR and results in a proton density weighted image, while the second echo has a long TE and a long TR and results in a T2 weighted image. The second echo has less amplitude than the first echo because more T2 decay has occurred by this point. Spin echo sequences provide high quality images, but require long scan times.

Fast or turbo spin echo sequences (FSE or TSE) are a faster version of conventional spin echo. These sequences incorporate a series of 180° rephrasing pulses, each one producing a spin echo (echo train), and after each rephasing, a phase-encoding step is performed. Thus, more than one phase encoding is

performed per TR, and more than one line of k-space is filled every TR (unlike in conventional spin echo sequences), hence reducing the overall scan time. However compared to gradient echo sequences, FSE or TSE take longer to traverse k-space because data cannot be sampled during the application of an RF pulse, though unlike gradient echo sequences signal loss from dephasing is eliminated. In addition all the RF pulses have a heating effect on patients, which can be great enough to reduce the speed of the scan. This sequence can be combined with inversion recovery (IR) sequences to suppress signal from certain tissue classes such as CSF.

The traversal of K space in spin echo sequences is complex as the 180° RF pulse causes the point to which K space has been crossed to be mirrored to the opposite side in both up-down and left-right directions. For this reason in spin echo sequences, the frequency gradients needed to reach the left side of K space and begin data collection are two identical lobes either side of the 180° RF pulse.

1.6.2.2 Gradient echo sequences

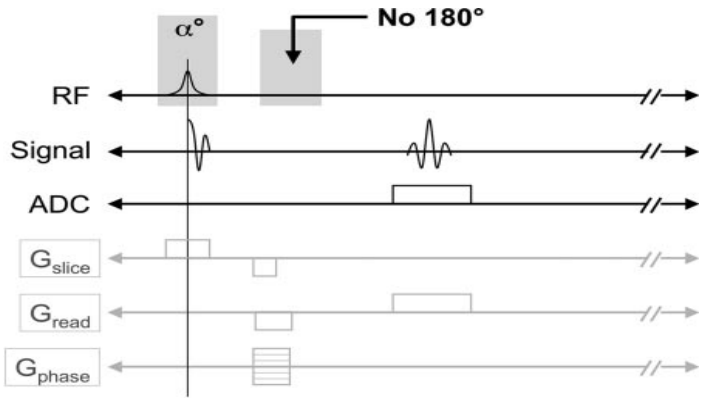

Figure 1.9 – A gradient echo sequence – The differences from a spin echo sequence include the fact that the initial RF pulse is less than 90°, and there is no 180° RF pulse. Signal dephasing and rephasing is carried out by gradient pulses (273).

Gradient echo sequences (see figure 1.7) are sequences that use a gradient to rephase spins, instead of a 180° RF pulse as used in a basic spin echo sequence. In a typical sequence an RF excitation pulse is followed by a relaxation period, and then gradient reversal to produce rephasing of spins. The magnitude and duration of the RF pulse determines the flip angle or angle through which NMV moves away from B_0 during resonance. When a flip angle other than 90° is used, only part of the longitudinal NMV is converted

to transverse magnetisation, unlike in spin echo sequences where all the longitudinal magnetization is converted to transverse magnetization. For this reason, the signal to noise ratio in the gradient echo sequences, is less than in spin echo sequences. However the smaller flip angle and lack of a 180° RF pulse allow TR to be much shorter than in spin echo sequences resulting in very fast imaging times.. After the RF pulse is withdrawn T2* decay occurs before T1 and T2 processes have had a chance to occur, and the magnetic moment within the transverse plane starts to dephase. A gradient is then applied that causes a change in the local magnetic field strength, and hence changes the precessional frequency, and phase of the spins. This therefore rephases the magnetic spins, so that a signal is produced in the receiver coil. This is the gradient echo signal, as opposed to a spin echo sign, because a gradient was used to create it. In a gradient echo pulse sequence, rephasing is performed by the frequency-encoding gradient, and a negative gradient pulse accelerates dephasing, while rephasing is produced by a reversed polarity gradient. Gradient rephasing is less efficient than RF rephrasing, as it has no effect on dephasing caused by T2* effects. For this reason T2 weighted gradient echo images are usually called T2* images to reflect the presence of T2* effects. However, gradient rephasing is quicker than RF rephasing, and gradient echo sequences have shorter TEs and TRs than spin echo sequences. In gradient echo sequences the TR and flip angle together determine the T1/proton density weighting, while the TE controls the T2* weighting. T1 weighted images have large flip angles in order to shift the majority of the NMV into the transverse plane, and short TR and TE values to minimise T2* effects. T2* weighted images have small flip angles to ensure the majority of the NMV remains in the longitudinal axis preventing saturation, and long TE and TR values to produce maximum T2* effects, and reduce saturation respectively. Proton density weighted images have small flip angles so that most of the NMV remains in the longitudinal axis minimising saturation and T1 effects, and long TR and short TE values to minimise T1 effects and T2* effects respectively.

Gradient echo sequences are designed to utilise the steady state phenomenon. The steady state is created when the TR is shorter than the relaxation times of tissues and the flip angle is not 90° as in a spin echo sequence. The energy inputted into the system via the flip angle, equals the energy out of the system during the TR period. This in turn enables the use of shorter TR times, and faster scans. There is co-existence of both longitudinal and transverse magnetisation, and in particular the latter does not have time to decay during pulse sequence, but builds up over several TR periods. In gradient echo sequences that use the steady state there are two signals available to produce the final gradient echo that is used to

form the image. The FID image contains mainly T2* and T1 weighted information, especially if TE is short. The stimulated echo (or residual transverse magnetisation created across several TR periods) contains mainly T2* and T2 weighted information, especially if the TE is long. Gradient echo sequences can be classified according to whether the residual transverse magnetisation is in phase (coherent) or out of phase (incoherent). The types of gradient echo sequences include coherent gradient echo, incoherent gradient echo, steady state free precession, balanced gradient echo, and fast gradient echo.

K space traversal in gradient echo images is relatively straightforward. The starting point for K space traversal is usually the centre, and when the frequency encoding gradient is negative in order to dephase the FID, K space is traversed in a right to left direction, whose distance depends on the amplitude of the negative lobe of the frequency encoding gradient. If the phase encode gradient is positive, a line in the top half of K space is traversed. The larger the amplitude of the phase gradient, the higher up in K space that a line is traversed with data from the echo. The frequency-encoding gradient is then turned positive, and during its application, data are read from the echo, and K space is traversed from left to right. The distance travelled depends on the amplitude of the frequency-encoding gradient. If the phase gradient is negative, then a line in the bottom half of k space is traversed in the same manner.

1.6.2.3 Echo planar imaging (EPI)

Echo planar imaging (EPI) (see figure 1.8) is a very fast acquisition method based on gradient echo imaging, that fills all lines of K space in a single repetition or TR (single shot – SS), or in multiple repetitions (multishot – MS). Single or multishot techniques in which spin echoes are generated using 180° RF pulses, instead of gradient echoes, are known as single- or multi-shot turbo spin echoes (SS-TSE or MS-TSE), and are slower than techniques using gradient rephasing. In EPI sequences based on gradient rephasing, multiple echoes are generated by the oscillation of the frequency-encoding gradient, and each echo accrues a phase-encoding by a constant or "blipped" phase-encoding gradient. A plane of k-space is thus traversed within a single TR. There are initial negative phase-encoding and frequency-encoding blips to move to the corner of k-space, the frequency-encoding oscillating waveform then traverses k-x backwards and forwards while the blipped phase-encoding gradient increments along k-y space. The resultant trajectory is a raster scanning of k-space, rather like an oxen ploughing a field.

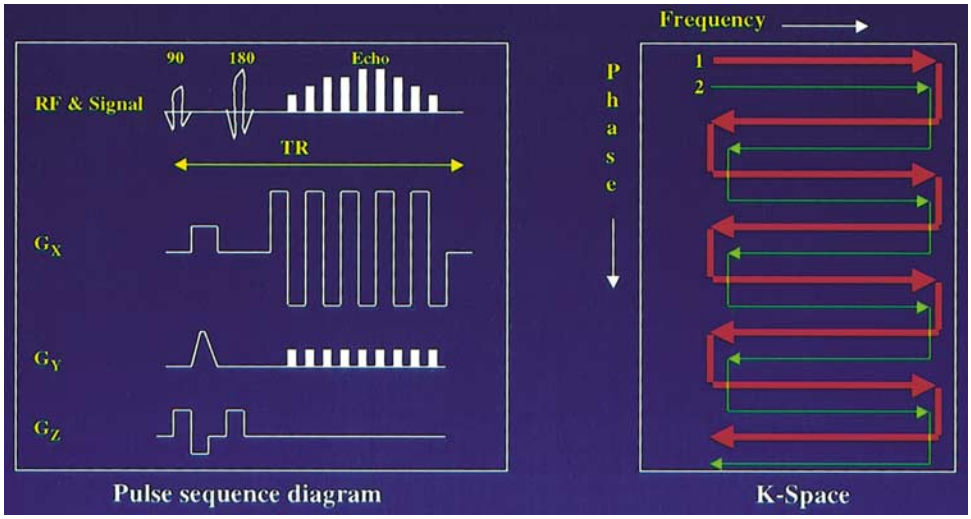

Figure 1.10 – An echo-planar imaging sequence (275). Within each TR period, multiple lines of imaging data are collected. Gx = frequency-encoding gradient, Gy = phase-encoding gradient, Gz = section- selection gradient.

Given that all echoes must be encoded before the transverse magnetization has decayed to zero, EPI images contain poor SNR and significant amounts of T2* decay. However their SNR per unit time is good. Multishot techniques, where K space is acquired in segments may ameliorate this problem, at the cost of increased scan time. K space techniques that can improve the speed of acquisition include, partial or fractional averaging, the use of an asymmetric or rectangular FOV, centric imaging or parallel imaging. In the latter technique, multiple receiver coils are used during the sequence. Each coil gathers data specific to their own unique lines of k space, hence decreasing the scan time by a factor equivalent to the number of coils, because the number of shots or trajectory duration needed to fully sample the image is reduced.

In order to achieve different contrasts in EPI sequences, any type of RF pulse may precede the sequence. Two examples include gradient and spin echo EPI. In gradient echo EPI (GE-EPI) a variable RF pulse is used. In spin echo EPI (SE-EPI) a 90° excitation pulse followed a 180° rephasing RF pulse are used, and followed by EPI readout of gradient echoes. The rephasing pulse helps reduce artefact caused by magnetic field inhomogeneities and chemical shift. SE-EPI sequences may take longer than GE-EPI sequences, but provide better image quality. In all single shot techniques, TR is infinitely long, and PD/T2 weighting is achieved by using a short/long effective TE, which corresponds to the time between the excitation pulse, and filling of the centre of K space. T1 weighting is achieved by the application of an inversion pulse

before the excitation pulse in order to produce saturation, or by using a short TR and varying the flip angle as in any other gradient echo sequence.

1.6.2.4 Advantages and disadvantages of EPI

The rapidity of EPI based acquisitions enable the freezing of physiological motions in the brain, and are critical to modern fMRI and diffusion MRI techniques. However these techniques do have a number of problems, primarily due to the absence of an RF refocusing pulse in gradient echo EPI sequences which are used in fMRI (spin echo sequences are used in diffusion MRI). Chemical shift in the frequency axis is relatively small, as each echo is acquired rapidly, but chemical misregistration along the phase axis can be a problem due to the length of time needed for the train of phase encodes. This results in the phase encodes being applied at different times after excitation, whereas in standard spin and gradient echo sequences the different phase encodes are acquired at the same time after excitation. Other artefacts include blurring caused by T2* decay, and ghosting caused by errors in the timing and shape of the readout gradients. Finally, susceptibility artefact leading to geometric distortions and signal loss, can also be a significant problem due to the fact that different tissues magnetize to different degrees which results in precessional frequency and phase differences. This leads to a shift in pixel position in the phase encoding direction, causing geometric distortions which leads to dephasing at the interface of these tissues, and resultant signal loss. The 180° rephasing pulse used in spin echo sequences is effective at compensating for such phase differences at air-tissue and fat-water interfaces, but gradient echo sequences do not compensate for it.

1.6.3 Diffusion MRI

1.6.3.1 Basic principles

Diffusion can be defined as a mass transport process that occurs naturally, and results in molecular mixing without the need for bulk motion. It occurs as a result of collisions between molecules in the liquid or gas state. The trajectory of each molecule can be described as a 'random walk' in three-dimensional space, in that a molecule stays in one place for a fixed time T, before moving to a new, random location. This is best exemplified by Robert Brown's observation in 1827 of the perpetual motion of pollen grains suspended in water caused by collisions with smaller diffusing particles (276). It is impossible to predict where a particular molecule may diffuse to, though

predictions can be made about the overall displacement of molecules. Fick was the first to mathematically describe this process (277).

$J = -D\Delta C$

J = net particle flux (vector), C = particle concentration, and D = diffusion coefficient (constant)

He highlighted that the rate of flux was proportional to the concentration gradient as well as the diffusion coefficient. The diffusion coefficient is dependent on the size of the diffusing particles, and the temperature and microstructural features of the environment. Diffusion occurs even at thermodynamic equilibrium, although there may be no net flux. Einstein later formulated a more comprehensive description of diffusion by using a probabilistic framework, and introducing the concept of a 'displacement distribution' which quantifies the fraction of particles that travel a certain distance within a particular timeframe, or the probability that a single particle will undergo a given displacement (278). In free diffusion this displacement distribution can be modelled as a Gaussian function, whose width grows with larger diffusion coefficients. The peak distribution is at zero displacement, and there is equal probability of displacement a given distance from the origin, regardless of the direction of diffusion. Mathematically this can be described as follow:

$(x^2) = 2D\Delta$

x^2 = mean-squared displacement of particles during , Δ = diffusion time, D = diffusion coefficient

Thus by measuring the displacement of water molecules over a period time, we can calculate the diffusion coefficient of water. If water molecules encounter tissue substructures along their random walk such as cell membranes, the mean-squared displacement will be smaller than in free water, and the diffusion coefficient will *appear* smaller. For this reason, in diffusion weighted imaging the term 'apparent diffusion coefficient' (ADC) is used.

1.6.3.2 Sensitizing MR acquisition to diffusion

Because diffusional processes are influenced by the geometrical structure of the tissue microenvironment, MRI sensitized to diffusion and using the bulk-average diffusion properties of water molecules, can be used to probe that structure. Practically any MRI sequence can be

sensitized to diffusion, and the underlying principles were first introduced by Stejskal and Tanner, who incorporated pulsed gradients into a traditional spin echo sequence (see figure 1.9) (279).

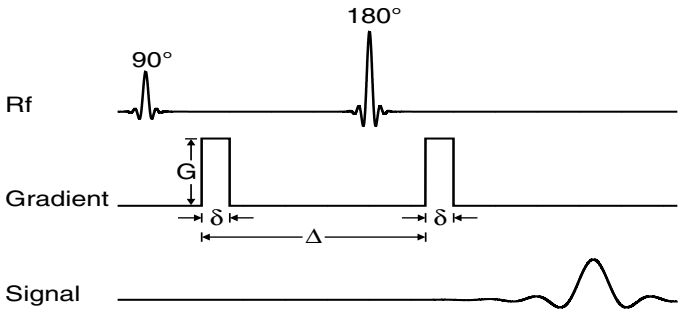

Figure 1.11 - A schematic of the pulsed field gradient spin echo MR technique. Δ = separation between two pulses, δ = pulse duration, G = pulse magnitude.

The first applied diffusion gradient confers a position-dependent precessional frequency, such that there is a gradient in phase accrual. This gain in phase is reversed by the application of a gradient of identical amplitude, duration and polarity, following 180° refocusing pulse. The phase accrual could also be reversed by application of a gradient of the same amplitude and duration, but opposite polarity.

When δ is short one can ignore the diffusion that takes place during the application of these gradient pulses. The pulses cause a net phase change, which can be expressed as:

$\Phi_1 = -qx_1$

x_1 is the position of the particle during the application of the first pulse

$q = \Upsilon\delta G$ where δ and G are the duration and magnitude of the gradient pulses, and Υ is the gyromagnetic ratio.

Similarly if a particle is situated at x_2 during the application of the second pulse, the net phase change due to the second pulse is expressed as:

$\Phi_2 = -qx_2$

The 180° RF pulse between the two gradient pulses reverses the phase changes caused by the first pulse (as well as all phases from all applied gradients, and off resonance) and therefore the net phase change is:

$\Phi_2 - \Phi_1 = -q\,(x_2 - x_1)$

It should be noted that all phase changes due to the B_0 field have been ignored because these are constant for all the spins. If the particles remain stationary, that is $x_1 = x_2$, there is no net phase change, in which case the spins are displaced by the same amount and the echo magnitude is solely due to T1 and T2 processes. However, because of diffusion or the random walk process, there is a distribution of displacements, and hence phases. The increase in phase accrued during the first period does not cancel out the phase decrement gained in the second period. Therefore, phase dispersion occurs, leading to loss of signal coherence and exponential attenuation of the signal by a factor that is the product of the diffusion coefficient D, and a factor b which is the degree of diffusion weighting. The degree of diffusion weighting, dictates the extent of phase dispersion, and depends on the strength of the field gradient or how strongly phase depends on position, the duration of the gradient or how long a spin experiences position dependent phase accrual, and the time interval between gradient applications, or the time for diffusion. Using a Gaussian model of diffusion, the b factor is given by the Stejskal-Tanner equation:

$b = (\Upsilon G\delta)^2(\Delta - \delta/3)$

b = diffusion weighting

Υ = gyromagnetic ratio

G =amplitude, δ = duration, and Δ = separation, of the magnetic field gradient pulses

1.6.3.3 Modelling and quantification of diffusion data

Assuming the diffusion of water molecules is Gaussian, MR signal attenuation E(q) due to diffusion is defined as the ratio of two MR signals. This can be mathematically defined as (279,280):

$E(q) = e^{-bADC}$

ADC = apparent diffusion coefficient

b = difference in diffusion weighting

The diffusion gradients can be applied in any direction, and the ADC can be quantified for any direction by collecting at least two sets of data with two different b-values. Typically at least one data set has no diffusion weighting (S_0) with b = 0, and another with a non-zero diffusion-weighting gradient in the direction of interest (S_D). By rearranging the above equation, the ADC can be defined as:

$ADC = Log [S_0/S_D] / b$

The ADC reflects diffusion in one direction only, but even when diffusion measurements are made in several directions S_0 need only be measured once. For all the gradients the signal loss relative to S_0 is due to diffusion related displacement in the direction of the applied gradient. The microstructure of tissue affects the diffusion of water molecules, and hence diffusion as measured by MRI can act as a probe to investigate changes in cellular structure that alter the diffusion of water molecules.

The most useful application of these principles has been the use of diffusion-weighted MRI in acute ischaemia or stroke (281). Here there is a reduction in the diffusion of water molecules or ADC, and therefore less signal attenuation, and areas of acute ischaemia appear bright on MRI. At the same time as this discovery, it was appreciated that measurements of the ADC in certain parts of the brain, depend on the direction of the applied diffusion encoding gradient (282). In some regions, the ADC is the same in all directions, and in these areas, diffusion is described as isotropic. In other regions diffusion has a directional preponderance due to the underlying white matter restricting diffusion in certain directions, and in these regions diffusion is described as anisotropic.

1.6.3.4 The diffusion tensor model

The characterisation of diffusion in ordered tissue cannot be described adequately by a single ADC, in view of the fact that there will be some directional preponderance, and the ADC will depend on

the direction of measurement. The diffusion tensor model is a more sophisticated description of diffusion in such tissues, where the displacement of water molecules per unit time is not the same in all directions. The diffusion tensor matrix is a three-dimensional covariance matrix of displacements in a given time (see figure 1.10).

$$\mathbf{D} = \begin{bmatrix} D_{xx} & D_{xy} & D_{xz} \\ D_{xy} & D_{yy} & D_{yz} \\ D_{xz} & D_{yz} & D_{zz} \end{bmatrix}$$

Figure 1.12 - The diffusion tensor matrix

The off-diagonal elements of the matrix reflect the correlation or covariance between molecular displacements in orthogonal directions. Therefore, for example, D_{xy} is the correlation of displacements along the x and y axes, and not the ADC measured with a diffusion encoding gradient along the x-y axis. For this reason, off-diagonal elements can take values of 0 or negative values, but the ADC in the equivalent direction can never be negative or zero. A graphical representation of the tensor is an ellipsoid (see figure 1.11). This represents an envelope, where a molecule placed at the centre would diffuse with equal probability from the centre in all directions if diffusion is isotropic. If the diffusion is anisotropic, the long axis of the ellipsoid would be parallel to the long axis of the anisotropic medium. The eigensystem of the ellipsoid represents its internal frame of reference, where principal axes of diffusion are called eigenvectors (ε_1, ε_2, ε_3) and the lengths or corresponding eigenvalues (λ_1, λ_2, λ_3) represent the diffusion distance in a given time along the principal axes of the diffusion tensor. As the displacement in a given time is proportional to the square root of the diffusivity, the axes are scaled according to the square root of the eigenvalues. By definition the eigenvectors are orthogonal to one another, and eigenvalues are classified according to their magnitude such that $\lambda_1 \geq \lambda_2 \geq \lambda_3$. The orientation of the tensor is taken to be parallel to the principal eigenvector ε_1 which is the eigenvector associated with the largest eigenvalue. The principal eigenvector is assumed to be parallel to the dominant white matter fibre orientation within the voxel. As ε_2 and ε_3 are constrained to lie in a plane orthogonal to ε_1, they do not provide information about the orientation of additional fibre populations.

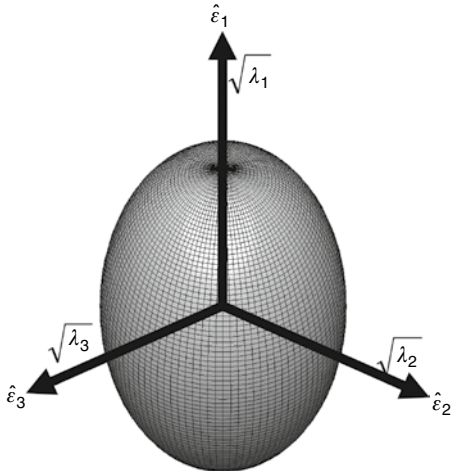

Figure 1.13 – Schematic of the diffusion tensor ellipsoid (283)

The calculation of the diffusion tensor from a series of diffusion-weighted signals was first formalised by Basser and Le Bihan (284,285). Analogous to the calculation of the ADC (see above), a scaling factor or b-matrix is derived for a given gradient, from its amplitude, duration and separation. This together with the signal attenuation for a given gradient is then used to calculate the tensor. As the tensor is symmetric there are only six unknown values to determine, and these can be derived from a minimum of six gradients applied in non-collinear, and non-coplanar directions in addition to one non-diffusion-weighted image. In practice more directions are used in order to reduce errors, with a fixed diffusion weighting. This is known as a spherical acquisition protocol. The tensor itself can be fitted in a number of ways, including weighted linear least squares, or non-linear least squares regression.

With the development of the diffusion tensor model it became possible to derive a number of rotationally invariant quantitative indices. The trace is the sum of the three diagonal elements of the diffusion tensor (i.e. Dxx + Dyy + Dzz), and is equal to the sum of its three eigenvalues. The trace/3 is the orientationally averaged mean diffusivity. The trace has the advantage that at low b-values, it is quite uniform throughout the brain (286), and therefore the effects of anisotropy do not confound the detection of diffusion abnormalities in for example acute ischaemic stroke (287). As b values increase differentiation between grey and white matter trace values increases, with the latter having smaller values (288).

Measurements of anisotropy can also be derived from the diffusion tensor model. Pierpaoli and Basser (289,290) were the first to propose that using measures that incorporated the normalised variance of the three eigenvalues about their mean had a low sensitivity to bias at low signal to noise ratios (SNR). The fractional anisotropy (FA) normalizes the variance of the tensor by its magnitude as a whole, and therefore represents the fraction of the tensor that can be assigned to anisotropic diffusion. It can have values from zero (when diffusion is isotropic) to one (when diffusion is constrained along one axis). As the SNR decreases the FA may increasingly overestimated (290). FA can be calculated as follows:

$$FA = \frac{\sqrt{(D_{xx} - D_{yy})^2 + (D_{yy} - D_{zz})^2 + (D_{zz} - D_{xx})^2}}{\sqrt{2\left(D_{xx}^2 + D_{yy}^2 + D_{zz}^2\right)}}$$

One of the limitations of MD or FA is that neither provides any information about the shape of the tensor. For example both a 'cigar-shaped' ($\lambda_1 \geq \lambda_2 = \lambda_3$) and 'pancake-shaped' ($\lambda_1 = \lambda_2 \geq \lambda_3$) tensor can give rise to high anisotropy. Possible solutions to this problem include the use of the skewness of the three eigenvalues as proposed by Basser (291) or the use of Westin metrics which describe an ellipsoid's spericity, linearity, and planarity (292).

1.6.3.5 The multi-tensor model

The diffusion tensor is clearly a very useful model in that it provides two important insights into tissue microstructure. Firstly it quantifies diffusion anisotropy, which is a useful index of white matter integrity. Secondly, it provides an estimate of the principal direction of axon fibres, which enables the use of tractography. However, the model is limited in that it can typically, only recover a single fibre orientation in each voxel. An individual voxel typically contains hundreds of thousands of axon fibres, and these can adopt a wide number of complex configurations. The Gaussian model of diffusion upon which it is based, breaks down when there are kissing, or crossing fibre populations within a voxel which has implications for techniques such as tractography where such information is critical.

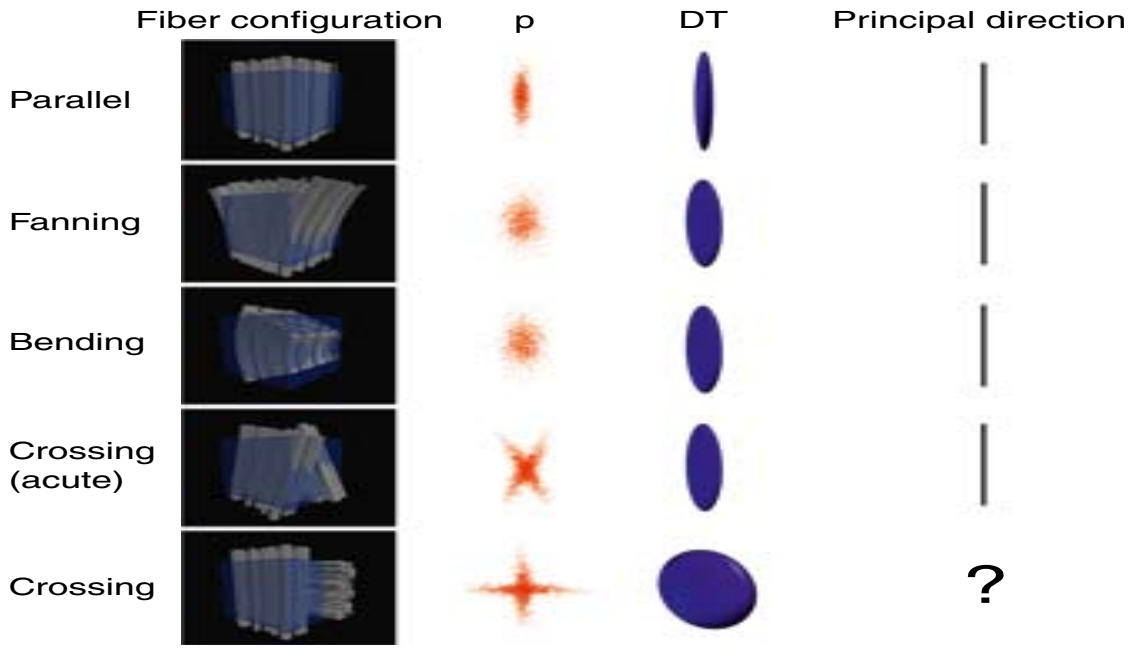

Figure 1.14 – Examples of fibre orientations that can occur in single voxels, and how they are modelled by the diffusion tensor model (DT). p = scatter pattern of molecules during diffusion time from one starting position [edited from (283)]

Figure 1.12 demonstrates that when all fibres run in one direction within a voxel, p (the scatter pattern of diffusion of molecules during the diffusion time) is anisotropic, the diffusion tensor is ellipsoid in shape, and the principal direction is parallel to that of the underlying fibres. When fibres fan or bend within a voxel the diffusion tensor is less anisotropic and its shape is between prolate and oblate. The principal direction of the tensor is still a good estimate of the mean overall fibre direction, but clearly the tensor fails to convey information about the overall shape of the underlying fibres. Indeed fanning and bending fibres are indistinguishable from one another using the tensor model. When fibres are crossing obliquely, the diffusion tensor models an identical non-ellipsoid shape as seen for bending/fanning fibres. Moreover, the principal direction derived from the tensor is wrong. When fibres are crossing orthogonally, p has a cross-shaped contour, and yet the diffusion tensor is unable to capture this shape, and the closest Gaussian approximation is an oblate sphere. In this case, the model breaks down.

The observation that the Gaussian model breaks down in areas of crossing fibres (293), prompted the development of multi-tensor models. This is also a parametric technique, and based on the principal that fibre-crossings can be resolved by modelling distinct fibre populations separately. The multi-tensor model assumes that a voxel contains 'n' distinct groups or populations of fibres, and that diffusing molecules stay within only one population, and that there is no exchange between populations. Each population is modelled by a separate diffusion tensor. The p for the whole voxel is the sum of the Gaussians that each DT represents, weighted by the fraction of the volume that each population occupies. In theory the multi-tensor model can model any number 'n' of distinct fibre populations, but in practice the number of measurements, and noise level limit the number of orientations that can be reliably resolved. Most published studies using the multi-tensor model, use a maximum of n=2. Unlike the simpler DT model, the parameters of the multi-tensor model cannot be expressed as a linear function, and model fitting needs non-linear optimisation. Once the multi-tensor model is fitted, the principal eigenvector of each tensor provides a separate fibre orientation estimate.

The multi-tensor model has a number of limitations. As 'n' increases, the number of parameters within the model increases, and adds to its complexity and instability. Constraints on the model can reduce the complexity and stabilise fitting. These include the use of cylindrical symmetry on the component DTs, or spatial regularization techniques, which ensure voxel-to-voxel coherence (294). Another approach to simplifying the multi-tensor model, is to separate free and restricted compartments. Behrens et al do this by using a 'ball and stick' approach (295). This assumes that water molecules belong to one of two populations: a restricted population of water molecules corresponding to white matter fibres with scatter pattern p_r and a free population that does not interact with fibres and has scatter pattern p_f. An isotropic Gaussian model is used for p_f, and p_r, but in the latter, the DT has only one non-zero eigenvalue so that particles move only in the fibre direction. The 'ball and stick' model can be extended naturally to model multiple fibres, by increasing the "sticks" in the model. Similar approaches have been used by others, but more sophisticated models have been used for the 'ball' and 'stick' in order to capture more complicated fibre orientations such as fanning or bending (296,297).

Another problem with the multi-tensor model is that it assumes that the number of distinct fibre populations is known, and this can cause problems, because the two-tensor model can become unstable when only one population of fibres is present, and produce erroneous results. A number of approaches have been introduced to deal with this problem. Parker and Alexander (298) use the spherical-harmonic voxel-classification algorithm (293) to classify voxels as isotropic, one-fibre, or two-fibre, though this method does not extend beyond 2 fibre populations. Behrens et al use a Bayesian approach (299).

1.6.3.6 Artefacts and diffusion imaging

There are three primary sources of error in diffusion imaging acquisition, namely eddy currents, gradient non-linearities and motion artefact. Background and RF noise can also be a problem in diffusion imaging as in any other quantitative MRI technique, but more so at higher b values.

1.6.3.6.1 Eddy currents

The gradient coils used to create magnetic fields within an MRI scanner, also produce magnetic fields outside the coils, which can generate electrical currents or 'eddy currents' in neighbouring conductive surfaces. The prolonged decay of these currents can create lags in the responsiveness of the gradients. In typical structural imaging sequences, the gradients are applied briefly, and therefore induced eddy currents tend to cancel one another out, with the rise and fall of the pulse. In DWI sequences, in order to achieve adequate b values, gradients are applied for longer durations and are unipolar, and therefore the eddy currents do not cancel one another out. Eddy currents have two unwanted effects. Firstly they affect the field gradient giving rise to a difference between the actual, and prescribed b-matrix. This is exacerbated in pulse-gradient spin echo sequences typically used in DWI, which have a small bandwidth in the phase-encoded direction, such that errors in the desired gradient are exacerbated. Secondly, a slowly decaying field during readout of an image causes geometrical distortion of the DWI. This type of warping is typically more significant than those produced by constant magnetic field inhomogeneities as it is not constant through the entire readout, and changes with each diffusion encoding gradient direction. Both effects can lead to significant, and systematic effects in the estimated diffusion parameters or tensor applied to each voxel, as the actual gradient applied to the tissue is different from the

prescribed gradient in each DWI volume. In addition, if uncorrected, some pixels will be in different locations for each diffusion-weighted image, hence corrupting the final synthesised image.

Eddy current effects can be minimised both during acquisition, and with post processing methods. Active shielding of the gradient coils reduces the external magnetic fields produced by them, and in turn reduces eddy current effects. In individual scanners eddy current effects can be measured, and the shape of the applied gradient waveforms can be altered, in order to achieve desired magnetic field gradient outcome. Improved feedback mechanisms to the gradient amplifiers, can also help reduce this artefact. Finally, the use of split diffusion gradients with an additional refocusing RF pulse can be used to decrease eddy currents (300). The latter method is based on the fact that Eddy currents are typically proportional to the slew duration and rate of gradients applied (ie magnitude of the gradient change). By bringing the positive and negative phases of diffusion gradients closer together in time by splitting gradients, the eddy current effects tend to cancel one another out.

Common post-acquisition methods for correction of eddy current distortions rely on the fact that these distortions are time varying and therefore slice specific. Using this principle slices can be individually co-registered using cross-correlation or mutual information based cost functions, to matching non-diffusion weighted images (301). The shortcoming of this method is an assumption that there is no subject motion during acquisition, and that the eddy current deformations only encompass shift, shear and scaling along the phase encoded direction only. Other post-acquisition methods include collection of phase map and correction of the images depending on the effects that eddy currents have on it (302), or the use of phantoms in separate experiments to map eddy current fields (303). Perhaps the most popular post-acquisition method of correction is the approach taken to correct both eddy current distortion, and motion. This incorporates a full affine rigid body approach (3 rotations, 3 translations, 3 scales, 3 shears) to co-register the whole diffusion weighted volume to non-diffusion weighted images using packages such as FLIRT (304). The rigid components are used to correct motions, and the additional degrees of freedom are used to correct eddy current distortions. However, this method is limited by its inability to take into account non-linear deformations across slices in a given volume. A better method might be to

model both how eddy currents evolve spatially and temporally, and subject motion, and then correct both simultaneously (305).

1.6.3.6.2 Gradient non-linearity and magnetic susceptibility gradients

Within the imaging volume there should be a linearly increasing magnetic field, but outside the imaging volume, this field should drop off as quickly as possible. At the same time the maximum rate at which magnetic fields can change in time is limited because of the potential for heating effects and nerve stimulation. As a result of these conflicting demands, the gradient of the field, and therefore diffusion weighting, is often not linear within the imaging volume, and this non-linearity can vary in different directions across the imaging volume. This can cause the b-matrix to be spatially varying and lead to systematic errors in the determination of the diffusion tensor in each voxel. Some of these artefacts can be reduced in a number of ways, and shimming for example, is a process whereby the static magnetic field is made more homogenous over the region of interest (306) .

A related problem is that of discontinuity in magnetic susceptibility at tissue/air interfaces, such as in brain regions adjacent to sinuses. This produces local magnetic field gradients that can degrade and distort DWIs, especially during echo-planar imaging. The additional gradients lead to changes in the magnetic field experienced by protons, and changes in their precessional frequency. This causes geometric warping of images, and signal variation including signal voids/pile up, and resulting variation in the b matrix, and errors in the estimation of the diffusion tensor. Furthermore, magnetic field inhomogeneity within a voxel can cause increased dephasing, and resulting signal loss and reduction in effective resolution.

Geometric distortions of the EPI data make it difficult to directly overlay fMRI activations or DTI data directly on co-registered high-resolution scans. Acquisition methods that may improve these artefacts include parallel imaging reconstruction, which reduces the duration of the sampling trajectory and hence the time for dephasing of the spins, and imaging techniques that increase bandwidth in the phase-encoded direction (307). In the gradient reversal method (308) k space is sampled in two opposite directions, such

that the resulting images have equal but opposite warping in the phase encoded direction. That is, the pair of images have distortions which are matched in magnitude, but the direction in which the images are stretched or squashed is reversed. This reveals the degree of warping, which can then be compensated for by stretching or squashing the image in the opposite direction. Both images can then be averaged for improved SNR. This method can prove particularly effective when combined with the acquisition of field distortion maps that describe the displacements. Images can be unwarped using techniques that map the local field in the head, though these approaches can reduce signal to noise (309).

1.6.3.6.3 Motion artefact

In diffusion imaging, large diffusion weighted gradients are required to be sensitive enough to pick up the phase shifts caused by diffusion of water molecules, and generate signal decay. As a result of this, diffusion acquisition can be exquisitely sensitive to the motion of tissue, both within and outside of voxels. This motion originates from several sources, and includes head motion and cardiac pulsation. Both sources of motion, when in the direction of the diffusion-weighting gradient, can cause a change and shift in the phase of the spins (310).

Head motion during the application of diffusion weighting gradients can be modelled as a rigid body motion and includes translation and rotation, which cause changes and shifts in phase across voxels respectively. Motion artefact corrupts data acquisition in several ways. Firstly, it corrupts the Fourier encoded phase data, reducing image quality, and causing 'motion artefact'. If all the data is acquired after a single diffusion-weighting gradient, the motion-related phase changes are constant in all k-space measurements, and the Fourier encoding is not corrupted. However, if data is collected after several shots, the motion during the diffusion weighting for each shot will be different, and differences in motion related phase will be apparent across k-space causing problems with Fourier encoding. This will result in loss of image quality and artefacts. For this reason, diffusion weighted imaging is typically carried out with single shot techniques, which mean that motion-related phase changes are constant across an image for a given set of data. Related to this, shifts in k-space data due to rotational head movements, can also lead to significant artefact in asymmetrical data sampling acquisitions. For this reason, in single shot methods of acquisition, asymmetrical sampling is minimized. The symmetrically measured part of k-space must be large

enough to encompass all phase variations due to motion-induced phase. Motion artefact can be dealt with in two ways. Firstly, during acquisition, a patient should be comfortable and well padded in order to minimise motion. Secondly, post-acquisition, rigid body transformations can be used to remap data to the non-diffusion weighted scans.

Cardiac pulsation artefact is not as easy to model as motion artefact, as it induces non-rigid body motions, which in turn lead to a non-linearly changing phase in spins within voxels, an effect quite separate from that of the diffusion effect. This non-linear change in spin phase within voxels, leads to phase incoherence, and reduced signal from a voxel, even with single shot techniques (311). This has detrimental effects on quantitative measurements derived from the tensor model as well as tractography. However, cardiac pulsation artefact is predictable in that it occurs with each heartbeat. It can therefore be minimized by using cardiac gating to acquire data, and by reducing voxel size (312). Alternative post-acquisition approaches include post-hoc rejection of contaminated data points, including the RESTORE approach (313).

1.6.3.6.4 Background and RF noise

Increasing diffusion weighting or decreasing voxel size can reduce the SNR to such a degree that some DWI signals are close to background noise level. Estimation of the ADC can typically be corrupted in those directions in which ADC is highest leading to underestimations of the diffusion tensor and mean diffusivity (314). RF noise can also cause errors in estimates derived from the tensor model, and a variety of methods have been developed to minimise such errors (315).

1.6.3.7 Optimal parameters and acquisition methods

For reasons elucidated above, the most popular method of diffusion imaging is single shot echo planar imaging (SSEPI). The single shot and EPI based nature of the sequence reduces motion related artefact, and also reduces the acquisition time of the scan, which is critical when diffusion is measured in more than one direction, at different b values. Partial k-space coverage reduces the duration of the trajectory, and reduces the T2 decay of the signal for this k-space centre, which increases the MRI signal. At the same time more symmetrical sampling is used to prevent artefacts that can arise in asymmetrically collected data due to head rotation, and cardiac gating helps to

prevent signal loss from tissue shearing during the application of diffusion weighting gradients. The use of velocity compensated diffusion gradients may also be useful in reducing many of the artefacts described above (316) , but is limited by the fact that it significantly reduces any applied diffusion weighting or increases TE.

The overall aim of a diffusion MRI experiment is to increase the sensitivity of the MR signal values, or a derived metric, to a change in isotropy and direction, or an average value of diffusion. The maximum b-value, and number and arrangement of diffusion gradient vectors, are particularly relevant to this aim, and the choice of these parameters is significantly influenced by the choice of diffusion model. For example in order to use a multi-tensor model Alexander and Barker (294) recommend the use of a b value of 2200 to 2800s mm^{-2}, and acquisition of data in 64 gradient directions. With these settings, a two-tensor model can resolve 60° crossing consistently with an SNR of 16. When a maximum b-value is chosen, the diffusion-weighting gradient duration, and thus the diffusion time, are typically minimized to reduce T2 signal loss and overall scan time. The choice of other sequence parameter values when designing a DW SSEPI pulse sequence is contingent on balancing a number of factors. These include desired scan time, desired voxel size, SNR, geometric warping, and resolution. These factors are discussed in the section above entitled "Signal to noise ratio and spatial resolution".

There are alternative methods to the use of SSEPI for data acquisition, though they are less popular. Fast spin echo sequences take longer as data collection cannot occur during RF pulse application, but warping and signal loss from dephasing inherent in EPI based sequences are eliminated by the refocusing pulses. Multishot methods are useful in diffusion imaging because they reduce the echo train duration for each shot, which increases SNR and reduces blurring from spin dephasing and T2 losses. However multishot sequences are considerably slower than single shot methods as the diffusion weighting must be repeated during each shot. They are also limited by the problem of motion artefact though this can be improved by 'navigator correction', which is a method of measuring and removing phase corruption from movement (317). Finally, and most recently, PROPELLER (periodically rotated overlapping parallel lines with enhanced reconstruction) based

FSE and EPI methods can significantly improve motion related artefact, but at the expense of other factors.

1.7 Analysis of diffusion tensor imaging

The sensitisation of MRI acquisition to the diffusional properties of water molecules results in the acquisition of a large amount of quantitative data. This data can be analysed in a variety of ways. The primary methods used to compare such data across subjects include region of interest analysis, whole brain methods of analysis, and tractography-based analysis.

1.7.1 Region of interest analysis

The earliest analysis of diffusion MRI data incorporated region of interest (ROI) methods. In these methods, an ROI is drawn in a specific area of the brain, on the basis of an a priori hypothesis and anatomical knowledge. ROIs are typically drawn on co-registered high-resolution images, or non-diffusion weighted b0 images. Parameters within the ROI, such as MD or FA, are then calculated, and compared within groups, or correlated with other data. The advantages of this method are that specific regions can be chosen on the basis of hypotheses. The disadvantages are that significant abnormalities may be missed in regions that are not selected. In addition, ROI placement is highly operator dependent, and subject to both the anatomical rules used to select the ROI, and potential registration errors. It can therefore be very difficult to place ROIs accurately for small or thin white matter tracts, especially given partial volume issues. A more sophisticated approach is to use tractography to identify voxels from which to take FA (or any other measure) values for cross-subject comparison. In these approaches, the relevant tracts are typically identified using hand-drawn seed regions, or constraining the tractography with hand-drawn ROIs. Tractography can be used to overcome the problem of co-registering equivalent regions in subjects, as the summary statistics can be derived from anatomically corresponding regions in each subject's native space.

1.7.2 Whole brain analysis

The multi-tensor diffusion model described in previous chapters is capable of providing a range of voxelwise, scalar values such as FA, MD, and tensor eigenvalues. In order to compare and spatially localise interesting differences in these parameters across the *whole* brain, a variety of methods have been utilised. These include voxel-based morphometry (VBM) and tract based spatial statistics (TBSS). These methods differ in their approach to the problem of achieving accurate correspondence across subjects.

1.7.2.1 Voxel Based Morphometry (VBM)

VBM was originally developed for finding localised difference in grey matter density in T1-weighted structured brain images between two groups of subjects (318,319). VBM can be carried out in a number of software packages including SPM and FSL. The VBM method can be outlined as below:

1) Choose a target template for registration of the subject images. This may be a standard space template such as the MNI152, or a study-specific template created from the subjects themselves. The MNI152 template corresponds to an average of 152 T1-weighted structural images in 'MNI space'. The primary purpose of such a coordinate system is to allow the alignment of data into a common space, and the reporting of meaningful voxel coordinates.
2) Align all the structural images of the subjects to the chosen template using linear and then non-linear registration methods.
3) Segment each subject's structural image into different tissue types, and for the purpose of standard VBM, only the grey matter (GM) images are used for analysis.
4) Smooth the output (segmentation) data. Smoothing produces an image, which provides a measure of the balance between the GM and non-GM voxel count. Smoothing also improves any effects of misalignment from imperfect registration, and increases sensitivity when the extent of smoothing matches the expected effect size. Finally, smoothing also ensures that the data is Gaussian in nature, which maintains the validity of the Gaussian random field theory (GRF) which are used for thresholding. Smoothing is typically applied with a Gaussian linear filter at between 4 and 16mm full width half maximum (FMWM).
5) Carry out a univariate, voxelwise statistical analysis using the general linear model (GLM). After the pre-processing steps described above, the data can be considered to be in the form of a 4D image, where the 4^{th} dimension is subject number. Univariate modelling processes each voxel separately using the general linear (a form of multiple regression) across subjects. The GLM approach creates a design matrix that contains a column for each variable of interest or co-variate. Each row corresponds to a separate subject. Model parameters (one for each column in the model) are adjusted so as to minimize the residual

errors or noise in the model fitting. Contrasts are employed to investigate the effects of interest within the model.

6) The fitting of a cross-subject model to the data results in a raw statistics image such as a Z (or F or T)-statistic, which shows how well the model, fits the data compared to the error in its fitting. One z-statistic image is generated for each contrast. The final stage in the analysis requires that the statistics image is thresholded in order for inferences to be drawn about the significance of the results. The simplest method of is voxel based thresholding, where each voxel's raw statistic value is tested for significance at a set threshold. A more sensitive method is cluster-based thresholding, where the raw statistic image is thresholded (cluster forming threshold) at a specific but arbitrary level (e.g. Z > 2.3), and clusters of contiguous supra-threshold voxels are found. The size of each cluster is then tested for significance by estimating the p-value corresponding to the size, and how this compares to a critical cluster size threshold value. This method identifies clusters of extended signal, which are likely to have greater statistical significance than individual voxels considered in isolation. The resulting Z-statistic (or F or T) image is then corrected for multiple comparisons across voxels (or clusters), by applying a family-wise error rate. A standard Bonferonni correction is overly conservative, and for this reason Gaussian random field (GRF) theory (320) is applied which takes into account the fact that neighbouring voxels are not independent by virtue of their intrinsic and applied smoothing.

Since the original description of the VBM method, a number of modifications have been suggested (319). These include the use of the GM segmentation, rather than the raw structural data, to drive the registration process, and the modulation of the segmentation output after non-linear registration in order to compensate for local changes in volume caused by the alignment process. The VBM method has also been applied to the analysis of diffusion-related images, and most commonly FA images directly. The above steps are employed in this form of analysis, though registration is carried out using the FA images directly, and the amount of smoothing that should be carried out is open to question.

The advantages of a VBM-style voxelwise analysis is that they are fully automated, easy to apply, and investigate the whole brain without the need for specification of regions of interest. However, VBM also has a number of methodological limitations that can limit the interpretability of results (321). Residual misalignment between images can give rise to partial volume effects, and the misinterpretation of data. Where FA images are used in VBM it is important to check whether differences are seen on the edge of white matter tracts, and therefore that effects are not related to GM/WM partial volume effects. A number of approaches have been suggested for the problem of alignment, including the use of FA images to drive linear alignment across subjects, or more sophisticated methods using high degrees-of-freedom non-linear methods, and tensor components of diffusion data (322). The second limitation of VBM based analysis, is the arbitrary choice of smoothing extent applied to the images. Jones et al (323) demonstrate clearly how differing smoothing kernels, can cause considerable variation in the results of a VBM based FA analysis of schizophrenia data. Smoothing also exacerbates partial volume effects, such that it can be difficult to estimate whether FA changes in data are driven by a change in FA data, or changes in the relative amounts of different tissue types.

1.7.2.2 Tract Based Spatial Statistics (TBSS)

Tract based spatial statistics or TBSS is a relatively, newly developed method that attempts to minimise the limitations of VBM (324,325). It has also been shown that the analysis of diffusion data with TBSS has greater cross-session and cross-subject repeatability, than VBM (324). The steps involved in the application of TBSS are as follows:

1) The first step involves the registration of all subjects' FA images into a common space using linear and non-linear registration tools, namely FLIRT (304) and FNIRT (324) in FSL. Typically the target image is the standard space template FMRIB58_FA image, although study-specific templates can also be derived using methods to identify the most 'typical' subject of the entire group. The FMRIB58_FA image was created by using the average of 58 FA images from healthy adults aligned to the MNI152 T1 weighted template.
2) The transformed images are then averaged to create a mean FA image, which shows that white matter tracts that are common across subjects on average. This mean FA image is then fed into a skeletisation programme, which generates a skeleton image containing

tracts that are common to all subjects. The skeleton represents each tract as single line or surface, which runs down the centre of the tract. During the skeletisation process, the local surface perpendicular direction is estimated, and a search is carried out in this direction to identify the voxel with the highest FA. This voxel is then designated as the centre of the tract. The skeleton is subsequently thresholded in order to restrict analysis to points within the white matter which have been successfully aligned across all subjects, and away from grey matter and CSF in order to minimise partial volume effects, and away from those areas which have not been well aligned across subjects.

3) Each subject's FA image is then 'projected' onto the mean FA skeleton. That is, at each point in the skeleton, a given subject's FA image is searched in the perpendicular tract direction to find the maximum FA value, and assign this value to the skeleton voxel. In this way any residual misalignments from the initial non-linear registration are corrected. Because the corrections occur in a perpendicular direction (the direction in which FA varies most), and not a parallel direction (the direction in which FA varies least), group analysis should not be confounded by misregistration or partial volume effects.
4) The statistical analysis of the resulting data is similar to the processes described above for a VBM analysis. However, there are two critical differences employed in TBSS which theoretically should make it more robust. Firstly, although cluster-based thresholding is more sensitive than voxel-based thresholding, it is limited by the choice of initial choice of threshold which is typically arbitrary. Threshold free cluster enhancement (TFCE) enhances cluster-like areas in a raw z-statistic map in a more continuous way, without the need for an initial hard thresholding (326). Each voxel value subsequently contains information not only about the strength of the raw test statistic, but also about the spatial extent of the local signal. Secondly, the statistical analysis of diffusion data is limited in that it is typically not Gaussian in nature due to both the data and its pre-processing (323). For this reason, the significance of clusters cannot be determined as the 'null distribution' for the statistical image is unknown. Similarly, methods of thresholding such as GRF cannot be applied. Instead, TBSS incorporates permutation-based methods in order to estimate the null distribution empirically by repeatedly randomising the order of subjects in the data relative to the model (327). Multiple comparison correction can also be applied

via the application of permutation testing, by building up a null distribution of the maximum test statistic across the brain, against which the actual statistic values can be tested.

1.7.3 Tractography based analysis

Tractography is the process of integrating voxelwise fibre orientations into a pathway that connects remote brain regions. It is one of the few tools available for identifying and measuring white matter pathways non-invasively and in-vivo in human subjects. All tractography techniques rely on the assumption that the diffusion of water molecules is hindered to a greater extent across a white matter axis, than along it. By sensitizing MRI to the diffusional properties of water molecules along many different orientations, one expects to see diffusion preferred in orientations that correspond to white matter orientation. Thus all tractography algorithms attempt to find paths through data fields, along which diffusion is least hindered. There are many different tractography algorithms, but these can be broadly divided into streamline and probabilistic models.

1.7.3.1 Streamline tractography

This is the simplest and earliest model of tractography. The evolution of a streamline through data acquired with the diffusion tensor model is based on the fact that as the streamline passes through a voxel, it has a tangent that is parallel to the local vector information, which is assumed to be the first eigenvector of the diffusion tensor. That is, the streamline propagates in manner parallel to the fibre orientation by using local vector information on a step-by-step basis. A mathematical differential equation can be used to describe the evolution of such a streamline (328).

$dr(s)/ds = \varepsilon_1(r(s))$

where $r(s)$ is the [x, y, z] location that is a distance s alone a streamline and ε_1 is the first eigenvector of the diffusion tensor

The errors in streamline methods are threefold. Noise in the image can disrupt estimation of the dominant diffusion directions, and the diffusion model itself (eg the tensor model) may struggle to accurately describe the orientation of complex fibre anatomy. Jones has demonstrated that these types of errors are largest in CSF and grey matter, and in white matter as pathways approach the

cortex, or where more than one fibre bundle is present in a voxel (329). Both of these types of error are common to other models of tractography. However, streamline tractography is also susceptible to errors arising from interpolation and integration errors introduced during the tractography process. Importantly, these errors accumulate or compound along the streamline. The propagation of a streamline is defined in continuous space, but the diffusion data that local fibre orientations are derived from are acquired on an imaging grid, meaning there is only one measure of orientation in every voxel. It is therefore necessary to interpolate discrete measurements into continuous space, and discretize dr(s)/ds. A variety of interpolation methods have been used. The FACT algorithm uses the 'nearest neighbour' approach where the measurement from each voxel should be applied over the entire voxel (330). Others have shown that 'smooth' interpolation approaches using fibre orientation information from all neighbouring voxels are more accurate and less error prone (331). In order to discretize dr(s)/ds , models typically approximate a continuous derivative along a small step size h. These integration errors can accumulate or compound along the streamline, though they lessen with decreasing step size, and increasingly higher order descriptions of diffusion. Given the fact that errors accumulate along a streamline, and the fact that there is no mechanism to determine the degree of confidence that can be applied to a resulting streamline, alternative empirical rules must be applied to terminate a streamline when it reaches a point of high uncertainty. Two commonly used rules are a minimum FA threshold, and a maximum curvature threshold. The rational for an FA threshold is that regions of low FA are associated with a relatively larger degree of uncertainty regarding the principal diffusion direction, and therefore a large potential error for the next streamline step. The rational of a curvature threshold is that it is biologically implausible to find bends over large angles in white matter pathways over the scale of a voxel. If such a bend occurs in a streamline, it is more likely to be due to error than the underlying white matter trajectory.

1.7.3.2 Probabilistic tractography

Probabilistic approaches to tractography differ from deterministic techniques such as streamline tractography in that they model the uncertainty associated with any resulting streamline through diffusion data. This quantification of the probability of a given streamline allows one to propagate pathways through areas of high uncertainty where deterministic approaches are likely to

accumulate errors. All probabilistic models contain a function that characterises the uncertainty in fibre orientation, otherwise known as the uncertainty orientation density function (uODF). The fibre ODF (fODF) quantifies the fraction of fibre portions (fibres may vary in orientation along their length) within a voxel with each orientation. Mathematically it is a probability distribution on a sphere, where each point on the sphere corresponds to a unique orientation. The fODF therefore contains the information needed to estimate a meaningful measure of connectivity between two regions. However, the fODF cannot be measured directly, and instead diffusion MRI measures the diffusion ODF (dODF) within each voxel. This represents the orientational structure of diffusion within the voxel. Although diffusion is least hindered along the fibre orientations, there is still significant amounts of diffusion in other directions, and the dODF is much broader than the fODF. The uODF characterises the uncertainty in making inferences of fODF from dODF. That is, it characterises the uncertainty in the exact orientation of the principal diffusion direction, or fibre orientation, within a voxel.

1.7.3.2.1 Characterisation of the uncertainty

The uODF can be estimated in a number of ways. One approach is an empirical, non-parametric statistical approach based on data resampling called bootstrapping (329). This technique is based on the concept of permutation of data samples, each associated with multi-sample measurement, in order to construct an approximation of true distribution. However, such boot strapping techniques have two limitations. Firstly, the acquisition needs to contain at least two repeats of the data in order to characterise the uODF. Secondly, each of the bootstrapped data sets is derived from the same original data sets, and this can lead to underestimation in the estimate of uncertainty. An alternative approach is wild bootstrap, which only needs a single original data set (332). In this method, a model is fitted to the diffusion signal, which provides a set of fitting residuals. The residuals are then permuted randomly across the set of diffusion signals predicted by the model to form a 'new' set of noisy measurements. The model is then fitted to this 'new' set, and by repeating the process a number of times, a distribution of model parameters can be estimated.

The second approach to estimating the uODF, is to use a Bayesian model (295,299). Using this approach, the posterior probability density function (pdf) or uODF of the model parameters given

the data and model, is proportional to the likelihood of seeing the data set at these parameter values, multiplied by prior beliefs about the model parameters. The likelihood function in the model includes a number of parametric assumptions about the noise structure, and the relationship between the data and quantities of interest. The priors pertaining to the model include physical constraints on the estimation process or spatial smoothness of the diffusion orientation. There are a variety of techniques for solving Bayes' equation and recovering the posterior distribution, but one of the most popular is the Markov Chain Monte Carlo estimation process (MCMC). This process can however be computationally expensive, and it can be difficult to ascertain when convergence on the true distribution has occurred. Both Bayesian and boot strap approaches can accommodate multifibre populations (eg multi-tensor model) when estimating the uODF. The Bayesian approach is used in the FDT tractography algorithm incorporated in the FSL software suite.

The third approach for estimating the uODF is via a process of calibration. This approach utilises an approximate relationship between the shape of the uODF, the noise in the image, and features of the diffusion profile such as the FA in a tensor model (333,334). For example it is clear that regions of high uncertainty in the principal diffusion direction in a diffusion tensor model, occur in regions of low FA. If the data acquisition characteristics are known (eg. noise, diffusion sensitisation, encoding directions etc) it is possible to link features of the data such as anisotropy or the principal diffusion direction to the uncertainty in orientation by a calibration process, using synthetic test functions. This calibrative approach is inefficient when noise, or other characteristics vary significantly between experiments. The calibrative approach is used in the PICo algorithm used in this thesis.

1.7.3.2.2 The propagation of uncertainty in tractography

The determination of the uODF in each voxel captures the expected distribution of possible fibre orientations. In each voxel there is an infinite number of possible orientations that might be followed but with different levels of probability of being the correct orientation. There are therefore an infinite number of potential paths through the data from a seed region, but with differing levels of probability. There are a number of methods that used to exploit this information in the context of probabilistic tractography.

Monte carlo streamlines

Once the uODF has been determined in each voxel, a deterministic tracking algorithm such as streamlines, is applied to the data a large number of times in a Monte Carlo fashion (295,332–334). Each run uses a randomly selected sample from each uODF in the streamline, and the front of the streamline subsequently moves forward a discrete distance. By drawing many sample streamlines from the seed region, the entire spatial probability density function (PDF) from the seed region can be constructed. This continuous spatial distribution can then be tuned into discrete probabilities by counting the number of streamlines that pass through each voxel, or a second region of interest, and then dividing that number by the total number of sample streamlines. It should be noted that the discrete probabilities will depend on the number and size of voxels in the region of interest. Probabilistic tractography is more robust to noise and regions of uncertainty than deterministic approaches, because erroneous paths resulting from noise or areas of high uncertainty, tend to disperse quickly and give low probability values. For this reason, stopping criteria are typically not used in probabilistic approaches.

Front evolution approach

To date the tractography models described take a *local* integral approach, in that they track from a seed region sequentially either through the principal diffusion direction (streamlining) or through a distribution that represents the uncertainty on the estimate of the principal diffusion direction (probabilistic tractography). Another approach is to take two regions in the brain and look for the path of least resistance to diffusion along the *whole* path. This approach is *global* in nature, and transforms the tractography problem into a global optimisation problem that can be written as the minimization of a path integral. That is, at each point on a path the tangent of that point on the path may not align with the direction of maximum diffusivity, but the overall diffusion along the path will be higher than any other path connecting the two points of interest. In practice, this problem is solved by creating spatial maps that encodes the time integrated along the shortest possible path from the seed region to every other voxel in the brain. These 3D connectivity maps are built using a technique known as front evolution (335,336). This approach attempts to grow a region at speed through the data that is modulated by the underlying directionality of the diffusion data. Once the 3D map is constructed, the 'best tract' between two regions

of interest is the fastest route between the two regions. A global approach such as this is less sensitive to the local confounding effects including noise and modelling errors. As long as a tract is optimal along its whole length, local errors have little effect.

1.8 Diffusion MRI and epilepsy

As described in earlier sections of this thesis, structural MRI is central to the assessment of individuals with refractory epilepsy. It facilitates the identification of any lesion underlying the epileptogenic zone, and if surgical treatment is considered, depicts the relationship of the epileptogenic zone to eloquent areas of the brain such as the motor, language or memory areas and critical white matter tracts.

Diffusion based MRI can provide valuable information in the evaluation of an individual with epilepsy. Studies that utilise diffusion techniques in epilepsy can be divided into those that employ ROI or whole brain methods of analysis, and those studies that use tractography. Studies using the former method have been carried out immediately or soon after a seizure (peri-ictal and postictal), and between seizures (interictal). This method can potentially identify epileptogenic areas, including those that appear normal on standard MRI sequences. Tractography may be used to map white matter tracts, and their relationship to epileptogenic tissue and eloquent cortex. This information may be used to improve surgical planning in order to minimise post-operative deficits including language and visual field loss. Both approaches also have the potential to aid understanding of the acute and chronic patho-physiological effects of seizures on the brain.

The remainder of this section reviews the literature in these areas up to 2010. Beyond 2010, the relevant literature is discussed either in this section or where appropriate in the discussion sections of each of the results chapters in this thesis.

1.8.1 The biological basis of diffusion imaging

In the brain, diffusion is restricted by intra- and extra cellular boundaries, and represents the effects of several variable, independent factors (337). These include the presence of impermeable or semi-permeable membranes, macromolecules which hinder the diffusion of small molecules, and intra- and extra cellular microcirculatory effects . The measurement of water diffusion therefore provides a means of probing cellular integrity and pathology (338).

Diffusion anisotropy in cerebral tissue is highly heterogeneous due to several factors including, the concentration of macromolecules and intracellular organelles, regional differences in the density of nerve fibres, the degree of myelination, fibre diameter and the density of neuroglial cells (339). Anisotropy in white matter results from the organization of tissue as bundles of axons and myelin sheaths run in parallel, and the diffusion of water is freer and quicker in the long axis of the fibres, than in the perpendicular direction (339). Malformations or acquired insults cause disruption to the microstructural environment, and more often than not, a subsequent reduction in anisotropy. Such abnormalities may also lead to a reduction in cell density and/or expansion of the extra cellular space, resulting in an increase in MD/ADC. Seizure-associated changes in diffusion parameters are not static, but have a dynamic profile. These changes are observed in both animal and human studies, and generally show a pattern of early postictal depression in MD/ADC secondary to neuronal and glial cell swelling, followed by normalization, or transient/ chronic elevation of the ADC/MD secondary to neuronal damage causing cell loss and gliosis (340).

1.8.2 Peri- and postictal changes in diffusion

1.8.2.1 Animal studies

A considerable body of animal data has shown that diffusion weighted MRI can visualize the histopathological changes that result from seizures in animal models. The first reported study, by Zhong et al, demonstrated a fall of 15% in the ADC in bicuculline-induced status epilepticus in rats (341). Other models have shown similar reductions in ADC values which are in proportion to the severity of seizure activity (342). Diffusion tensor imaging has also been applied to animal models. Jansen et al (343) studied rats that had undergone febrile seizures at 24 hours and 8 weeks. They found transient changes in hippocampal T2 relaxation times at 24 hours but not 8 weeks, reduced ADC at 24 hours and 8 weeks, and no FA change at 24 hours, but an increased FA at 8 weeks. Although there was no change in hippocampal volumes, histological analysis of the hippocampi and amygdala at 9 weeks showed increased fibre density in the hippocampi, and reduced neuronal surface area in the amygdala.

The ictal and post-ictal changes seen in the ADC are similar to those seen in cerebral ischaemia, and both share a common biological basis, namely the loss of membrane function and ion homeostasis.

Cerebral ischaemia leads to a failure of energy metabolism, membrane dysfunction and cell death. Sustained seizures on the other hand lead to an increased metabolic rate. This is coupled to an increase in cerebral blood flow (344), so that cellular energy values are close to normal, though in prolonged ictal activity, the increased metabolic activity may not be matched by enhanced blood flow (345). The early ADC decline seen in prolonged seizures is thought to reflect cytotoxic oedema (346), and a decrease in the extra cellular space volume fraction of up to 30% at the area of maximum neuronal activity in the cortex (347). This in turn leads to increased extracellular tortuosity and decreased diffusivity. Seizures cause increased membrane ion permeability leading to an influx of sodium, calcium and water along the osmotic gradient which cannot be compensated for by an energy deficient sodium-potassium ion ATP pump (346). Intracellular cytoskeletal fragmentation which increases intracellular tortuosity and viscosity, may also contribute to restricted diffusion (348).

While cytotoxic oedema is the most common pathophysiological effect of seizures found in cortical grey matter, vasogenic oedema has also been reported less commonly in subcortical white matter (349). Animal studies have demonstrated that seizures can also trigger acidosis and the breakdown of the blood brain barrier (350). This, together with local vasodilatory effects, can give rise to vasogenic oedema and an increase in intercellular space, and consequently diffusivity (351).

Though cytotoxic oedematous changes are not necessarily irreversible, with prolonged seizures, diffusivity and the ADC can change permanently (351). Excitotoxic mechanisms mediated by excitatory amino acids, calcium influx, ATP depletion and lactate accumulation may lead to cell atrophy and death (352). This cell lysis results in an increase in extracellular space and an increase in diffusion above normal values, which correlates with histopathological changes in both the seizure focus and secondarily affected areas (353,354).

1.8.2.2 Human studies - status epilepticus

Early clinical studies assessed diffusion weighted imaging in patients with status epilepticus, and consisted predominantly of case reports. Inevitably these studies represent an extreme in terms of seizure duration and severity, which limits their utility in assessing diffusion MRI as a tool to aid

clinical localisation in a typical epilepsy patient. In a patient with focal motor status epilepticus consisting of clonic jerking of the right leg, a 27% relative decrease in the ADC was demonstrated in the motor cortex of the right leg was demonstrated (355). There was also a 31% relative increase in the ADC of the sub-cortical white matter. This finding was thought to represent a shift of water into cortical cells at the seizure focus, and a shift of water into extracellular space in remote white matter due to vasogenic oedema (347). Similar findings in other case reports hint at the complex osmotic relationship between epileptogenic and surrounding areas, and cytotoxic and vasogenic oedema (356,357). A small series has corroborated these results, and reported cortical ADC reductions of up to 36% during partial status epilepticus (358).

Early clinical reports also suggested that there were significant correlations between the areas of diffusion abnormalities, and increased perfusion and electrocorticographic abnormalities (359–361). In a study of 10 patients with complex partial status epilepticus there was correlation between focal swelling and hyperintensity on T2 weighted images and increased signal on DWI images (344). ADC values were reduced by 11 to 37%, and there was a close spatial correlation of diffusion weighted and perfusion imaging (PI) changes, hyperperfusion on SPECT, and localization of EEG focus. These abnormalities normalized in most patients by day 14. In other studies however, DWI revealed abnormalities in several different regions, and it was problematic to differentiate changes in areas of seizure focus, and changes in the epileptic cortical and sub cortical networks that underlie seizure spread (358,362). The authors therefore concluded that it would be difficult to locate the epileptogenic focus using DWI and PI alone.

1.8.2.3 Human studies - single seizures

There are more reported studies of diffusion imaging following (rather than during) single seizures. The interpretation of these studies is limited by a number of factors. These include, small numbers of heterogeneous patients, varying methods of analysis (including ROI and whole brain voxel based methods), lack of control groups or follow-up scanning, and wide variability in the duration of both seizure, and interval from seizure to scan. The major studies are summarised in table 1.12.

Diehl et al (363) carried out one of the first postictal series. Their results (see table 1.13) suggested that postictal DWI may help delineate epileptic areas in a minority of patients with TLE. The yield was low in patients with HS and single short seizures, and higher in patients with tumor or status epilepticus. Salmenpera et al used DWI to study changes in diffusivity after single seizures (364). In 21 patients with intractable focal epilepsy, postictal decreases were found in 52% seizures, but in 17% of seizures there were increases in MD. The analysis used voxel based methods to include data from the whole brain, and the resulting spatial distribution of diffusion changes was complex, with postictal changes in MD often being found distant to the putative seizure focus. This implied involvement of a widespread epileptic network, and not a single focus. The increases in MD, which were detected together with the decreases in postictal scans that were acquired soon after seizures, were thought to be due to vasogenic oedema. Concordance with the presumed epileptogenic focus was seen in only four patients, all of whom had postictal scans within 45 minutes of seizure onset. Repeated postictal scans showed a gradual return to baseline for both the increases and decreases in MD.

In an effort to minimize the delay between seizure and scan, Konermann et al (365) administered intravenous flumazenil, shortly before scanning. They consistently demonstrated significantly reduced ADC in hippocampi and parahippocampal gyri, ipsilateral to the seizure onset, in a series of 10 patients with refractory TLE. Further work by the same group without the use of flumazenil, identified diffusion changes postictally in only two out of nine patients, in whom complex partial seizures were of duration greater than 60 seconds, and seizure to scan time was less than 15 minutes. Generalized seizures were associated with global ADC change (366). The results of the original study may therefore have been confounded by the effect on flumazenil on haemodynamics, and in any case, flumazenil is not routinely used in clinical practice.

These studies suggest that the diffusion changes visualized with MRI after single seizures are more transient than those after status epilepticus, and are complex in terms of their distribution and evolution of change. The inherent difficulties in scanning patients directly after seizures, the evident involvement of a cerebral network and not of a single focus, and the physical limitations of spatial resolution limit the sensitivity of the technique in the localization of seizure foci.

Technological advancements such as, real time motion correction, open access scanners, and fast acquisitions may overcome these limitations and result in post-ictal diffusion MRI becoming a useful clinical tool.

Table 1.13 – Post-ictal diffusion studies

Authors	Findings
Diehl et al 2001 (363)	• 9 TLE patients scanned (7 with HS, 1 with tumour, 1 cryptogenic) 45 to 150 minutes after EEG-documented seizure • 2/7 TLE-HS had co-localising significant ↓ADC compared with contralateral side (one of the two was in status epilepticus) • Areas of diffusion change maximal adjacent to hippocampus (unclear if seizure onset or seizure spread zone)
Hufnagel et al 2003 (366)	• 9 refractory TLE patients scanned 2 to 210 minutes after seizure • Interictal ADC significantly elevated in affected hippocampus in all TLE patients • 2/9 patients had significant ↓ADC postictally compared to interictally and changes co-localised with postulated seizure focus
Konermann et al 2003 (365)	• 12 refractory focal epilepsy patients (10 with TLE) scanned before and after injection with flumazenil • At baseline TLE patients had ↑ADC in ipsilateral hippocampus compared with controls • Significant ↓ADC in all TLE patients postictally compared with interictally • Changes co-localised with seizure focus in TLE patients - ipsilateral hippocampus and parahippocampal gyrus
Oh et al 2004 (367)	• 9/14 patients had significant ↓ADC postictally compared to interictally • Changes co-localised with postulated seizure focus • Significant difference seen only in patients with neocortical ictal onset zones or in neocortical temporal portion of temporal lobe – authors hypothesise this is due to interictal chronic ↑ADC in hippocampus of mTLE patients masking any post-ictal decrease
Diehl et al 2005 (368)	• 18 refractory focal epilepsy patients (3 with TLE) scanned with DTI 30 to 300 minutes after seizure • VBM used for analysis • 13/18 had significant ↑MD in interictal image compared to controls • 9/18 patients had significant ↓MD postictally and in 6 of these patients was epileptic focus known • In 3/6 patients presumed epileptogenic zone co-localized with the area of MD decrease • No changes in FA seen suggesting that single short seizures cause changes in cell hydration but not the directionality of diffusion
Salmenpera et al 2006 (364)	• 21 refractory focal epilepsy (12 with TLE) patients scanned median interval of 53 minutes after seizure • VBM used for analysis • Focal diffusion changes (significant ↑ or ↓ in MD) seen in 52% of seizures postictally compared with interictally • Changes co-localised with postulated seizure focus in 4 patients • Repeated postictal scanning in 8 patients after further medial interval of 46 minutes showed postictal diffusion changes resolving

1.8.3 Interictal studies

Interictal studies of diffusion MRI applied to patients with epilepsy have concentrated on two broad areas. Most have explored the utility of diffusion imaging in determining the location, and extent of the epileptogenic zone, particularly in patients who have no abnormalities on standard structural MRI. This information has implications both for targeting potential epilepsy surgery, and its outcome. More recently, studies have assessed the nature and extent of changes in white matter in TLE, and how these might relate to both seizures and function.

1.8.3.1 The epileptogenic zone

1.8.3.1.1 TLE and HS

Early interictal diffusion imaging studies of patients with epilepsy, concentrated on MTLE and HS using ROI based techniques, and found increased average ADC values in sclerotic hippocampi, compared with the contralateral side and control subjects. This suggested structural disorganization and an expansion of extra cellular space, and was thought to reflect neuronal loss, reduction of dendritic branching, and microstructural changes associated with epileptogenesis (369–373). Studies using high resolution diffusion imaging and the tensor model replicated these findings and have also found lower FA values in the ipsilateral hippocampus compared to healthy control subjects, though to a lesser magnitude than mean diffusivity changes (374,375). Given the fact that the hippocampi are already visibly abnormal on structural MRI, interest subsequently developed in the utility of diffusion parameters as a prognostic tool for surgery. The evidence for this is mixed, with some studies suggesting ADC measures may be a useful independent post-operative prognostic indicator (376), and others reporting the opposite (377).

1.8.3.1.2 TLE and normal MRI

Diffusion based studies have also reported abnormalities in the diffusion parameters of hippocampi ipsilateral to seizure onset in patients with MTLE, which are normal on conventional MR (378). However, diffusion derived measurements alone do not have sufficient power as a diagnostic tool to lateralise pathology in this patient group. Londono et al showed that the combination of hippocampal volumetry and ADC asymmetry measurements was more sensitive to accurate seizure

localization in patients with mesial TLE, than either technique alone (379). Wehner et al (380) assessed 22 patients with TLE who underwent ATLR, and found that in the 14 patients with MRI defined hippocampal sclerosis, the ADC was significantly greater in the ipsilateral HC compared with the contralateral side, and could be used to lateralize the seizure focus. In the remaining patients without HS, the ADC of the hippocampi were not significantly different to the contralateral side, but were significantly less than in controls. Analysis of the resected specimens confirmed hippocampal sclerosis in those MR positive patients, but revealed gliosis only without any apparent neuron loss or hippocampal sclerosis in the MR negative group. The authors postulated that bilateral temporal lobe abnormalities in patients with TLE might explain why diffusivity did not provide lateralizing information in patients with non-lesional MRI, and this appears to be have been borne out by other similar studies (381).

1.8.3.1.3 Acquired lesions

Diffusion tensor imaging is also sensitive to patients with epilepsy and non-progressive acquired lesions such as head injuries, cerebral ischaemic lesions and perinatal hypoxia (198,382). Areas of increased MD and decreased FA correlate with abnormalities identified on visual inspection of conventional MR imaging, and are concordant with neuronal loss, gliosis and structural disorganization. Moreover, diffusion imaging can often pick up areas of pathology beyond the conventional margins of acquired lesions seen on standard MRI, again suggesting additional sensitivity from diffusion based imaging (198).

1.8.3.1.4 Developmental lesions

Diffusion MRI may also be applied to patients with epilepsy and malformations of cortical development (MCD). Eriksson et al used a voxel based method to assess the whole brains of 22 patients with several types of MCD (383). Fifteen and eight patients had reduced anisotropy and increased diffusivity within the MCD respectively, which suggests a loss of directional organisation and relatively preserved cell density. Moreover, diffusion abnormalities were also found beyond the margins of the evident MCD in areas that appeared normal on conventional MRI. Consistent with these findings, Dumas et al used a ROI based method to assess both areas of MR visible abnormality, and normal appearing cerebral tissue in 15 patients (384). They identified

significantly reduced anisotropy in normal appearing white matter adjacent to, and 2-3 cm distant from several types of cerebral lesion, including MCDs. Histological examination of resected normal looking tissue revealed the presence of occult abnormalities such as gliosis, infiltrative tumour cells and axonal loss. Together these findings suggest that diffusion imaging can often pick up areas of pathological abnormality beyond the conventional margins seen on standard MR images, which has implications for the surgical resection margins of these areas. More recent studies using other functional modalities in correspondence with diffusion MRI, appear to corroborate that diffusion parameters may correlate not only with the epileptic lesion zone, but also the epileptogenic zone in patients with visible MCDs. Widjaja et al, using ROI based techniques and several diffusion parameters (FA, MD and the three eigenvalues) demonstrated that up to 6 out of 8 patients with visible MCD had diffusion abnormalities that correlated with MEG dipole clusters (385). Similarly Lippe et al demonstrated correlations in 8 children between grey matter hypometabolism in the seizure onset zone on PET studies, and diffusion parameters (FA, ADC, parallel and perpendicular diffusivity) in adjacent white matter (386).

1.8.3.1.5 Cryptogenic epilepsy

Interictal diffusion imaging may also contribute to the identification of focal abnormalities in patients with focal epilepsy, and unremarkable conventional MRI. In one of the earliest studies using whole brain analysis techniques, increased diffusivity was found in eight patients and reduced anisotropy was found in two patients out of a total of 30 patients with refractory focal epilepsy, and unremarkable conventional MRI (198). In seven, the areas of abnormal diffusion corresponded with the localization of EEG focus. A group analysis of the nine patients with electro clinical seizure onset localizing to the left temporal region revealed a significant increase in diffusivity, and reduction in anisotropy within the white matter of the left temporal lobe. The areas of abnormal diffusion were postulated to be caused by disruption in the microstructural environment due to aetiological factors such as occult dysgenesis, or acquired damage, or as a result of repeated seizures leading to neuron loss, gliosis, and expansion of the extra cellular space. This study suggested that diffusivity is a more sensitive diffusion index than anisotropy for identifying occult abnormalities in patients with normal, conventional MRI. This may represent expansion of the extra cellular space but retention of the overall structural organization of the

white matter tracts. A patient from this study, with cryptogenic frontal lobe epilepsy, had focally increased MD in the right frontal lobe. Subsequent intracranial EEG concluded that this was the area of seizure onset, and led to a resection. Histopathologic examination of the resected specimen showed marked white matter gliosis, associated with structural disorganization, and expansion of the extra cellular space (387). Six years after surgery, seizures had been reduced by more than 50% the preoperative rate.

Subsequent studies have substantiated these findings, and investigated the correlation between DTI measurements and stereo-electroencephalographic (SEEG) recordings in patients with cryptogenic focal epilepsy (388,389). These studies have found good spatial concordance between epileptiform activity on EEG and diffusion abnormalities in nearly 50% (6/13 and 4/9 respectively) patients. They also found again that diffusivity, rather than anisotropy measures, correlated better with electroclinical data. Furthermore, in those patients who have undergone surgery for their epilepsy, this has often translated into a good postoperative outcome, suggesting that while DTI alone cannot localize epileptogenic or epileptic lesion zones, it can provide additional information over conventional MRI in the identification of occult abnormalities. When this information is combined with other imaging modalities the epileptogenic zone can be more precisely defined. Thivard et al (390) studied 20 patients with cryptogenic epilepsy, all of whom had had intracranial EEG to localize the epileptogenic zone. The sensitivity and specificity of interictal PET, and VBM applied to structural and DTI data in individual patients were compared. PET had the greatest sensitivity (75%), compared to DTI (40%) and structural (35%) analysis. However, DTI had a greater specificity (60%) compared to both PET (35%) and structural data analysis (30%). The authors concluded that combining PET and DTI in cryptogenic cases was the most efficient strategy for highlighting pertinent abnormalities that co-localised with the intracranial EEG data.

Despite the encouraging nature of these results, it is important to note that in several of the aforementioned studies, details of the 'conventional' MRI sequences used were not available. Tertiary referral centres can increase their diagnostic yield in patients with refractory epilepsy, with the use of epilepsy specific, high-resolution volumetric imaging (186). In those cases that remain 'MR negative' after such imaging, interictal diffusion imaging may have a role to play. The

derivation of quantitative diffusion parameter maps and their analysis either by ROI or VBM methods provides a useful tool in the localization of subtle structural abnormalities. However, care is needed as a number of different diffusion parameters have been used in the aforementioned studies, and yet their biological underpinnings are not yet fully understood. Therefore diffusion imaging is best utilized as part of a multimodality evaluation that should include interictal and ictal EEG recordings, neuro- psychiatric and psychological evaluations and other imaging modalities such as PET, SPECT or magnetoencephalography (MEG).

1.8.4 Tractography

Tractography has been increasingly used in patients with epilepsy in order to image white matter tracts and their relationship with both the epileptogenic zone and eloquent cortex. Tracts can also be treated as ROIs for further quantitative and qualitative assessment in order to understand the effect of seizures on brain structure, function and development. Furthermore, the use of tractography in this manner, can help to improve surgical planning and minimise postoperative deficits in language and vision. To date, most studies have concentrated on the application of this technique to TLE, which is the most common epilepsy syndrome, and this will be the focus of the remainder of this chapter.

1.8.4.1 Microstructural white matter changes in TLE

Traditionally TLE-HS has been thought of as an epilepsy syndrome where structural changes are limited to the hippocampus itself. With the development of advanced techniques such as quantitative MRI and MR volumetry (86), MR spectroscopy (391) and VBM (392), it is evident that structural abnormalities are more widespread than demonstrated by conventional MRI. Tractography based studies appear to support this consensus. In one of the first studies to use tractography, the authors segmented two white matter pathways, the fornix and cingulum, in patients with TLE and unilateral HS and reported a bilateral reduction in FA in both limbic structures (393). Given that there are direct connections between the hippocampus and these limbic structures, the authors speculated that their results might reflect downstream axonal Wallerian degeneration from the primary site of pathology in the hippocampus. A further study by the same group comparing patients with TLE and HS and those without HS, is supportive of this

hypothesis. They found that while patients with TLE but without mesial temporal sclerosis have widespread changes in white matter, these changes were not as extensive or as severe as those seen in TLE with mesial temporal sclerosis (394). Other groups have also put forward the hypothesis of downstream degeneration. Kim et al (395) used ROI based techniques applied to the splenium of the corpus callosum, and demonstrated reduced FA values compared to controls. However, they then applied tractography to this area, and demonstrated direct connections to the temporal lobe. From this they inferred that extra-temporal changes in microstructure may represent downstream white matter degeneration, secondary to the primary injury. One issue that has arisen from these studies is whether the changes in diffusion parameters reflect genuine, underlying structural changes, or are secondary to seizure activity. While some studies have demonstrated correlations between white matter DTI findings and duration of epilepsy (396,397), other studies have failed to demonstrate such a correlation (398–400). Concha et al (401) attempted to address this problem by assessing a group of patients with unilateral TLE who underwent surgery and were seizure free for a year after surgery. They found that the abnormalities in diffusion parameters persisted, and therefore concluded that the diffusion findings might reflect white matter microstructural changes, which may even predispose individuals to the development of TLE.

Diffusion based studies using manual ROI and whole brain techniques have also added to the weight of evidence suggesting that unilateral TLE is associated with widespread changes. Arfkanis et al (398) published the first study of DTI in 15 TLE patients, and applied simple ROI based techniques to structures outside of the temporal lobe, namely the internal and external capsule and corpus callosum. They reported lower FA in many of these structures compared to controls, but duration of epilepsy was not correlated with the diffusion indices from any of the structures. Gross et al (400) using identical methods also demonstrated bitemporal and extratemporal abnormalities in 11 patients with TLE and HS. Again they found no correlation with the duration of epilepsy, and in addition the diffusion abnormalities bore no relation post-operative seizure outcome. Whole brain techniques by their very nature are able to assess areas beyond the ipsilateral temporal lobe, and have also demonstrated bilateral changes together with extratemporal abnormalities. Thivard et al (399) were the first to perform a VBM analysis of DTI data in 31 patients and 36 controls.

Three areas of abnormality were identified; increased MD in the ipsilateral hippocampus and temporal structures, associated with a decreased FA; decreased MD in the contralateral hippocampus, amygdala and temporal pole; and finally a decreased FA in ipsilaterally in posterior extratemporal regions. None of the abnormalities correlated with clinical parameters such as duration of epilepsy, age of onset, or seizure frequency. The authors suggested that structural or functional abnormalities (metabolic changes, subtle structural lesions) might extend beyond the seizure onset zone in unilateral mesial TLE associated with HS.

1.8.4.2 Language networks

In addition to assessing the effect epilepsy may have on white matter microstructure, tractography can also be used to elucidate aspects of neuronal plasticity, or structural reorganisation secondary to epilepsy. When combined with functional data it provides an opportunity to understand the relationship between structure and function in patients with TLE. The lateralisation of language is a well-recognised aspect of brain function. fMRI studies have shown that about 95% of right handed subjects are left-hemisphere dominant for language, and greater atytpical (bilateral or right hemisphere) is seen in left-handed subjects (402). fMRI studies have also shown that there is a higher incidence of atypical language dominance in preoperative left TLE patients (403). Overall these findings suggest that dominant hemisphere lesions can cause reorganisation of language to the contralateral hemisphere. Tractography in healthy control subjects has demonstrated that the connections between Broca's and Wernicke's area are lateralised, with stronger connections in the left hemisphere (404). Subsequently, Powell et al (405)combined fMRI and tractography in patients with unilateral TLE, and in controls. Verb generation and reading comprehension paradigms were used to define functional regions, which were used to generate starting regions for tractography. Tractography was carried out using diffusion images acquired with a high angular resolution technique, and a probabilistic algorithm. Controls and right TLE patients had a left-lateralised pattern of both language related activations, and associated white matter organisation. Left TLE patients showed more symmetrical language activations, along with reduced left hemisphere and increased right hemisphere white matter pathways, in comparison with both controls and right TLE patients. Correlations between measures of structure and function in both left and right TLE patients were found, with subjects with more lateralised functional activation

having more lateralised white matter pathways. The correlation between structure and function in TLE patients has been reported by other groups in a similar study (406), and in controls (404). In view of this correlation, other groups have explored whether tractography may provide a means of lateralising language independent of fMRI. Ellmore et al (407) using Wada lateralisation as a gold standard determined that a DTI derived asymmetry index of the arcuate fasciculus was about 10% less accurate than fMRI in lateralising language in epilepsy patients. The study is limited by the heterogeneous patient population, not all of whom had TLE. Yet it suggests that diffusion MRI may have a role to play in language lateralisation in patients unable to undergo fMRI, and may be synergistically combined with fMRI. Ultimately, given the cross-sectional nature of these studies it is difficult to elucidate whether functional reorganisation leads to structural reorganisation, or whether structural changes occur as a result of HS or seizures, and serve as an anatomical substrate upon which atypical language function develops. Longitudinal studies are needed in order to answer these questions.

In addition to a better understanding of the effect of epilepsy on structure and function of language, tractography may also have a role in the prevention of postoperative language deficits. A study has demonstrated that preoperative knowledge of language connections, enables the prediction of language decline following ATLR (408). In this study a significant correlation was demonstrated between lateralisation of language connections prior to dominant-hemisphere ATLR and postoperative language decline. That is, those patients with more extensive connections ipsilateral to the side of resection suffered a greater language decline. The authors of this study also demonstrated a correlation between age of onset of epilepsy and lateralisation of connections, such that the earlier the age of onset, the more bilateral the connections, which appeared to be protective against postoperative decline.

1.8.4.3 Visual pathways and preoperative planning

ATLR can also cause clinically significant visual field defects (VFD) in up to 10% of patients. Indeed, in 5% it can be severe enough to render the patient ineligible for a driving license, despite being seizure-free (409). Typically, VFDs after ATLR occur in the superior homonymous field contralateral to the resection and are due to disruption of fibres of Meyer's loop. The anterior

extent of the Meyer loop is not visualized on conventional imaging and varies from person to person (410). As a consequence the occurrence and extent of a postoperative VFD cannot be accurately predicted by conventional MRI, or from the extent of resection performed. Tractography has been used to demonstrate the optic radiation in normal subjects (411), and has been applied to pre- and post-operative surgical patients with AV malformations and tumours in and around the visual pathways. Kikuta et al (412) carried out pre- and post-operative tractography in 10 such patients, and were able to predict the magnitude of pre- and post-operative visual field loss from the geometrical relationship between the optic radiation and AV malformation. A recent study demonstrated application to temporal lobe surgery for epilepsy. The optic radiation was visualized before and after ATLR, and disruption of Meyer's loop was demonstrated in a patient who developed a quadrantanopia (413). In a similar vein, other studies have demonstrated the utility of tractography in the resection of neoplasms that are in close proximity to eloquent subcortical white matter tracts (414). There are however, technical challenges to be overcome, to enable the co-registration of pre-operative tractography with the T1-weighted MR images used to guide neurosurgical interventions. When these are surmounted, preoperative tractography of the optic radiation and other vital white matter connections, will be able to be displayed when planning and undertaking surgical procedures (415). Further, the advent of per-operative MRI will allow the correction of the movement of tracts caused by craniotomy, and will improve the accuracy of the data, to aid surgical planning and result in a lower risk of post-operative deficits.

2 Common Methods

2.1 Introduction

This chapter describes the methodology that was common to the studies described in the subsequent chapters. Information is provided on subject recruitment, MR data acquisition, and diffusion MRI analysis. The following results chapters refer back to this section. Where a particular method was used only in a single study it is included in the relevant chapter, along with any other related information.

2.2 Subject recruitment and ethics approval

Patients were recruited from the epilepsy clinics at the National Hospital for Neurology and Neurosurgery, London, UK, and the National Society for Epilepsy, Chalfont St Peter, UK. All had medically refractory TLE and were undergoing pre-surgical evaluation at the National Hospital for Neurology and Neurosurgery. Further details on patient demographics, neurological and neuropsychological test results, and surgical outcome data are included in each chapter where relevant. All the control subjects were English-speaking healthy volunteers with no history of neurological or psychiatric disease. All studies were approved by the National Hospital for Neurology and Neurosurgery and the Institute of Neurology Joint Research Ethics Committee, and informed written consent was obtained from all subjects.

2.3 Acquisition of clinical data

All patients had undergone structural MRI (185) and hippocampal volumetry according to a previously published protocol (189). All patients underwent video-EEG, and were on anti-epileptic medication. Handedness was determined using the Edinburgh Hand Preference Inventory (416). The frequency, type and date of last seizure as well as current medications were determined in all patients each time they were scanned. All patients had a baseline standardised neuropsychological assessment and in those undergoing surgery, this was repeated postoperatively (417). Specific components of the neuropsychological assessment were used in this thesis, and are described within the relevant results chapters.

2.4 MR data acquisition

All MRI studies except for those in chapter 3 were performed on a 3T GE Excite II scanner (General Electric, Wakashua, Milwaukee, Wisconsin, USA). Standard imaging gradients with a maximum

strength of 40mTm-1 and slew rate 150Tm-1s-1 were used. All data were acquired using a body coil for transmission, and 8-channel phased array coil for reception. The scanning protocol also included a coronal T1-weighted volumetric acquisition sequence with 1.1mm-thick slices, and hippocampal volumes were determined using a previously described method (189). All MRI acquisitions, both structural and diffusion, were repeated post-operatively in those patients who underwent surgery.

2.5 Diffusion tensor imaging acquisition

The DTI acquisition sequence was a single-shot spin-echo planar imaging (EPI) sequence, cardiac gated with TE=73ms, TR of 30 RR with triggering occurring on every QRS complex. Sets of 60 contiguous 2.4mm-thick axial slices were obtained, covering the whole brain, with diffusion sensitizing gradients applied in each of 52 non-collinear directions (maximum b value of 1200mm2s-1 (δ=21ms, Δ=29ms, using full gradient strength of 40mTm-1)) along with 6 non-diffusion weighted (b=0) scans. The gradient directions were calculated and ordered as described elsewhere (418). The parallel imaging factor (SENSE) was 2. The field of view was 24cm, and the acquisition matrix size was 96x96, zero filled to 128x128 during reconstruction so that the reconstructed voxel size was 1.875 x 1.875 x 2.4 mm3. The DTI acquisition time for a total of 3480 image slices was approximately 25 minutes, depending on subject heart rate. During the acquisition, radiographers routinely checked for gross head movement in real time. Data that suffered from significant movement artefact were excluded from analysis. High-resolution echo planar imaging (HR-EPI) images were also acquired with geometric distortions to match those of the DTI data, and used primarily in chapters 3 and 7 (419).

2.6 Diffusion tensor imaging analysis

The diffusion MRI data was analysed using a variety of methods. These included whole brain analysis methods based on VBM as implemented in SPM (318) and TBSS as implemented in FSL (324). We also used tractography based analysis methods including the PICo algorithm as implemented in the Camino package (333,420,421), and the FDT algorithm as implemented in FSL (295,422). The specific details pertaining to each method employed are described in the relevant results chapters.

2.7 Statistical analysis

All statistical analyses were carried out using SPSS v16 and v18 (backwards compatible).

3 Connections of the Medial Temporal Lobe and Material Specific Memory Impairment in Unilateral Temporal Lobe Epilepsy

This chapter describes a study using diffusion tractography to study the connections of the medial temporal lobe in a group of normal subjects, and patients with temporal lobe epilepsy. The material in this chapter has been published (see publications section).

3.1 Objectives

The aim of this study was to delineate the main connections of the parahippocampal gyrus (PHG), a white matter pathway located in the medial temporal lobe that is closely related, structurally and functionally, to the hippocampus. We hypothesised that in patients with TLE these connections would be impaired ipsilateral to the seizure focus, and that the degree of any such impairment would correlate with material specific memory function.

3.2 Introduction

The structural connections of the hippocampus and the medial temporal lobe to the rest of the brain are of significant interest. Parahippocampal structures are critically implicated in the generation and propagation of seizures in TLE (423,424), and are essential for declarative memory (425). As described in chapter 1, longitudinal neuropsychological studies have shown that persisting epilepsy is associated with progressive memory impairment. Those who undergo anterior temporal lobe resection (ATLR) are at further risk of memory impairment, the nature of which depends on whether surgery is on the language dominant or non-dominant side.

Neuropsychological assessment, quantitative MRI, and latterly functional MRI (fMRI) indicate the role of the medial temporal lobe structures (MTL) in sustaining material specific memory functions (426), and the reorganisation of memory that occurs with TLE (427). These and lesion deficit studies (428,429) have shown that memory deficits in TLE and after ATLR are related to the *functional* integrity of the parahippocampal structures. However the structural integrity of the parahippocampal gyrus in TLE has not been evaluated, or related to function.

As described in chapter 1, the parahippocampal gyrus has direct and extensive connections with the hippocampus and dentate gyrus, and acts as the mediator of translation of temporary hippocampal information storage to a more permanent storage in cortical association areas (430). A study by Powell et al (431) used tractography to map connections from a seed point in the anterior PHG in healthy controls. It demonstrated connectivity between the PHG and anterior temporal lobe, orbitofrontal areas, and posterior temporal and extrastriate occipital areas in healthy control subjects. Direct connections between the hippocampus and parahippocampus were also visualised in this study. These findings are consistent with animal tracer studies, which have demonstrated that there are widespread connections from sensory-specific and multimodal association cortices that converge on the parahippocampal gyrus (432–434). For these reasons, the parahippocampal gyrus is potentially of interest in the assessment of patients with TLE. The structural white matter connections of an epileptic focus may underlie epileptogenic networks, and spread of epileptiform activity within those networks. In addition, the integrity of white matter tracts connecting cortical areas sub serving cognitive functions such as memory, may be necessary for normal function. A better understanding of the white matter changes present in patients with TLE may lead to the development of surrogate markers of treatment outcome, and improved patient selection for, and planning of, epilepsy surgery. This in turn in may maximise the chance of seizure remission, and minimise the risk of cognitive impairment.

3.3 Methods

3.3.1 Subjects

We studied 18 patients (median age 33.5 years; range 22-47 years; 11 males) with medically refractory TLE undergoing pre-surgical evaluation at the National Hospital for Neurology and Neurosurgery, London, UK. All patients had undergone structural MRI at 1.5T (185). Of the eight left TLE patients, seven had hippocampal sclerosis (HS) (one also had a ganglioglioma in the left fusiform gyrus) and one had a MTL dysembryoblastic neuroepithelial tumour (DNET). Of the ten right TLE patients, seven had HS, one had a right MTL glioma, another had a right MTL DNET, and the other had right superior temporal focal cortical dysplasia (FCD). Video-EEG had confirmed seizure onset in the MTL ipsilateral to the clinically defined seizure site, and all patients had a normal, contralateral hippocampus based on qualitative and quantitative MRI criteria (435).

All patients were on anti-epileptic medication, and were fluent English language speakers. Handedness was determined using the Edinburgh handedness inventory (416), and language dominance was determined using a range of fMRI tasks which have been described previously and include the use of verbal fluency, and reading tasks (404). All patients underwent a standardised pre-surgical neuropsychological assessment (436). Patient demographics, neurological test results, and surgical outcome data are listed in table 3.1. The ILAE classification of post-operative seizure outcome following epilepsy surgery was used (437). We also studied 10 right-handed native English speaking, healthy volunteers (median age 29.5 years; range 23 to 50 years; 7 female) recruited locally at our institution. The study was approved by the National Hospital for Neurology and Neurosurgery and the Institute of Neurology Joint Ethics Committee, and informed written consent was obtained from all subjects.

3.3.2 MR data acquisition

MRI studies were performed on a 1.5T GE Signa Horizon scanner (General Electric, Wakashua, Milwaukee, Wisconsin, USA). Standard imaging gradients with a maximum strength of $22mTm^{-1}$ and slew rate $120Tm^{-1}s^{-1}$ were used. All data were acquired using a standard quadrature birdcage head coil for both RF transmission and reception. The scanning protocol also included a coronal T1-weighted volumetric acquisition sequence with 1.5mm-thick slices, and hippocampal volumes were determined according to a previously described method (438).

3.3.3 Diffusion tensor imaging

The DTI acquisition sequence was a single-shot spin-echo planar imaging (EPI) sequence, cardiac gated (triggering occurring every QRS complex) (439), with TE=95ms. Sets of 60 contiguous 2.3mm-thickness axial slices were obtained, covering the whole brain, with diffusion sensitizing gradients applied in each of 54 non-collinear directions (maximum b value of $1148mm^2s^{-1}$ (δ=34ms, Δ=40ms, using full gradient strength of $22mTm^{-1}$)) along with 6 non-diffusion weighted (b=0) scans. The field of view was 24cm, and the acquisition matrix size was 96x96, zero filled to 128x128 during reconstruction so that the reconstructed voxel size was 1.8 x 1.8 x 2.3 mm^3. The

DTI acquisition time for a total of 3600 image slices was approximately 25 minutes (depending on the heart rate).

We used the method of Parker and Alexander (333,420) to reduce fibre orientation ambiguities in voxels containing fibre crossings. Voxels in which the single tensor fitted the data poorly were identified using the spherical-harmonic voxel-classification algorithm of Alexander et al (293). In these voxels a mixture of two Gaussian probability densities was fitted and the principal diffusion directions of the two diffusion tensors provided estimates of the orientations of the crossing fibres (440). In all other voxels a single tensor model was fitted. For all voxels, fractional anisotropy (FA) maps were generated from the single tensor fit (286,290).

3.3.4 Tractography

All scans were transferred to a Unix workstation for processing. We used the PICo algorithm extended to cope with crossing fibres (333,420) to track from anatomically defined regions of interest (ROIs) within the parahippocampal gyrus. This algorithm adapts the commonly used streamline approach to exploit the uncertainty due to noise in one or more fibre orientations defined for each voxel. This uncertainty is defined using probability density functions (PDFs) constructed using simulations of the effect of realistic data noise on fibre directions obtained from the mixture model (333). The streamline process is repeated using Monte Carlo methods to generate maps of connection probability or confidence of connection from the chosen start region(s).

The anatomical definition of the ROI was based on a previously published tractography analysis of the parahippocampal gyrus in healthy subjects (431). Viewing the FA images in three orthogonal planes using MRIcro (http://www.psychology. nottingham.ac.uk), the centre of the white matter tract just anterior to the brainstem, and posterior to the cerebral peduncles was selected, such that the parahippocampal gyrus was defined at its longest in the corresponding sagittal view (figure 3.1). The corresponding coronal slice was then used to select two adjacent voxels in a left-right direction, such that they both lay within the white matter tract on axial and sagittal views. This process was repeated in one anterior and one posterior coronal slice. This method was chosen as

the parahippocampal gyrus runs anterior to posterior, inferior to superior and medial to lateral within the medial temporal lobe. The principal eigenvector of each voxel, when viewed using PICo and projected on the axial plane was orientated anterior-posterior. A threshold of FA ≥ 0.1, and curvature threshold of 180° were set for tractography.

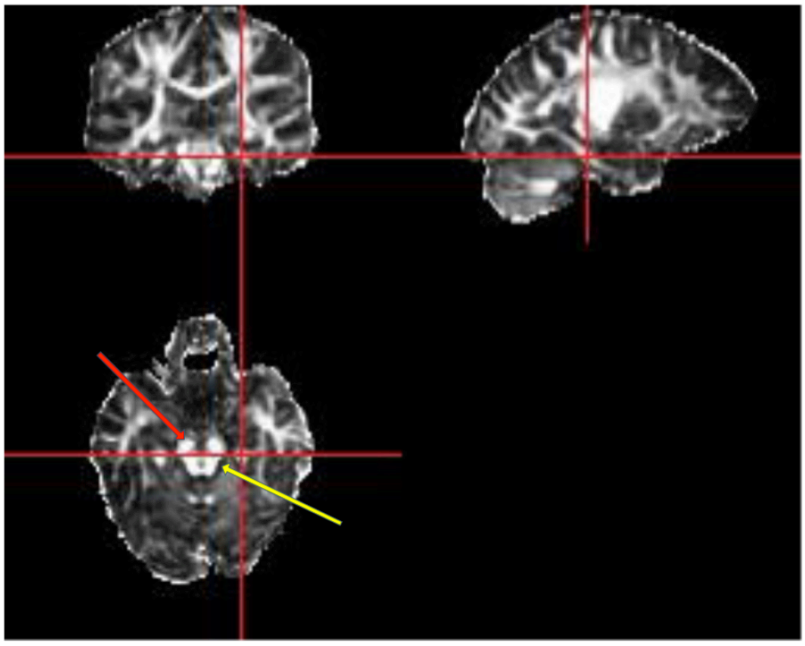

Figure 3.1 - Axial, coronal and sagittal views of a single subject FA map. The red arrow points towards the cerebral peduncles, and the yellow arrow points towards the brainstem. The white matter of the parahippocampal gyrus is readily identifiable in the crosshairs in all three corresponding views.

Table 3.1 – Clinical data for all patients

	Age/ gender	Handedness	Age of epilepsy onset (years)	Duration of epilepsy (years)	Seizure types and frequency (per month)	Post-op outcome (ILAE Class)	MRI and pathological diagnosis	Clinical and EEG diagnosis	Right HV (cm^3)	Left HV (cm^3)	Hippocampal volume ratio (%)	Total intracranial volume (cm^3)	AEDs (mg/day)	Language dominance
1	25/F	Right	17	8	CPS 8 SGTC 0.5	1	Left HS	Left TLE	2.73	1.35	49.5	1690	TPR 150 LTG 200	Left
2	37/M	Left	1	36	SPS 12 CPS 4	2	Left HS	Left TLE	3.3	1.88	56	1750	VPA 800 CBZ 800 LVT 2000	Left
3	33/M	Right	1	32	SPS 4 CPS 4	1	Left HS	Left TLE	2.83	2.02	71	1650	PMD 500 CBZ 1200 CLB 10 TPR 175 LVT 4000	Left
4	32/F	Right	22	10	SPS 30 CPS 5 SGTC 0.25	N/A (Died)	Left HS	Left TLE	2.36	1.79	75.9	1530	OXC 1050 TPR 200	Left
5	28/M	Right	3	25	CPS 1	1	Left HS	Left TLE	3.08	1.42	46	1710	LVT 3000 LTG 600	Left
6	31/M	Right	10	21	CPS 50 SGTC 3	1	Left MTL DNET	Left TLE	3.73	3.8	98	1870	CBZ 1200 CLN 1.5 LTG 100	Left
7	34/M	Right	21	13	CPS 5	(No surgery)	Left HS	Left TLE	2.23	1.9	85	1720	LVT 2000 VPA 2000	Left
8	37/F	Right	1	36	SPS12 CPS8 SGTC 1	3	Left HS, L fusiform gyrus ganglioglioma	Left TLE	2.8	2.38	85	1350	CBZ 1000 CLB 10	Left
9	25/M	Right	5	20	CPS 3	N/A (No surgery)	Right HS	Right TLE	1.84	2.35	78	1500	PHT 200 LVT 3000	Left
10	47/M	Right	13	34	CPS 1	2	Right HS	Right TLE	1.04	2.77	37.5	1460	LVT 500 PHT 300 CBZ 800	Left
11	41/F	Right	14	27	CPS 4	1	Right superior temporal FCD	Right TLE	2.6	2.67	97	1520	TGB 15	Left
12	44/F	Right	14	30	CPS 4	1	Right HS	Right TLE	2.61	3.03	86	1550	LVT 750 PHT 400 CLB 10	Left
13	44/M	Right	14	30	CPS 4	?1	Right HS	Right TLE	2.78	3.05	91	1760	CBZ 800 LVT 1000	Left
14	36/M	Left	15	21	SPS 6 CPS 6 SGTC 3	1	Right MTL glioma	Right TLE	3.12	2.77	89	1520	CBZ 1600 CLB 20 LTG 400	Right
15	46/F	Right	8	38	CPS 5	1	Right HS	Right TLE	1.75	2.69	65	1470	TPR 600 PMD 1000 OXC 2400	Left
16	31/F	Right	19	12	CPS 2	4	Right HS	Right TLE	2.3	2.56	89.75	1400	CBZ 1600 LVT 1000	Left
17	29/M	Right	9	20	CPS 30 SGTC 4	3	Right HS	Right TLE	2.27	2.98	76	1630	VPA 2400	Left
18	22/M	Left	18	4	CPS 3 SGTC 0.33	1	Right MTL DNET	Right TLE	2.49	2.55	97.6	1680	VPA 2000 GBP 600	Left

M=male, F=female, SPS=simple partial seizure, CPS=complex partial seizure, SGTC=secondarily generalised seizure, N/A=not available, HS=hippocampal sclerosis, MTL=mesial temporal lobe, DNET=dysembryoblastic neuroepithelial tumour, TLE=temporal lobe epilepsy, TPR=topiramate, LTG=lamotrigine, VPA=sodium valproate, CBZ=carbamazepine, LVT=levetiracetam, PMD=primidone, CLB=clobazam, OXC=oxcarbamazepine, CLN=clonazepam, PHT=phenytoin, TGB=tiagabine, GBP=gabapentin.

3.3.5 Neuropsychological tests

The list learning and design learning tests were used by our neuropsychologists to assess material specific memory function (417). In the verbal learning task the subject is read a list of 15 words five times, and on each presentation attempts to recall as many of the words as possible. The overall percentage of correct responses was used as the measure of verbal memory efficiency. For non-verbal memory we employed a design-learning task; the subject is presented with a visual design on five occasions with recall being tested after each presentation. The percentage of correct responses over the five trials was used as a second measure of non-verbal memory efficiency. These tests form part of our presurgical memory assessment in TLE cases, and have proven least affected by performance anxiety, have a good test-retest reliability and are sensitive indicators of medial temporal lobe function (436). Neuropsychological test results are listed in table 3.2.

Neuropsychological test results of patients

Group	Mean VIQ	Mean PIQ	Mean VL	Mean DL
Left TLE	82	90	59	59
Right TLE	89	97	65	63

VIQ=verbal IQ, PIQ=performance IQ, VL=verbal learning, DL=design learning.

Table 3.2 – Neuropsychological test results of patients

3.3.6 Data analysis

All data were analysed using SPSS (11.0.0). It was first verified whether all parameters were normally distributed using the Kolmogorov-Smirnov test for normal distribution. Group differences for age were determined by a one-way analysis of variance (ANOVA), and gender distribution was assessed using the Pearson's χ^2 test. The age of onset of epilepsy, duration of epilepsy, and frequency of complex partial (CPS) and secondarily generalized seizures (SGS) in right and left TLE patients were compared using the Mann-Whitney test.

Each subject's output tractography connection probability map was spatially normalised by mapping into a standard space using the MNI template provided by SPM2 (Wellcome Department of Imaging Neuroscience, London; http://www.fil.ion.ucl.ac.uk/spm). Binary masks at a threshold connection probability value of 0.05 were then constructed. Our group has previously demonstrated in this same group of patients and control subjects, that the threshold 0.05 strikes a balance between losing non-specific low probability connections, while retaining the main body of the pathways (404). Binary masks at this threshold were therefore averaged across each group, to produce variability (or commonality) maps indicating the degree of spatial variability and overlap of the identified connections (441). A voxel commonality value C of 1.0 indicates that every individual had a connection identified in this voxel, while a C value of 0 indicates that none of them did (441). Tracts were then assessed visually in all three planes for visual symmetry and size/extent using MRIcro.

Normalised tract volumes were calculated for the connecting tracts from the left and right PHG of each control and patient at a threshold of 0.05 (442). An asymmetry index for volume (AI_{vol}) defined as AI_{vol} = [100 x (Right Volume-Left Volume)]/[(Right Volume+Left Volume)/2] was calculated (Jutila et al. 2001), and the mean values between groups compared using a one way ANOVA analysis. Comparisons between the control AI values, and left and right TLE AI values were carried out using post-hoc Dunnett t-tests. Two way mixed ANOVA with one between subjects factor (group – controls or TLE (both left and right)) and one within subjects factor (hemisphere – left or right) was used to test for the effect of interaction between group and hemisphere on volume, and unpaired *T*-tests were used to compare the patient and control group tract volumes.

The mean FA of the connected volume was calculated in native space for the left and right tracts in controls and patients. This was carried out by multiplying the binary masks defined above with that subject's whole brain FA image, and calculating the mean intensity value of the voxels. An asymmetry index for FA (AI_{FA}) defined as AI_{FA} = [100 x (Right FA-Left FA)]/[(Right FA+Left FA)/2] (443) was calculated, and the mean values between groups compared using one way ANOVA analysis. Comparisons between the control AI values and left and right TLE AI values were carried out using post-hoc Dunnett t-tests. Two way mixed ANOVA with one between subjects factor

(group – controls or TLE (both left and right)) and one within subjects factor (hemisphere – left or right) were used to test for the effect of an interaction between group and hemisphere on FA, and unpaired *T*-tests were used to compare the patient and control group tract FA values.

Pearson's correlation test was used to evaluate the evidence for a correlation of hippocampal volume with tract volume and FA, and tract volume with tract FA, ipsilateral and contralateral to the seizure focus. Performance on material specific memory measures was investigated for evidence of a correlation with tract volume and FA in right and left TLE groups, omitting patient 14 because of his atypical language dominance.

3.4 Results

3.4.1 Demographic analysis

There was no significant difference in the mean age or gender distribution of participants in the three groups (controls, left TLE, right TLE). There was no significant difference in the age of onset, duration of epilepsy or frequency of CPS and SGS between left and right TLE patients.

3.4.2 Qualitative tract analysis

In controls, PHG connections were visually symmetric. Connections between the para-hippocampal gyrus and anterior temporal lobe, orbitofrontal areas and posterior temporal and extrastriate occipital areas were observed as documented previously (431). There was a clear decrease in ipsilateral compared with contralateral connections in left TLE (figure 3.2), though an ipsilateral reduction was not evident in the commonality map of the right TLE group (figure 3.3).

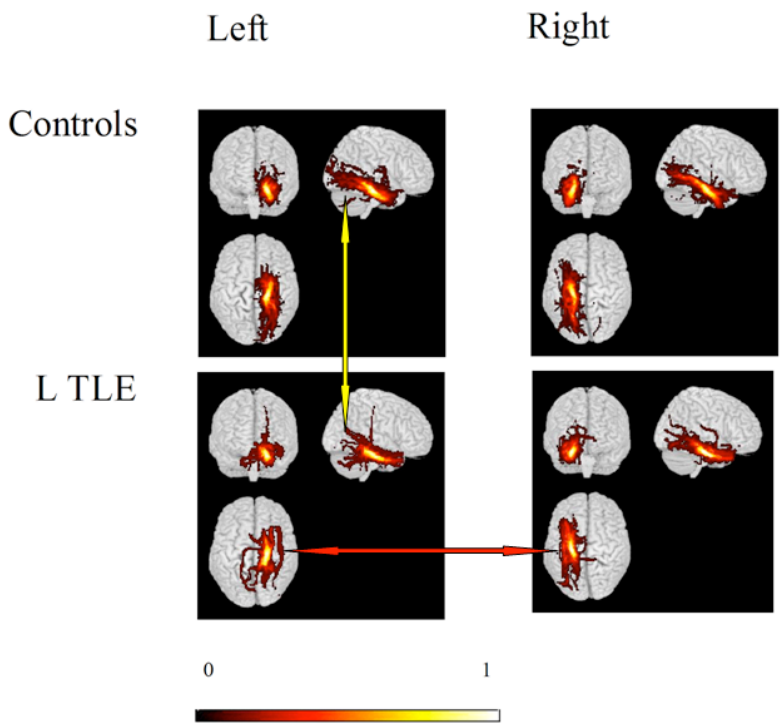

Figure 3.2 - Group maps of the parahippocampal gyrus tracts comparing left TLE patients against controls. Tracts are projected onto a 3d rendered brain template. A voxel commonality value of 1.0 indicates that each individual had a connection identified in this voxel while a value of 0.0 indicates that none of them did. In controls, PHG connections were symmetric. There is more marked asymmetry of connections in left TLE patients compared with controls. There is a decrease in ipsilateral compared with contralateral connections in left TLE, such that the body of the PHG appears smaller (red arrow). In addition, fewer connections to the occipital lobe are present in left TLE patients compared with controls (yellow arrow).

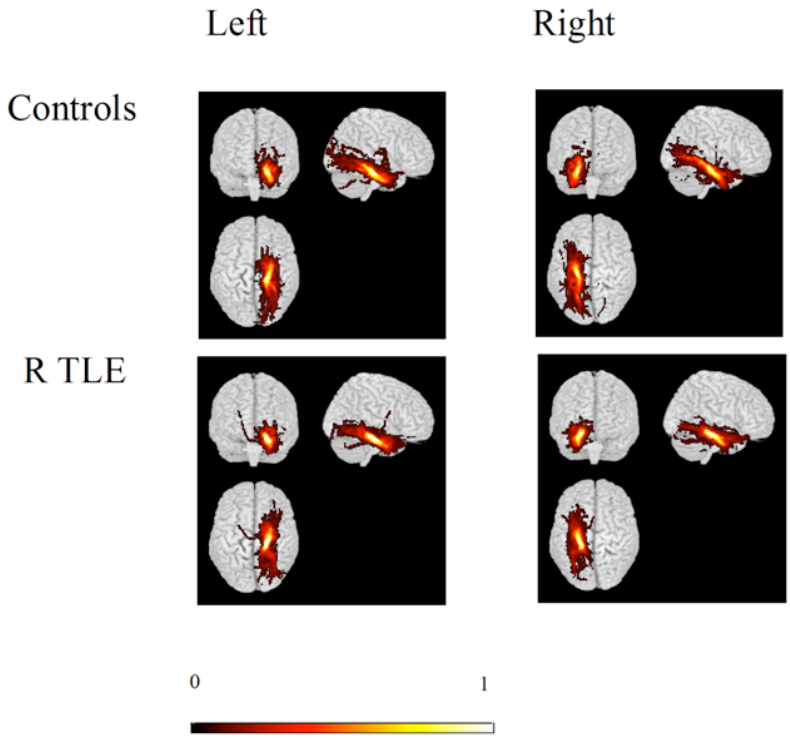

Figure 3.3 - Group maps of the parahippocampal gyrus tracts comparing right TLE patients against controls. Tracts are projected onto a 3d rendered brain template. A voxel commonality value of 1.0 indicates that each individual had a connection identified in this voxel while a value of 0.0 indicates that none of them did. In controls, PHG connections were symmetric. There is more marked asymmetry of connections in left TLE patients compared with controls and right TLE patients.

3.4.3 Quantitative tract analysis

There was a significant difference in AI_{vol} between groups [F (2,25) = 3.31 p = 0.05]. The AI_{vol} was greater in left TLE patients than in controls (p = 0.05) with a mean 22% reduction in volume on the left (table 3.3). There was no significant difference between the AI_{vol} in right TLE patients and controls. There was no significant interaction between group and hemisphere for tract volume, and no significant differences between left and right volumes in left/right TLE patients, and controls.

There was a significant difference in AI_{FA} between groups [F (2, 25) = 4.92 p=0.02], attributable to reduced FA on the left in left TLE (p = 0.02 against controls). There was no significant difference between the AI_{FA} in right TLE patients and controls. There was a significant interaction between group and hemisphere on tract FA [(F2, 25) = 4.35 p=0.02], with FA being lower on the left in left TLE patients, compared with controls (p=0.03). Although a similar trend was present in right TLE patients, with FA being lower on the right side compared with controls, this was not significant (p=0.06).

	Controls	Left TLE	Right TLE
Left volume±SE (mm^3)	7130±605	5756±810	7030±653
Right volume±SE (mm^3)	6791±959	7424±1052	6411±1019
AI Volume±SE (%)	−8.58±12.50	26.22±7.06*	−17.72±14.2
Left FA±SE	0.29±0.05	0.26±0.01*	0.27±0.01
Right FA±SE	0.29±0.01	0.29±0.01	0.26±0.01
AI FA±SE (%)	−0.99±3.26	11.80±4.67*	−5.26±3.70

AI=asymmetry index=[100×(right−left)]/[(right+left)/2].
*=$p \leq 0.05$ compared with control subjects.

Table 3.3 - Asymmetry indices of FA and volume, and mean absolute values of FA and volume in controls and patients

3.4.4 Correlation of tract volume and FA with material specific memory

All but one patient were left hemisphere dominant for language. Patient 14 was left handed and right hemisphere dominant on both fMRI and intracarotid amytal testing. He was therefore omitted from the correlation analysis. In the left TLE patients, FA of the left PHG connections were correlated significantly with pre-surgical verbal learning (r = 0.88, p=0.002), and right FA correlated significantly against pre-surgical design learning (r = 0.63, p=0.05) (figure 3.4). Left and right tract volumes were not significantly correlated with verbal learning and design learning, respectively. In the right TLE patients, there were no significant correlations between left or right tract FA or volume, with pre-operative verbal learning or design learning respectively.

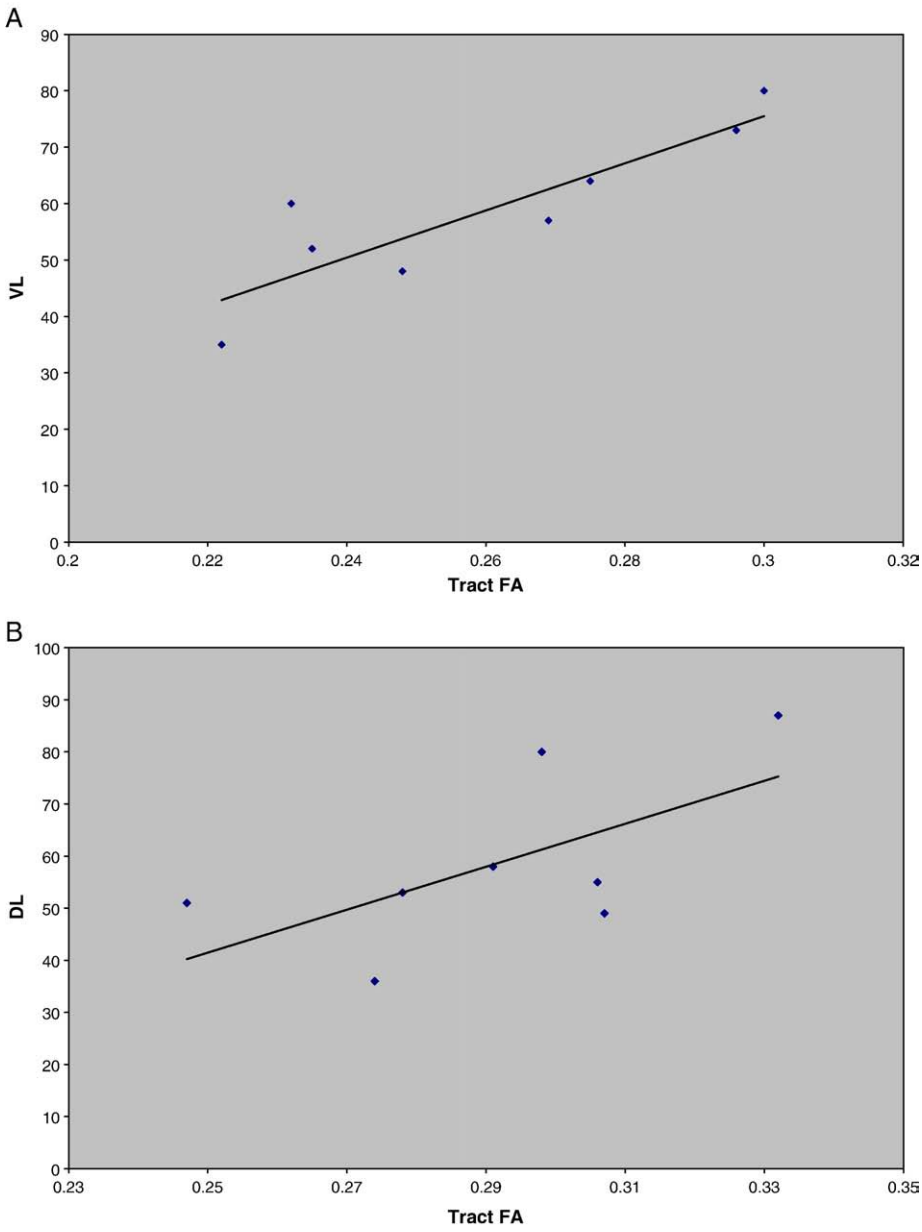

Figure 3.4 - The correlation of material specific memory against left PHG FA in left TLE patients where VL=verbal learning (r=0.876, p≤0.05) and DL=design learning (r=0.630, p≤0.05).

3.4.5 Correlations of hippocampal volumes with tract volumes and tract FA

There was no significant correlation between ipsilateral hippocampal volume and ipsilateral tract volumes or FA, nor between contralateral hippocampal volumes and contralateral tract volume or FA.

3.4.6 Correlation analysis of tract volume with tract FA

There was a significant correlation between tract FA and tract volume (r = 0.61, p=0.008) ipsilateral to seizure focus (figure 3.5), but not contralateral to seizure focus.

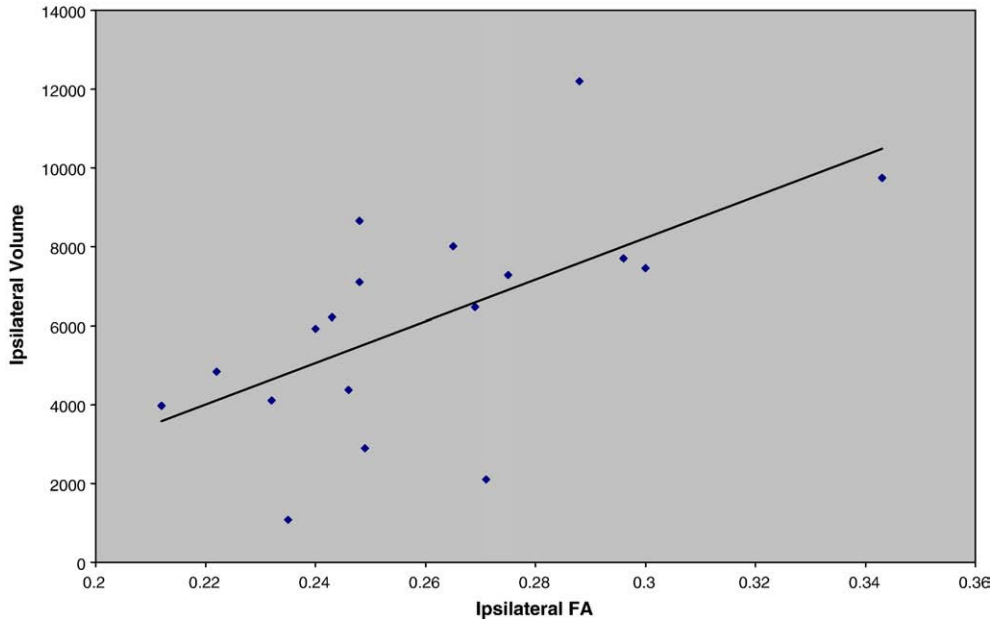

Figure 3.5 - The correlation between FA and volume of the parahippocampal gyrus in TLE patients, ipsilateral to seizure focus (r=0.606, p≤0.05).

3.5 Discussion

Our principal finding was that in TLE the white matter connections of the parahippocampal gyrus ipsilateral to the seizure focus had smaller volumes and decreased FA. This was statistically significant in left but not right TLE patients. Furthermore, in left TLE, decreased FA was associated with poorer performance on both material specific memory measures. These results are consistent with the hypothesis that TLE involves dysfunction and structural changes in a network that includes the parahippocampal gyrus.

3.5.1 Connections of the parahippocampal gyrus

The connections of the human parahippocampal gyrus, visualized with tractography, have been described in a control population (431). Using a different tractography algorithm (Fast Marching Tractography or FMT), connectivity was found between the parahippocampal gyrus and the

anterior temporal lobe, orbitofrontal areas, posterior temporal lobe and extra-striate occipital lobe via the lingual and fusiform gyri. These findings are similar to those in this control group. The demonstration of the connections of the medial temporal lobe may provide an explanation for some aspects of seizure semiology seen in patients with TLE. For example ipsilateral motor automatisms may be due to seizure spread from the medial temporal lobe focus to ipsilateral frontal and cerebellar lobes. Functional SPECT studies provide some support for these potential pathways of propagation, and have demonstrated cerebral perfusion changes during temporal lobe seizures in ipsilateral frontal, occipital and cerebellar lobes (444,445). More recently, subsequent to the publication of this study, Hamandi et al (446) published a case report in which they used EEG-fMRI to define a seed point for tractography in the left anterior temporal lobe in a patient with cryptogenic TLE. The authors demonstrated connections between the site of temporal lobe activation, and an occipital lobe region where activation also correlated with EEG changes.

3.5.2 Microstructural white matter changes of the parahippocampal gyrus

This was the first study to use tractography to quantitatively assess the structural changes in the parahippocampal gyrus in TLE. Prior to the publication of this study, several volumetric MRI (447,448) and voxel-based morphometry (VBM) studies assessing grey matter (392,449–451) had investigated the extra-hippocampal structural changes in unilateral TLE. The parahippocampal gyrus or its sub-regions including the entorhinal cortex, parahippocampal cortex and perirhinal cortex were affected in TLE in these studies. Several studies also suggested that the degree of atrophy and regional distribution was more extensive in left compared to right TLE, though none were specifically designed to evaluate this (449–452). Our study was the first to show that the white matter connections of the parahippocampal gyrus are affected by unilateral TLE, and that this process appeared to be more severe in left TLE compared with right TLE.

Since the publication of this study, several studies have been published, which have used diffusion MRI data in order to assess white matter structure (see table 3.4). Most of these studies have derived FA or MD values from tracts, and compared them to a control population. Of those studies that have assessed the parahippocampal gyrus or region (453–457), all reported ipsilateral reduction in FA in left TLE patients compared to controls, while right TLE patients were less

affected. These studies have used a variety of methods of analysis including simple ROI approaches, deterministic tractography and the application of tractography atlases, but none have used probabilistic tractography. In an attempt to negotiate the heterogeneity of these studies in terms of the white matter tracts studied, diffusion sequence acquisition parameters, analysis methods and patient demographics, Otte et al (458) recently published a meta-analysis of 13 cross-sectional studies looking at an array of white matter tracts including many of those listed in table 3.4. Their overall findings are concordant with the results of this study. They concluded that FA was reduced significantly in ipsilateral compared to contralateral white matter, particularly in those tracts most closely connected to the temporal lobe. Of note, the average, pooled reduction for all white matter in FA was 0.026, which corresponds closely to the differences found in this study. Although this meta-analysis was not geared to assess differences between left and right TLE patients, a number of recent tractography based papers have demonstrated that changes in white matter integrity are greater in left TLE compared to right TLE patients, as demonstrated in this study (455,457).

Authors	Analysis Method	Tract(s)/white matter studied	L:R TLE (number of patients)
Arfkanis et al (2002) (398)	ROI	ACC, PCC, AIC, PIC, EC	15 in total (no further details)
Concha et al (2005) (393)	Tractography (deterministic)	Fornix, CG	5:3
Lui et al (2005) (453)	ROI	HC, PHG	9:11
Gross et al (2006) (400)	ROI	Genu and splenium CC, EC, IC	7:4
Rodrigo et al (2007) (459)	Tractography (deterministic)	UF	0:10
Diehl et al (2008) (460)	Tractography (deterministic)	UF	18:10
Lin et al (2008) (397)	Tractography (deterministic)	UF, AF	10:2
McDonald et al (2008) (454)	Tractography (atlas)	AF, CST, fornix, IFOF, UF, PHC	9:8
Kim et al (2008) (395)	ROI	CC	4:6
Ahmadi et al (2009) (455)	Tractography (deterministic)	CG, PHG, SLF, ILF, UF, fornix, ATR, IFOF	10:11
Concha et al (2009) (394)	Tractography (deterministic) and ROI	Tractography – fornix, CG, tapetum of splenium of CC ROI – genu of CC, EC	17 all unilateral HS 6:2 all non-lesional (5 bilateral)
Knake et al (2009) (456)	ROI	ant/middle/post CC, SFG, IFG, TL, PHG, HC	12:0
Wang et al (2010) (461)	ROI	FL, OL, CC, IC, EC, caudate, putamen, thalamus	19 in total (no further details)
Kemmotsu et al (2011) (457)	Tractography (atlas)	Fornix, PHC, UF, ILF, IFOF, AF	18:18
Kim et al (2011) (462)	Tractography (deterministic)	AF, UF	13:12
Kucukboyaci et al (2012) (463)	Tractography (atlas)	UF, AF, SCG, IFOF	11:9
Liacu et al (2012) (464)	Tractography (deterministic)	fornix, SCG, ICG	7:2 (all unilateral HS) 8:1 (all non-lesional)
Keller et al (2012) (465)	ROI	HC, TL / FL white matter, thalamus	41:21

ACC – anterior corpus callosum, PCC – posterior corpus callosum, AIC – anterior limb internal capsule, PIC – posterior limb internal capsule, EC – external capsule, UF – uncinate fasciculus, AF – arcuate fasciculus, CST – corticospinal tract, IFOF – inferior fronto occipital tract, UF – uncinate fasciculus, PHG – parahippocampal gyrus, CG – cingulate gyrus, SLF – superior longitudinal fasciculus, ILF – inferior longitudinal fasciculus, ATR – anterior thalamic radiations, CC – corpus callosum,

SFG – superior frontal gyrus, IFG – inferior fronal gyrus, TL – temporal lobe, HC – hippocampus, FL – frontal lobe, OL – occipital lobe, IC – internal capsule, SCG – superior cingulum, ICG – inferior cingulum, PHC – parahippocampal cingulum

Table 3.4 – Summary of main ROI and tractography studies in TLE

3.5.3 Parahippocampal connections and memory in temporal lobe epilepsy

The memory deficits associated with TLE, particularly left TLE, can be disabling. Consequently, much attention has been focused on the effects of both chronic TLE and ATLR on memory. While the hippocampus plays a critical role in the initial formation of memories (425), the parahippocampal region is thought to be involved in the intersection between perception and memory, and the translation of material into a more permanent storage in the cortical association areas (425). Animal models have shown that the parahippocampal region is important for recognition memory (425,466), and that selective lesions to the parahippocampal area can severely impair memory (467). Furthermore, the functions of the medial temporal lobe are highly lateralized and the classic model of material specific memory predicts that lesions in the left hippocampal system impair verbal memory retrieval (468), while those in the right hippocampal system affect non-verbal memory, though these findings are less consistent (469).

In left TLE patients there was a significant correlation between parahippocampal tract FA and material specific memory measures on both the left and right sides. No significant correlations were seen with respect to tract volume in left TLE, and neither volume nor FA in right TLE. The finding of fewer occipital connections in the left TLE group compared with right TLE patients and controls may be significant in this respect (figures 3.2 and 3.3). Animal models suggest that potential roles for these connections may involve the priming of mesial temporal lobe structures to facilitate the consolidation of visual memory, or enhancing the visual processing of emotionally significant stimuli (467,470). Visual cues may be important not only for non-verbal memory, but may also be useful in verbal memory. This could explain the correlation of FA found with verbal **and** non-verbal memory in left TLE patients. In the right TLE patients the occipital connections did not seem to be as affected, and hence these patients may have been able to use visual cues to aid both verbal and non-verbal memory. In this study, it also appears that tractography derived para-hippocampal FA is a more sensitive marker than volume of the functional integrity of tracts that form the hardwiring of circuits needed for memory (471). Other tractography studies have shown that FA is a more sensitive and robust measure than volume of pathology in white matter tracts (472). In biological terms the interpretation of reduced anisotropy is complex (339), and depends

on the context or disease in which it is found (473). In epilepsy, it may represent neuronal loss, gliosis, and structural disorganisation (474).

Several other studies have also observed correlations between MRI findings and memory dysfunction in TLE. Some have shown a correlation between left and right hippocampal MRI volumes, and verbal and non-verbal memory respectively (436,475,476). Others have shown correlations between hippocampal T2-signal, or abnormalities of MR spectroscopy and material specific measures (477,478). There have also been studies published that have observed that the relationship between the side of pathology and memory dysfunction appears to be more evident in those with left TLE than right TLE. Alessio et al evaluated the relationship between several medial temporal lobe structures and memory in 39 patients, and found a correlation between the degree of left sided hippocampal atrophy and verbal memory deficits, but not between right sided hippocampal atrophy and visual memory deficits (469).

Prior to the publication of this study, only one study had assessed potential correlations between white matter microstructure and cognitive function. Lui et al (453) examined 18 TLE patients using ROI based methods and found correlations between apparent diffusion coefficients (ADC) in the left and right hippocampi and parahippocampal gyri and, verbal and non-verbal memory respectively. Subsequently, Wang et al (461) using similar ROI based methods, also demonstrated correlations between left frontal and right occipital white matter and category fluency. Since the publication of this study, there have been several reports of correlation between white matter microstructural changes and cognitive function, using a variety of approaches. Diehl et al (460) demonstrated that increased MD of the left uncinate fasciculus was associated with poorer performance on auditory memory tasks in patients with left TLE. Similarly, reduced FA and higher MD values in the right uncinate fasciculus were associated with poorer visual memory performance in left TLE patients. As in this study, no correlations between white matter microstructure and cognitive function were seen in right TLE patients.

Other studies have concentrated on the integrity of multiple white matter regions or tracts simultaneously and how these might relate to cognitive function. Riley et al (479) used whole brain

analysis techniques, and demonstrated that a high FA in the anterior temporal lobe correlated with better performance on delayed memory tasks, and in the mesial temporal lobe with better immediate memory performance. Bilateral anterior lobe cerebellar FA was positively correlated with executive functioning. No correlation was found between the frontoparietal regions and cognitive performance. Other studies have used tractography based techniques, to demonstrate that a distributed network may relate to cognitive function. Kucukboyaci et al (463) related the integrity of four fronto-posterior white matter association tracts to executive functioning. In this study the authors demonstrated that compared to healthy controls, correlations between fronto-temporal tract integrity and executive functioning were absent or attenuated in patients with TLE. The authors of this study interpreted these findings as suggesting a breakdown of typical structure-function relationships in TLE that may reflect aberrant developmental or degenerative processes. Macdonald et al (454) also related the integrity of multiple white matter tracts to cognitive function, but used a white matter atlas based on controls in TLE patients. Despite the limitations of this method, the authors of this study found that decreased FA in many of these white matter tracts, or in combinations, especially in the left hemisphere, were associated with verbal memory and language performance. However, no correlations were found between white matter integrity and non-verbal memory or fluency. In view of the fact that many of the correlations of white matter integrity occurred in tracts other than those regarded as relevant to the specific cognitive tasks in question, the authors concluded that memory and language cognitive function was related to a widely distributed white matter network. Most recently, Winston et al (480) have applied whole brain analysis methods to DTI data and found significant correlations between white matter and working memory. In left HS, gray matter loss was seen in the ipsilateral hippocampus and parietal lobe, with maintenance of the gray matter volume of the contralateral parietal lobe associated with better performance. White matter integrity within the frontoparietal network, in particular the superior longitudinal fasciculus and cingulum, and the contralateral temporal lobe, was associated with working memory performance. In right HS, gray matter loss was also seen in the ipsilateral hippocampus and parietal lobe. Working memory performance correlated with the gray matter volume of both frontal lobes and white matter integrity within the frontoparietal network and contralateral temporal lobe.

Finally, in addition to correlations between white matter structure and neuro-psychology assessments, some groups have reported correlations with functional activation in fMRI studies. Voets et al (481) reported significant reductions in functional connectivity between bilateral medial temporal lobe, occipital and left orbitofrontal regions in left TLE patients during a memory-encoding task. This altered orbitofrontal activity was directly related to measures of fornix tract coherence, that is FA, in patients. Their results suggested that specific fibre pathways may play a central role in functional plasticity in TLE, and highlighted the importance of network-based analysis approaches.

3.5.4 Limitations of study

Only modest numbers of patients and controls were available for this study, as the scanner used was decommissioned and replaced with a 3T instrument. These small numbers, particularly in the left TLE group, may have contributed to the pattern of observed changes in left but not right TLE patients. Furthermore, for this reason several morphological and functional factors that can influence cognition and memory in chronic epilepsy were not included as co-variates in the statistical analysis such as seizure frequency. The pathological basis of TLE was not homogenous throughout the group, and the degree of hippocampal atrophy was varied. This may partly explain the poor lateralisation seen on the neuropsychological evaluation of the patients. Secondly the spatial resolution of the tractography was limited and we did not separately evaluate the entorhinal cortex, parahippocampal cortex, and perirhinal cortex. The entorhinal cortex is considered to be the route by which data reaches the hippocampus. The perirhinal, and parahippocampal cortex on the other hand, provide the incoming connections to the entorhinal cortex, conveying information from the polymodal and unimodal cortices (116). A sub-regional analysis is an area that should be explored in future tractography studies. Finally the comparison of the group tractography maps in TLE patients and controls was carried out qualitatively. In future studies it would be useful to carry out this analysis quantitatively using a package such as SPM.

3.5.5 Conclusion

This tractography study has shown disruption of the architecture and atrophy of the connections of the parahippocampal gyrus ipsilateral to the seizure focus in patients with refractory TLE, and

these structural changes were associated with memory deficits evident on psychometric testing. This information has both diagnostic and prognostic implications. Larger, longitudinal studies at a higher resolution will enable both sub-regional analysis, and the investigation of other factors that may contribute to neuronal loss and structural changes, and subsequent memory impairment in patients with TLE.

4 VBM Using SPM and TBSS Analysis of Patients with Mesial Temporal Lobe Epilepsy and Hippocampal Sclerosis

This chapter describes a study comparing the use of VBM and TBSS based methods to study the differences in diffusion parameters between controls and patients with temporal lobe epilepsy. The material in this chapter has been published (see publications section), and was the first paper in the literature to apply TBSS to TLE patients, and compare its results with those of VBM. It was also the first study using these techniques to report extra temporal and contralateral white matter changes. The findings in this study have subsequently been validated by several published studies that report similar findings.

4.1 Objectives

The previous chapter explored the use of tractography defined ROIs to explore differences in white matter microstructure between patients and controls. However, given the literature at the time, we also hypothesised that the overall differences in white matter microstructure between TLE patients and controls were likely to be present in a distributed network. Therefore, the aim of this study was to use whole-brain analysis techniques, without a priori assumptions, in order to localise these differences, and assess whether they correlated with neuropsychology. The secondary aim of this study was to compare the sensitivity of two whole brain analysis techniques, namely VBM and TBSS.

4.2 Introduction

Traditionally TLE-HS has been thought of as an epilepsy syndrome where structural changes are limited to the hippocampus itself. With the development of advanced techniques such as quantitative MRI and MR volumetry (86), MR spectroscopy (391) and VBM of T1 images (451), it is evident that structural abnormalities are more widespread than demonstrated by conventional MRI. As discussed in the last chapter ROI and tractography studies corroborate these findings. However, the limitation of an ROI-based approach is that it is restricted to predefined regions and is subject to operator bias. In order to overcome this and enable the study of the whole brain, voxel-based techniques have been developed, the most well known being Statistical Parametric

Mapping (SPM) (318). Our group have already shown the usefulness of voxel-based DTI analysis in MR negative patients and those with acquired lesions or malformations of cortical development (198,383), as described in chapter 1. A methodological issue associated with the SPM approach is the spatial normalization that is required to make anatomically different subjects comparable in each individual voxel. Even with non-linear warps it is usually not possible to achieve a perfect match, therefore smoothing is necessary to account for some residual error and make the data conform more closely to the underlying model of Gaussian fields. An alternative method for the whole brain analysis of diffusion data, instead of trying to match each and every voxel in different subjects, projects DTI data on a common pseudo anatomical skeleton and therefore does not need smoothing (324). This technique, otherwise known as Tract-Based Spatial Statistics (TBSS), is available as part of the FSL software package.

Since most functions in the human brain are not represented in a single anatomical structure but rather occur in systems it is of merit to analyze which white matter connections or networks show diffusion abnormalities in mTLE. We used both SPM and TBSS to report the diffusion changes throughout the brain without prior constraints in patients with mTLE and HS. We also discuss methodological differences between the two voxel-based approaches.

4.3 Methods

4.3.1 Subjects

We studied 33 consecutive patients with unilateral HS and mTLE undergoing presurgical evaluation at the National Society for Epilepsy. Unilaterality of HS was determined on qualitative and quantitative criteria (hippocampal T2 relaxation time and volumetry) (435). All patients had a pathological small-to-big hippocampus volume ratio (< 90%) and increased ipsilateral T2 relaxation times (table 4.1). In total, 21 had left-sided (left HS) and 12 had right-sided hippocampus sclerosis (right HS). The median age for the left HS group was 44 years (range 17 – 62, 8 female), the median age of the right HS group was 39 years (range 22 – 54, 6 female). We also included 37 normal controls (median age 39, range 18 – 70, 19 female). Of these 34 subjects were right and 3 left-handed. Handedness and additional clinical information about the patient group is

given in table 4.1. Clinical variables and quantitative imaging scores were analyzed with SPSS v11 (SPSS Inc., Chicago, IL, USA).

Table 4.1 – Clinical and radiological data of the patient group

	Age	Gender	Duration	Seizure frequency (per month unless stated)	AH	Hand	Video-EEG	Surg	Group	HVR
1	43	M	12	SPS (daily), CPS (4–5)	–	R	L TLE (interictal)	No	LHS	52.4%,
2	42	M	41	SPS (daily), CPS (2–3), SGTC (3–4/year)	FC	R	R TLE	No	RHS	50.8%,
3	62	F	61	CPS (4)	–	R	L TLE	Yes	LHS	71.2%
4	51	M	46	SPS (2–3/day), CPS (1–2)	–	R	R TLE	Yes	RHS	63.8%
5	45	M	42	CPS (4), SGTC (2)	–	R	L TLE, some extratemporal features—for ICR	No	LHS	54.0%
6	44	M	29	CPS (2–3), SGTC (4/year)	FC	R	L TLE	No	LHS	39.3%
7	60	F	36	CPS (1–2)	–	R	L TLE, some extratemporal features—for ICR	No	LHS	71.4%
8	23	F	18	CPS (3), SGTC (1–2)	–	R	R TLE	Yes	RHS	69.9%
9	51	M	45	CPS (12–31)	FC	R	L TLE	No	LHS	44.1%
10	47	M	45	CPS (4)	FC	R	R TLE (interictal)	Yes	RHS	69.5%
11	37	F	33	CPS (1–2), SGTC (<0.5/year)	FC	R	L TLE	Yes	LHS	52.8%
12	58	M	17	CPS (5–8/week)			L TLE	No	LHS	65.7%
13	19	F	9	CPS (8)	FC	R	L TLE	Yes	LHS	53.1%
14	46	F	39	SPS (daily), CPS (4), SGTC (0.5)	–	R	R TLE–ICR L TLE	Yes	LHS	37.2%
15	62	M	37	CPS (1)	FC	R	L TLE	No	LHS	59.8%
16	42	F	31	CPS (4–6), SGTC (0.5)	–	R	R TLE	Yes	RHS	77.3%
17	30	M	20	CPS (6), SGTC (<1/year)	FC	R	R TLE (interictal)	No	RHS	57.2%
18	54	M	43	SPS (2), CPS (2)	–	R	R TLE	No	RHS	62.6%
19	36	F	32	CPS (2–3), SGTC (2–3)	HT	L	R TLE but some extratemporal features—to undergo ICR	No	RHS	69.2%
20	51	M	7	SPS (7–10/week), CPS (14), SGTC (<1)	–	R	BL TLE—to undergo ICR	No	LHS	51.7%
21	45	M	44	CPS (5)	FC	R	L TLE	No	LHS	65.7%
22	31	M	29	CPS (1)	FC	R	R TLE	Yes	RHS	41.0%
23	30	M	17	CPS (30–45/day), SGTC (1/year)	FC	R	R TLE	No	RHS	65.6%
24	22	F	11	SPS (10), CPS (4)	FC	L	L TLE	Yes	RHS	59.2%
25	17	F	15	CPS (8)	FC	R	L lateral TLE–ICR L mTLE	Yes	LHS	83.3%
26	45	F	32	CPS (1–2)	FC	R	R TLE	No	RHS	49.8%
27	19	F	18	SPS (2), CPS (2)	FC	R	L TLE	Yes	LHS	79.3%
28	33	M	8	CPS (15–30), SGTC (1)	FC	R	L TLE	Yes	LHS	56.6%
29	49	M	42	CPS (70–80)	FC	R	L TLE	No	LHS	56.6%
30	42	M	41	SPS (0.5), CPS (12), SGTC (<1)	FC	R	BL TLE–ICR L TLE	Yes	LHS	69.3%
31	41	M	23	SPS (12–15), CPS (10)	–	R	L TLE	No	LHS	85.9%
32	33	F	32	CPS (4), SGTC (1–2)	FC	R	L TLE	Yes	LHS	57.2%
33	29	M	8	CPS (56–84), SGTC (36–48)	–	R	L TLE	No	LHS	82.1%

Age and duration of epilepsy given in years; M = male; F = female; LHS = left hippocampus sclerosis; RHS = right hippocampus sclerosis; HVR = hippocampal volume ratio; SPS = simple partial seizures; CPS = complex partial seizures; SGTC = secondarily generalized tonic–clonic seizures; AH = antecedent history; FC = febrile convulsions; HT = head trauma; Hand = handedness; EEG = scalp EEG; TLE = temporal lobe epilepsy; ICR = intracranial recordings; Surg = had surgery.

4.3.2 Imaging protocol

We acquired the clinical T1 and DTI data on a 3T scanner (GE Excite II) using the sequences and parameters described in chapter 2.

4.3.3 Data analysis

All scans were transferred to a Linux workstation and processed with SPM5 (http://www.fil.ion.ucl.ac.uk/spm/), Matlab 7.3 (The MathWorks, Natick, MA) and FSL 3.3 (http://www.fmrib.ox.ac.uk/fsl/). First the DICOM files of each DTI acquisition were converted into a single multivolume ANALYZE 7.5 file. Next they were corrected for eddy currents with FSL "eddycorrect". This tool conducts an affine registration of every individual volume to the first b0 volume. After this coregistration step the 6 b0 volumes of each subject were extracted and averaged. The main diffusion tensor was fitted in each voxel with FSL DTIFit and the FA and MD maps were calculated.

4.3.3.1 SPM analysis

Initially a generic FA template was built from the control group since TBSS also uses a FA-based spatial normalization step. This was done by normalizing the extracted b0 image to the SPM5 EPI template and applying this transformation information to the FA maps and reslicing to 2mm cubic resolution. Afterwards the 37 normalized FA maps were averaged and smoothed with an 8mm FWHM Gaussian kernel to form the FA template. Next all native FA maps (patients and controls) were normalized to this template and resliced to 2mm cubic resolution as well. All normalization steps were done with SPM default settings that encompassed affine registration (12 degrees of freedom) and 16 non-linear iterations using a discrete cosine basis function with a frequency cutoff of 25 (482). The same transformation was applied to the MD maps and the native b0 images. The now normalized b0 images were then brain extracted with the FSL brain extraction tool ("bet") and the individual brain mask was applied to the normalized FA and MD images. To correct for individual masking errors with residual non-brain voxels a group brain mask was constructed from the control group by averaging all individual brain masks, smoothing with a 2mm FWHM Gaussian

kernel and thresholding at 0.5. This group mask then was applied to all FA and MD maps. Afterwards the normalized and brain extracted FA and MD maps were smoothed with an 8mm FWHM Gaussian kernel and a General Linear Model (GLM) was set up comparing the left HS and the right HS group against the controls with a 2-sample t-test. The contrast was generated with a 1-tailed t-contrast fully corrected for multiple comparisons with family-wise error correction (FWE) at a $p < 0.05$. The resulting SPM T maps were superimposed on the unsmoothed brain-extracted FA or MD template with MRIcro (http://www.sph.sc.edu/comd/rorden/mricro.html).

4.3.3.2 TBSS analysis

First the FA and MD maps were scaled with a factor of 10000 (FA) or 2000 (MD) to achieve an approximate intensity range of 0 to 10000 that was necessary for the further processing steps. Afterwards every FA map was non-linearly co-registered to every other FA map and the most representative subject was determined by automatically selecting the subject that needed the least amount of warping when all other subjects were warped to it. This representative target was then coregistered using an affine transformation to the MNI152 template and resampled to 1mm cubic resolution. All other FA maps were then likewise resampled by concatenating the non-linear transformation to the target with the transformation from the target to the MNI152 space. A mean FA image was generated by averaging all resampled FA maps, and a group skeleton was automatically constructed from these maps. In brief this process involves finding the main tract direction and reducing it to a tube or sheet. This process is described in more detail elsewhere (324). The skeleton is a pseudo-anatomical representation of the main fiber tracks. Next the locally highest FA values were projected onto this skeleton. A distance map automatically weighted the search area by the distance from the individual voxel to the skeleton. The same voxel used for the FA projection was also used to construct an MD skeleton. Thus, for each subject (patients and controls) an individual FA and MD skeleton was produced that was analyzed in a group comparison of left HS and right HS patients versus controls respectively using FSL "randomize" with 5000 permutations. This tool uses a permutation-based statistical inference that does not rely on Gaussian distribution of voxels (327). The resulting statistical maps were corrected for multiple comparisons at the cluster level with a p value of 0.05 and superimposed on the mean FA or MD image and the group skeleton.

4.3.3.3 Correlation analysis

In order to assess whether white matter changes might be related to seizures, a GLM was constructed to look for correlations between age of onset or duration of epilepsy, and white matter FA/MD changes.

4.3.3.4 Fibre tracking

Fibre tracking was done with FSL v3.3 Diffusion Tools (FDT). First the diffusion characteristics were calculated in each voxel with "bedpost" using a Markov Chain Monte Carlo sampling method (295). Afterwards probabilistic tracking was carried out with "probtrack" using a seed region manually defined in normalized space (see results for details of seed region). Tracking was carried out in individual native space; therefore the seeding mask was first back-normalized by inverting the individual normalization matrix created by SPM (see above) with the SPM deformations toolbox and applying this to the seeding mask. Afterwards tracking was initiated, the resulting native space tracks were again spatially normalized by applying the same matrix used to normalize the FA and MD maps. Voxel values as calculated by "probtrack" represent the number of samples passing through each voxels. Tracts were binarized using an empirically defined lower threshold of 100 and an upper threshold of infinity. Individual binarized tracks were averaged to form a group map and the resulting image was superimposed on the unsmoothed FA template with MRIcro for visualization.

4.4 Results

4.4.1 Clinical variables and quantitative scores

There was no significant age difference between left HS patients, right HS patients and controls. There also was no significant difference between the left HS and the right HS group for intracranial volume ($p=0.79$), hippocampus volume ratio ($p=0.99$), frequency of generalized seizures ($p=0.90$) or duration of epilepsy (in years) ($p=0.70$). A trend was observed with slightly higher frequency of complex partial seizures in the left HS group ($p=0.075$) and higher T2 relaxometry times of the affected hippocampus ($p=0.027$). As expected the left sided hippocampus volumes were smaller

for the left HS than the right HS group, and the right sided hippocampus volumes were smaller for the right HS group (all $p<0.001$). For normal-distributed variables (intracranial volume, hippocampal volume, T2 relaxometry) a t-test was used; for non-normal distributed variables a Wilcoxon-test was applied.

4.4.2 DTI findings

Detailed results are shown in figure 4.1 (SPM), figure 4.2 (TBSS) and table 4.2.

4.4.2.1 Left hippocampus sclerosis group

4.4.2.1.1 FA reduction

Both SPM and TBSS detected an FA decrease in the ipsilateral temporal lobe (figure 4.3). The pattern however was somewhat different: SPM showed significant reduction in the mesial temporal pole, the superior temporal gyrus leading to the central temporal white matter and middle temporal gyrus. TBSS additionally found FA reduction in the parahippocampal gyrus, the inferior and middle temporal gyrus and the crus and body of the ipsilateral fornix. In the contralateral temporal lobe small clusters of reduced FA were detected in the central white matter that were more widespread with TBSS.

FA was reduced in the anterior thalamus and cingulum, more on the ipsilateral side, using both SPM and TBSS. TBSS showed contiguous FA reduction in the anterior half of the cingulum, SPM in contrast showed isolated suprathreshold clusters but also more ipsilateral than contralateral (figure 4.4).

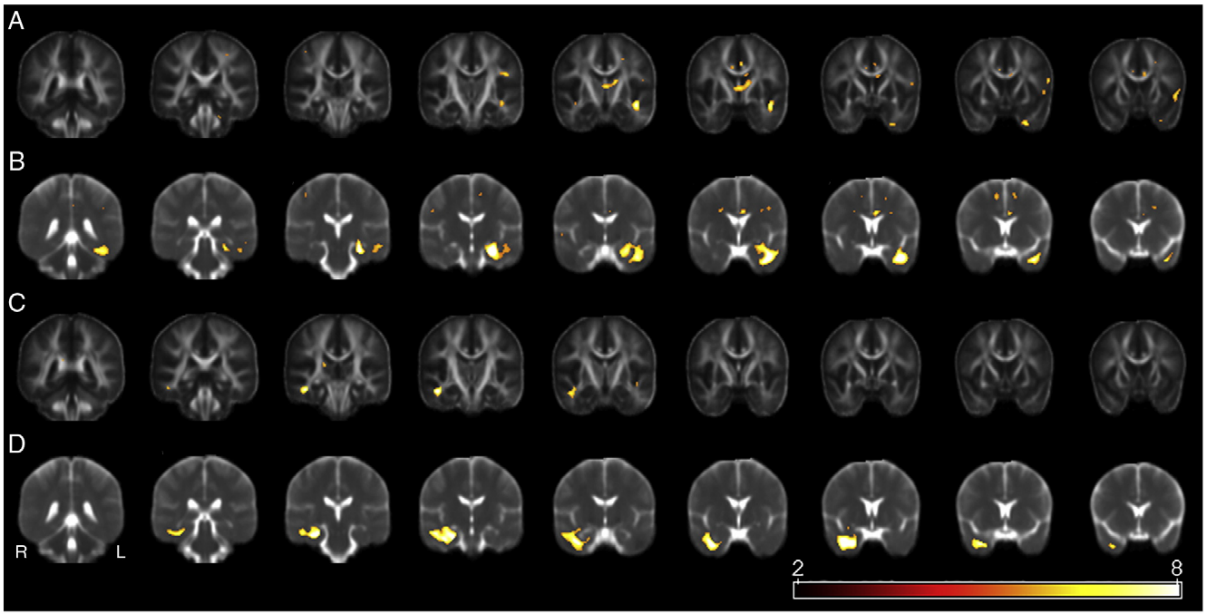

Figure 4.1 - SPM results. (A) FA decrease and (B) MD increase of the left HS group compared with controls. (C) FA decrease and (D) MD increase of the right HS group compared with controls. Colours symbolize T scores (see colour bar). FWE correction with p = 0.05. Left on image is patients right (radiological convention).

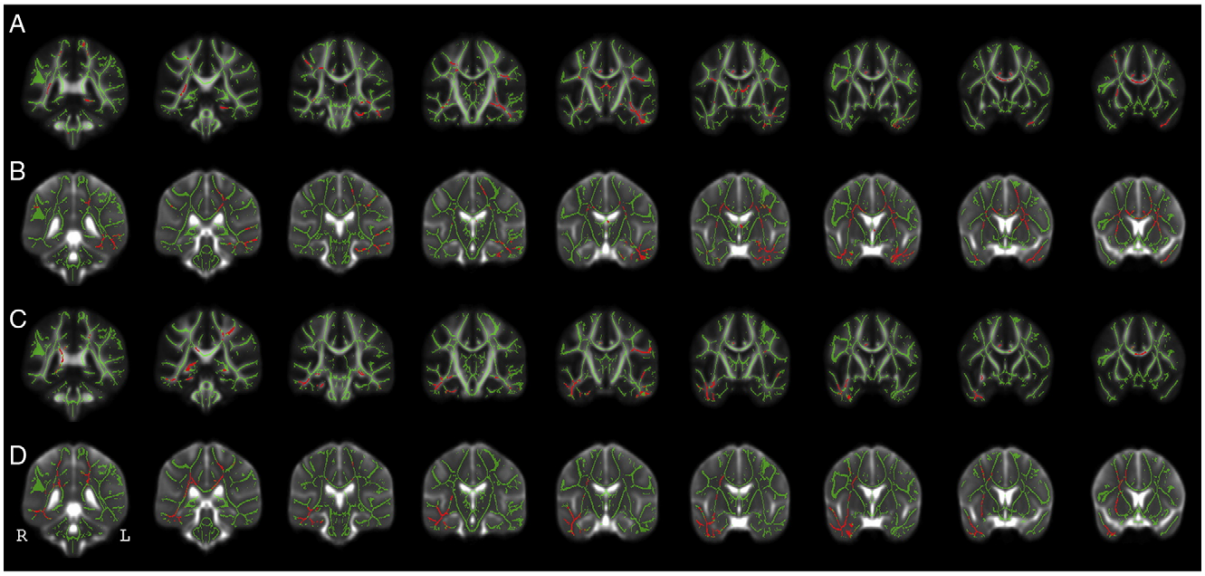

Figure 4.2 - TBSS results. (A) Significant FA decrease and (B) MD increase of the left HS group compared with controls. (C) Significant FA decrease and (D) MD increase of the right HS group compared with controls. Colours symbolize: Red=significant voxels at p=0.05 (corrected for multiple comparison at cluster level); green=group skeleton.

	SPM	TBSS
Left hippocampal sclerosis		
FA decrease		
Ipsilateral temporal lobe (L)	Mesial temporal pole (T=6.68, 74 Vx, −26 8 −42) Central white matter extending into the superior temporal gyrus (T=8.31, 175 Vx, −42 −6 −18)	Mesial temporal pole (p=0.002) Central white matter reaching into the inferior, middle and superior temporal gyrus (p=0.0002) Parahippocampal gyrus (p=0.0026)
Extratemporal limbic system	L>R anterior mesial thalamus (crossing midline ; T=6.77, 205 Vx, −2 −4 6) L>R cingulum (multiple cluster ; largest T=6.14, 115 Vx, −8 20 22)	L+R anterior mesial thalamus (p=0.0036+p=0.036) L body and crus of fornix (p=0.0036) L+R cingulum (p=0.0004+p=0.0084)
Other regions	L posterior inferior frontal gyrus (T=6.32, 39 Vx, −44 −14 24) L inferior frontal gyrus cortical (T=6.25, 68 Vx, −48 14 −6 and T=6.01, 25 Vx −56 10 16) L+R post-central gyrus (12 Vx+11 Vx) L occipito-temporal white matter (9 Vx) L+R superior occipital gyrus (10 Vx+6 Vx) L inferior anterior cerebellum (46 Vx)	L+R inferior frontal gyrus (p=0.0048+p=0.0174) L>R anterior corpus callosum (p=0.0004) L+R post-central gyrus (p=0.0212+p=0.01) L supramarginal gyrus (p=0.0076) L superior occipital gyrus (p=0.03) R superior frontal gyrus (p=0.0294) R posterior central temporal white matter (p=0.001) R external capsule (p=0.0482) L+R middle lateral cerebellum (p=0.0048+p=0.0028) R inferior anterior cerebellum (p=0.001)
MD increase		
Ipsilateral temporal lobe (L)	Coalescing cluster including hippocampus and central temporal white matter (T=11.3, 2298 Vx, −26 −16 −24; subclusters −38 2 −32 and −40 −42 −22)	Coalescing cluster including parahippocampal gyrus, central white matter and all temporal gyri (p=0.0002)
Extratemporal limbic system	L cingulum (T=6.63, −6 4 28)	L anterior mesial thalamus (p=0.0398) L+R cingulum (p=0.0008+p=0.004)
Other regions	L+R frontal lobe (multiple clusters, 2–32 Vx) L>R parietal lobe (multiple clusters, 5–90 Vx)	R central temporal white matter (p=0.0094) L+R anterior body of corpus callosum and pericallosal white matter (widespread) L+R external capsule (p=0.0006+p=0.0064) L+R post-central gyrus (p=0.0014+p=0.02) L occipito-parietal white matter (p=0.0164) L central cerebellum (p=0.028)
Right hippocampal sclerosis		
FA decrease		
Ipsilateral temporal lobe (R)	Central white matter extending into the superior and middle temporal gyrus (T=8.66, 235 Vx, 46 −14 −22) Parahippocampal gyrus (T=5.6, 1 Vx, 24 −18 −26)	Central white matter reaching into the inferior, middle, root of the superior temporal and fusiforme gyrus (p=0.0002) Parahippocampal gyrus (p=0.005)
Extratemporal limbic system	–	L+R crus of fornix (p=0.0002) R crus/body of fornix (p=0.0002) R cingulum (p=0.0296)
Other regions	L superior temporal gyrus (T=5.75, 9 Vx, −42 −6 −14) R postero-lateral thalamus (T=6.05, 13 Vx, 20 −24 12) R pericallosal white matter (T=5.76, 7 Vx, 14 −42 20)	L superior temporal gyrus (p=0.035) L inferior and middle temporal gyrus (p=0.0066) L posterior inferior frontal gyrus (p=0.0044) R occipito-temporal white matter (p=0.0256) R posterior pericallosal white matter (p=0.0096) L+R middle body of corpus callosum (p=0.014) L post-central gyrus (p=0.0092)
MD increase		
Ipsilateral temporal lobe (R)	Coalescing cluster including hippocampus and central temporal white matter (T=9.48, 1933 Vx, 36 −2 −36; subclusters 26 4 −36, 26 −18 −24 and 32 4 −14)	Coalescing cluster including parahippocampal gyrus, central white matter and all temporal gyri (p=0.0002)
Extratemporal limbic system	–	
Other regions	–	R frontal lobe white matter including the anterior pericallosal area and external capsule (widespread, p=0.0002) L+R superior parietal lobe white matter including posterior pericallosal area (widespread, p=0.0008+0.0012)

Suprathreshold FA decrease and MD increase clusters as detected by the two methods in the patient groups. T=SPM T score; Vx=Voxel; coordinates for SPM results are MNI-derived but since a custom FA template was used should be considered with caution. For TBSS, p values after correction for multiple comparisons at the cluster level are shown.

Table 4.2 – SPM and TBSS results

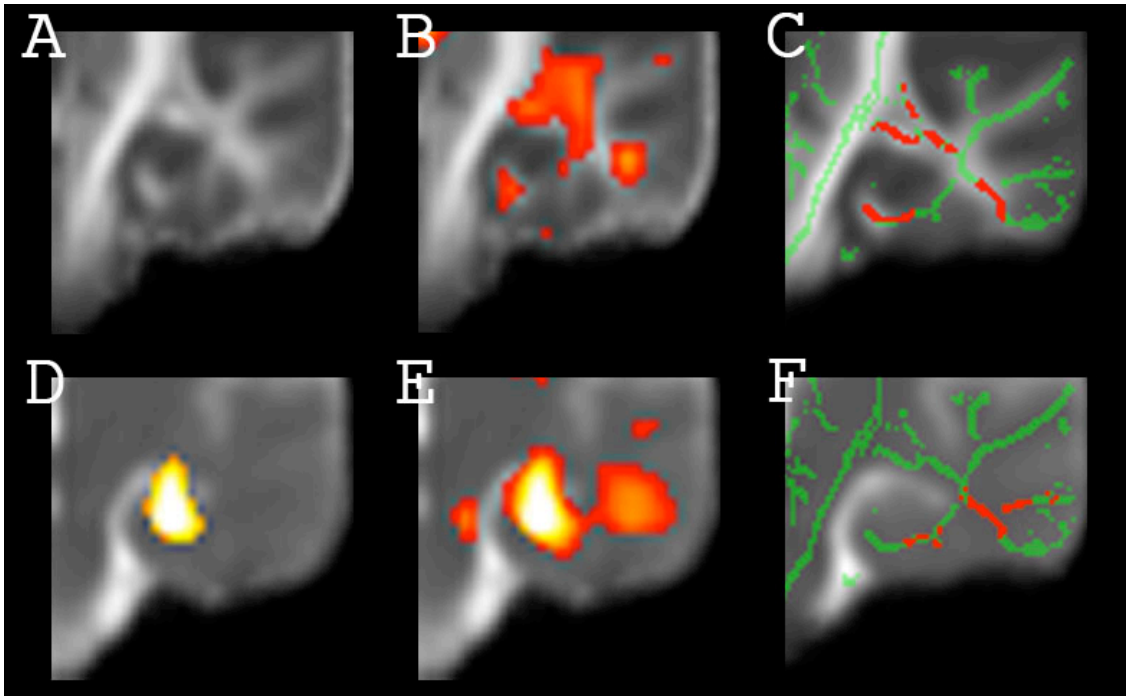

Figure 4.3 - Synopsis of results in the left HS group in the ipsilateral temporal lobe

FA reduction detected by SPM with (A) FWE correction (p=0.05), (B) uncorrected for multiple comparisons (p = 0.0001) and (C) TBSS results corrected for multiple comparisons at cluster level (p=0.05). MD increase detected by SPM with (D) FWE correction (p=0.05), (E) uncorrected for multiple comparisons (p = 0.0001) and (F) TBSS results corrected for multiple comparisons at cluster level (p=0.05). TBSS found FA reduction in the parahippocampal gyrus, inferior temporal gyrus and deep temporal white matter. SPM detected no changes with FWE but could find similar changes at lower threshold levels. Clear cut MD increase was detected by SPM in the ipsilateral hippocampus that was only detected marginally by TBSS.

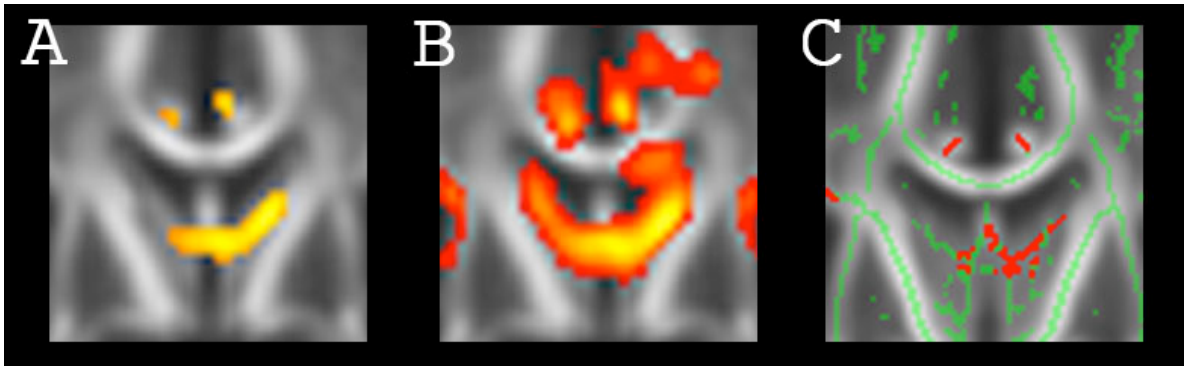

Figure 4.4 - Synopsis of FA reduction in left HS with SPM and TBSS at the anterior thalamus and cingulum region. SPM results displayed with (A) FWE correction (p=0.05) and (B) uncorrected for multiple comparisons (p = 0.0001). (C) TBSS results displayed corrected for multiple comparisons at cluster level (p=0.05). SPM and TBSS show clear FA reduction in the anterior thalamus more on the ipsilateral side and FA reduction in the cingulum bilaterally. SPM however does not show contiguous changes but rather patchy clusters. Also note the effect of the smoothing in (B) with suprathreshold FA reduction reaching into the left lateral ventricle and the corpus callosum. TBSS additionally shows FA reduction reaching into the body of the fornix that is not detected by SPM at either threshold level.

FA was reduced in the ipsilateral superior frontal gyrus with both techniques, again being more widespread with TBSS. Both techniques also showed FA reduction in the ipsilateral posterior inferior frontal gyrus, and this was more extensive using TBSS.

Clusters of FA reduction were also found in the superior post-central gyrus bilaterally, and the ipsilateral superior occipital gyrus more on the ipsilateral side. Only TBSS showed changes in the anterior body of the corpus callosum and the contralateral occipito-temporal white matter. In the cerebellum SPM detected a cluster in the ipsilateral inferior anterior region, whereas TBSS showed bilateral changes in the middle lateral region. No FA increase (left HS > controls) was detected with either technique.

4.4.2.1.2 MD increases

SPM showed increased MD in the ipsilateral hippocampus in the left HS group compared to controls (figure 4.3). Changes also affected nearly the entire temporal lobe focused on the central white matter. TBSS showed comparable findings in the central temporal white matter. The hippocampus however was only marginally detected given it is a grey matter region that is not part of the skeleton. Smaller changes were found in the inferior frontal gyrus, more on the ipsilateral side, and the superior frontal gyrus bilaterally. MD was increased in the cingulum; SPM showed ipsilateral changes whereas TBSS found bilateral clusters more on the ipsilateral side. Multiple small clusters of MD increases were detected in the parietal lobe bilaterally but clearly more on the ipsilateral side and the frontal lobe bilaterally. TBSS also showed increased MD in the anterior body of corpus callosum and the corona radiate, more ipsilaterally. TBSS also detected a MD increase in the contralateral central temporal lobe white matter and the ipsilateral body of the fornix. No MD decrease was detected with either technique.

4.4.2.2 Right hippocampus sclerosis group

4.4.2.2.1 FA reduction

SPM detected decreased FA in the central ipsilateral temporal white matter and a one voxel cluster in the parahippocampal gyrus. There also was a small cluster in the contralateral superior temporal gyrus and the ipsilateral dorsal thalamus. TBSS showed far more widespread reductions in FA: in the ipsilateral temporal lobe including the parahippocampal gyrus, the inferior, middle and superior temporal gyri (figures 4.1 and 4.2). FA was reduced in the crus of the fornix bilaterally, more so ipsilaterally and the ipsilateral body of the fornix. In the contralateral superior temporal gyrus reduced FA was detected. TBSS additionally found clusters of FA decrease in the inferior and middle temporal and posterior inferior frontal gyrus. There also were less significant clusters in the ipsilateral occipito-temporal white matter, the midline middle body of the corpus callosum and the ipsilateral posterior pericallosal area. No FA increase (right HS > controls) was detected with either technique.

4.4.2.2.2 MD increase

With SPM MD increase was confined to the ipsilateral temporal lobe including the hippocampus, parahippocampus, inferior and middle temporal gyrus and central temporal white matter. No extratemporal or contralateral clusters were found.

TBSS showed similar changes in the ipsilateral temporal lobe and included the ipsilateral superior temporal gyrus but only marginally detected the hippocampus. Widespread MD increase was detected in the ipsilateral frontal lobe including the external capsule and bilaterally in the parietal lobe including the posterior pericallosal area. No MD decrease (right HS < controls) was detected with either technique.

4.4.2.3 Fibre tracking

Outside the ipsilateral temporal lobe and the limbic system one consistent finding was an FA decrease detected by both SPM and TBSS in the posterior part of the inferior frontal gyrus in the left HS group (figures 4.1 and 4.2). TBSS showed bilateral changes in this region for the left HS group and also an FA decrease in the left, contralateral, side for the right HS group. In order to visualize which track was involved in this highly consistent finding, a seeding mask was manually generated out of the suprathreshold cluster detected by SPM in this region (left inferior frontal gyrus, cluster size 39 voxel, coordinates -44 -14 24). Tracking was initiated in all 37 control subjects. The resulting group track clearly showed the arcuate fasciculus connecting the inferior frontal gyrus to the superior temporal lobe, and also demonstrated tracks projecting into the post-central gyrus and the inferior longitudinal fasciculus projecting to the temporal pole (figure 4.5).

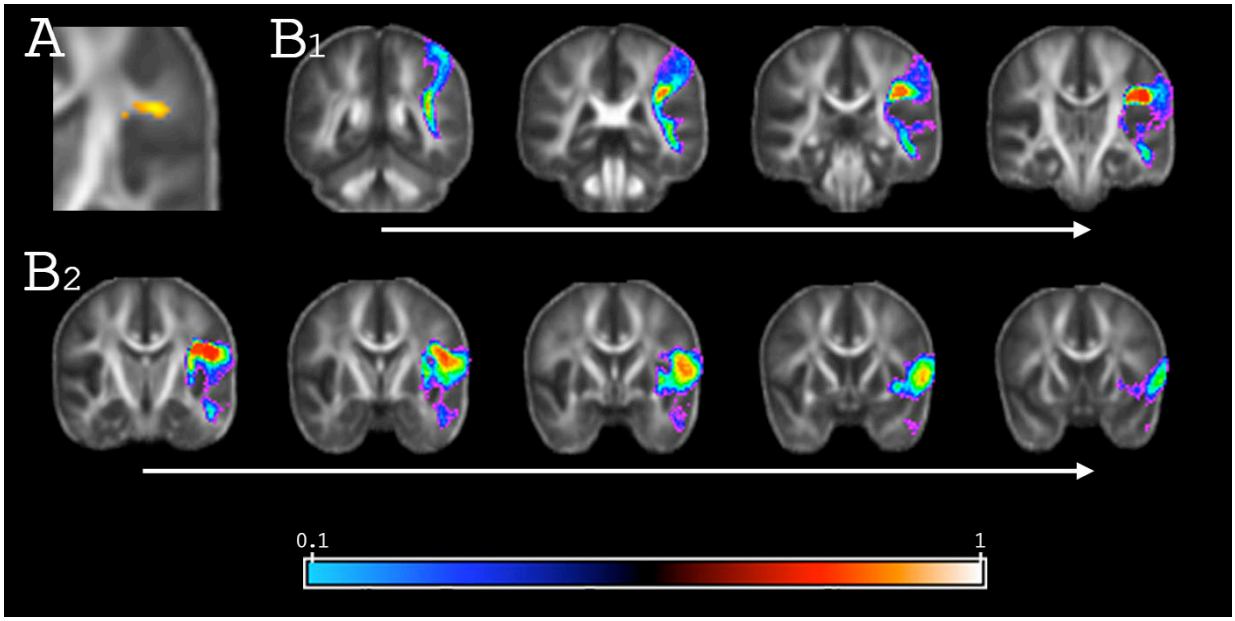

Figure 4.5 - Fibre tracking results. Probalistic tractography seeded from an area of FA decrease (A) in the left root of the post-central gyrus leading towards the inferior frontal gyrus in the left HS group as detected by SPM. (B1+B2) Group map of the 37 control subjects displayed from posterior to anterior showing the arcuate fasciculus and projection fibres leading towards the inferior frontal, superior and middle temporal and post-central gyrus.

4.4.2.4 Correlations with age of onset and duration of epilepsy

No significant clusters were found to correlate with age of onset or duration of epilepsy using either SPM or TBSS.

4.5 Discussion

This is the first study to compare the application of VBM and TBSS to detect microstructural differences in white matter. Prior to the publication of this study, only one other study had employed whole brain analysis (VBM) of diffusion MRI in TLE patients (399). Our findings are consistent with this study, but also suggest TBSS is a more sensitive technique, that facilitates the detection of other white matter regions affected in TLE. DTI changes with reduced FA and increased MD were found in the ipsilateral temporal lobe, the limbic system and the inferior frontal gyrus including the AF. Contralateral temporal lobe changes were also detected, as were widespread bilateral changes of lower significance level.

4.5.1 Methodological considerations

From a theoretical point of view TBSS has some advantages over SPM for voxel-based DTI comparison (324). It should be more precise in achieving spatial comparability by projecting the data on a common skeleton than the SPM approach in which each and every voxel would need to be matched between subjects. The absence of a need for smoothing also aided precision and reduced problems from partial volume effects and cross-contamination of different tissues e.g. high CSF signal for MD. Another advantage is the reduced number of voxels and thus a far smaller multiple comparisons problem. In our study the expectation of a higher sensitivity for identifying white matter changes with TBSS was confirmed. Changes found by SPM were also detected by TBSS but were usually more extensive. When using a lower threshold (uncorrected p=0.0001) in SPM, suprathreshold clusters previously only detected by TBSS became evident (figures 4.3 and 4.4) as well. However without a clear prior hypothesis correction for multiple comparisons is needed in a voxel-based study to minimize false positive findings. Given the different statistical methods used by SPM (general linear model with family-wise error correction) and TBSS (non-parametric permutation based inference with cluster-level error correction) a direct comparison of statistical thresholds is challenging. Neither method found increased FA or decreased MD. This is in disagreement with a study done at 1.5 T that found decreased MD in the contralateral temporal lobe (399). Postictal diffusivity decrease, due to cytotoxic edema, has been demonstrated previously (364). However in the interictal period such changes are more difficult to explain since even in patients with ischemic stroke diffusivity decrease is resolved after 4 weeks, and in the chronic state increased diffusivity is seen (483).

An obvious feature of TBSS is that it is restricted to the skeleton, and thus will be insensitive to changes in grey matter, such as the hippocampus, that were detected using SPM. This is of particular concern when applying this technique to pathology located largely in grey matter (hippocampus). In addition, the SPM approach was a lot faster computationally since TBSS usually needs to compute N x N number of non-linear registrations to find the most representative target. In our study this step alone took approximately 14 days of processing using a set of 1-4 parallel dual-core AMD Opteron workstations. However newer versions of TBSS that use a predefined FA

template should be faster, especially when processing large subject numbers (see later results chapters).

4.5.2 White matter microstructural differences

DTI changes in mTLE with HS, as manifested by increased MD and reduced FA, were not confined to the involved hippocampus but affected a larger network. It is of note that although many structures were affected in common, there were differences between left HS and right HS.

4.5.2.1 Ipsilateral temporal lobe

The ipsilateral temporal lobe was affected in left HS and right HS, although the pattern visualized was dependent on the technique used (SPM or TBSS) and the side of the focus (left HS or right HS). Increased MD was detected in the ipsilateral hippocampus by SPM in both groups. TBSS however, which does not include the hippocampus as part of the skeleton, only gave marginal results (figure 4.3). No FA reduction was found in the hippocampus but TBSS demonstrated FA reduction in the parahippocampal gyrus. This finding is consistent with those reported in chapter 3. This finding is also in line with previous ROI based studies of the hippocampus that found MD to be more sensitive than FA for lateralizing mTLE (374,375). The parahippocampal gyrus is the main input tract for the hippocampus and changes of this region concordant with the severity of HS have already been found in volumetric studies (86). Suprathreshold clusters of FA reduction in the ipsilateral temporal lobe were found in the mesial temporal pole and in the central temporal white matter extending into the central superior temporal gyrus. TBSS also detected reduced FA in the inferior and middle temporal gyri. Significant increases of MD were more widespread, involving the whole central white matter and all temporal lobe gyri. Findings were more extensive for the left HS than the right HS group but the patterns were similar. It however is important to point out that our right HS group was smaller then the left HS group and the difference in spatial extent could be at least partially due to lower statistical power (see below). Extrahippocampal changes of the ipsilateral temporal lobe have already been demonstrated with a variety of different techniques including volumetry (Moran et al., 2001)(86), voxel-based morphometry (VBM) (484), T2 relaxometry (485) and DTI (399).

4.5.2.2 Limbic system

In the left HS group the entire circuit of Papez showed DTI changes to some extent (figures 4.3 and 4.4). Increased MD was found in the involved hippocampus and FA reduction was detected in the ipsilateral fornix and in the anterior thalamus, with some MD increase in this region as well. The cingulum showed FA reduction bilaterally, particularly on the ipsilateral side and MD was increased ipsilaterally. In the parahippocampal gyrus, FA was reduced and MD increased ipsilaterally.

In the right HS group, the changes were subtler. MD was equally increased in the ipsilateral hippocampus, FA was reduced in parts of the fornix, bilaterally and FA was reduced and MD increased in the ipsilateral parahippocampal gyrus. In the thalamus there was only a small cluster in the dorso-lateral region and no findings in the anterior mesial region. The cingulum also showed an ipsilateral FA decrease, only with TBSS.

There is considerable evidence for the involvement of the limbic system in TLE, with thalamic atrophy and gliosis in 14 epilepsy patients, 11 of whom had HS (58). There are imaging reports of thalamic atrophy in mTLE (486,487) and increased diffusivity in the thalamus in children with TLE (488). VBM of segmented T1-weighted scans showed atrophy of the thalamus and the cingulate gyrus in TLE (449,451). More recently as described in the previous chapter, a number of tractography based studies have also demonstrated marked extensive, and bilateral limbic white matter abnormalities in unilateral TLE (393).

It is interesting to speculate why involvement of the limbic system was more widespread in left HS than right HS. In part, the right HS group was smaller (12 versus 21 patients) and statistical power could therefore be lower. In fact with lower thresholds of p=0.2 (FWE for SPM or cluster level correction for TBSS) some contralateral cingulum involvement could be detected but the anterior thalamus still did not show any changes and the clusters still were smaller then those seen in the left HS group. The main clinical measures of severity (duration of epilepsy and frequency of generalized seizures) were not different between the groups. The finding of a difference between left and right TLE groups is consistent with the results of the previous chapter. In addition, other

studies including those based on grey matter VBM (392,452), diffusion tractography (455,457) and white matter volumetric techniques (465) have also demonstrated differences between left and right TLE that cannot be attributed to differences in clinical variables. This reinforces the idea that they can be viewed as pathologically distinct entities. The cause of the differences seen in left and right TLE patients may be due to a combination of architectural, connectivity, physiological and developmental differences between the hemispheres. For example, the asymmetry of cerebral structure and function is well established (404,459), and it is possible that seizure propagation is more widespread in the dominant hemisphere on the basis of a pre-existing better connectivity.

4.5.2.3 Contralateral temporal lobe

In the left HS group, SPM detected no contralateral temporal lobe DTI changes. TBSS however showed an increased MD in the central contralateral temporal lobe white matter and a zone of decreased FA, posteriorly. In the right HS group, there was no MD increase in the contralateral temporal lobe but FA reductions were detected in the left superior temporal gyrus, and only by TBSS in the middle and inferior temporal gyrus as well.

This is the first study using a whole brain approach that demonstrates contralateral increases in MD or decreases in FA. Increased T2 relaxation times have been described in the contralateral hippocampus (190,489) and the central temporal white matter in TLE (485). DTI changes in the contralateral hippocampus have also been noted (380,399,488). In our study, even when lowering thresholds to p=0.0001 uncorrected, no such contralateral hippocampus changes could be found. The lack of contralateral hippocampus changes could be due to the fact that our study population was a pre-surgical cohort, and patients with bilateral hippocampus changes on quantification are usually not considered for epilepsy surgery.

4.5.2.4 Extratemporal and extralimbic changes

An interesting finding was a FA decrease in the root of the left posterior inferior frontal gyrus, in both the left HS and the right HS groups. With TBSS FA reduction was bilateral in this region for the left HS group although significance was higher ipsilateral. The inferior frontal gyrus is part of the language network and is the site of Broca's area which is connected to Wernicke's area in the

superior temporal gyrus via the arcuate fasciculus (AF) (405). It appeared plausible, therefore, that the reduced FA in this region may be due to changes in this tract between the temporal and frontal lobes. To evaluate this hypothesis we initiated fibre tracking from the cluster of decreased FA as detected by SPM and calculated a group tractography map for the control group (figure 4.5). It was evident that the AF did traverse through this region. Previous DTI studies of the AF have shown lateralization in healthy controls with higher FA values in the left AF for right-handed subjects (404). In left-handed subjects another study found increased relative fibre density in the left AF, irrespective of right-sided language lateralization (490). In TLE, language lateralization seems to be driven away from the epileptogenic focus with corresponding reductions in FA (405). In the present study we found left-sided FA reduction even in right HS patients and a bilateral but more left than right-sided FA reduction in left HS patients. This may be due to the fact that the dominant (usually left) side has pre-existing higher FA values and bilateral changes may therefore be easier to detect on this side since a uniform statistical threshold is always applied.

FA was also reduced in the anterior part of the body of the corpus callosum in the left HS and also in the right HS group. This part of the corpus callosum holds commissural fibers for pre-motor areas (491) and the significance of this finding in TLE is unclear at present.

We also found FA reduction of the external capsule contralaterally for the left HS group. Comparable changes were found with ROI-based DTI (400). The FA reduction and MD increase in the parietal and occipital lobe found more in the left HS group are of uncertain significance and may represent a more generalized loss of integrity and structure.

4.5.3 Validation of results and neurobiological considerations

Following the publication of this study, several studies have been conducted using comparable techniques, which report similar findings. These studies are summarized in table 4.3. Afzali et al (492) compared VBM and TBSS, and conclude that TBSS is more sensitive to white matter changes, and results in more localized findings. The studies by Shon et al (493) and Riley et al (479) corroborate the findings reported in our study. They also found extratemporal and bilateral white matter changes in TLE patients, particularly in those patients with left sided TLE. Similarly,

tractography and ROI based studies, as outlined in the previous chapter, including the meta-analysis by Otte et al (458), report widespread and bilateral white matter changes in unilateral TLE. These results are reassuring, but prompt two related questions. The first relates to the biological basis of the changes in diffusion parameters, and the second relates to whether the changes seen are a cause or consequence of seizure activity.

4.5.3.1 Biology of diffusion changes

Since the publication of the results reported in this study, two studies have combined DTI and histological analysis in order to shed light on the underlying white matter changes found in TLE patients. In the first study Concha et al (494) reported on postsurgical fimbriae specimens from people with TLE. In this study they found an increased extra-axonal fraction, reduced axonal membrane circumference, and reduced myelination. The pre-surgical FA values correlated significantly with the reduction in axonal membrane circumference, and showed a trend towards decreased myelin thickness. There were no significant correlations between histology and MD values. Ultimately in the future, histopathology-MRI studies such as this should be used to understand the biological substrate of changes in FA, and axial/radial diffusivity. In the second study, van Eijsden et al (495) studied juvenile rat white matter after pilocarpine induced status epilepticus. The authors reported decreased staining with luxol fast blue (myelin marker) that preceded a reduction in corpus callosum and fornix FA. The authors concluded that changes in myelination rather than changes in axonal integrity were predominantly responsible for diffusion changes apparent on MRI.

Authors	Whole-brain analysis technique	No of TLE patients (left:right)	DTI abnormalities
Thivard et al 2005 (399)	VBM	18:17	Ipsilateral hippocampus / temporal pole / parahippocampal gyrus / parietal and frontal lobes Contralateral non-sclerotic hippocampus / amygdala / temporal pole
Riley et al 2010 (479)	TBSS	10:2 (combined group – ipsilateral v contralateral)	Ipsilateral anterior/medial temporal / cerebellum Contralateral fronto-parietal
Shon et al 2010 (493)	VBM	12:7 (with HS) 10:8 (no HS)	Ipsilateral hippocampus / posterior cingulum / corpus callosum Contralateral occipital / temporal - only in LTLE Ipsilateral posterior fornix / posterior cingulum - only in LTLE
Afzali et al 2011 (492)	TBSS and VBM	11:8 (combined group)	TBSS more sensitive than VBM Left and right parahippocampal gyrus / superior-middle-inferior temporal gyri / fornix / inferior frontal gyrus / anterior corpus callosus / post central gyrus Unable to differentiate between LTLE and RTLE as groups combined

Table 4.3 – Reported studies using whole brain assessment of diffusion MRI

4.5.3.2 Cause or consequence?

Despite widespread agreement regarding the extent and severity of white matter changes that are seen in patients with TLE, the pathophysiological mechanisms underlying the generation of such changes remains unknown. A number of hypotheses have been proposed which include altered brain development, and plasticity-related reorganization of local and global white matter networks. Perhaps the most intuitive explanation of such changes is that they are the direct effect of axonal damage and associated secondary Wallerian degeneration in ipsilateral bundles due to repetitive seizure spread, and the effect of interictal spike propagating through the white matter epileptic network. In support of this hypothesis, Concha et al (496) have recently published a study in which they evaluated point-wise differences in diffusion parameters along the uncinate, inferior longitudinal and arcuate fasciculi at group and subject levels. They report a centrifugal pattern of increased MD, which tapers off as tracts exit the temporal lobe probably. The authors concluded that this reflects astrogliosis related to chronic seizure activity in the vicinity of the focus, rather than being due to hippocampal damage, and indeed they reported the same findings in patients with TLE but normal hippocampi. In support of this hypothesis, in a volumetric ROI based study by Keller et al (465), the authors observed correlations between the duration of epilepsy and FA of several ROIs along an anatomically plausible route, that included the ipsilateral parahippocampal gyrus, temporal lobe white matter, the thalamus bilaterally, and posterior regions of the corpus callosum that contain temporal lobe fibres. However, in contrast to this finding, none of the whole brain studies listed in table 4.5 showed significant correlations between white matter microstructure and parameters such as duration of epilepsy, age of onset, or seizure frequency. This is in accordance with the findings in our study. One reason for this could be that those studies using whole brain analysis, including the study reported here, are underpowered, and results are unable to survive whole brain correction. An alternative explanation is that there is another pathophysiological process underlying the white matter changes. One hypothesis proposes that widespread white matter changes are due to the initial lesion of the epileptogenic process that underlies and precedes seizure onset. Bonhila et al (497) combined a grey matter VBM study with probabilistic tractography from the hippocampus. They identified a decrease in hippocampal probabilistic tractography in patients with MTLE in limbic areas. A significant relationship between

loss of hippocampal connections and regional grey matter volume atrophy was found involving the putamen, pallidum, middle and inferior temporal areas, amygdala and ceberellar hemisphere. In view of the correlation between hippocampal disconnection and regional atrophy, the authors concluded that hippocampal deafferentation might contribute to extrahippocampal brain damage in TLE. The findings by other groups that white matter abnormalities are not as widespread or as severe in patients with TLE without HS compared to patients with TLE and HS, is supportive of this hypothesis (394,493). Ultimately, the white matter microstructural changes present in patients with TLE may be due to a combination of the above processes. In order to distinguish between them it may be necessary to study patients with hippocampal atrophy but without epilepsy, or the effects of longstanding seizures in patients with refractory primary generalized epilepsy.

4.6 Conclusion

This study has demonstrated that unilateral mTLE was associated with changes in a large network. Extensive reduction of FA and increased MD was evident in the limbic system in the left HS and to a lesser extent the right HS group. Further DTI changes were evident in the ipsilateral temporal lobe and the AF. There were differences in the pattern of changes between the left HS and right HS group with more widespread changes in left HS including the entire limbic system. In the right HS group contralateral findings in the temporal lobe and the inferior frontal gyrus were more prominent. It will be interesting to examine the limbic system and the other major projections of the temporal lobe that could play a key role in seizure propagation and to evaluate correlations with functional, neuropsychological scores and outcome after anterior temporal lobe resection.

5 The Structural Plasticity of White Matter Networks Following Anterior Temporal Lobe Resection

This chapter describes a study assessing the changes in white matter microstructure that occur after anterior temporal lobe resection. The material in this chapter has been published (see publications section).

5.1 Objectives

The previous chapter demonstrated that there were widespread, microstructural white matter differences between patients with TLE and controls. In this chapter we study the nature of white matter changes after epilepsy surgery. Because many fibre tracts are severed during surgery, understanding the effects of surgery on remaining white matter networks could have important clinical implications for predicting postsurgical morbidity. In addition, by assessing the nature of the white matter changes, particularly in areas distant from the surgery, where post-surgery Wallerian degeneration is expected to be minimal, one may gain a better understanding of the underlying mechanisms responsible for preoperative white matter changes. Reversible white matter diffusion abnormalities would be in favor of plasticity related changes secondary to either seizure cessation or the effects of surgery, while irreversible alterations would be compatible with axonal or myelin degeneration secondary to the underlying epileptogenic process.

5.2 Introduction

Though up to 80% of these patients may be rendered seizure free by surgery, up to 40% are also at risk of post-operative decline in memory and language functioning (205). Several functional magnetic resonance imaging (fMRI) and magnetoencephalography (MEG) studies have attempted to elucidate the functional reorganisation that occurs after surgery (498–503). Few studies have assessed the structural consequences of epilepsy surgery (401,504–506). Moreover, none of these studies have longitudinally assessed the nature of white matter changes after neurosurgery, and how these changes relate to functional and neuropsychological outcome in patients. The non-invasive, in-vivo nature of diffusion MRI allows for the longitudinal evaluation of white matter tracts in individuals. Whole-brain, voxel-wise analysis of data obviates the need for restriction to a

priori regions which can bias the interpretation of such data, and provides morphometric information regarding the changes that may occur in white matter after neurosurgery. There are several voxel based methods that can be applied. As demonstrated in the previous chapter tract based spatial statistics (TBSS) encompasses high sensitivity to, and excellent interpretation of, white matter tract changes in patients with temporal lobe epilepsy. This method uses a non-linear form of registration specifically optimised for diffusion data, and projects data from individual patients onto an alignment-invariant, group tract representation. This precludes the need for spatial smoothing of data, which can hinder the sensitivity and interpretation of the results, particularly in those patients who have had surgery (323,324). Significant clusters identified at a group level by such methods, can then be deprojected and back normalised into individual subjects in order to provide quantitative information in each subject that can be statistically analysed. These regions can also be used as seed regions for tractography which provides complementary information regarding the morphology of those areas identified with voxel based methods.

We applied these techniques to a group of patients with TLE in whom DTI data was acquired before and after anterior temporal lobe resection. The aims of this study were, first, to assess on a voxel-wise basis, and without any a priori hypothesis, the location and extent of structural white matter changes after temporal lobe surgery. Second, to investigate the causes of these changes and how they relate to expressive language function outcome in these patients.

5.3 Methods

5.3.1 Subjects

We studied 26 left (mean 37 years, range 18 – 62 years, 10 male) and 20 right (mean 37 years, range 22 – 52 years, 8 male) TLE patients, all of whom were medically refractory. All patients underwent pre-surgical evaluation, and subsequent anterior temporal lobe resection for the treatment of their epilepsy, at National Hospital for Neurology and Neurosurgery, London, UK. All patients had undergone structural MRI at 3 Tesla (3T) (185), and video-EEG had confirmed seizure onset in the temporal lobe ipsilateral to the resection. 6/26 left and 2/20 right TLE patients, also had intracranial recordings to localise seizure onset to the temporal lobe ipsilateral to the

resection. Four of the 26 patients with left TLE, had normal structural MRI, and histopathology of the resected specimen revealed end folium sclerosis. Two of the 20 right TLE patients had anterior temporal lobe cavernomas, and one had a normal structural MRI and histopathology of the resected specimen revealed end folium gliosis. All remaining patients had HS identified on MRI ipsilateral to seizure onset, and all patients had a normal, contralateral hippocampus based on qualitative and quantitative MRI (435). Post operative histopathology confirmed the MRI findings in all cases. All patients were taking anti-epileptic medication and all, except two patients with LTLE, spoke English as a first language. Handedness was determined using the Edinburgh handedness inventory (416), and language dominance was determined using a range of fMRI tasks which have been described previously, and include the use of verbal fluency measures (404). In brief, this paradigm consisted of a blocked experimental design with 30 seconds activation blocks alternating with 30 seconds of cross-hair fixation during the baseline condition over 5.5 minutes. During the activation phase, subjects were asked to covertly generate different words beginning with a visually presented letter (A, S, W, D and E). The data were analysed using statistical parametric mapping (SPM5) (Wellcome Trust Centre for Imaging Neuroscience (http://www.fil.ion.ucl.ac.uk/spm/)). Scans from each subject were realigned using the mean image as a reference, spatially normalised into standard space (using a scanner specific template created from 30 healthy controls, 15 patients with left hippocampal sclerosis and 15 patients with right hippocampal sclerosis) and spatially smoothed with a Gaussian kernel of 10 mm FWHM. Lateralisation indices were derived in subjects using the bootstrap method of the SPM lateralisation index toolbox (507), which was applied to the verbal fluency contrast in the middle and inferior frontal gyri. Patients with a laterality index of < -0.4 or > 0.4 were described as left and right dominant respectively, while those patients with laterality indices between -0.4 and 0.4 were described as having bilateral representation of language (508).

The standard neurosurgical procedure undergone by these patients, consisted of removal of the temporal pole, opening of the temporal horn, followed by en bloc resection of the hippocampus with a posterior resection margin at the mid brainstem level. Typically, the anterior-posterior extent of the temporal lobe resection as measured from the temporal pole to the posterior margin of resection, is 30% and 35% of the distance from the temporal pole to the occipital pole after left and right anterior temporal lobe resection respectively.

Patient demographics, clinical information and surgical outcome data (based on the ILAE classification of post-operative seizure outcome (227)) at the time of the post-operative scan following epilepsy surgery are listed in Table 5.1.

5.3.2 Neuropsychology

All patients, except the two in whom English was not their first language, completed the McKenna Graded Naming Test pre- and post-operatively. In this test, the subject is asked to name 30 black and white line drawings of increasing difficulty. The total number of items correctly named is the performance indicator (509). The same patients also performed two verbal fluency tests pre- and post-operatively. In the first letter fluency test, the patient is given 60 seconds to produce as many words starting with the letter "S", and in the second category fluency test the subject is asked to name as many animals as possible. The total number of words correctly produced is the performance indicator (510). Using these raw values, the percentage change following surgery of each parameter was calculated using the following formula [(Post-operative value – Pre-operative value)/(Pre-operative value)]*100. We expected a high degree of correlation between the letters "S" and "A" in the pre-operative scores, post-operative scores and percentage changes in verbal fluency. Therefore we used a principal components analysis within SPSS v14.0 (SPSS inc. Chicago, USA) to identify a factor accounting for the largest component of variance amongst each of these three pairs of scores. For all three pairs, both measures were entered into a principal components analysis, from which the first principal component was extracted, and used to represent overall pre- and post-operative verbal fluency and change in verbal fluency following surgery.

5.3.3 MR data acquisition

We acquired the clinical T1 data on a 3T scanner (GE Excite II) using the sequence and parameters described in chapter 2. A single investigator (MY) manually segmented the surgical resection area of each patient's post operative T1-weighted volumetric MR scan, creating individual regions of interest (ROI). These ROIs were used to quantify the volume of resection in each patient.

5.3.3.1 Diffusion tensor imaging acquisition

The DTI data was acquired on the 3T scanner using the sequence and parameters described in chapter 2.

5.3.4 Diffusion tensor imaging processing

All scans were transferred to a Linux Sun Ultra 40 workstation and processed with FSL 4.1.3 (http://www.fmrib.ox.ac.uk/fsl/) (422). The DICOM files of each DTI acquisition were converted into a single multivolume NifTI file. This file was then corrected for eddy current distortion, and movement artefact by affine registering, every individual volume to the first b=0 volume. After this co-registration step the 6 b=0 volumes of each patient were extracted and averaged. A single investigator (MY) used the average of the post-operative b=0 images to manually segment the surgical resection area in each patient, creating individual ROIs. Each ROI was then transformed into an inverse binary mask. The main diffusion tensor and its eigenvalues (λ_1, λ_2, λ_3) and eigenvectors were then estimated for each voxel (284), along with the summary parameters fractional anisotropy (FA) and mean diffusivity (MD) (290). By sorting the eigenvalues in order of decreasing magnitude for each voxel ($\lambda1 > \lambda2 > \lambda3$), $\lambda1$ represents the diffusivity along the primary diffusion direction, that is along the fibre axis, and is referred to as the axial diffusivity $\lambda \parallel$. The averaged water diffusivities perpendicular to the axonal fibres, $\lambda2$ and $\lambda3$ are referred to as $\lambda \perp = (\lambda2 + \lambda3)/2$, or the radial diffusivity (511).

In order to align all FA data into a common space, the following procedure was applied separately for left and right TLE patients. First, all patients' pre-operative FA data were aligned to the FMRIB58_FA standard space template supplied with FSL, using the nonlinear registration tool FNIRT (512,513), which uses a b-spline representation of the registration warp field (514). Secondly, each patient's post-operative FA image was co-registered to its pre-operative FA image using the linear registration tool FLIRT (304,515) and FNIRT. During this registration step the surgical ROI created from the post-operative b=0 image was used to de-weight this area, such that the registration process ignores the information under the mask and prevents the surgically resected area contributing to the image registration (516,517). Finally, the warps derived from each of the two steps were combined, and the resulting warp was applied to the native, post-

operative FA image in each subject. In this manner all pre- and post-operative data for subjects were aligned in a common space, and all images including post-operative data were re-sampled only once. Following this, voxel-wise statistical analysis of the FA data was carried out in the left and right TLE groups separately, using TBSS (Tract-Based Spatial Statistics (324). The mean FA image across all pre- and post-operative images in each group was created, thinned, and thresholded at FA > 0.2 to create a mean FA skeleton which represents the centres of all tracts common to the group (324). Each patient's aligned FA and MD data were then projected onto this skeleton and the resulting data fed into voxel-wise cross-subject statistics.

In order to achieve accurate inference, including appropriate correction for multiple comparisons over space, we used permutation-based, non-parametric inference on a voxel-by-voxel basis (327). A paired t-test (5000 permutations) was used to assess the location and extent of significant increases and decreases in the FA and MD between pre- and post-operative scans in each group. Threshold free cluster enhancement was used to correct results for multiple comparisons, and results were considered significant for $p < 0.05$. Threshold free cluster enhancement is more sensitive than traditional cluster based methods of thresholding, and does not require the setting of an arbitrary, initial cluster-forming threshold, or need a large amount of data smoothing (326). Significant clusters were superimposed on the mean FA image and the MNI152 template supplied by FSL. FSLview and its atlas tools (International Consortium of Brain Mapping DTI-81 white matter labels atlas and John Hopkins University white matter probabilistic tractography atlas) in addition to general neuroanatomy atlases (518,519) were used to anatomically label the location of significant clusters in MNI152 space.

In order to both validate and investigate our results further at an individual subject level, we de-projected and reverse-normalised significant clusters of changes in FA into their native pre- and post-operative images. Using these native clusters, mean pre- and post-operative FA, MD, $\lambda \parallel$, and $\lambda \perp$ values were calculated by masking the corresponding whole-brain diffusion parameter images with the clusters. Pre- to post-operative percentage changes in each parameter in these clusters were then calculated using the equation above. These clusters were also masked with the b=0

derived surgical masks in order to exclude those CSF filled areas within the area of resection, which would confound the results.

5.3.5 Tractography

In order to assess the patterns of connections of selected clusters derived from the whole brain analysis, fibre tracking was carried out using FMRIB's Diffusion toolbox (FDT) v2.0 (http://www.fmrib.ox.ac.uk/fsl/) (422). In both groups, the diffusion characteristics were calculated in each voxel in each patient using a Markov Chain Monte Carlo sampling method (295). In order to improve tractography in areas of crossing fibres, a two tensor model was applied to the data (299). Probabilistic tracking was then seeded using the local maxima derived from the significant clusters obtained with the whole brain TBSS analysis. Tracking was carried out in individual native space, and therefore, the seeding mask was de-projected and reverse-normalized before tracking was initiated. Tractography used default parameter settings (5000 iterations, 80 degrees curvature threshold) and tracts were thresholded at 10% of the number of streamlines generated. The resulting, thresholded, native space tracks were then spatially normalized by applying the same transformation matrix used to normalize the FA map in each patient. Tracts were then binarised and averaged to form a group map, which was superimposed upon the FSL MNI-152 T1 template with FSLview for the purpose of visualisation. In these "group variability" maps, each pixel reflects the percentage of subjects that contained a particular tract seeded with clusters derived from the whole brain analysis. This approach enables the visualisation of the consistency of the core of such tracts across a group of subjects.

5.3.6 Statistical analysis of clinical data and native clusters

Statistical analyses were performed with SPSS v14.0 (SPSS inc. Chicago, USA), and the threshold for statistical significance was set at $p < 0.05$. The normality of distribution of continuous, clinical variables was tested using the Kolmogorov-Smirnov test. Clinical variables (age, sex, age of onset of epilepsy, duration of epilepsy, resection volume, interval from surgery to post-operative scan, number of seizure free patients at time of post-operative scan, the average number of drugs before and after surgery) in left and right temporal lobe epilepsy groups were then compared using the independent samples t-test (continuous normally distributed variables), the Mann-Whitney U-test

(continuous non-normally distributed variables), and the Chi squared exact test (categorical variables).

The Kolmogorov-Smirnov test was also used to test the distribution of all DTI related native cluster parameters, and mean pre- and post-operative cluster diffusion parameters were compared using paired t-tests (continuous normally distributed variables), and the Wilcoxon signed ranks test (continuous non-parametrically distributed variables). The relationship between diffusion parameters, and Graded Naming Test and verbal fluency scores was assessed using Pearson's correlation test. A repeat partial correlation controlling for IQ and language laterality was also carried out.

5.4 Results

5.4.1 Clinical data

The clinical characteristics of the subjects studied are listed in table 5.1. There were no significant differences in the age or duration of epilepsy of the left TLE and right TLE patients at the time of surgery, and no significant difference in the number of pre- or post-operative medications between left TLE and right TLE patients. The mean left anterior temporal lobe resection volume was 18% smaller than the mean right sided resection [$t = -2.04$ (44), $p = 0.047$]. There were no significant differences in pre- and post-operative numbers of medications in either left TLE or right TLE patients. There was no significant difference in age of onset, duration of epilepsy, or interval from surgery to post-operative scan between left TLE and right TLE groups. There were no significant differences in either the gender distribution or the numbers of patients who were seizure free at the time of post-operative scans.

	LTLE (range)	RTLE (range)
No of subjects	26	20
Sex – no of males	10	8
Mean age in years	37 (18 – 62)	37 (22 – 52)
Average age of epilepsy onset in years	9 (1 – 26)	10 (1 – 37)
Average duration of epilepsy in years	28 (8 – 60)	27 (6 – 47)
Average language lateralisation index	-0.64 (-0.97 – 0.63)	-0.41 (-1 – 0.48)
Average surgical resection volume in mm3	21,087 (8809 – 30761)	24,942 (10368 – 39025)
Average interval from surgery to scan in days	127 (90 – 193)	141 (85 – 351)
Number of patients of given ILAE class at time of post-operative scan	Class 1 - 21 / 81% Class 2 - 2 Class 3 - 1 Class 4 - 1 Class 5 – 1	Class 1- 14 / 70% Class 2 - 1 Class 3 - 4 Class 4 - 1
Average number of pre-operative medications	2 (0 – 4)	2 (2 – 3)
Average number of post-operative medications	2 (1 – 4)	2 (1 – 3)

Table 5.1 – Summary of the clinical characteristics of left and right temporal lobe epilepsy patients

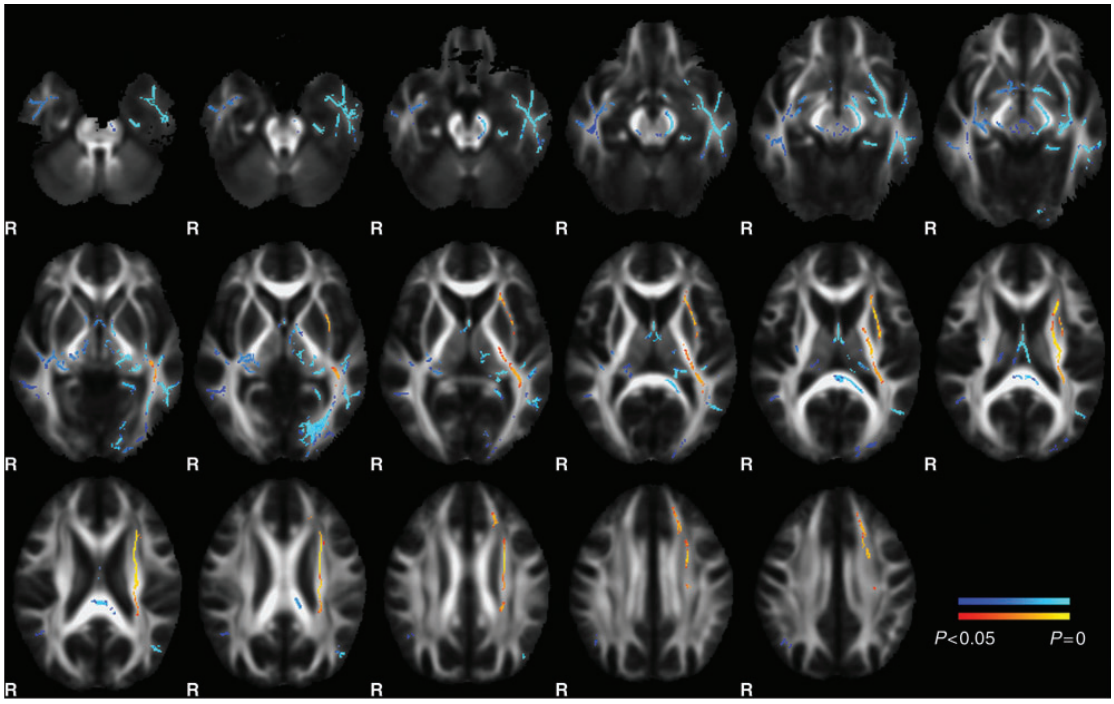

Figure 5.1 - Threshold free cluster enhanced corrected (p<0.05) results of the whole brain tract based spatial statistics analysis of FA after left anterior temporal lobe resection. The left side of the brain is on the right side of the image. R = right. Significant clusters representing increases (red to yellow) and decreases (blue to light blue) in FA after surgery are projected onto the mean FA template derived from all pre- and postoperative left temporal lobe epilepsy patients. For clarity, the group FA skeleton is not shown. The area of resection is visible inferiorly in the left temporal lobe where the white matter bundles are absent. FA reduction after left anterior temporal lobe resection is apparent in the left temporal and occipital lobes, fornix, splenium and anterior commissure. There are also decreases in fractional anisotropy to a lesser extent in the contralateral hemisphere. FA increases are present in the external capsule, posterior limb of the internal capsule and corona radiata. See table 5.2 for more detail regarding the anatomical location of local maxima.

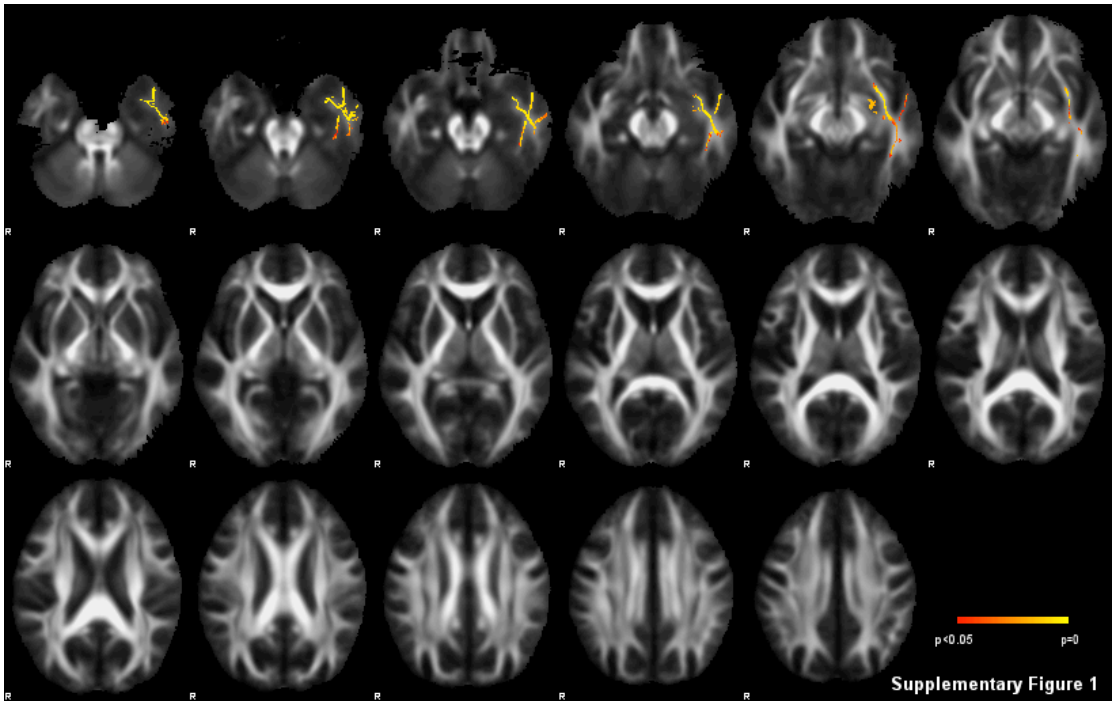

Figure 5.2 - Threshold free cluster enhanced corrected ($p<0.05$) results of the whole brain TBSS analysis of MD after left anterior temporal lobe resection. The left side of the brain is on the right side of the image. R = right. Significant clusters representing increases (red to yellow) in MD after surgery are projected onto the mean FA template derived from all pre- and postoperative left temporal lobe epilepsy patients. For clarity, the group FA skeleton is not shown. The area of resection is visible inferiorly in the left temporal lobe where the white matter bundles are absent. MD increases are predominantly located in the vicinity of the area of surgical resection, including the temporal portion of the uncinate fasciculus and inferior longitudinal fasciculus.

Post-operative reduction of FA after left ATLR	Left inferior longitudinal fasciculus (p<0.001) (may also contain fibres of left fronto-occipital fasciculus posteriorly) Right inferior longitudinal fasciculus – temporal portion (p=0.025) Left parahippocampal gyrus (p<0.001) Left cerebral peduncle (p<0.001) (containing corticopontine, corticospinal, and corticobulbar fibres) Left uncinate fasciculus – temporal portion and portion lying on anterior floor of external capsule (p<0.001) Left inferior fronto-occipital fasciculus – portion lying in anterior floor of the external capsule superior to left uncinate fasciculus (p<0.001) Left fornix (crura, and columns) (p<0.001) Right fornix (crura, and columns) (p<0.001) Body of fornix (p<0.001) Left geniculo-calcarine tract (p<0.001) Splenium of corpus callosum/forceps major (p<0.001) Left superior longitudinal fasciculus – temporal portion connecting to superior, and middle temporal gyri (p<0.001) Left anterior commissure (p<0.001) Right anterior commissure (p=0.022) Right retrolenticular internal capsule (p=0.021)
Post-operative increase in FA after left ATLR	Left anterior corona radiata (p=0.014) Left posterior corona radiata (p=0.006) Left superior corona radiata (p=0.006) Left anterior-dorsal limb internal capsule (p=0.001) Left posterior limb internal capsule (p=0.005) Left retrolenticular region internal capsule (p=0.015) Left external capsule (p=0.008) Left superior frontal gyrus white matter (p=0.014) Left inferior frontal gyrus white matter (p=0.013)
Post-operative increase in MD after left ATLR	Left inferior longitudinal fasciculus – temporal portion (p<0.001) Left uncinate fasciculus – temporal portion (p<0.001) Part of left anterior commissure (p=0.014) Left anterior floor external capsule – containing fibres of uncinate fasciculus and inferior fronto-occipital fasciculus (p=0.03)

Table 5.2 - Summary of significant local maxima clusters found in whole brain analysis of left TLE patients after left ATLR (anterior temporal lobe resection).

Maximum p values of local maxima clusters are given in brackets.

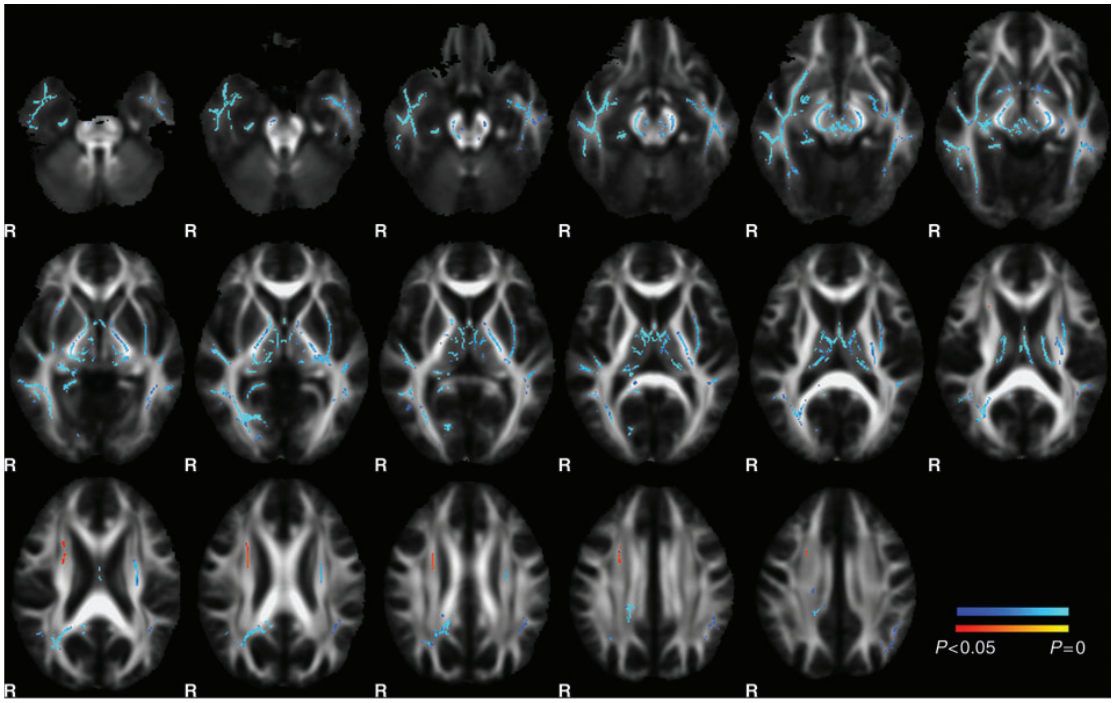

Figure 5.3 - Threshold free cluster enhanced corrected (p<0.05) results of the whole brain tract based spatial statistics analysis of FA after right anterior temporal lobe resection. Significant clusters representing increases (red to yellow) and decreases (blue to light blue) in FA are projected onto the mean FA template derived from all pre- and postoperative right temporal lobe epilepsy patients. For clarity, the group FA skeleton is not shown. The area of resection is visible inferiorly in the right temporal lobe where the white matter bundles are absent. The left side of the brain is on the right side of the image. R = right. FA reduction after right anterior temporal lobe resection is apparent in the right temporal lobe, occipital lobe, fornix, splenium, anterior commissure and both cerebral peduncles. There are also decreases in FA to a lesser extent in the contralateral hemisphere. In comparison to patients undergoing a left anterior temporal lobe resection, there is only a very small area of increased FA in the anterior corona radiata.

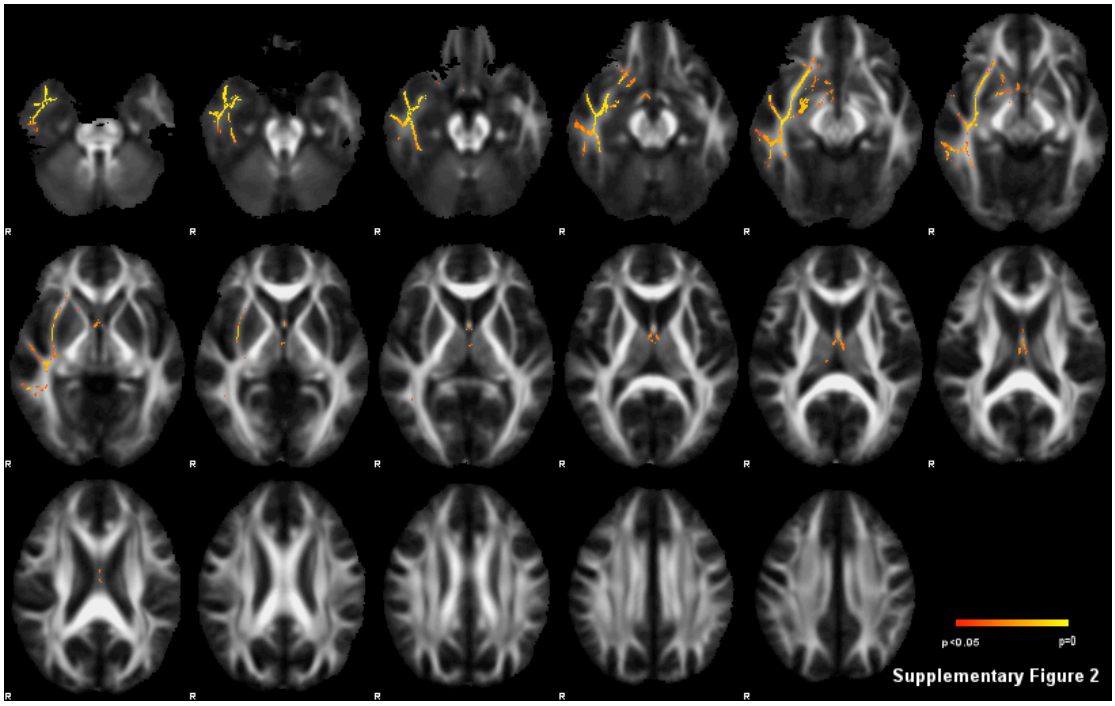

Figure 5.4 - Threshold free cluster enhanced corrected ($p<0.05$) results of the whole brain TBSS analysis of MD after right anterior temporal lobe resection. Significant clusters representing increases (red to yellow) in MD after surgery are projected onto the mean FA template derived from all pre- and postoperative right temporal lobe epilepsy patients. For clarity, the group FA skeleton is not shown. The area of resection is visible inferiorly in the right temporal lobe where the white matter bundles are absent. The left side of the brain is on the right side of the image. R = right. The location of the increase in MD is similar, though more extensive, to that seen after left anterior temporal lobe resection. MD increases are predominantly located within the surgical resection zone itself as well as its penumbra.

Table 5.3 - Summary of significant local maxima clusters found in whole brain analysis of right TLE patients after right ATLR (anterior temporal lobe resection).

Maximum p values of local maxima clusters are given in brackets.

Post-operative reduction of FA after right ATLR	Right inferior longitudinal fasciculus (p<0.001) (may also contain fibres of left fronto-occipital fasciculus posteriorly) Left inferior longitudinal fasciculus (p=0.013) (may also contain fibres of left fronto-occipital fasciculus posteriorly) Right parahippocampal gyrus (p<0.001) Right cerebral peduncle (p<0.001) (containing corticopontine, corticospinal, and corticobulbar fibres) Left cerebral peduncle (p=0.012) (containing corticopontine, corticospinal, and corticobulbar fibres) Right uncinate fasciculus – temporal portion and portion lying on anterior floor of external capsule (p<0.001) Right inferior fronto-occipital fasciculus – portion lying in anterior floor of the external capsule superior to left uncinate fasciculus (p<0.001) Left external capsule (p=0.012) Right fornix (crura, and columns) (p<0.001) Left fornix (crura, and columns) (p<0.001) Body of fornix (p<0.001) Right geniculo-calcarine tract (p<0.001) Splenium of corpus callosum/forceps major (p=0.015) Right superior longitudinal fasciculus – temporal portion connecting to superior, and middle temporal gyri (p<0.001) Right anterior commissure (p<0.001) Left anterior commissure (p=0.013) Left posterior limb of internal capsule (p=0.012)
Post-operative increase of FA after right ATLR	Right superior corona radiata (p=0.034)
Post-operative increase in MD after right ATLR	Right inferior longitudinal fasciculus – temporal portion (p<0.001) Right uncinate fasciculus – temporal portion (p<0.001) Part of right anterior commissure (p=0.015) Right anterior floor external capsule – containing fibres of uncinate fasciculus and inferior fronto-occipital fasciculus (p=0.007) Part of body of fornix (p=0.029) Right crura of fornix (p=0.026) Left crura of fornix (p=0.026)

5.4.2 Whole brain analysis - left TLE patients

Following left anterior temporal lobe resection there were significant decreases in FA in the main fibre tracts ipsilateral to the side of surgery, and also to a lesser extent in the contralateral hemisphere (figure 5.1). The areas of decreased FA corresponded to one contiguous, large cluster of 15,240 voxels ($p<0.001$). The local maxima of this cluster were determined, in order to investigate the anatomy of this cluster further (table 5.2). The most significant decreases in FA were on the left side in the geniculo-calcarine tract and its projection to the lingual/occipital fusiform gyri, and intracalcarine cortex, part of the inferior longitudinal fasciculus, parahippocampal gyrus, crura of the fornix, anterior commissure, and the anterior temporal portions of the superior longitudinal fasciculus. There were also significant decreases of FA in the temporal portion of the left uncinate fasciculus that connects to the temporal pole, and the anterior floor of the external capsule. The latter structure contains fibres of the uncinate and inferior fronto-occipital fasciculi. Less significant decreases in FA were also noted on the contralateral side in the fornix, anterior commissure and temporal portion of the inferior longitudinal fasciculus. Analysis of the de-projected, pre- and post-operative native clusters (table 5.4) confirmed that there was a significant mean 7.08% decrease in FA in these areas post-operatively ($z=-3.845$, $p<0.001$) due mainly to a mean 7.77% increase in $\lambda\perp$ ($z=-3.883$, $p<0.001$). MD was also significantly increased by a mean 4.75% post-operatively in these areas ($z=-3.735$, $p<0.001$).

There were also widespread increases in FA evident an average of 4.5 months after left anterior temporal lobe resection, consisting of a single contiguous cluster of 3412 voxels ($p<0.001$) (figure 5.1). This cluster extended across a number of regions that included the anterior, posterior and superior corona radiata, the posterior limb (including the retrolenticular region) and dorsal part of the anterior limb of the internal capsule, and the external capsule (table 5.2). Analysis of the de-projected, native pre- and post-operative clusters (table 5.4) using paired t-tests confirmed a mean 7.84% post-operative increase in FA in this area [$t = -7.470$ (25), $p < 0.001$]. This was due to a mean 2.95% post-operative increase in $\lambda\parallel$ ($t = -3.363$ (25), $p = 0.002$), and a mean 4.74% decrease in $\lambda\perp$ ($t = 3.336$ (25), $p = 0.003$) (table 5.4). There was no significant difference in MD values (mean -0.76%) in these clusters between pre- and post-operative patients.

Post-operative increases in MD were more limited consisting of a cluster of 2917 voxels ($p<0.001$). This cluster was restricted in distribution to those anterior portions of the inferior longitudinal fasciculus and uncinate fasciculus lying predominantly within the area of resection in patients (figure 5.2 and table 5.2). There were no significant decreases in MD after surgery.

5.4.3 Whole brain analysis - right TLE patients

There were similar patterns of decreases in FA after right anterior temporal lobe resection, with a single significant cluster consisting of 19,248 voxels ($p<0.001$) (figure 5.3). The local maxima of this cluster are described in more detail in table 5.3. Analysis of the pre- and post-operative de-projected, native cluster confirmed that there was a significant mean 6.76% reduction in FA in these areas ($z = -4.178$, $p<0.001$), that was predominantly due to a mean 8.43% increase in $\lambda\perp$ ($z = -3.709$, $p<0.001$) (table 5.4). MD was also significantly increased post-operatively in these areas by a mean 5.36% ($z=-3.467$, $p<0.001$) (table 5.4).

The location of the increase in MD was similar to that seen after left anterior temporal lobe resection, and consisted primarily of a cluster of 5850 voxels located within the surgical resection zone itself as well as its penumbra ($p<0.001$) (figure 5.4).

In contrast to the effects of left anterior temporal lobe resection, there was a very limited pattern of post-operative FA increases after right anterior temporal lobe resection. A small, 255 voxel, peripheral white matter cluster within the anterior corona radiata was noted ($p<0.001$) (figure 5.3). In view of the comparatively, small nature of this cluster, and its location in the periphery of the white matter skeleton, where mis-registration between scans is more likely, it was not analysed further. There were no significant post-operative decreases seen in MD using whole brain analysis.

Table 5.4 - Summary of the mean diffusion parameters of back normalised clusters identified from the whole brain analysis. Note in left and right TLE patients the area of resection in each patient has been masked out so that results are not confounded by the CSF filled surgical lacunae. (se=standard error)

	Left TLE Native Cluster FA Increase			Left TLE Native Cluster FA Decrease			Right TLE Native Cluster FA Decrease		
	Pre-Op	**Post-Op**	**% change**	**Pre-Op**	**Post-Op**	**% change**	**Pre-Op**	**Post-Op**	**% change**
FA (se)	0.47 (0.006)	0.51 (0.007)	7.84 (1.06)	0.37 (0.006)	0.35 (0.005)	-7.08 (0.94)	0.39 (0.007)	0.36 (0.005)	-6.76 (1.12)
MD mm^2/sec x 10^{-6} (se)	770 (7.12)	764 (7.77)	-0.76 (1.06)	856 (20.10)	895 (18.90)	4.75 (1.08)	819 (11.90)	864 (17.90)	5.36 (0.98)
$\lambda \parallel$ mm^2/sec x 10^{-6} (se)	1208 (12.22)	1242 (11.30)	2.95 (0.85)	1210 (18.67)	1226 (17.90)	1.42 (0.77)	1177 (10.46)	1203 (19.50)	2.13 (0.81)
$\lambda \perp$ mm^2/sec x 10^{-6} (se)	551 (6.70)	524 (8.17)	-4.74 (1.41)	680 (21.00)	730 (19.60)	7.77 (1.40)	640 (13.00)	694 (17.30)	8.43 (1.28)

5.4.4 ROI analysis

In order to ensure that these results were not related to potential confounds associated with the realignment and spatial normalisation of white matter tracts, we defined manual ROIs over the ipsilateral internal and external capsule on the raw, untransformed pre- and post-operative FA images of all patients who underwent left and right anterior temporal lobe resections. The ROIs were drawn over three consecutive axial slices beginning with the first slice in which the internal capsule could be clearly delineated from the external capsule. The anterior and posterior extents of the ROI were defined by lines tangential to the splenium and genu of the corpus callosum respectively (figure 5.5). After left anterior temporal lobe resection there was a significant mean 5.80% increase in FA in this regions [$t = 3.709$ (25), $p = 0.001$]. In contrast, there was no significant change in FA in this region after right anterior temporal lobe resection.

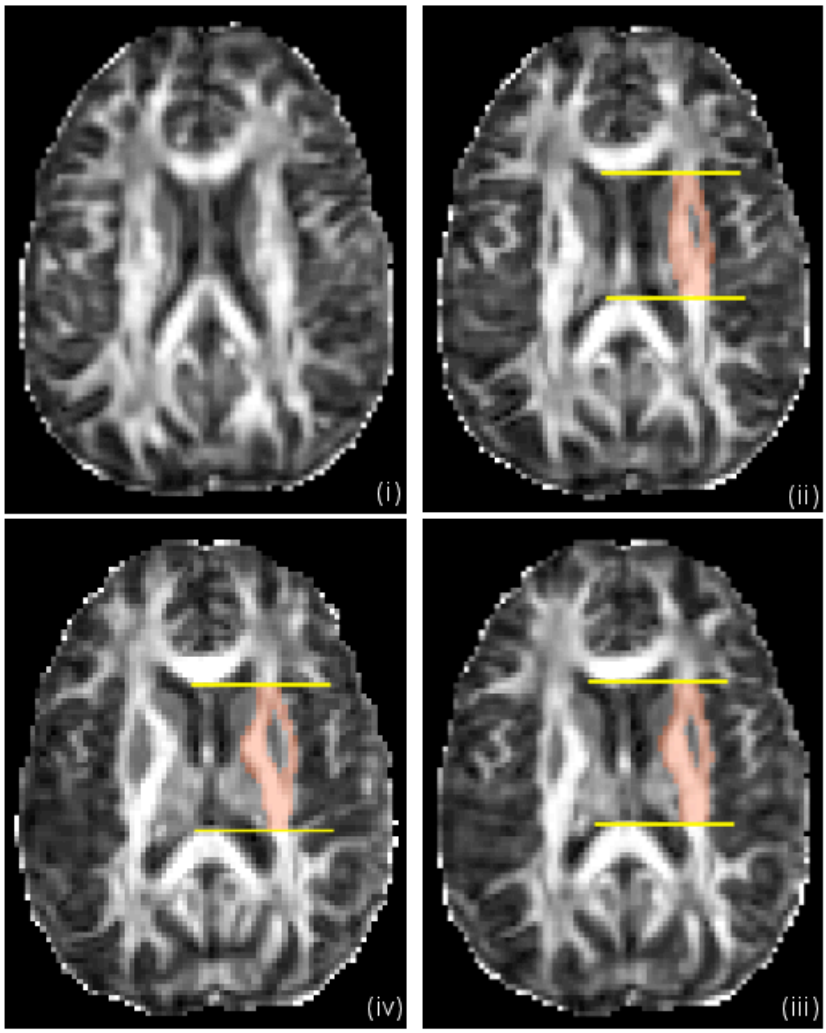

Figure 5.5 - An example of the method used to draw manual regions of interest (ROI) around the internal and external capsule. The first axial slice where the internal and external capsule were clearly differentiated was identified (ii) and ROIs were then drawn around the internal and external capsules over three consecutive slices (ii to iv). The anterior and posterior extents of the ROI were defined by lines tangential to the splenium and genu of the corpus callosum (yellow lines).

5.4.5 Analysis of cluster of increased FA after left anterior temporal lobe resection

Having identified the increase in FA after left anterior temporal lobe resection, we explored potential artefactual causes for this finding. While, scan-scan variability between pre- and post-operative acquisitions may confound results, previous assessments of such variability that have been carried out by our group suggest that this variability is of the order of 1 to 2% (520). This is significantly smaller than the changes observed in the present study. FA represents the degree of directionality of diffusion within individual voxels, and is therefore higher in voxels containing a single fibre population compared to two, crossing or kissing fibre populations. It is plausible therefore that if this cluster contains a predominance of voxels with two fibre bundles pre-operatively, and one of these bundles is directly or indirectly connected to the area of resection, downstream Wallerian degeneration may cause an apparent increase in FA (521). We rejected this explanation as there was no significant difference in the proportion of voxels within the pre- and post-operative deprojected native clusters modelled as containing two fibre populations by the DTI processing.

An alternative explanation for the changes observed changes relates to the mechanical shift that can occur in the brain after surgery. Removal of the anterior temporal lobe may cause deformation of other parts of the brain, leading to stretching of nerve fibre bundles which may result in an increase in FA. If this hypothesis is correct larger volumes of resection should cause greater shift in the remainder of the brain, and potentially more stretching of white matter. We refuted this hypothesis as there was no significant correlation between the surgical resection volume and the percentage change in FA, $\lambda \parallel$ or $\lambda \perp$ after surgery. Further, the mean right anterior temporal lobe resection volume was greater than the equivalent resection on the left and the increases in FA were seen only after left sided resections.

In order to assess the relationship of the increase in FA to seizure freedom and language we stratified all patients undergoing a left anterior temporal lobectomy into several subgroups. These included seizure-free (ILAE Class I – 21 patients) and non-seizure free (ILAE Class II to IV – 5 patients) groups at the time of their post-operative scan, and left (19 patients), bilateral (4

patients) and right (1 patients) hemisphere language dominant patients at the time of their surgery. A formal statistical comparison between the two groups is limited by the small numbers of patients in the non-seizure free and right hemisphere dominant groups. However, both non-seizure free and left hemisphere/bilaterally dominant patients had greater increases in FA compared to seizure-free (9.0% versus 7.4%) and right hemisphere dominant (7.6%/7.4% versus 3.9%) patients respectively.

5.4.6 Verbal fluency and naming after left anterior temporal lobe resection and relationship to cluster of increased FA

As expected, there were significant correlations between the category and letter fluency scores preoperatively ($r = 0.689$, $p<0.001$) and postoperatively ($r = 0.686$, $p<0.001$), and between the percentage change in category and letter fluency after surgery ($r = 0.421$, $p = 0.020$). Three principal components were therefore extracted and used to represent pre- and postoperative verbal fluency and the percentage change in verbal fluency. There was no significant correlation between pre- or post-operative mean FA in this cluster and pre-operative verbal fluency (figure 5.6a). However there was a significant correlation between the pre- and postoperative mean FA in this cluster, and post-operative verbal fluency ($r=0.482$, $p=0.009$ and $r=0.469$, $p=0.010$ respectively) (figure 5.6b). These correlations remained significant after correction for IQ and language lateralisation ($r=0.443$, $p=0.020$ and $r=0.435$, $p=0.022$).

This association was primarily underpinned by $\lambda \parallel$, and there was a correlation between percentage change in both verbal fluency and $\lambda \parallel$ after left anterior temporal lobe resection. That is, patients with the biggest increases in $\lambda \parallel$ after surgery had the smallest declines in verbal fluency ($r=0.398$, $p=0.027$). Again this correlation remained significant after correction for IQ and language lateralisation ($r=0.457$, $p=0.016$). It should be noted that all of the above correlations remained significant when letter and category fluencies were considered separately.

There was also a significant correlation between pre- and post-operative $\lambda \parallel$ in this cluster and the post-operative graded naming test score ($r=0.388$, $p=0.030$ and $r=0.480$, $p=0.009$ respectively), but not the pre-operative graded naming test score. In view of the apparent importance of $\lambda \parallel$ we

tested for a correlation between the percentage increase in this parameter and the interval between temporal lobe resection and post-operative scanning. Although there was a positive trend this was not significant due to the presence of an outlier who was the only patient with an ILAE outcome of class V in this group (figure 5.7). After exclusion of this outlier, this trend was significant ($r=0.400$, $p=0.024$), and the correlations between the diffusion parameters and verbal fluency and graded naming test scores remained significant.

In order to assess the specificity of these correlations we also calculated the global, mean pre- and postoperative FA across the whole brain. Neither of these measures correlated with pre- or postoperative verbal fluency or graded naming test scores. Furthermore, there was no correlation between the global percentage change in $\lambda \parallel$ and the interval between temporal lobe resection and post-operative scanning.

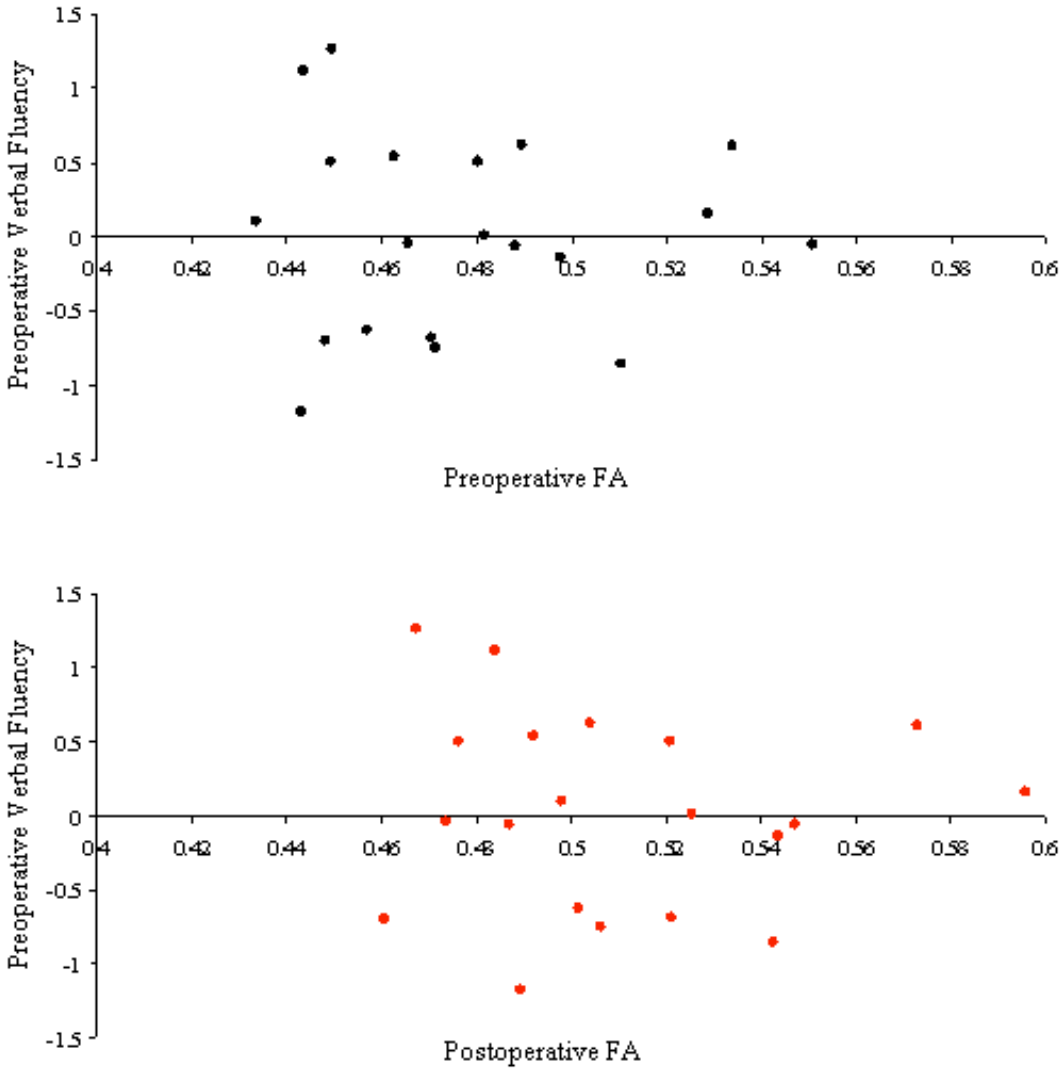

Figure 5.6 a and b – Scatterplots of pre- and post-operative verbal fluency scores against pre- and post-operative mean fractional anisotropy in left posterior limb internal capsule, external capsule and corona radiata.

(a) - Scatterplots of verbal fluency scores against mean fractional anisotropy in left posterior limb internal capsule, external capsule and corona radiata before (black dots) and after (red dots) left anterior temporal lobe resection. There was no significant correlation between the mean fractional anisotropy in this cluster before and after left anterior temporal lobe resection, and pre-operative verbal fluency scores.

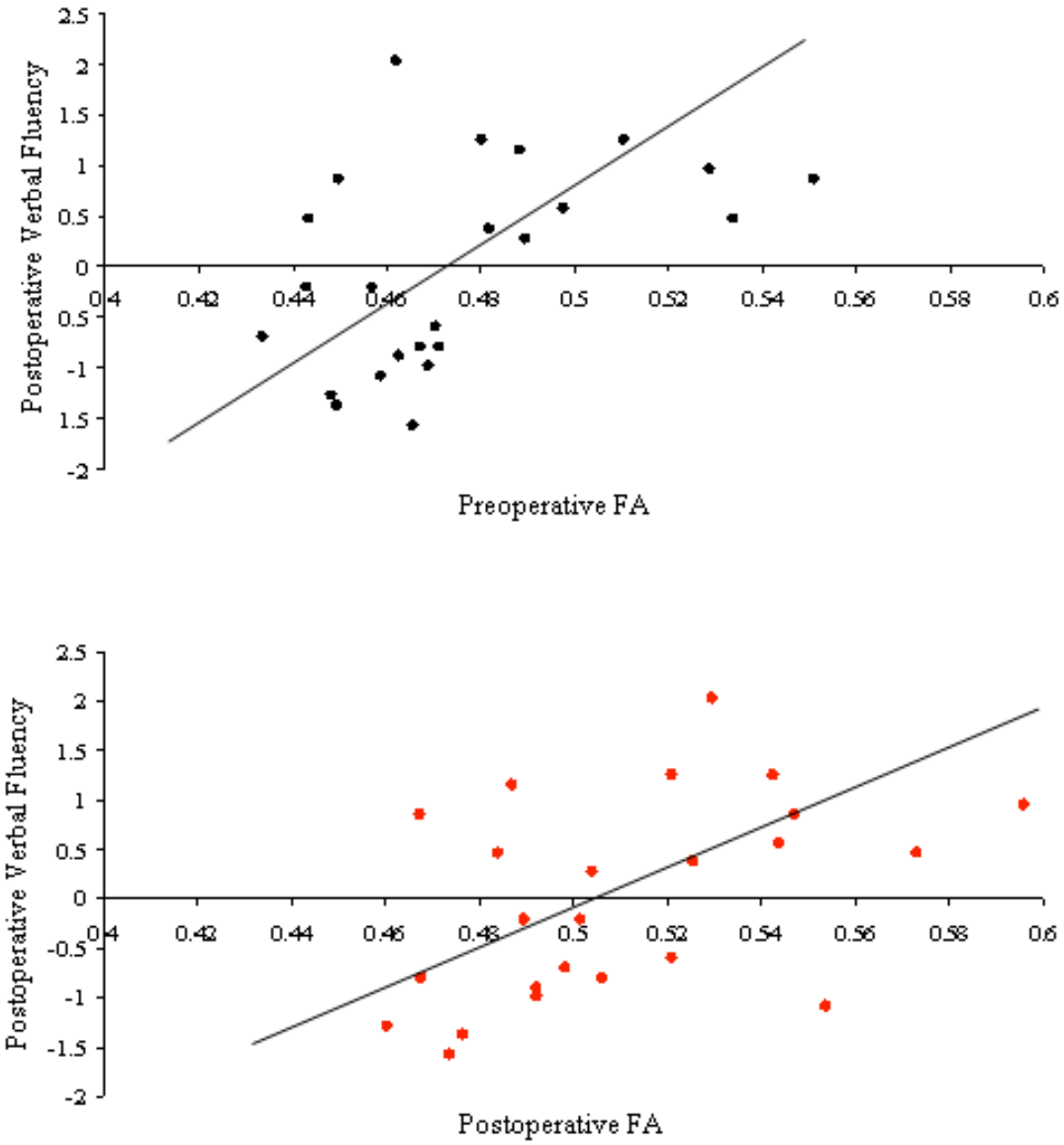

(b) - Scatterplots of verbal fluency scores against mean fractional anisotropy in left posterior limb internal capsule, external capsule and corona radiata before (black dots) and after (red dots) left anterior temporal lobe resection. There was a significant correlation between the mean fractional anisotropy in this cluster before and after left anterior temporal lobe resection, and post-operative verbal fluency (r=0.482, p=0.009 and r=0.469, p=0.010 respectively).

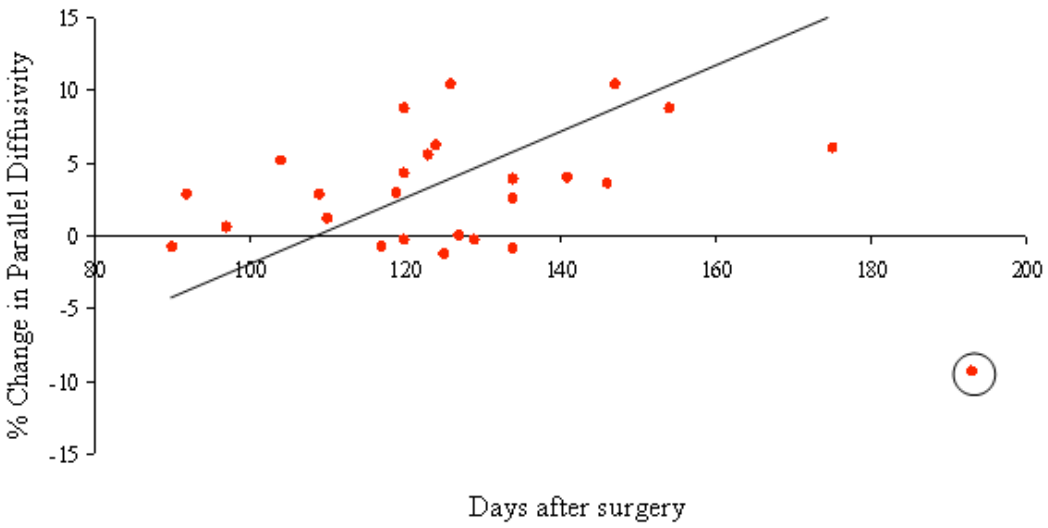

Figure 5.7 - Scatterplot and regression line of percentage change in $\lambda_{\parallel}$ in the cluster showing an increase in fractional anisotropy after left anterior temporal lobe resection against interval between surgery and imaging. The circled point is an outlier, and when removed from the analysis, the correlation is significant (r=0.400, p=0.024).

5.4.7 Tractography

Post-operative tractography from those areas demonstrating an increase in FA after surgery in left anterior temporal lobe resection is shown in figure 5.8. The group variability map of this network of connections consisted of two predominant pathways. The first was a network of connections running from the precentral gyrus, though the posterior limb of the internal capsule limb to the corticospinal tract and pons. The second pathway consisted of connections from premotor and prefrontal areas, the superior and inferior frontal gyrus (including the deep frontal operculum), and passed via the external capsule to the posterior, superior temporal gyrus and angular gyrus. As this pathway passes through the external capsule it is ventral and medial to the arcuate fasciculus/superior longitudinal fasciculus whose anatomical location is also shown in figure 5.8 for reference. The distribution of the group variability maps (figure 5.8) approximates to the ventromedial language network, that is distinguishable from the arcuate fasciculus/superior longitudinal fasciculus, that make up the dorso-lateral language network (522).

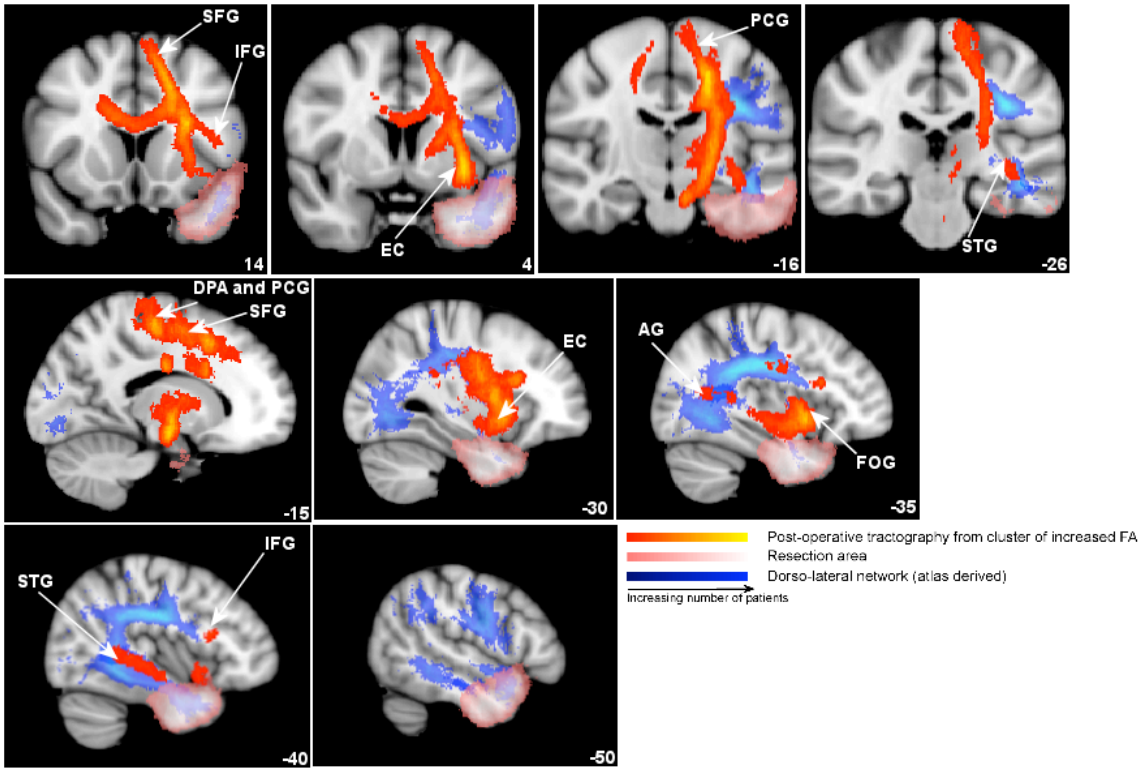

Figure 5.8 - Group variability map (thresholded at 0.2) of tractography results after seeding from the local maxima of the cluster identified as showing an increase in fractional anisotropy after left anterior temporal lobe resection. Tracts are superimposed upon the MNI152_T1_1mm_brain image supplied with FSL. The group variability map (yellow-red, with yellow representing voxels identified by the tractography in all subjects) visualises connections from the precentral gyrus via the internal capsule, and connections from the premotor and prefrontal areas, the superior and inferior frontal gyrus (including the deep frontal operculum), which pass via the external capsule to the posterior, superior temporal gyrus and angular gyrus. This network of connections is medial to the traditional dorso-lateral language pathway composed of the arcuate fasciculus and inferior longitudinal fasciculus. The latter pathway is shown for reference in blue, and is derived from the JHU white matter tractography atlas supplied with FSL. Also shown is the group variability map for the surgical resection area (dark pink to light pink) created from the postoperative b=0 images (thresholded at 0.3). It is evident that after an anterior temporal lobe resection the dorso-lateral language connections may be more susceptible to resection and damage than the ventro-medial connections. MNI coordinates are shown on each slice. (DPA=dorsal premotor area, PCG=precentral gyrus, SFG=superior frontal gyrus, EC=external capsule, AG=angular gyrus, FOG=fronto-orbital gyrus, STG=superior temporal gyrus, IFG=inferior frontal gyrus)

5.5 Discussion

This study demonstrates the structural consequences of anterior temporal lobe resection on white matter networks in patients with temporal lobe epilepsy. Areas of decreased FA and increased MD were evident after both left and right sided resections. There were also significant focal post-operative increases in FA after left anterior temporal lobe resections. The location of these changes, their correlation with language function, and presence only after left sided temporal lobe surgery and with greater increases occurring after longer intervals from surgery, suggests that they may be related to structural plasticity relevant to language function after surgery. This information is likely to be important for the planning of epilepsy surgery and prediction of post-operative language function, and for the understanding of brain recovery following injury.

5.5.1 Post-operative reduction in FA

Prior to the publication of this study, three published studies had assessed the structural consequences of epilepsy surgery on white matter (401,504,505). Schoene-Bake et al. carried out a TBSS analysis of diffusion data of 21 right and 19 left temporal lobe epilepsy patients. All but two of the patients underwent a selective amygdalo-hippocampectomy (SAH). Healthy controls were used as a comparison group for post-operative patients due to lack of pre-operative data. Overall, the distribution of reduction in FA was similar to the current study, both ipsilaterally and contralaterally, although we have observed more extensive changes post-operatively. This is not surprising given that anterior temporal lobe resection removes more brain tissue than an amygdalo-hippocampectomy, and the lack of preoperative data in the Schoene-Bake et al study (505).

Decreased FA can be caused by decreased diffusivity parallel to axonal fibres or by increased perpendicular diffusivity (339,523). In the present study, the decrease in FA in those white matter networks connected to the area of resection was caused by an increase in $\lambda_{\perp}$ that was relatively larger than the decrease in FA. Concha et al assessed the effects of a corpus callostomy in three subjects, and reported similar findings (504). The changes in diffusion parameters after surgery evolved from an acute pattern approximately one week after surgery, to a more chronic pattern several months after surgery. The biggest and most significant reductions in FA were closest to the

surgical lesion. In the present study, the contralateral reductions in FA, which were furthest from the area of resection, also appear to be less marked than those areas close to the area of resection. Electron microscopy studies of the basis of reduced FA have proposed that increases in $\lambda\perp$ are caused by reduced axonal density and increased extra-axonal fraction (524,525) or decreased myelin (526,527). In the present study the decrease in FA is likely to be related to Wallerian degeneration of nerve bundles disconnected from afferent and/or efferent structures, which in turn may cause myelin degradation and decreased axonal packing. Concha et al (504) also reported a chronic increase in $\lambda\parallel$, which we observed. Based on evidence from animal models, in this context, this may be due to loss of axons and intra-axonal structures such as neurofilaments and microtubules, thereby reducing the barriers to parallel diffusivity (528). Overall, the increase in $\lambda\perp$ and $\lambda\parallel$ also give rise to an increase in MD in those areas identified as showing a decrease in FA after surgery.

Since the publication of this study in 2010, there have been a further four studies assessing the nature of white matter changes after temporal lobe epilepsy surgery (529–532). The findings of these studies are in keeping with the results reported in this chapter. Two of these studies include postoperative scans acquired at more than one post-operative time point, and will be discussed in more detail in the following chapter (530,532). The study by Liu et al (529) scanned 6 patients 5 times after surgery, the longest post-operative scan period being 4 months. They studied the diffusion parameters derived from tractography of the fornix, and demonstrated that in the first week after surgery there was both an expected reduction in $\lambda\parallel$, and an unexpected reduction in $\lambda\perp$ and MD. However, in the longer term their results were in keeping with this study; there was a reduction in FA in the fornix driven primarily by an increase in $\lambda\perp$. In addition, more severely affected patients had changes in diffusion parameters in the contralateral fornix, as reported in this chapter. The authors concluded by suggesting that the chronic diffusion changes in the fornix were compatible with myelin degradation, while the acute changes may reflect beading and swelling of the axolemma, granular disintegration of the axonal neurofilaments, ischemia induced cytotoxic edema, and/or changes in the extra-axonal space including inflammatory changes and gliosis. The findings of the study by Nguyen et al (531) are broadly supportive. They also assessed the fornix using tractography in 12 patients (combined left and right TLE) before and after surgery, and

demonstrated a reduction in FA in the fornix ipsilateral to the side of surgery. However, in contradiction to the findings of Liu et al and our findings, they also reported an increase in contralateral fornix FA and a non-significant trend for patients with higher FA in the contralateral fornix to have a higher memory postoperatively. Their results suggest that epilepsy surgery may also result in structural reorganisation or a form of structural plasticity, as well as Wallerian degeneration.

5.5.2 Post-operative increase in FA

We observed extensive post-operative increases in FA after left anterior temporal lobe resection using unbiased whole brain analysis methods, which had not been reported in post-operative studies prior to the publication of this study (401,504,505). In both studies by Concha et al. patient numbers were small, and the ROI approach used limits investigation to *a priori* defined regions. However, one of the regions assessed, included the external capsule (401). Though the authors did not report *significant* post-operative increases in FA in this region, their data suggest a trend towards a post-operative increase in FA underpinned by an increase in $\lambda \parallel$ and decrease in $\lambda \perp$. In the study by Schoene-Bake et al. the lack of pre-operative data may have reduced the sensitivity to detect post-operative increases in FA (505). Finally, the patients assessed in these three studies, predominantly underwent selective amygdalo-hippocampectomy, and not anterior temporal lobe resection. In the current investigation, the longitudinal design with pre- and post-operative data, the whole-brain analysis techniques and a relatively large number of patients undergoing anterior temporal lobe resection enabled detection of increases in FA, and an ROI analysis of the raw data confirmed the robustness of these findings. This is supported by a recent study which assessed white matter changes after hemispherectomy in 10 children (533). The authors of this longitudinal study used a TBSS based analysis, and reported an increase in FA in the contralateral corona radiata, which also correlated with time after surgery.

Of the four post-operative diffusion studies published since 2010, two also report widespread increases in FA after temporal lobe surgery (530,532). Both studies utilise ROI based methods, which though more sensitive due to a smaller multiple comparison problem than whole brain methods, depend on an a priori hypothesis. Faber and colleagues (530) reported increases in FA

after surgery in 20 left TLE patients in regions that included: bilateral thalamic radiations, bilateral inferior fronto-occipital fasciculi, left corticospinal tract, left inferior fronto-occipital fasciculus, left inferior longitudinal fasciculus, and left superior longitudinal fasciculus. Macdonald et al (532) reported less widespread increases in FA, but noted a trend for FA increases primarily in the ipsilateral corticospinal tract after surgery.

The post-operative increase in FA in the present study was caused by both an increase in $\lambda \parallel$, and a decrease in $\lambda \perp$. For this reason the MD of this cluster was unchanged post-operatively. There are several potential causes of these observed changes. We demonstrated that mechanical stretch of white matter tracts, or a decrease in the proportion of voxels modelled as containing two fibre bundles, are unlikely to be contributing factors. The widespread distribution of the increase in FA, the lack of similar changes after right anterior temporal lobe resections, and the absence of a correlation between resection volume and percentage change in diffusion parameters, argue against these possible explanations. Furthermore, while stretching of white matter bundles may explain a decrease in $\lambda \perp$ due to increased axonal packing, this would not explain the increase in $\lambda \parallel$, which tends to decrease with reduced axonal calibre (527,534).

Post-operative increases in FA could also be due to seizure cessation after surgery. Concha et al found persistent bilateral white matter diffusion changes post-operatively, and proposed these were probably secondary to irreversible structural damage such as myelin degradation and axonal degeneration, and may be related to the underlying epileptogenic process. However, they also acknowledged that Wallerian degeneration related to surgery may mask structural changes associated with functional recovery (401). More recently, Yasuda et al carried out a whole-brain VBM comparison of pre- and post-operative T1- weighted data in 67 patients with TLE (506). The authors identified significant increases in white matter concentration in the ipsilateral temporal and frontal lobes after temporal lobe surgery, with a distribution similar to that observed in the present study. However, because both left and flipped right TLE patients were analysed together, it is impossible to ascertain whether there were differences in these increases in left and right TLE groups. The authors suggested that these findings were a consequence of seizure cessation in association with reversible metabolic dysfunction and neuronal plasticity. That interpretation is in

keeping with several PET and MR spectroscopy studies that have suggested post-operative reversal of pre-operative, extra-temporal metabolic dysfunction in TLE (535–538). There is also evidence that the cortical and subcortical networks underlying propagation of secondarily generalised seizures predominate between the midbrain, basal ganglia and thalamus (539). The white matter connecting these structures consists primarily of subcortical tracts which pass through the internal capsule and corona radiata (540), and is broadly consistent with the location of the increases in FA identified in the present study. Despite this, our observation that seizure free patients had smaller mean increases in FA than non-seizure free patients, suggests that seizure freedom is not the sole cause of increased FA observed after surgery. Rather, the location of these increases in FA confined to left temporo-frontal white matter tracts, and the observation that left hemisphere language dominant patients have larger increases in FA after left temporal lobe surgery than right hemisphere dominant patients, suggests that another major cause of these changes may be related to the structural plasticity of language networks after anterior temporal lobe resection.

5.5.3 Language and structural plasticity

Advanced magnetic resonance imaging techniques and analyses have shown that there is considerable capacity for, not only functional but also structural, reorganization after brain injury in the adult human brain (541–544). Traditional tract tracing techniques in animal models have highlighted the central role of white matter reorganization in this process (545–547), and diffusion based MRI techniques corroborate these findings. For example, studies of patients with blindsight highlight the scope of white matter reorganization underlying preservation of visual abilities after occipital cortical lesions (548,549). Similarly, studies of animal models of spinal cord injury demonstrate the correlation between diffusion MRI derived measurements, and immuno-histological markers of plasticity (550).

The premise that the post-operative increases in FA after left anterior temporal lobe resection may be in part related to the plasticity of language networks after surgery is substantiated for two reasons; the location of these changes is in keeping with the current understanding of the neuro-anatomical basis of language, and there are significant correlations between independent neuro-psychometric data and the mean diffusion parameters derived from these clusters. Models of

language postulate the existence of an expressive language area in the left ventrolateral frontal region (Broca's area) (551) which is connected to temporo-parietal language regions via the arcuate fasciclus (552). Recent diffusion based MRI studies suggest that the arcuate fasciculus has much more extensive putative cortical terminations beyond the classical limits of Broca's and Wernicke's area, to include the dorsal premotor cortex, the dorsolateral prefrontal cortex and the anterior middle and inferior temporal gyri (553–556). Furthermore, tract tracing studies in primates, suggest that the arcuate fasciculus is not a single, direct, white matter connection between frontal and temporo-parietal regions, but instead is part of a dorsal stream of connections which includes parts of the superior longitudinal fasciculus and the middle and inferior longitudinal fascicule (522,555,557). Current standard tractography techniques do not have the spatial resolution needed to resolve these corticocortical pathways (555). However, these connections have been visualized in humans and primates using high resolution diffusion techniques (558–560). These studies have also identified a second, parallel, ventral language circuit which is located medial to this dorsal pathway. This runs from the ventrolateral prefrontal and orbitofrontal cortex, and inferior and middle frontal gyri, through the extreme capsule dorsal to the uncinate fasciculus, to the posterior/middle superior temporal gyri, where it merges with the fibres of the middle longitudinal fasciculus which is lateral to it, and connects to the inferior parietal lobe and angular gyrus (522,555,560–564). Current in vivo diffusion tensor imaging lacks the spatial resolution to unambiguously differentiate between the external and extreme capsules by means of FA maps alone. For this reason, the post-operative increases in FA appear to be localized to the external capsule of the TBSS skeleton in the present study. However, tractography seeded from these areas demonstrates the presence of connections linking temporo-parietal areas with the ventral prefrontal areas, and inferior frontal gyrus, which is consistent with the ventromedial language pathway (figure 5.8). The other morphological features identified by the post-operative tractography in this study are also concordant with the current understanding of language networks, including connections from the dorsal prefrontal areas, superior frontal gyrus, precentral gyrus and premotor areas, which overlap with parts of the dorsal language network, and connect to parts of the basal ganglia. These areas are likely to be important for final speech production, and higher order articulatory control of speech (555,565).

Damage to this distributed network may occur following left anterior temporal lobe resection, and is most likely to affect the dorsal rather than ventromedial pathway because of the former's lateral position, and the anterior extent of fibres connecting to the superior and middle/inferior temporal gyri. In contrast, the ventral pathway is more medial and connects to the posterior/middle superior temporal gyrus (figure 5.8), and may therefore be less susceptible to injury (438). This ventro-medial pathway may therefore have a greater propensity to undergo plasticity related changes relevant to language functioning after surgery. This contention is substantiated by the presence of significant correlations between pre- and post-operative mean FA and $\lambda \parallel$ values and post-operative verbal fluency and naming scores, but *not* pre-operative scores. It appears that the most significant component of this correlation is the increase in $\lambda \parallel$ after surgery, demonstrated by the correlation between the percentage change in $\lambda \parallel$ and the percentage change in verbal fluency after left anterior temporal lobe resection. Whilst there is debate as to the specific role of each pathway with respect to language functions (566), some functional overlap seems likely with both pathways contributing to a high proficiency in verbal communication (522). The biological interpretation of a pattern of increased $\lambda \parallel$ in concert with decreased $\lambda \perp$ is not well defined, but may be primarily related to an increase in myelination (567) in addition to an increase in axonal calibre (534) and neurofilament density (568).

The predominance of the ipsilateral, rather than contralateral, white matter network with respect to language function after surgery, is corroborated by the few longitudinal studies that have assessed the functional reorganization of language after epilepsy surgery (500,503,569). Although these studies have used differing methods, they all highlight the importance of the ipsilateral hemisphere (503,569), and intra-hemispheric reorganization of language after dominant temporal lobe resection (500). The study by Pataraia et al also demonstrated ipsilateral inferior displacement of receptive language activation after anterior temporal lobe resection (500). In the most recent fMRI longitudinal study of pre- and post-operative TLE patients Bonelli et al demonstrated that post-operatively ipsilateral recruitment of language systems including the posterior hippocampal remnant was important for maintaining language, and reorganisation to the contralateral hemisphere was less effective (261). Furthermore, larger studies in patients with other forms of brain injury, such as stroke, also support that it is the repair and strengthening of

ipsilateral, neighbouring networks that is more important, than the recruitment of contralateral homologous regions (570).

The current study suggests a structural correlate to the concept of ipsilateral reorganisation and recovery of function, with augmentation of the ventro-medial language network, consequent to surgical damage to the dorsal-lateral language pathway. We suggest that the focal increases in FA seen in the ventro-medial language network after left anterior temporal lobe resection represent in part an attempt to reorganise language function after brain injury caused by surgery. Importantly, the observed correlation between pre-operative diffusion parameters and post-operative language outcome suggests that the pre-operative state of the ventro-medial language network is important, and that if this network is already in "active service", left anterior temporal lobe resection will have less impact on language functioning. Further studies are needed to clarify whether diffusion imaging or tractography of this ventral network might provide predictive information regarding the risk of language dysfunction after anterior temporal lobe resection, and moreover whether it can provide functional landmarks that can be used to guide surgery in order to minimise post-operative language dysfunction. Further longitudinal investigations with more time points following surgery will clarify the time course of these changes in FA.

5.5.4 Limitations

Whole brain and tractography methods of analysis of diffusion data have several limitations. The presence of brain lesions can cause problems with the normalization of images to standard space when using whole brain methods. We have attempted to minimize these complications by registering the post-operative images to their pre-operative counterparts using hand drawn cost function masks over the areas of resection, before then normalizing all images to a common space. We incorporated this method within the framework of TBSS which is specifically optimized for the registration of diffusion data. The confirmation of our whole brain findings, using native cluster information, and hand drawn ROIs lends confidence to the robustness of the methods employed in this study. The resolution of tractography images is several orders of magnitude lower than the nerve bundles under examination. A single voxel contains numerous fibre populations, some of which may be kissing or crossing, and this is particularly problematic in the fronto-temporo-

parietal areas assessed in this study. Although, the multiple fibre model, and probabilistic tractography approach employed in this study, may be able to partly deal with these problems, ultimately higher resolution in vivo diffusion imaging techniques are needed to precisely delineate the many subcomponents of the language network. The delineation of individual white matter tracts connecting different, language relevant cortical areas, in association with functional data, should facilitate a better understanding of the functional specificity of these white matter subcomponents. The use of a language laterality index derived from an expressive, rather than receptive, fMRI task that activates the frontal lobe may also be a limiting factor, given that the targeted surgical area is the temporal lobe. However, though it might be useful to have a measure of receptive language function, crossed dominance is uncommon, and damage to white matter tracts after surgery is as likely to affect frontal, as well as temporal, lobe functioning (571). Further, the language deficit encountered after anterior temporal lobe resection is commonly of word finding, and not of receptive function (572). The correlations between neuropsychology and diffusion data noted in this study were not corrected for multiple comparisons due to the small numbers of patients studied. However, even with an adjusted Bonferonni significance level of 0.05/4, the correlations remain significant, and the broad theme of this study is consistent.

5.6 Conclusion

We have used whole-brain voxel based analysis of diffusion tensor imaging to assess the morphometric changes in white matter following left and right anterior temporal lobe resection. While widespread decreases in FA occurred after left and right-sided resections, only the left anterior temporal lobe resections were followed by an increase of FA in an extensive area. The location of these changes and the results of tractography seeded from this area suggest that it is part of the parallel, ventro-medial language network. This is corroborated by a significant correlation between the diffusion parameters of this region and post-operative language function. These findings have important implications for our understanding of the response of the brain to injury, and may prove useful in the planning of epilepsy surgery in order to minimize post-operative language dysfunction.

6 Evaluation of White Matter Changes at Two Time Points After Anterior Temporal Lobe Resection - Prediction of Language Decline

This chapter extends the previous study in a subgroup of patients by assessing the longitudinal changes in white matter microstructure that occur at approximately 4 months and 1 year after anterior temporal lobe resection. In addition, it demonstrates how knowledge of these changes can be used to aid prediction of post-operative language deficits. The material in this chapter has been submitted for publication (see publications section).

6.1 Objectives

The previous chapter demonstrated that widespread, white matter changes occur approximately 4 months after anterior temporal lobe resection. Some of these changes may represent plasticity related processes underlying language function. In this chapter we aim to understand the progression of white matter changes at further time points after surgery, and how they may aid prediction of post-operative language decline.

6.2 Introduction

To date, only two studies (530,532) have studied the nature of white matter changes after temporal lobe surgery at more than one time point beyond 4 months after surgery. Both studies were reported after the publication of the results reported in the last chapter, and give contradictory results. Macdonald et al suggest that white matter changes do not progress beyond 2 months post-operatively, whereas Faber et al suggest that remodelling of brain connectivity after surgical intervention continues for longer time periods. While the study by Faber et al does not explore the functional implications of such white matter changes, Macdonald et al demonstrate that at least some of the reduction in FA seen post-operatively in patients may be related to visual field deficits.

We have previously hypothesized that increases in FA after anterior temporal lobe resection may in part represent structural plasticity in language related networks. As outlined in chapter 1, up to 40% of patients (253,254) may suffer a clinically significant naming decline after dominant anterior temporal lobe resection. The ability to predict which patients may suffer significant language

deficits is therefore of critical importance. The use of fMRI and preoperative cognitive function in predicting language decline after surgery was discussed in chapter 1. The largest, and most recent, longitudinal fMRI study assessing language in TLE patients undergoing surgery (261) highlighted that pre-operative language fMRI, and pre-operative naming ability can be used to accurately predict post-operative decline in naming ability. The more language is lateralised pre-operatively to the side of surgery, and the higher pre-operative language function, the greater the decline after surgery. Interestingly, this study also highlighted that postoperatively, it is ipsilateral hemispheric recruitment of language centres that is important for maintaining language function, and reorganisation to the contralateral hemisphere is less effective after surgery.

In this study we firstly hypothesise that white matter changes continue to develop 12 months after anterior temporal lobe resections. Secondly, given the importance of these regions for language function (as outlined in the previous chapter), we hypothesise that the preoperative quantification of diffusion parameters in these areas, together with preoperative fMRI and pre-operative language scores, can be used to predict post-operative language function at 12 months.

6.3 Methods

6.3.1 Subjects

We studied 12 left (mean 34 years, range 19 – 52 years, 3 male) and 14 right (mean 36 years, range 23 – 52 years, 6 male) TLE patients, all of whom were medically refractory. These patients were a subgroup of those studied in the last chapter. All patients underwent pre-surgical evaluation, and subsequent anterior temporal lobe resection for the treatment of their epilepsy, at National Hospital for Neurology and Neurosurgery, London, UK. All patients had undergone structural MRI at 3 Tesla (3T) (185), and video-EEG had confirmed seizure onset in the temporal lobe ipsilateral to the resection. 2/12 left and 0/14 right TLE patients, also had intracranial recordings to localise seizure onset to the temporal lobe ipsilateral to the resection. Two of the 12 patients with left TLE, had normal structural MRI, and histopathology of the resected specimen revealed end folium sclerosis. Two of the 14 right TLE patients had anterior temporal lobe cavernomas, and one had a normal structural MRI and histopathology of the resected specimen revealed end folium gliosis. All remaining patients had HS identified on MRI ipsilateral to seizure onset, and all patients had a

normal, contralateral hippocampus based on qualitative and quantitative MRI (435). Post-operative histopathology confirmed the MRI findings in all cases. All patients were taking anti-epileptic medication. Handedness was determined using the Edinburgh handedness inventory (416), and 3/12 left and 1/14 right TLE patients were noted to be left handed. A language lateralisation value was determined using a range of language fMRI tasks in manner identical to that described in the last chapter.

The standard neurosurgical procedure undergone by these patients, consisted of removal of the temporal pole, opening of the temporal horn, followed by en bloc resection of the hippocampus with a posterior resection margin at the mid brainstem level. Typically, the anterior-posterior extent of the temporal lobe resection as measured from the temporal pole to the posterior margin of resection, is 30% and 35% of the distance from the temporal pole to the occipital pole after left and right anterior temporal lobe resection respectively.

Patient demographics, clinical information and surgical outcome data based on the ILAE classification of post-operative seizure outcome (227) at the time of the post-operative scan following epilepsy surgery are listed in table 6.1.

6.3.2 Neuropsychology

Patients completed the McKenna Graded Naming Test pre- and post-operatively at approximately 4 and 12 months after surgery. In this test, the subject is asked to name 30 black and white line drawings of increasing difficulty. The total number of items correctly named is the performance indicator (509). The same patients also performed two verbal fluency tests pre- and post-operatively at approximately 4 and 12 months after surgery. In the first letter fluency test, the patient is given 60 seconds to produce as many words starting with the letter "S", and in the second category fluency test the subject is asked to name as many animals as possible. The total number of words correctly produced is the performance indicator (510). Using these raw values, the percentage change following surgery of each parameter was calculated using the following formula [(Post-operative value – Pre-operative value)/(Pre-operative value)]*100.

	LTLE (range)	RTLE (range)
No of subjects	12	14
Sex – no of males	3	6
Average age in years	34 (19 – 52)	36 (23 – 52)
Average age of epilepsy onset in years	10 (2 – 26)	13 (1 – 37)
Average duration of epilepsy in years	24 (8 – 47)	24 (6 – 47)
Average language lateralisation index	-0.66 (-0.97 to 0.63)	-0.47 (-1 to 0.48)
Average interval from surgery to 1st postoperative scan in days	132 (97 – 193)	128 (96 – 194)
Average interval from 1st postoperative scan to 2nd postoperative scan in days	366 (269 – 688)	368 (243 – 675)
Average interval from surgery to 2nd postoperative scan in days	498 (391 – 785)	496 (352 – 791)
Number of patients of given ILAE class at time of 1st post-operative scan	Class I = 9 Class II = 1 Class III = 1 Class IV = 0 Class V = 1	Class I = 10 Class II = 1 Class III = 3 Class IV = 0 Class V = 0
Number of patients of given ILAE class at time of 2nd post-operative scan	Class I = 7 Class II = 2 Class III = 1 Class IV = 2 Class V = 0	Class I = 8 Class II = 1 Class III = 2 Class IV = 3 Class V = 0
Average number of pre-operative medications	2 (0 – 4)	3 (2 – 3)
Average number of post-operative medications at time point 1	2 (1 – 3)	3 (1 – 3)
Average number of post-operative medications at time point 2	2 (1 -3)	3 (1 – 5)

Table 6.1 - Summary of the clinical characteristics of left and right temporal lobe epilepsy patients

6.3.3 MR data acquisition

All patients were scanned before, and approximately 4 and 12 months after surgery. We acquired the clinical T1 data on a 3T scanner (GE Excite II) using the sequence and parameters described in chapter 2. A single investigator (MY) manually segmented the surgical resection area of each patient's post-operative T1-weighted volumetric MR scan at each time point, creating individual regions of interest (ROI).

6.3.3.1 Diffusion tensor imaging acquisition

The DTI data was acquired on the 3T scanner using the sequence and parameters described in chapter 2.

6.3.4 Diffusion tensor imaging processing

As in the previous chapter, the DICOM files of each DTI acquisition of each subject were processed in an identical fashion to that described in the previous chapter in order to derive FA, MD, axial and radial diffusivity maps. In order to align all FA data into a common space, the following procedure was applied separately for left and right TLE patients. First, all patients' pre-operative FA data were aligned to the FMRIB58_FA standard space template supplied with FSL, using the nonlinear registration tool FNIRT (512,513), which uses a b-spline representation of the registration warp field (514). Secondly, each patient's post-operative FA image, at both time points after surgery, were each co-registered to its pre-operative FA image using the linear registration tool FLIRT and FNIRT (304,515). During each registration step the surgical ROI created from the relevant post-operative b=0 image was used to de-weight this area, such that the registration process ignores the information under the mask and prevents the surgically resected area contributing to the image registration (516,517). The warp derived from co-registering each post-operative image to the pre-operative was combined with the pre-operative warp for each of the two post-operative images. The resulting combined warp was then applied to each native, post-operative FA image in each subject. In this manner the pre-operative, and each of the post-operative, scans for subjects were aligned in a common space, and all images including both post-operative scans were re-sampled only once. Following this, voxel-wise statistical analysis of the FA data was carried out in the left and right TLE groups separately, using TBSS (Tract-Based Spatial Statistics (324). The mean FA image across the pre- and both post-operative images in each group was created, thinned, and thresholded at FA > 0.2 to create a mean FA skeleton which represents the centres of all tracts common to the group. Each patient's aligned FA data were then projected onto this skeleton and the resulting data fed into voxel-wise cross-subject statistics.

In order to achieve accurate inference, including appropriate correction for multiple comparisons over space, we used permutation-based, non-parametric inference on a voxel-by-voxel basis (327). A tripled two-group difference test or triple t-Test (5000 permutations) was used to assess the location and extent of significant increases and decreases in the FA between the pre- and each of the post-operative scans in each group. This test is a natural extension of the paired t-test, where

subjects are scanned under 3 conditions. We used six contrasts in each group of patients, which are listed below:

Contrast 1 – po2 (post-operative 2) > po1 (post-operative 1)

Contrast 2 – po1 (post-operative 1) > po2 (post-operative 2)

Contrast 3 – po2 (post-operative 2) > pr (pre-operative)

Contrast 4 – pr (pre-operative) > po2 (post-operative 2)

Contrast 5 – po1 (post-operative 1) > pr (pre-operative)

Contrast 6 – pr (pre-operative) > po1 (post-operative 1)

As in the previous chapter, threshold free cluster enhancement (TFCE) was used to correct results for multiple comparisons, and results were considered significant for $p < 0.05$. Significant clusters were superimposed on the mean FA image and the MNI152 template supplied by FSL. FSLview and its atlas tools (International Consortium of Brain Mapping DTI-81 white matter labels atlas and John Hopkins University white matter probabilistic tractography atlas) in addition to general neuroanatomy atlases (518,519) were used to anatomically label the location of significant clusters in MNI152 space.

In order to both validate and investigate our results further at an individual subject level, we de-projected and reverse-normalised significant clusters of changes in FA into their native pre- and post-operative images at both time points. Using these native clusters, mean pre- and post-operative (at both time points) FA, MD, $\lambda \parallel$, and $\lambda \perp$ values were calculated by masking the corresponding whole-brain diffusion parameter images with the clusters.

6.3.5 Statistical analysis of clinical data and native clusters

Statistical analyses were performed with SPSS v14.0 (SPSS inc. Chicago, USA), and the threshold for statistical significance was set at $p < 0.05$. The normality of distribution of continuous, clinical variables was tested using the Kolmogorov-Smirnov test. Clinical variables (age, sex, age of onset of epilepsy, duration of epilepsy, interval from surgery to first and second post-operative scans, interval from surgery to second post-operative scan, number of seizure free patients at time of

second post-operative scan, the average number of drugs before and after surgery at each time point) in left and right temporal lobe epilepsy groups were then compared using the independent samples t-test (continuous normally distributed variables), the Mann-Whitney U-test (continuous non-normally distributed variables), and the Chi squared exact test (categorical variables).

A mixed design MANCOVA (multivariate analysis of covariance) was carried out, where the repeated measure was time (3 levels – preoperative, first postoperative, second postoperative scan), the between subject factor was group (2 levels – left and right TLE), and the dependent variables were graded naming test score, and letter and category fluency. The language lateralisation index was a covariate. The sign of this index was reversed for right TLE patients such that for both left and right TLE patients, the more negative the value, the greater the degree of language lateralisation to the side of seizure onset and surgery. All assumptions of the MANCOVA model including homogeneity of the regression slopes, multivariate normality, and homogeneity of the co-variance matrices were tested and met. Five of the right TLE patients missed at least one of the three longitudinal assessments of naming or category/letter fluency, and were excluded from the neuropsychology analysis.

A hierarchical, multiple linear regression was carried out across a combined group of left and right TLE patients in view of the small numbers of patients, and the fact that patients with atypical language dominance were present in both groups. The predictor variables initially used in the model were preoperative graded naming test score, and the degree of language lateralisation to the side of surgery. The mean FA in a cluster of preoperative white matter was entered as a third parameter. The dependent variable was the percentage reduction in GNT score at approximately 12 months after surgery. Two of the right TLE patients had not been assessed for GNT scores at the time of the final post-operative assessment, and were therefore excluded from the regression analysis.

6.4 Results

6.4.1 Clinical data

The clinical characteristics of the subjects studied are listed in table 6.1. There were no significant differences in the age or duration of epilepsy of the left TLE and right TLE patients at the time of surgery. There were no significant differences between left or right TLE patients in pre- and early or late post-operative numbers of medications. There was no significant difference between left TLE and right TLE groups in age of onset, duration of epilepsy, or interval from surgery to either post-operative scan. There were no significant differences between left and right TLE groups, in either the gender distribution or numbers of patients seizure free at the time of either of the post-operative scans.

6.4.2 Whole brain analysis – FA and left TLE patients

Following left anterior temporal lobe resection there were significant changes in FA noted only in the following contrasts 3, 4, 5, and 6:

Contrast 3 – po2 (post-operative 2) > pr (pre-operative)
Contrast 4 – pr (pre-operative) > po2 (post-operative 2)
Contrast 5 – po1 (post-operative 1) > pr (pre-operative)
Contrast 6 – pr (pre-operative) > po1 (post-operative 1)

The remaining, following contrasts 1 and 2 resulted in no significant results after whole brain correction:

Contrast 1 – po2 (post-operative 2) > po1 (post-operative 1)
Contrast 2 – po1 (post-operative 1) > po2 (post-operative 2)

At the first time point after surgery, there were decreases in FA in the main fibre tracts ipsilateral to the side of surgery, but not in the contralateral hemisphere as documented in the previous chapter (figure 6.1a and b). The ipsilateral, significant decreases in FA were similar to those described in

left TLE patients in the last chapter (figure 6.1a and b). These were present in the geniculo-calcarine tract and its projection to the lingual/occipital fusiform gyri, and intracalcarine cortex, part of the inferior longitudinal fasciculus, parahippocampal gyrus, anterior commissure, and the anterior temporal portions of the superior longitudinal fasciculus. There were also significant decreases of FA in the temporal portion of the left uncinate fasciculus that connects to the temporal pole, and the anterior floor of the external capsule. The latter structure contains fibres of the uncinate and inferior fronto-occipital fasciculi. Though there were no changes in FA that reached significance between the first and second post-operative scans, it is apparent that some of the reductions in FA present in the geniculo-calcarine tract that were present in the first post-operative scan had disappeared by the time of the second post-operative scan (circled in figure 6.1a).

As demonstrated in the previous chapter, there were also widespread increases in FA at the first time point after surgery (an average of 4.5 months) in a similar location to that described in the previous chapter (figure 6.1a and b). Although there was no significant change (either increases or decreases) in FA between the two post-operative scans, when compared to the pre-operative scans, this cluster of increased FA became more widespread and extended into the external capsule by the second time point after surgery (figure 6.1b). The cluster of increased FA extended across a number of regions that included the anterior, posterior and superior corona radiata, the posterior limb (including the retrolenticular region) and dorsal part of the anterior limb of the internal capsule, and the external capsule (figure 6.1a and b).

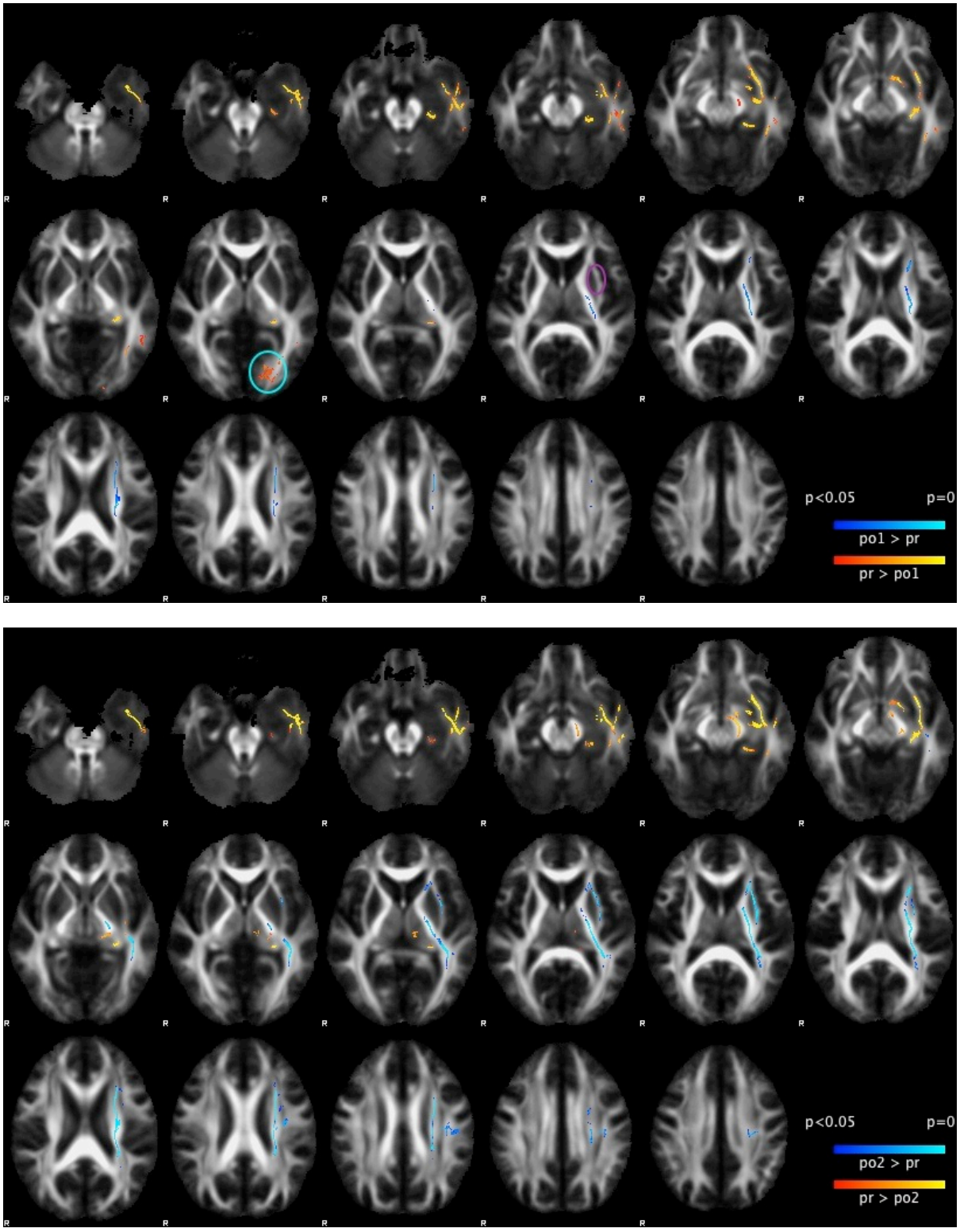

Figure 6.1 a (top) and b (bottom) - TFCE corrected (p<0.05) results of the whole brain TBSS analysis of changes in FA at two time points after left anterior temporal lobe resection (pr = pre-operative, po1 = 1st post-operative time point, po2 = 2nd post-operative time point). The left side of the brain is on the right side of the image. R = right. Significant clusters representing increases

(blue to light blue) and decreases (red to yellow) in fractional anisotropy after surgery are projected onto the mean fractional anisotropy template derived from all pre- and postoperative left temporal lobe epilepsy patients. For clarity, the group fractional anisotropy skeleton is not shown. The area of resection is visible inferiorly in the left temporal lobe where the white matter bundles are absent. Figure 'a' shows the changes in FA at the first time point after surgery, and figure 'b' shows the changes in FA at the second time point after surgery. Fractional anisotropy reduction after left anterior temporal lobe resection is apparent in the left temporal and occipital lobes, and anterior commissure. Areas of reduced FA present in the ipsilateral geniculo-calcarine tract at the first post-surgical scan in figure 'a' are not present at the time of the second post-surgical scan in figure 'b' (magenta circle). FA increases are present in the external capsule, posterior limb of the internal capsule and corona radiate (figure 'a' and 'b'). Areas of increased FA are more extensive at the time of the second post-operative scan in figure 'b' compared to the first post-operative time point in figure 'a', especially in the external capsule (purple circle).

6.4.3 Whole brain analysis – FA and right TLE patients

Following left anterior temporal lobe resection there were significant changes in FA noted only in the following contrasts 1, 3, 4, and 6:

Contrast 1 – po2 (post-operative 2) > po1 (post-operative 1)

Contrast 3 – po2 (post-operative 2) > pr (pre-operative)

Contrast 4 – pr (pre-operative) > po2 (post-operative 2)

Contrast 6 – pr (pre-operative) > po1 (post-operative 1)

The remaining, following contrasts did not result in significant FA changes after whole brain correction:

Contrast 2 – po1 (post-operative 1) > po2 (post-operative 2)

Contrast 5 – po1 (post-operative 1) > pr (pre-operative)

The significant results are shown in Figure 6.2a, b and c. There was a widespread reduction in FA approximately 4 months after surgery both ipsilaterally, and contralaterally (figure 6.2a). The most significant reduction in FA was apparent in the right temporal lobe, occipital lobe, fornix, splenium, anterior commissure and both cerebral peduncles. There were also decreases in FA to a lesser extent in the contralateral hemisphere, though these were less significant (figure 6.2a). Much of this reduction in FA appears to be reversible, as by the second post-operative time point, most of the reduction in FA compared to the pre-operative scan, was localised to areas seen at the second post-operative time point in left TLE patients (figure 6.2c). That is, reduced FA was present in part of the geniculo-calcarine tract, part of the inferior longitudinal fasciculus, the para-hippocampal gyrus, anterior commissure, and the anterior temporal portions of the superior longitudinal fasciculus. There were also significant decreases of FA in the temporal portion of the left uncinate fasciculus that connects to the temporal pole, and the anterior floor of the external capsule, which contains fibres of the uncinate and inferior fronto-occipital fasciculi. The significant results of contrast 1 [po2 (post-operative 2) > po1 (post-operative 1)] confirm the reversible nature of a significant proportion of the initial post-operative reduction in FA by demonstrating a widespread increase in FA in the second compared to first post-operative scan (figure 6.2b).

No significant increase in FA was seen at the first post-operative time point compared to the pre-operative scan. However, by the time of the second post-operative scan there was a large cluster of increased FA compared to the post-operative scan, in a distribution that was almost identical to that seen in left TLE patients at the same time point. That is, the cluster extended over the external capsule, posterior limb of the internal capsule and corona radiate (figure 6.2c).

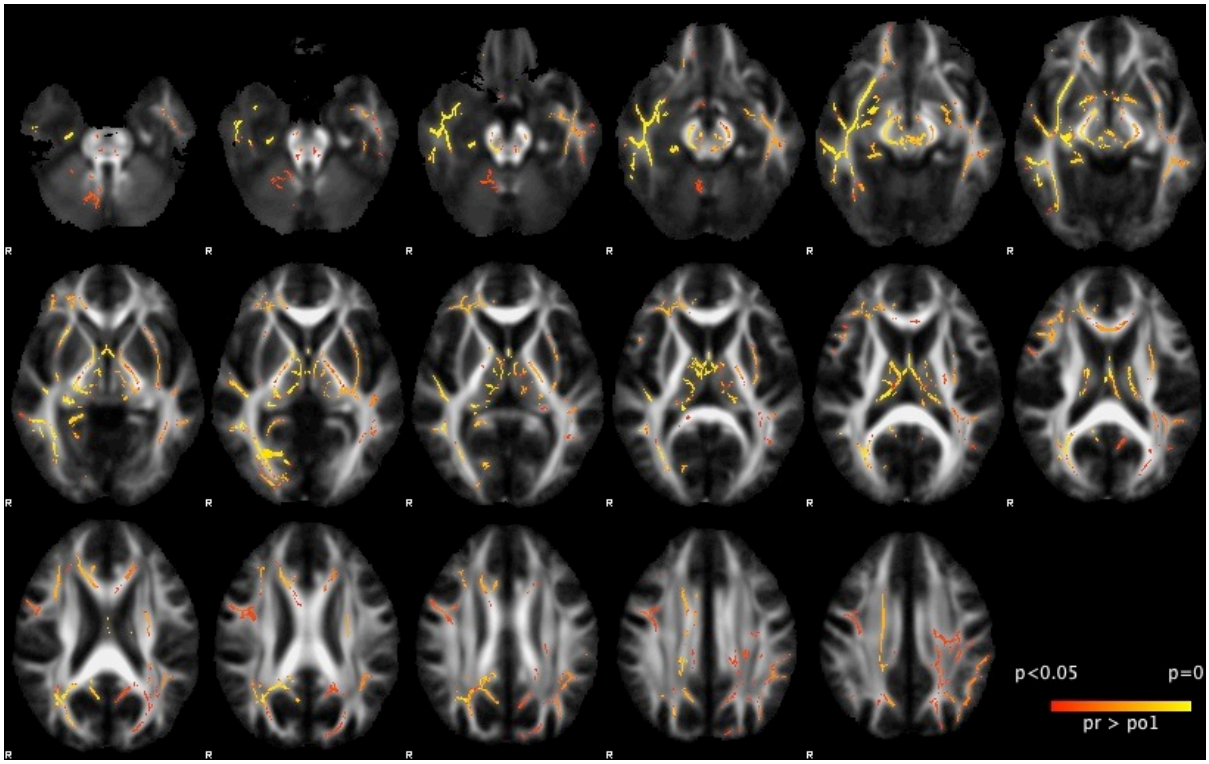

Figure 6.2a

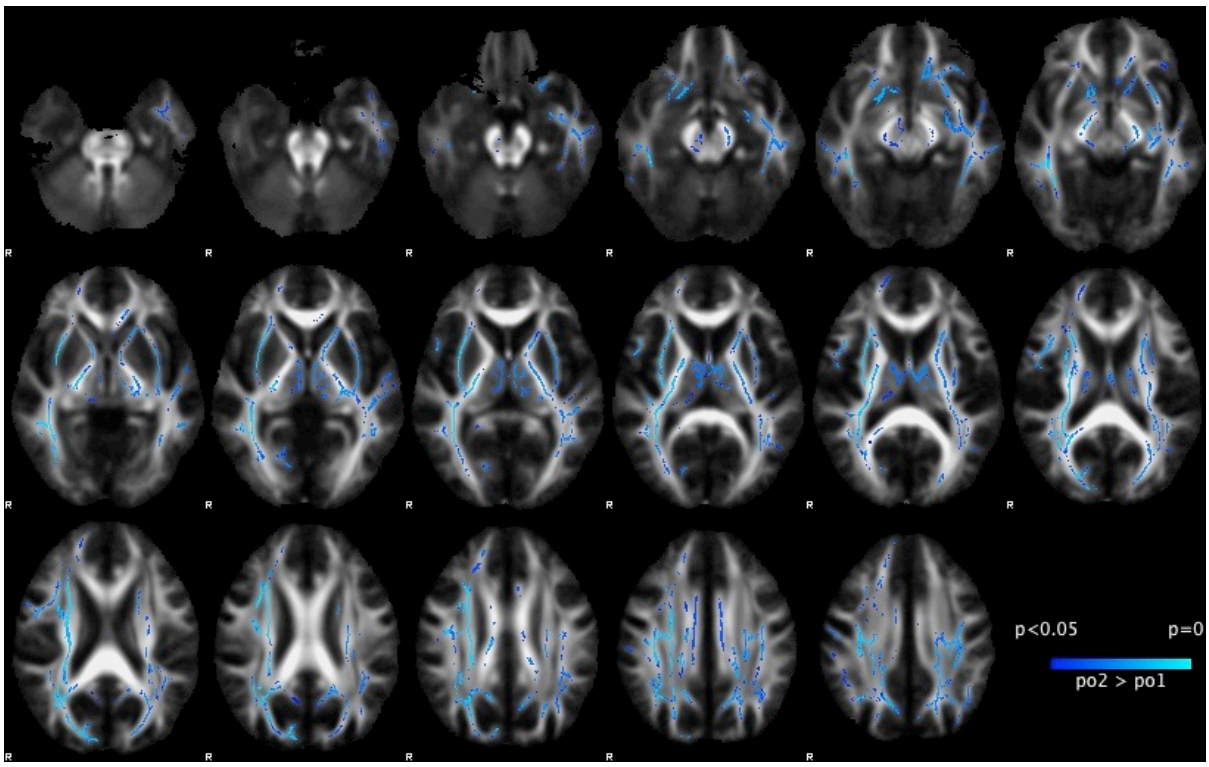

Figure 6.2b

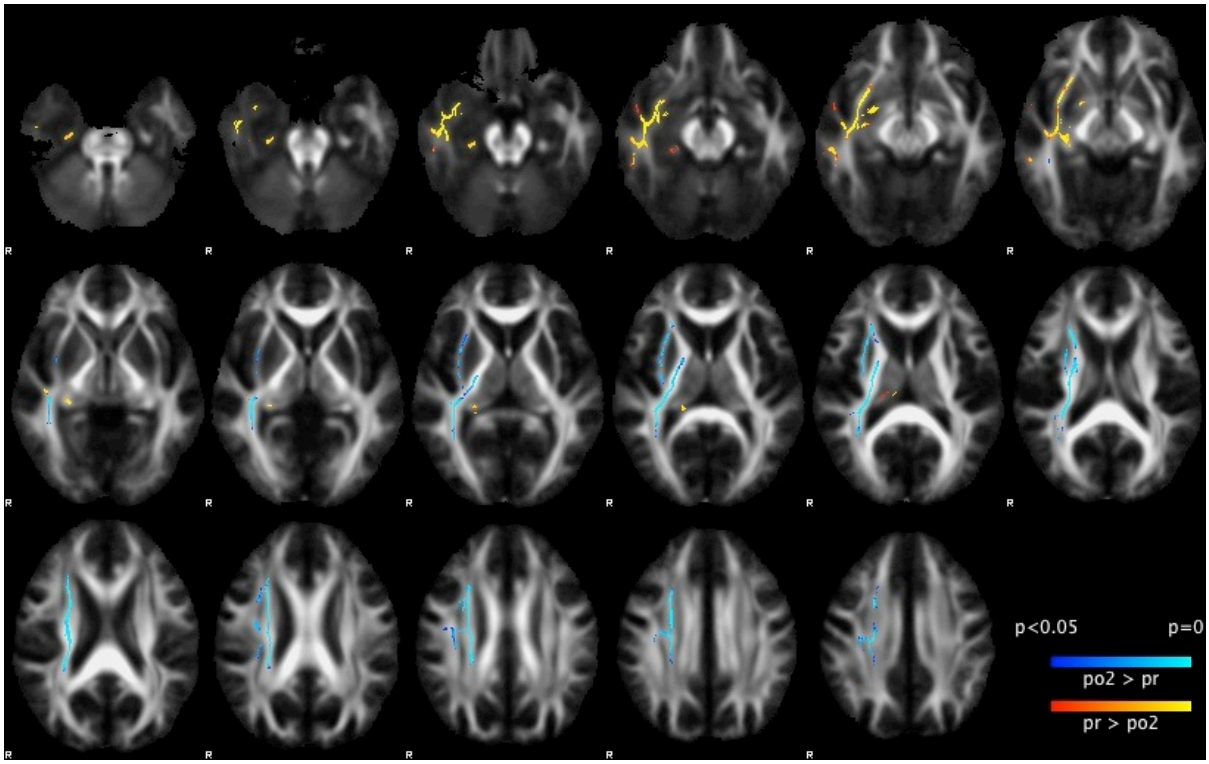

Figure 6.2c

Figure 6.2 a to c - TFCE corrected (p<0.05) results of the whole brain TBSS analysis of FA at two time points (pr = pre-operative, po1 = 1st post-operative time point, po2 = 2nd post-operative time point) after right anterior temporal lobe resection. The left side of the brain is on the right side of the image. R = right. Significant clusters representing increases (blue to light blue) and decreases (red to yellow) in fractional anisotropy after surgery are projected onto the mean fractional anisotropy template derived from all pre- and postoperative left temporal lobe epilepsy patients. For clarity, the group fractional anisotropy skeleton is not shown. The area of resection is visible inferiorly in the left temporal lobe where the white matter bundles are absent. Figure 'a' shows the changes in FA at the first time point after surgery, figure 'b' shows the changes in FA between the first and second time points after surgery, and figure 'c' shows the changes in FA at the second time point after surgery. While there is a widespread reduction in FA seen in RTLE patients immediately after surgery (6.2a), this appears to be reversible (6.2b), and is not present by 12 months after surgery (6.2c). Though no increase in FA is apparent at the first time point after surgery, an increase in an identical, ipsilateral distribution to that seen in left TLE patients is seen by the second time point after surgery (6.2c).

6.4.4 Whole brain analysis – Cluster of increased FA in left and right TLE patients at second time point after surgery compared to before surgery

Having identified that the post-operative cluster of increased FA in the external capsule appears to take longer to develop in right compared to left TLE patients, we explored the changes in diffusion parameters across time in this cluster (contrast 3) in both groups of patients (figure 6.3 and table 6.2). Overall, the increase in FA was driven primarily by a greater decrease in $\boldsymbol{\lambda}_{\perp}$ relative to an increase in $\boldsymbol{\lambda}_{\parallel}$, as demonstrated in the previous chapter. This reduction in $\lambda_{\perp}$ occurred at a quicker rate in left, compared to right, TLE patients, and therefore was present earlier in left TLE patients (figure 6.3).

	Left TLE Native Cluster FA Increase					Right TLE Native Cluster FA Increase				
	Pre-Op	**Post-Op1**	**% change (pr-po)**	**Post-Op2**	**% change (po1-po2)**	**Pre-Op**	**Post-Op1**	**% change (pr-po)**	**Post-Op2**	**% change (po1-po2)**
FA (se)	0.48 (0.01)	0.52 (0.01)	7.62 (2.35)	0.53 (0.01)	3.79 (1.97)	0.45 (0.01)	0.47 (0.01)	5.69 (1.98)	0.51 (0.01)	6.82 (1.81)
MD mm^2/sec x 10^{-6} (se)	774 (9.58)	750 (12)	-2.6 (1.81)	750 (9.7)	0 (1.19)	744 (10.9)	750 (9.9)	0.61 (0.86)	730 (12)	-2.19 (0.98)
$\lambda \parallel$ mm^2/sec x 10^{-6} (se)	1200 (20)	1240 (18)	0.98 (1.17)	1260 (19)	1.73 (0.62)	1140 (11)	1180 (13)	3.17 (0.53)	1190 (15)	0.96 (0.78)
$\lambda \perp$ mm^2/sec x 10^{-6} (se)	549 (10)	510 (12)	-6.42 (2.66)	500 (6.6)	-2.01 (2.12)	545 (14)	533 (10)	-1.89 (1.73)	503 (12)	-5.63 (1.70)

Table 6.2 - Summary of the mean diffusion parameters of back normalised cluster of increased FA identified from the whole brain analysis (contrast 3) at the second time point after surgery in left and right TLE patients (se = standard error, po1-po = percentage difference between preoperative and 1st postoperative scan, po1-po2 = percentage difference between 1st and 2nd postoperative scans).

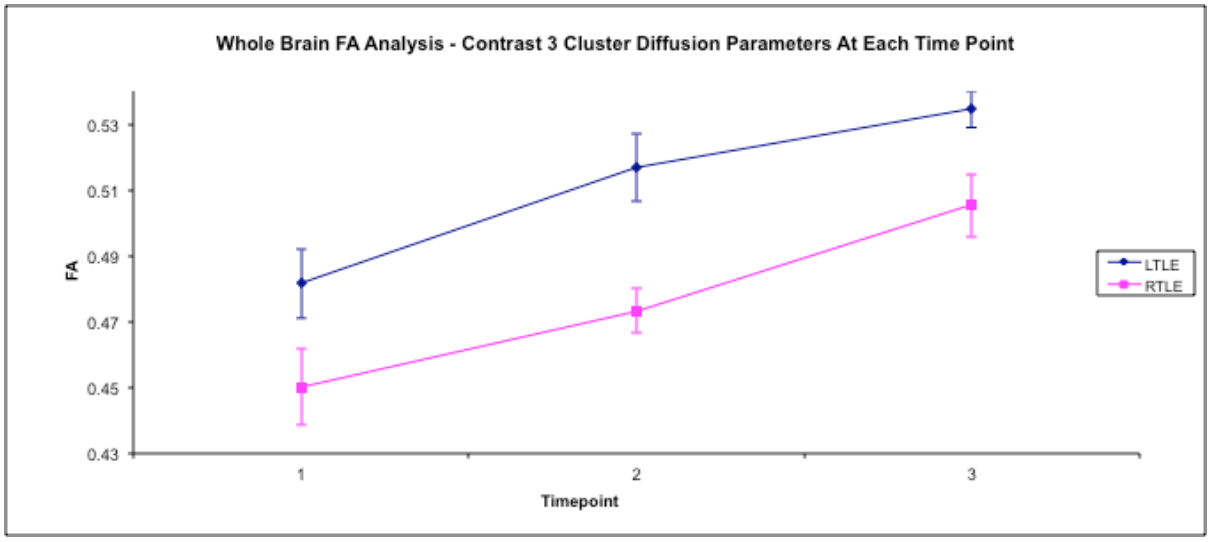
Whole Brain FA Analysis - Contrast 3 Cluster Diffusion Parameters At Each Time Point
FA
0.53
0.51
0.49
0.47
0.45
0.43
1
2
3
Timepoint
LTLE
RTLE

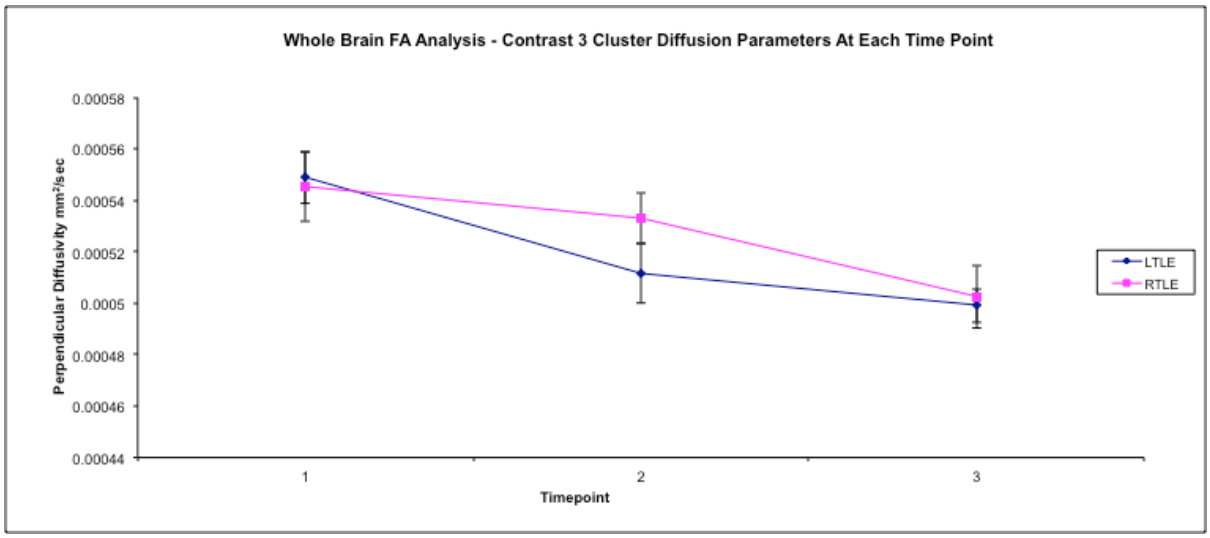
Whole Brain FA Analysis - Contrast 3 Cluster Diffusion Parameters At Each Time Point
Perpendicular Diffusivity mm²/sec
0.00058
0.00056
0.00054
0.00052
0.0005
0.00048
0.00046
0.00044
1
2
3
Timepoint
LTLE
RTLE

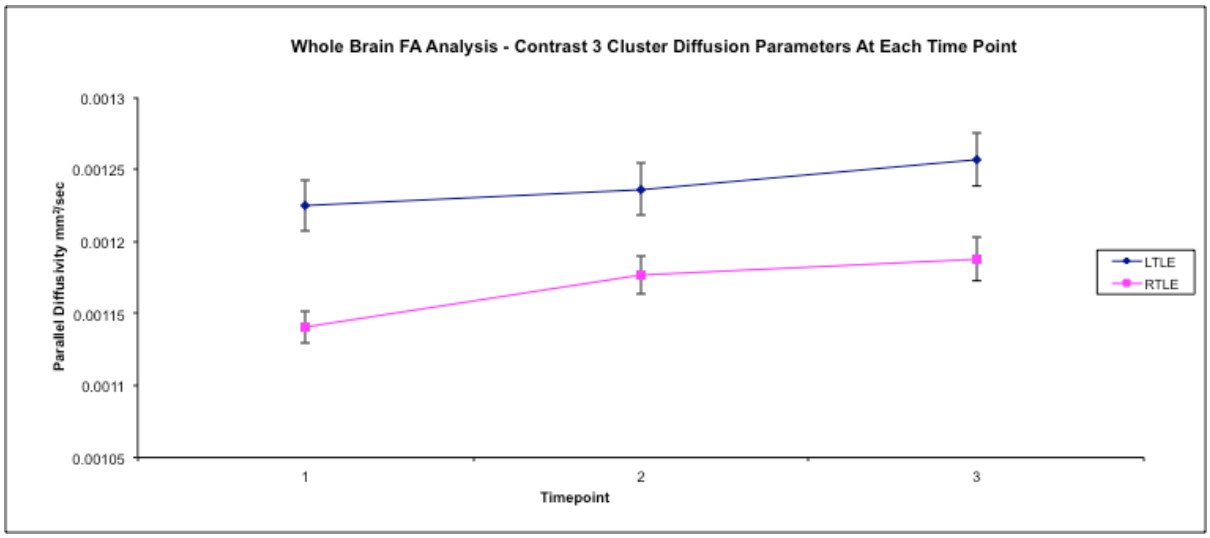
Whole Brain FA Analysis - Contrast 3 Cluster Diffusion Parameters At Each Time Point
Parallel Diffusivity mm²/sec
0.0013
0.00125
0.0012
0.00115
0.0011
0.00105
1
2
3
Timepoint
LTLE
RTLE

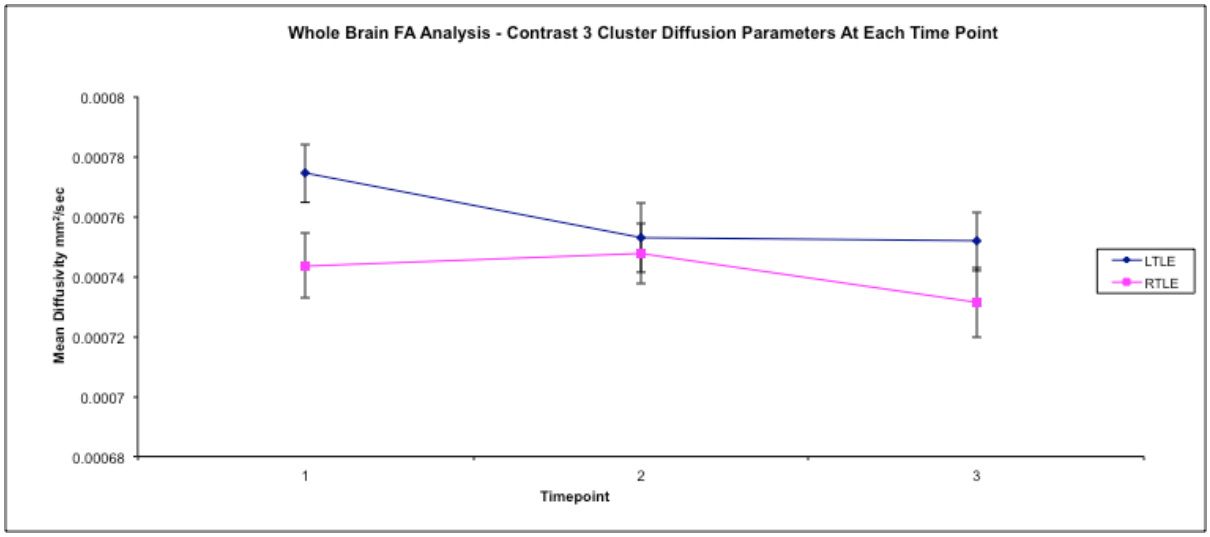

Figure 6.3 – Graphs illustrating the change in mean (+/- se) diffusion parameters within the back-normalised cluster of increased FA identified from the whole brain analysis (contrast 3) at the second time point after surgery in left and right TLE patients. Time points 1, 2 and 3 refer to the pre-operative, 1st post-operative and 2nd post-operative scans. The graphs show changes in FA, $\lambda_{\perp}$, $\lambda_{\parallel}$ and MD respectively. The whole brain analysis revealed a significant increase in FA in left TLE patients at both post-operative time points. This increase was only apparent at the 2nd post-operative scan in right TLE patients. This is due to the greater initial reduction in $\lambda_{\perp}$ in left TLE patients (see second graph down).

6.4.5 Neuropsychology results

The neuropsychology results at each time point are shown in table 6.3. There was no significant difference between the groups on the combined dependent variable of language ability [F(6,13) = 0.278, p = 0.841, Wilks lamda = 0.950, partial eta squared = 0.05]. There was a significant effect of time (preoperative, post-operative 1, post-operative 2) on the combined dependent variable of language ability, F(6,13) = 7.131, p=0.002, Wilks' Lamda = 0.233, partial eta squared 0.767. Analysis of each individual dependent variable, using a Bonferroni adjusted alpha level of 0.017 showed that there was no contribution of letter [F(2,36) = 4.234, p = 0.022, partial eta squared = 0.190] or category [F(2,36) = 3.460, p = 0.042, partial eta squared = 0.161] fluency to the effect of time. Only GNT differed significantly with time [F(2,36) = 7.150, p = 0.002, partial eta squared = 0.284]. Planned contrasts showed that there were significant differences between consecutive GNT

scores. It should be noted that when the analysis was re-run with the exclusion of the covariate, language lateralisation index, there was a significant interaction between group and time for GNT [F(2,38) = 0.015, partial eta squared = 0.198] but not letter or category fluency. Planned contrasts showed that this interaction was present as the final post-operative GNT score was significantly less than the pre-operative score in left but not right TLE patients.

The results of this MANCOVA analysis highlighted that GNT, and not fluency, was most at risk after surgery. This language component was therefore used in the linear regression model below. The MANCOVA model also highlighted that the use of a language lateralisation covariate, enabled analysis of both left and right TLE patients together.

	LTLE 1 (SE)	**LTLE 2 (SE)**	**LTLE 3 (SE)**	**RTLE 1 (SE)**	**RTLE 2 (SE)**	**RTLE 3 (SE)**
Flu S	14.7 (1.7)	14.0 (1.3)	17.8 (1.6)	14.1 (1.7)	13.8 (1.5)	16.3 (1.3)
Flu A	18.9 (1.4)	16.3 (1.8)	21.1 (1.4)	18.4 (1.9)	16.4 (1.7)	19.8 (1.8)
GNT	15.8 (1.5)	12.5 (1.9)	14.3 (1.7)	15.0 (1.9)	14.4 (2.1)	18.5 (1.6)

Table 6.3 – Composite table of neuropsychology scores in left and right TLE patients at each time point (1 = pre-operative time point, 2 = first post-operative time point, 3 = second post-operative time point)

6.4.6 Prediction of language decline after anterior temporal lobe resection

In the previous chapter we hypothesised that the cluster of increased FA in ipsilateral white matter structures in left TLE patients represented structural remodelling pertinent to language function. Both pre- and postoperative FA values correlated significantly with post-operative language function. In view of this, we hypothesised that the cluster of increased FA present in right TLE patients in an identical location was also relevant to language, but took longer to appear in the non-dominant hemisphere. Given the importance of this ipsilateral, white matter network for naming function after surgery, we hypothesised that the preoperative FA in this region could be used to predict graded naming outcome at 12 months. A hierarchical, linear regression model across both left and right TLE groups revealed that higher mean preoperative FA in the ipsilateral cluster of increased FA was a significant predictor of better outcome in GNT scores at 12 months. The model also predicted that higher preoperative GNT scores and language lateralization to the side of

surgery predicted worse language outcome, as has been demonstrated in other studies. The results of the linear regression are shown in table 6.4.

	B	SE B	β	p value
Step 1				
Constant	96.2	23.5		
Language laterality	30.3	9.9	0.49	0.006
Pre-operative GNT score	-5.3	1.4	-0.63	0.001
Step 2				
Constant	-66.2	75.6		
Language laterality	37.8	9.6	0.62	0.001
Pre-operative GNT score	-5.4	1.3	-0.64	0.000
Pre-operative FA	354.7	158.2	0.34	0.037

Note R^2=0.488 for Step 1; ΔR^2=0.103 for Step 2

Table 6.4 – Results of linear regression where B = unstandardized coefficient, SE = standard error, β = standardised coefficient

Partial residual plots for each predictor are shown in figure 6.4, and showed homoskedacity, and that residuals from the analysis were normally distributed. There was no correlation between residual terms.

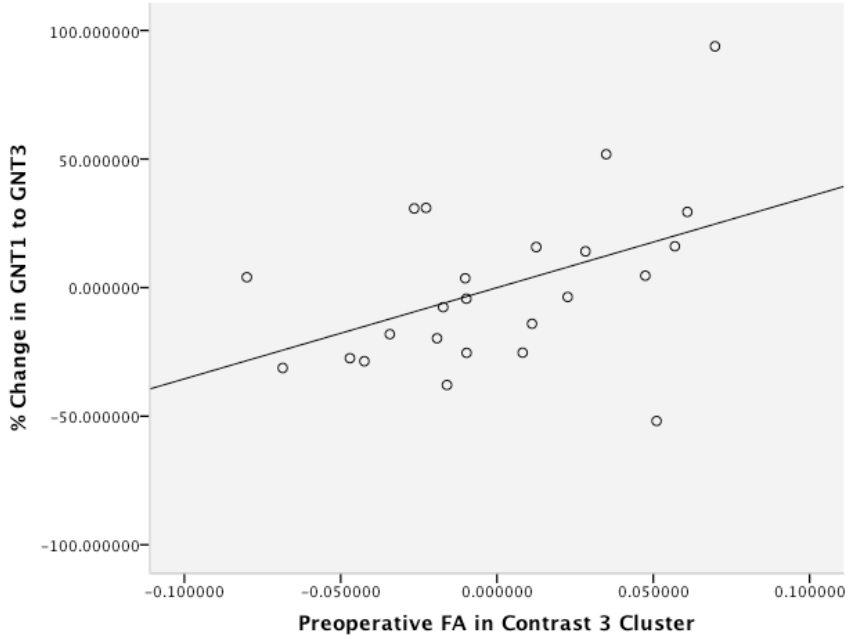

Figure 6.4a

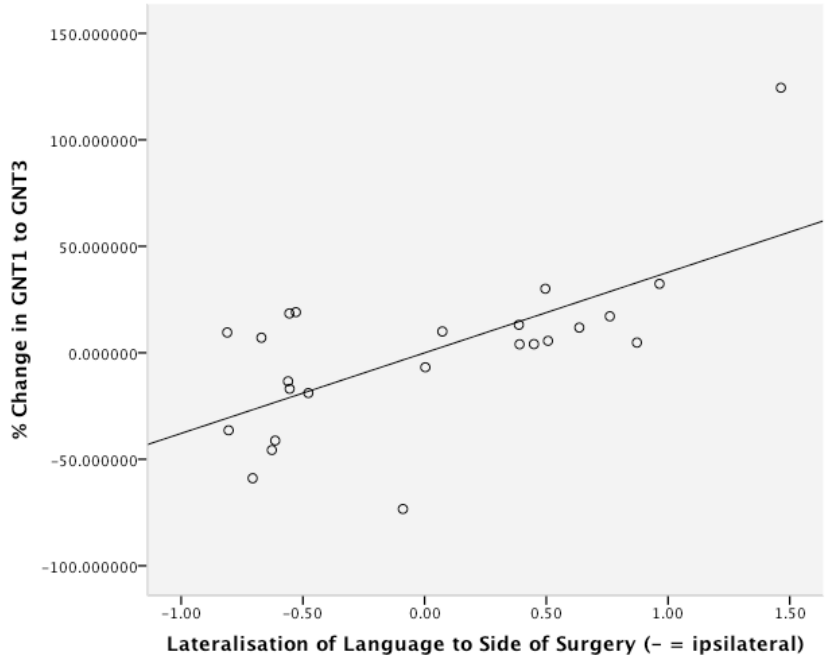

Figure 6.4b

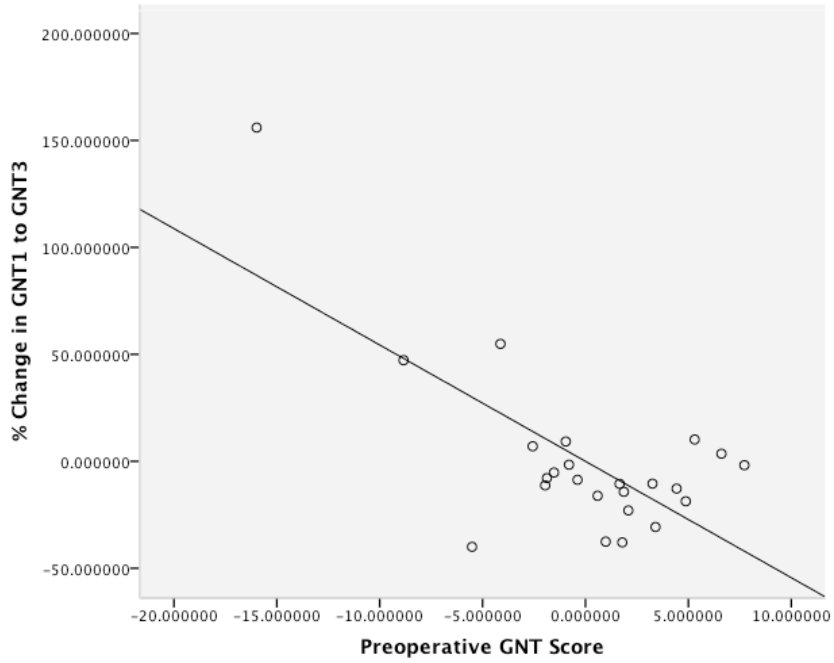

Figure 6.4 c

Figure 6.4 – Partial residual plots demonstrating the variance attributable to the model in pre-operative GNT score, language lateralisation to the side of surgery, and preoperative FA in the significant white matter network identified in contrast. a) The lower the pre-operative FA in the white matter network, the greater the decline in GNT at the second time point after surgery (r^2 = 0.201). b) The more lateralised language function is pre-operatively to the side of surgery, the greater the decline in GNT at the second time point after surgery (r^2 = 0.435). c) The higher the pre-

operative GNT score, the greater the decline in GNT at the second time point after surgery (r^2 = 0.485)

6.5 Discussion

In this study we have demonstrated that white matter changes in FA after anterior temporal lobe resection are part of a dynamic process in both left and right TLE patients. We have extended our findings in the previous chapter, by demonstrating that similar, ipsilateral, white matter increases in FA are apparent in both left and right TLE patients at approximately 12 months after surgery, but take longer to develop in right TLE patients. We have also demonstrated that preoperative FA in these areas, together with preoperative language function and lateralization, are predictive of language outcome after anterior temporal lobe resection across all TLE patients. Preoperative DTI may therefore aid the improved prediction of language outcome after anterior temporal lobe resection.

6.5.1 Dynamic changes in FA over 12 months

Two previous studies have assessed changes in FA up to at least 12 months after temporal lobe surgery. Faber et al (530) studied 20 left TLE patients, who underwent selective amygdalohippocampectomies. Thirteen of the patients were scanned after 3 to 6 months, and thirteen 12 months or later after surgery. However, only six patients had repeat MRI scans at both 4 and 12 months after surgery, and this is the main limitation of the study. The authors conducted a whole brain analysis and reported both corrected, and uncorrected ROI based results. In the corrected whole brain analysis they observed a decrease in FA values in ipsilateral temporal lobe fibre tracts, which was more widespread in the late than early postoperative group, when both were compared to their respective pre-operative scans. They interpreted these findings as continuing Wallerian degeneration associated with the resected epileptogenic focus over 1 year after surgery. In our study we found no further FA reduction between the first and second post-operative time points, or when either time point was compared to the respective pre-operative data. Part of the reason for this difference may be due to the fact that the main analysis in the study by Faber et al is not truly longitudinal. Interestingly, in the whole brain analysis of the subgroup of 6 patients who had had longitudinal scans, there were uncorrected significant results demonstrating extratemporal FA increases at the late compared to the early time points. But because of the small group the authors refrained from interpreting these results further.

In the uncorrected ROI based analysis Faber et al reported post-operative extra-temporal increases and decreases in FA, that are more widespread than those seen in the whole brain analysis, and similar to those reported in this study. Ipsilateral regions showing a post-operative increase in FA included the anterior thalamic radiation, corticospinal tract, inferior fronto-occipital fasciculus, inferior longitudinal fasciculus and superior longitudinal fasciculus. Contralateral regions showing a post-operative increase in FA included the anterior thalamic radiation and inferior fronto-occipital fasciculus. The areas showing a reduction or increase in FA were less or more widespread respectively, in the late post-operative group in comparison to the pre-operative data, than was observed in the early post-operative group compared to the pre-operative data. For example, clusters of post-operative decline in FA seen in the ipsilateral parietal lobes in the early post-operative group, were not seen in the late post-operative group when compared to pre-operative scans. The authors interpreted this finding as dynamic remodelling continuing beyond 6 months after surgery. This is similar to our findings. We noted significant widespread increases in FA between the early and late post-operative periods in the right TLE patients. In the left TLE patients, although no significant changes were noted between the early and late postoperative scans, we did note that the comparison of late post-operative and pre-operative scans resulted in fewer significant areas of reduced FA in the ipsilateral parietal lobe, than the comparison of early post-operative and pre-operative scans. The increase in FA between the early and late post-operative scans may partly reflect reversal of changes caused by surgery. This may explain why there was a more widespread increase in FA in right TLE patients between the early and late post-operative periods. In both this study and that of the previous chapter, right TLE patients have a more widespread decline in FA in the immediate post-operative period, which may be related to the fact that these patients have a significantly bigger anterior temporal lobe resection. However it is important to note that the increase in FA seen at the second time point after surgery compared to the pre-operative scans, represents in both left and right TLE an increase in FA from baseline and *not*, a partial recovery of a decrease in FA following surgery.

The second study to assess longitudinal changes in white matter after temporal lobe surgery is by Macdonald et al (532). This study reported an analysis of 4 left and 5 right TLE patients 2 months

after anterior temporal lobe resection. Four of these patients were also scanned 12 months after surgery. The analysis was ROI based, and used a tractography atlas to define ROIs. The authors reported a significant reduction in FA 2 months after surgery in ipsilateral fibre tracts transected during surgery (para-hippocampal cingulum, uncinate fasciculus, inferior longitudinal fasciculus, and fornix), as well as in fibre tracts not directly transected (inferior fronto-occipital fasciculus and corpus callosum). Additional decreases in FA were not observed from 2 months to 1 year after anterior temporal lobe resection, though a trend was noted for FA to increase in the ipsilateral corticospinal tract relative to the pre-operative scan. These findings are broadly in agreement with those in our study, where no further decreases in FA were noted after 4 months. The absence of more widespread, and significant increases in FA in the study by McDonald et al may be due to limited sensitivity caused by small numbers of subjects, and an ROI based analysis method. We speculate that changes in distributed networks that underlie language function, and which do not correspond to simple, specific white matter tracts, are easier to detect with whole brain compared to ROI based methods.

6.5.2 Cluster of increased FA in right TLE patients

In this study we have replicated, using smaller subgroups of patients, the findings from the previous chapter. We have demonstrated a significant increase in FA in an extensive region of white matter in left, but not right, TLE patients approximately 4 months after surgery. However, we have also shown that by approximately 12 months after surgery, right TLE patients have also developed a region of increased FA relative to the preoperative data, that is ipsilateral to the side of resection and almost identical in anatomical location to that seen in left TLE patients at 12 months. As explained in the previous chapter, we hypothesize that the increase in FA in this region in right TLE patients also partly represents structural plasticity underlying language, or possible other cognitive functions, but that it takes longer to develop in the non-dominant hemisphere. Assessment of the native cluster shows that the difference in the speed of increase in FA in left and right TLE patients is predominantly driven by a more rapid, initial decline in $\lambda_{\perp}$ in left compared to right TLE patients. It is perhaps not surprising that changes take longer to appear in the non-dominant hemisphere. Recent clinical, and imaging research demonstrates that language function cannot be simply dichotomized to the left hemisphere. Although the left hemisphere is the superior language processor, it is now clear that the right hemisphere is also important for language

processing including elements such as prosody, paralinguistic aspects of speech production, reception, and interpretation, and prelexical, lexical and postlexical components of visual word recognition (573). Impairment of these aspects of language function may be subtler clinically, and are not assessed with current neuropsychology tests. In addition, recent fMRI studies of patients after anterior temporal lobe resection highlight that it is ipsilateral temporal and frontal lobes, rather than the contralateral hemispheres, that are critical for post-operative material specific memory and language function respectively (261,270). For this reason, it is perhaps not surprising that structural changes and FA increases appear to predominate in the hemispheres ipsilateral to surgery. fMRI studies of other disorders such as middle cerebral artery stroke also demonstrate that reorganization of language function to the contralateral hemisphere after stroke is associated with poor language performance, and that it is ipsilateral reorganization that is critical (574).

6.5.3 The prediction of post-operative naming decline

A number of studies have attempted to identify factors that might be used to predict language and naming decline after anterior temporal lobe resection (260,261). These studies have highlighted that pre-operative language fMRI lateralization to the opposite hemisphere to surgery, and a lower pre-operative GNT score are predictive of a smaller naming decline after surgery. We have demonstrated that the higher the pre-operative FA in the ipsilateral white matter network encompassing the anterior/posterior/superior corona radiata, the posterior limb/the dorsal anterior limb of the internal capsule, and the external capsule, the lower the decline in naming ability at 12 months in both left and right TLE patients. This is in keeping with the findings from the previous chapter, where both the pre- and post-operative FA in this region correlated with post-operative, but not pre-operative, language function. The regression model reported in this study shows that while both pre-operative language fMRI ($\beta = 0.62$) and pre-operative naming ability ($\beta = -0.64$) are more powerful predictors than pre-operative FA ($\beta = 0.34$) of language decline after surgery, the latter variable, independent of language lateralisation and pre-operative naming ability, adds approximately 10% accuracy to the predictive model of language decline.

6.5.4 Limitations

The limitations of this study are similar to those highlighted in the previous chapter. In addition, we combined both groups for the regression analysis for several reasons; the small numbers of patients in

both left and right TLE groups, the presence of patients with atypical language dominance in both groups, and the fact that by 12 months the cluster of increased FA was present in an almost identical locations in both groups. Furthermore, the linear regression model highlights the significant contribution of preoperative FA to the predictive model, *independent* of pre-operative naming ability and language lateralization. In this regard, such a model may be clinically more useful, by being applicable to all patients undergoing anterior temporal lobe resection. In the future, larger independent pre-operative data sets are needed to assess the ability of this model to predict language deficits after surgery, and such studies are ongoing.

6.6 Conclusion

We have extended the findings of the previous chapter, and demonstrated that clusters of increased FA are present after surgery, ipsilaterally in right TLE patients, in a similar location to left TLE patients. However, these changes take longer to appear in right TLE patients. Pre-operative mean FA in these regions provides additional, independent information to the prediction of post-operative language deficits. These findings have important implications for how pre-operative diffusion MRI may be used to minimize post-operative language deficits. The pre-operative white matter network identified in this study can be used to together with pre-operative fMRI and neuro-psychology to predict those patients at highest risk of post-operative language deficits.

7 Defining Meyer's Loop – Temporal Lobe Resections, Visual Field Deficits and Diffusion Tensor Tractography

This chapter assesses the utility of tractography in delineating the optic radiation and Meyer's loop, and whether this information together with resection size is predictive of visual field deficits after anterior temporal lobe resections. The techniques first developed in this chapter, and the accompanying published paper (see publications section), have been subsequently replicated in several other publications.

7.1 Objectives

In the previous two chapters I have used whole brain methods of analysis to demonstrate how diffusion based data may aid the prediction of language deficits after anterior temporal lobe surgery. The primary objective of this chapter is to assess the utility of tractography in outlining Meyer's loop and the optic radiation, and to assess whether this information together with the size of the anterior temporal lobe resection is predictive of post-operative visual field deficits.

7.2 Introduction

As outlined in chapter 1, anterior temporal lobe resection (ATLR) is a well-established, and effective means of treatment for patients with refractory temporal lobe epilepsy (205). However, this procedure can be complicated by a visual field deficit (VFD), typically a contralateral superior quadrantanopia. This is caused by damage to the anterior and inferior portion of the optic radiation, also known as Meyer's loop (575). The reported incidence of post-operative visual field deficits varies from 68% (576) to 100% (577) of patients undergoing anterior temporal lobe resections. In 25% to 46% of patients the VFD may be severe enough to fail the current visual field criteria set by the UK Driver and Vehicle Licensing Authority (DVLA), even if they are seizure free (409,578). This is very significant because most patients cite the ability to drive as one of the five most important factors that would contribute to their complete rehabilitation (579). Several factors give rise to the variability in the figures reported in these studies, including the heterogeneity of methods used to assess VFDs (409), and differences in the nature and extent of

surgery (580). Equally important, is the inter-individual variability in the anatomy and anterior extent of Meyer's loop (410).

This anatomical heterogeneity cannot be assessed with conventional MRI, because variations in white matter signal are subtle. White matter tracts, such as the optic radiation, cannot therefore be accurately parcellated from surrounding tissue. Using diffusion tensor imaging (DTI) and tractography, we investigated the relationship of Meyer's loop to anatomical landmarks such as the tip of the temporal horn and temporal pole in patients undergoing anterior temporal lobe resections. We also investigated whether these measurements, together with the extent of resection, correlated with the severity of post-operative VFDs.

7.3 Methods

7.3.1 Subjects

We studied 21 consecutive patients (mean age 37 years, range 18 – 62 years, 10 male) with medically refractory TLE undergoing pre-surgical evaluation at the National Hospital for Neurology and Neurosurgery, London, UK. All patients had undergone structural MRI at 3 Tesla (3T) (185), and video-EEG had confirmed seizure onset in the medial temporal lobe (MTL) ipsilateral to the clinically defined seizure site. None of these patients had previously used vigabatrin. In two of the 11 patients with left sided TLE, structural MRI was normal, and post-operative histopathology confirmed the presence of end folium sclerosis. Of the 10 right TLE patients, two had anterior temporal lobe cavernomas and one also had HS. All remaining patients had HS identified on MRI ipsilateral to seizure onset, and all patients had a normal, contralateral hippocampus based on qualitative and quantitative MRI criteria (435). Post-operative histopathology confirmed the MRI findings in all cases. All patients were taking anti-epileptic medication, and were fluent English language speakers. Handedness was determined using the Edinburgh handedness inventory (416), and language dominance was determined using a range of fMRI tasks which have been described previously, and include the use of verbal fluency, and reading tasks (404). We also studied 20 right-handed, native English speaking, healthy volunteers (mean age 42, range 20 to 63, 8 male). All controls were left hemisphere language dominant as determined by the analysis of verbal fluency fMRI tasks as described in previous chapters.

Patient demographics, clinical information and surgical outcome data (based on the ILAE classification of post-operative seizure outcome (227)) following epilepsy surgery are listed in table 7.1.

7.3.2 MR data acquisition

We acquired the clinical T1 data on a 3T scanner (GE Excite II) using the sequence and parameters described in chapter 2. High resolution echo planar imaging (HR-EPI) images were also acquired with geometric distortions to match those of the DTI data (419).

7.3.3 Diffusion tensor imaging acquisition

The DTI data was acquired on the 3T scanner using the sequence and parameters described in chapter 2.

7.3.4 Diffusion tensor imaging (DTI) processing

All scans were transferred to a Linux workstation. The DICOM files of each DTI acquisition were converted into a single multivolume ANALYZE 7.5 file, and were then corrected for eddy currents using the "eddy-correct" algorithm implemented in FSL v4.1 (http://www.fmrib.ox.ac.uk/fsl/). This tool conducts an affine registration of every individual volume to the first non-diffusion weighted (b = 0) volume. After this co-registration step, the six b = 0 volumes of each subject were extracted and averaged. A multi-tensor model was fitted to the diffusion data using the open source Camino toolkit (http://www.camino.org.uk/) (581). We used the method of Parker and Alexander to reduce fibre orientation ambiguities in voxels containing fibre crossings (333,420). Voxels in which the single tensor fitted the data poorly were identified using a spherical-harmonic voxel-classification algorithm (293). In these voxels a two-tensor model was fitted, and the two principal diffusion directions of the two diffusion tensors provided estimates of the orientations of the crossing fibres. In all other voxels a single tensor model was fitted.

7.3.5 Tractography

The tractography analysis was carried out using the PICo algorithm (420) extended to multiple fibres as implemented in the Camino package (333,421). Start regions for tractography were based upon previously published work by our group (413,582) (figure 7.1). We used the program MRIcro (http://www.psychology.nottingham.ac.uk), to visualise images and create masks. We identified the lateral geniculate nucleus (LGN) on fractional anisotropy (FA) and principal diffusion direction (PDD) maps by selecting the axial slice at the level of the transition from the posterior limb of the internal capsule to the cerebral peduncle. At this level part of Meyer's loop could typically be seen on the PDD map (figure 7.1). Seed masks, consisting of voxels antero-lateral to the LGN at the base of Meyer's loop, with main eigenvectors orientated in an anterior-medial to posterior-lateral orientation, were identified and positioned in white matter from coronal views. Previous studies have shown that probabilistic algorithms can have difficulty in tracking Meyer's loop if seed voxels are placed directly at the lateral geniculate nucleus (295). Contiguous voxels, with principal directions in an anterior-posterior direction, were also selected in order to ensure that the entire coronal cross-section of Meyer's loop was encompassed. The volumes of seed masks were standardised for all subjects (15 voxels).

Patient number	Age/gender	Handedness/language dominance	Age of epilepsy onset (yrs)	Duration of epilepsy (yrs)	Clinical and EEG diagnosis	Operation	Postoperative outcome (ILAE class)[a]
1	50/M	R/L	16	34	L TLE	L ATLR	5
2	52/M	R/L	6	46	R TLE	R ATLR	1
3	62/F	R/L	1.5	61	L TLE	L ATLR	1
4	48/M	R/L	2.5	45.6	R TLE	R ATLR	1
5	20/F	R/L	11	9	L TLE	L ATLR	1
6	46/F	R/L	7	39	L TLE	L ATLR	3
7	43/F	R/L	12	31	R TLE	R ATLR	3
8	31/M	R/R	2	29	R TLE	R ATLR	1
9	22/F	L/L	10	11	R TLE	R ATLR	1
10	19/F	R/L	1	18	L TLE	L ATLR	3
11	18/F	R/L	3	15	L TLE	L ATLR	1
12	43/M	R/L	1	42	L TLE	L ATLR	1
13	32/F	R/L	4	33	L TLE	L ATLR	1
14	37/F	R/L	7	25	R TLE	R ATLR	1
15	30/F	R/L	18	20	R TLE	R ATLR	1
16	33/F	R/L	7	32	R TLE	R ATLR	b
17	34/M	R/L	26	8	L TLE	L ATLR	1
18	43/M	R/L	13	31	L TLE	L ATLR	1
19	36/M	R/L	23	13	L TLE	L ATLR	b
20	30/M	R/L	13	17	R TLE	R ATLR	4
21	48/M	R/L	30	18	R TLE	R ATLR[c]	1

[a] = at 12 months follow-up, [b] = ILAE class 1 at 3 months follow-up (12 month follow-up data not available), [c] = modified sparing hippocampus
M = male, F = female, R = right, L = left

Table 7.1 - Patient demographics, clinical information and surgical outcome data.

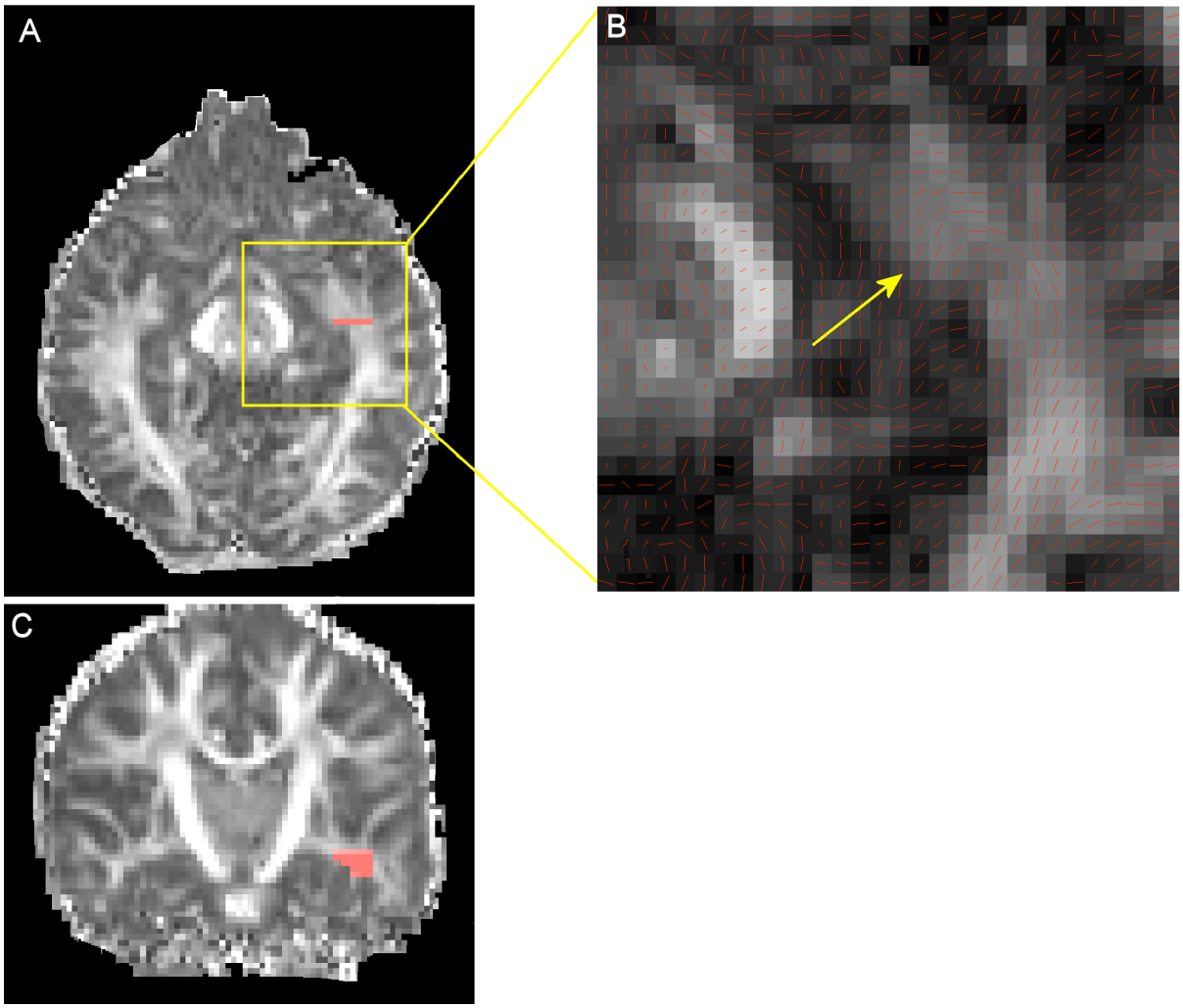

Figure 7.1 - Seed region selection using fractional anisotropy images (seed voxels are shown in red). (A) Axial slice where transition from the external limb of the internal capsule to cerebral peduncle is visible. (B) Magnified area of axial slice with principle diffusion direction map overlaid on each voxel (red lines). Part of Meyer's loop can be seen clearly (see arrow). (C) Seed voxels with principal diffusion direction in anterior-medial to posterior-lateral direction are selected in the corresponding coronal slice at the base of Meyer's loop.

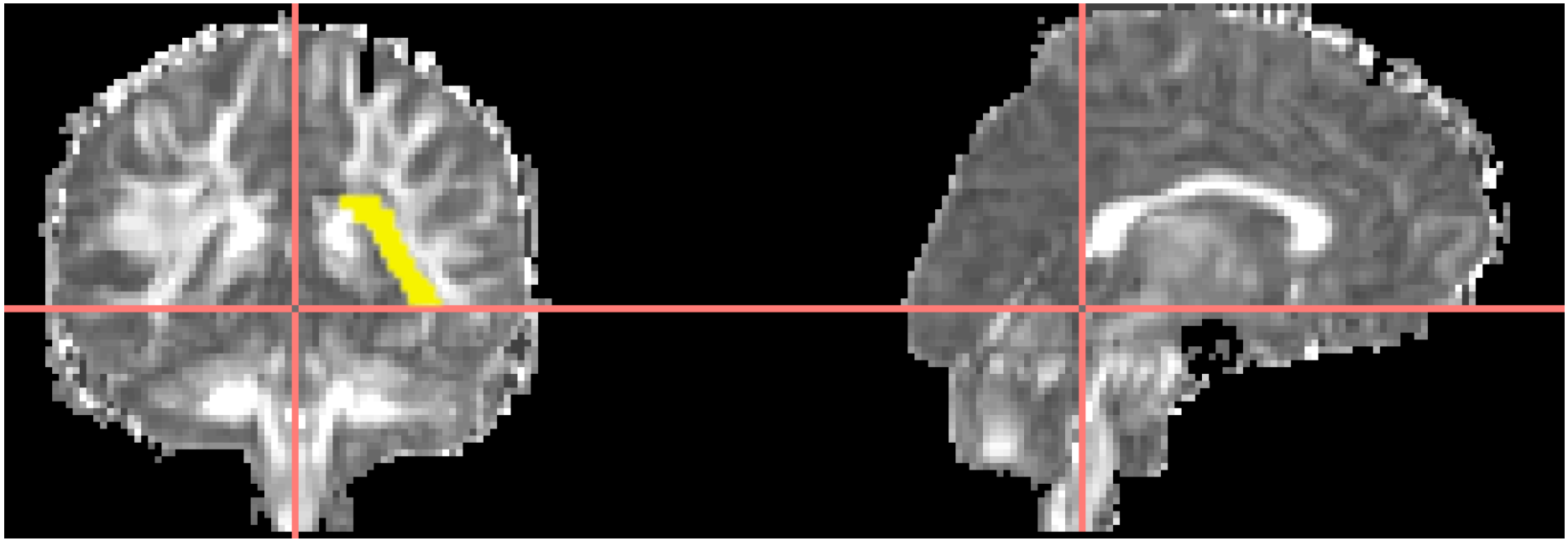

Figure 7.2 - Way point selection using fractional anisotropy images (waypoint voxels are shown in yellow): The coronal slice immediately posterior to splenium of corpus callosum is shown—a way point is superimposed at the level of the occipital horn of the lateral ventricle including the stratum sagittal.

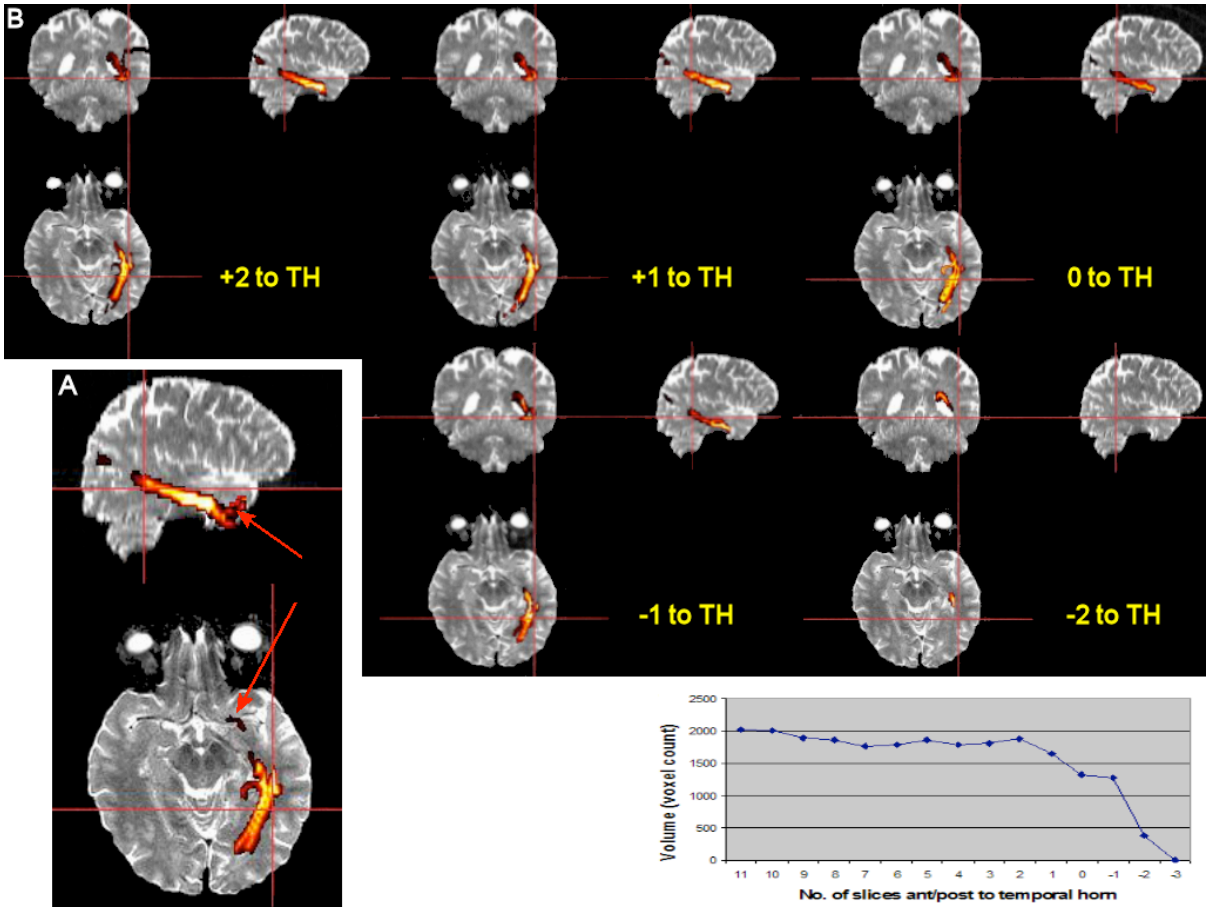

Figure 7.3 - (A) Resulting tract without use of fronto-temporal exclusion mask—the red arrow indicates some of the artefactual connections that can arise in areas including the uncinate fasciculus and fronto-occipital fasciculus, making it difficult to estimate the tip of Meyer's loop. (B) Iterative tracking using fronto-temporal exclusion mask. All images contain tracts thresholded at the same value and overlaid on distortion matched high-resolution EPI images. The graph is of tract volume against position of exclusion mask ('+' = anterior; '-' = posterior) relative to the tip of the temporal horn (TH). The graph and associated images demonstrate the thinning that occurs in the bulk of the optic radiation once the coronal exclusion mask reaches a coronal position 1 slice anterior to the temporal horn. At this position ≥10% of the tract volume is lost, and this is chosen as the exclusion mask to be used.

All studies were carried out using 50000 Monte Carlo iterations, an angular threshold of 90 degrees and an FA threshold of 0.1, in order to ensure that the paths detected would not erroneously enter areas of cerebrospinal fluid, and yet had sufficient angular flexibility as to allow tracking of Meyer's loop.

As described in similar studies (582,583), we used a way mask to restrict the pathway to the hemisphere ipsilateral to the seed mask, and extended posterior to the splenium of the corpus callosum within the wall of the occipital horn of the lateral ventricle (figure 7.2). It is widely accepted that the optic radiation passes through this region (584). All streamlines from the seed region that did not pass through this waypoint were discarded. In addition, a coronal exclusion mask that included the entire fronto-temporal area was used to remove artefactual connections to neighbouring bundles including the uncinate fasciculus, fronto-occipital fasciculus and anterior commissure (figure 7.3). This is a common problem when probabilistic tractography is applied in regions of adjacent white matter bundles. Rather than placing this mask on the basis of visual discrimination of Meyer's loop from artefactual connections, its coronal position was determined using an objective, iterative process. Tracts were initially generated from the seed region using an exclusion mask placed 25mm anterior to the temporal horn. This process was repeated, but in each consecutive trial, the mask was moved posteriorly by one voxel. All streamlines from the seed region that intersected with the exclusion mask were discarded. When this mask coincided with the optic radiation, visible thinning of the estimated trajectory of the optic radiation was evident, and typically coincided with a reduction in tract volume ≥ 10%. Therefore, in cases where it was visually difficult to discern thinning with consecutive slices, the mask that first resulted in a reduction in tract volume ≥ 10% followed by further, consistent reduction in volume, was chosen as the exclusion mask. This mask was then used in conjunction with the seed and way masks described above (figure 7.3).

Using this method, connectivity distributions were generated from every voxel in the seed mask, and thresholded to include only those with a probability of ≥ 5 %. Mask generation and tractography was repeated in 10 randomly selected patients in order to determine the intra-observer variation in the delineation of the anterior extent (ML-TP) of the optic radiation. The

correlation coefficient was 0.94, which suggested good reproducibility. On repeated analysis by the same observer, the average variation in the anterior extent of Meyer's loop was 2 mm, and the maximum variability was 4 mm. Pre- processing of tractography data, and the tractography itself required ~1 and 6h, respectively per subject, using a Linux based Sun Ultra workstation.

7.3.6 Quantitative and qualitative analysis

Pre-operative mean b = 0 images and distortion matched HR-EPI images were co-registered using SPM5 in order to ensure that they were in the same orientation (Wellcome Department of Imaging Neuroscience, London; http://www.fil.ion.ucl.ac.uk/spm). We qualitatively inspected the anatomy of resulting tracts by overlaying them onto the co-registered HR-EPI images. We also assessed the distance between the most anterior extent of Meyer's loop and the temporal pole (ML-TP) and tip of the temporal horn (ML-TH). These landmarks were identified using the pre-operative mean b = 0 images, with the aid of the distortion matched HR-EPI images.

7.3.7 Resection size estimates

All resections were carried out by a single surgeon (AM) who performed a modified Spencer approach. In this approach the lateral ventricle is localised by proceeding from the middle fossa floor up the collateral sulcus. The size of resection was measured using a previously described method, based on the post-operative T1-weighted images (577). Using MRIcro to visualise the images, the anterior-posterior extent of resection was estimated by measuring the distance from the anterior tip of the middle cranial fossa formed by the sphenoidal bone (which had previously contained the resected temporal pole) to the posterior margin of the resection. Distances were measured using sagittal images that intersected the midbrain and lateral wall of the temporal horn, as the optic radiation runs through this region. In the event of resection margins being irregular, we used the most posterior aspect of the resection in the peri-ventricular white matter, which typically also corresponded to the most medial point of resection. In order to compensate for variations in head size and field distortions caused by MRI, the extent of resection was expressed as a fraction of the distance between the anterior tip of the middle sphenoid fossa to the occipital pole (anterior temporal-occipital pole or AT-OP distance). To verify the accuracy of this method of using the tip of the fossa as a surrogate for the temporal pole, measures of the AT-OP distance were

obtained in the non-resected hemisphere, using the existing temporal pole to mark the anterior temporal position. T-tests showed no significant bias in the AT-OP estimates between the intact and resected hemispheres, despite the differences in methods.

7.3.8 Visual field assessment

All patients had post-operative Goldmann perimetry carried out by a consultant ophthalmologist (JA), at least three months after surgery, in order to decrease the likelihood of confounding temporary VFDs from brain oedema. The ophthalmologist was blinded to the results of tractography, and estimates of resection size. Perimetry was performed in a standardised fashion for each eye separately generating three isopters with the V4e, I4e and I2e targets. The results of perimetry were quantified using a previously described method to calculate the proportion of area lost for the three isopters (577). These values were averaged across all three isopters, and then across both eyes to give an overall estimate of visual field loss. Conventional isopter plotting will typically conceal the cartographic distortion error, which is inherent in the transposition of the isopter on the curved perimeter bowel onto flat, polar, azimuthal visual field charts (585,586). This can lead to the underestimation of visual field area, and any visual field loss measured by perimetry. However, this error should be similar across subjects for each isopter, and should therefore not affect the relationship between the anterior extent of Meyer's loop and visual field loss. Furthermore, because the central field is represented in all three isopters, unlike the periphery which is covered by fewer isopters, this method should weight the central field more than the peripheral field. Therefore, this should account for some of the physiological central magnification present in the optic nerve, which can confound any linear relationship between visual field loss, and axonal loss (587).

7.3.9 Statistical analysis

All statistical analysis was carried out using Stata v11.0.0 (Statacorp LP, Texas, USA). Group differences for age were determined by a one-way analysis of variance (ANOVA), and gender distribution was assessed using the Pearson's χ^2 test.

The relationship of interest was between the VFD, and the anterior extent of Meyer's loop. The size of the temporal lobe resection is a potential confounder of this relationship. Multiple regression analysis was therefore specified to model the relationship between VFD as a dependent variable, and ML-TP and resection size as independent variables. Both variables were entered into the model simultaneously. Partial regression plots were inspected for outliers and heteroskedacity, and residuals tested for normality using the Shapiro-Wilkes test. The Durbin-Watson test was used to test for the independence of the error terms. In view of the fact that any linear relationship between the anterior extent of Meyer's loop, and visual field loss may be confounded by the lack of a 'one-to-one' relationship between field loss and axonal numbers, we also carried out a categorical analysis of the data using a 2 x 2 contingency table, and Fisher's exact test.

We also carried out a two way mixed ANOVA with one between subjects factor (group – controls or TLE (both left and right)) and one within subjects factor (hemisphere – left or right), to test for the effect of group, hemisphere, or an interaction between group and hemisphere, on ML-TP. Prior to this analysis it was first verified that all parameters were normally distributed using the Shapiro-Wilkes test for normal distribution.

7.4 Results

7.4.1 Demographic analysis

There was no significant difference in the mean age or gender distribution of participants in the three groups (controls, left TLE, right TLE).

7.4.2 Resection size and visual field deficits

Right ATLRs averaged 34% of the TP-OP distance, compared with 31% for left ATLR (table 7.2), though this difference was not statistically significant. Six of the 11 patients undergoing a left ATLR had a post-operative VFD, compared with 3 of the 10 patients undergoing a right ATLR. Three of these patients (two post left ATLR, one post right ATLR) would fail DVLA criteria to be granted a UK driving license. Although left ATLRs tended to result in bigger VFDs than right ATLRs (mean of 26% compared with 22% of superior contralateral quadrant, averaged across three isopters and both eyes) this was not statistically significant. The post-operative VFDs tended to be incongruous,

with loss of field extending from the vertical meridian towards the horizontal meridian, in keeping with previous reports (577) (figure 7.4).

7.4.3 Qualitative analysis:

In all subjects the anterior portion of Meyer's loop typically passed over the roof of the temporal horn (figure 7.5 a), before then turning posteriorly to pass along the lateral inferior aspect of the temporal horn (figure 7.5 b). Fibres then passed laterally to the occipital horn of the ventricle (figure 7.5 c), and terminated in the calcarine sulcus, and occipital pole (figure 7.5 d).

Table 7.2 – Results of quantitative analysis of Meyer's loop

VFD expressed as a percentage of superior quadrantic field. This is calculated by averaging the proportion of quadrantic field loss across three isopters (V4e, I4e and I2e) and both eyes as measured by Goldmann perimetry. ML-TP = distance between the most anterior extent of Meyer's loop and the temporal pole, and tip of the temporal horn (ML-TH). The extent of resection is expressed as a fraction of the distance between the anterior tip of the middle sphenoid fossa to the occipital pole (AT-OP).

Group	L ML-TP (mm) Mean SE Range	R ML-TP (mm) Mean SE Range	L ML-TH (mm) Mean SE Range	R ML-TH (mm) Mean SE Range	Resection Size (%AT-OP) Mean SE Range	VFD (% superior quadrant) Mean SE Range
L TLE	31.5 1.5 24.4 to 39.4	35.3 1.2 28.1 to 41.3	2.0 1.3 -3.8 to 9.4	-3.3 1.3 -15 to 1.9	0.31 0.02 0.15 to 0.41	26 9 0 to 87
R TLE	35.4 1.2 30.0 to 43.1	34.2 2.0 26.2 to 43.1	-1.0 1.5 -7.5 to 7.5	1.3 1.2 -3.8 to 7.5	0.34 0.01 0.28 to 0.40	22 11 0 to 76
Controls	33.5 1.0 24.4 to 41.2	36.0 0.9 31.9 to 46.8	1.5 0.7 -3.7 to 9.4	-1.4 0.9 -11.2 to 3.7		

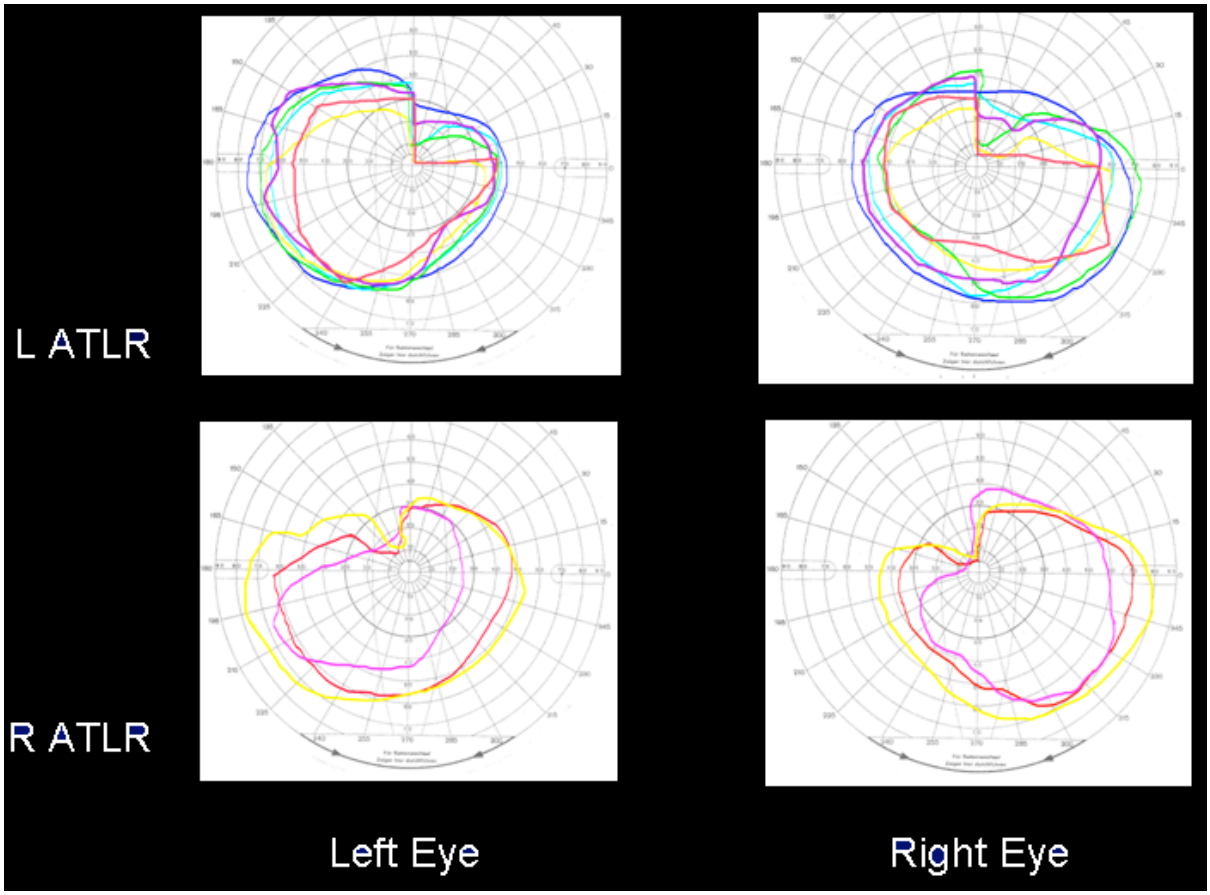

Figure 7.4 - Representative VFDs in one isopter only (I4e). Each colour represents a single patient. The range of magnitude of VFDs averaged across all three isopters was 22–87% of the superior contralateral quadrant in patients undergoing left ATLR, and 47–76% in patients undergoing right ATLR.

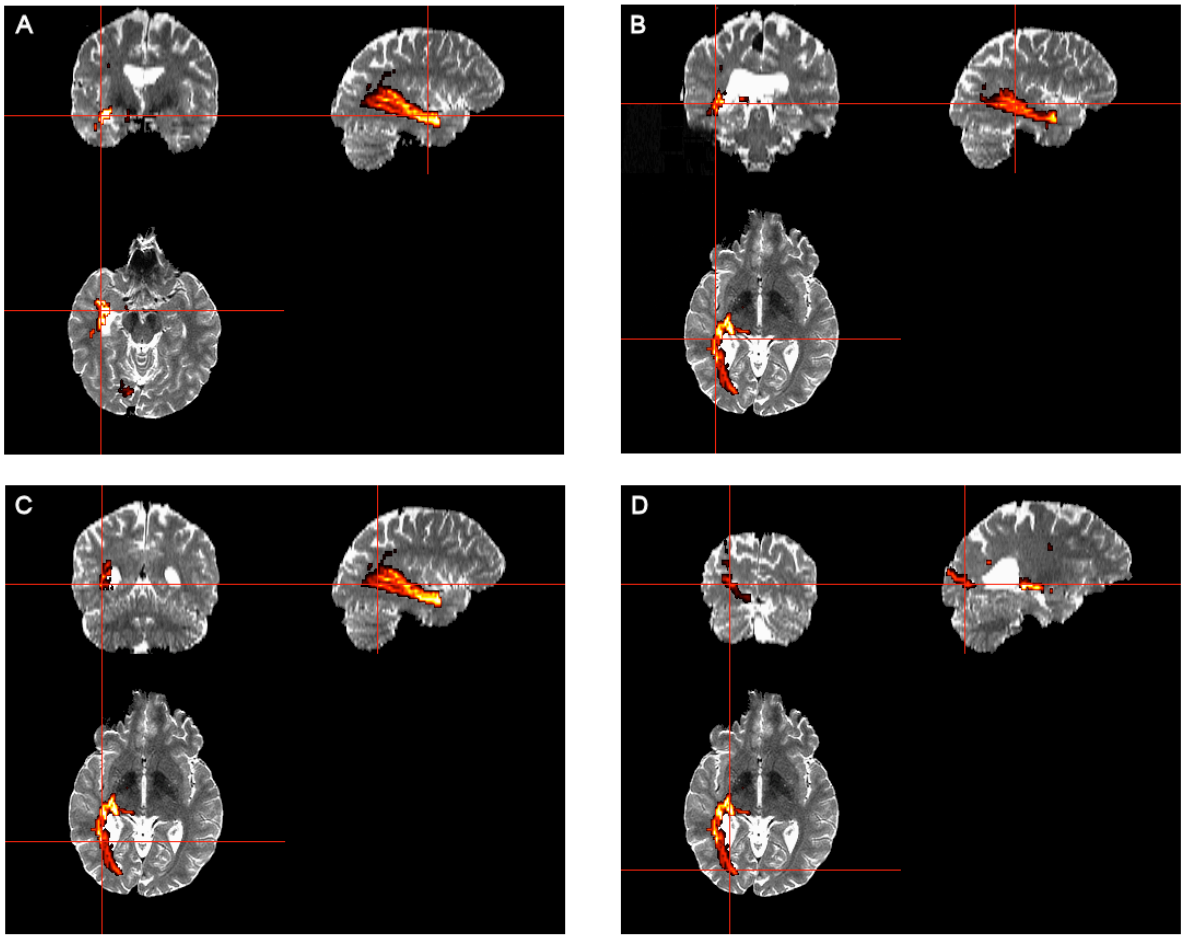

Figure 7.5 - Representative tract of the optic radiation of a single patient overlaid on a distortion matched HR-EPI image. (A) Anterior portion of Meyer's loop passing over the roof of the temporal horn. (B) Along the lateral inferior aspect of the temporal horn. (C) Along the lateral aspect of the occipital horn. (D) Termination in the calcarine sulcus, and occipital pole.

7.4.4 Quantitative analysis

In patients, the range of ML–TP was 24–43 mm (mean 34 mm), and the range of ML–TH was -15 to +9 mm (mean 0 mm). In controls, the range of ML–TP was 24–47 mm (mean 35 mm), and the range of ML–TH was -11 to +9 mm (mean 0 mm) (table 7.2). Following multiple regression analysis both ML-TP (ß = -0.80, $p < 0.001$) and resection size (ß = 0.41, $p < 0.05$) were found to be significant predictors of post-operative VFDs (adjusted $r^2 = 0.63$). Partial regression plots showed homoskedacity without significant outliers (figure 7.6), and residuals from the analysis were normally distributed. There was no correlation between residual terms.

The ANOVA analysis revealed a trend towards the left ML-TP being smaller than the right ML-TP across all groups ($p=0.072$). There was no interaction between groups and sides.

Fisher's test revealed a significant association between the anterior extent of Meyer's loop and whether a patient suffered a severe (>50%) quadrantic VFD $\chi^2(1) = 5.19$, $P = 0.01$ (two- tailed); if the anterior extent of Meyer's loop was <35 mm from the temporal pole, patients were more likely to suffer severe VFDs, irrespective of the size of resection. The threshold values used to categorize the data were chosen because 50% represented the midpoint of the VFD range and was regarded as the minimum cut-off for further binocular testing if seizure free patients wished to drive, and 35mm represented the approximate midpoint of the range of ML–TP distances found across controls and patients (table 7.2).

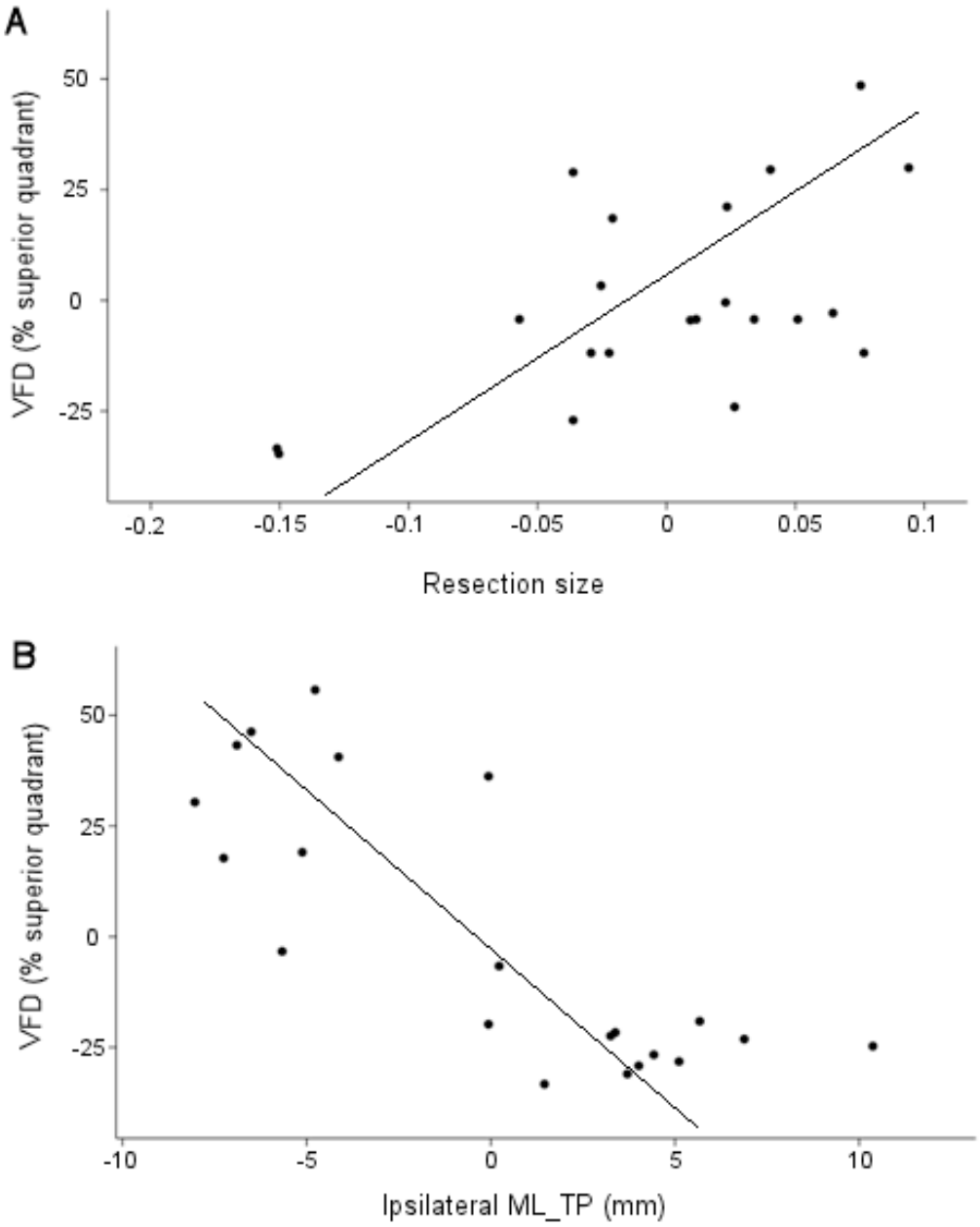

Figure 7.6 - Partial residual plots demonstrating the variance in ML–TP and resection size attributable to the model. (A) Extent of VFD against corrected anterior–posterior extent of temporal lobe resection (resection size), showing positive correlation $r^2 = 0.63$. (B) Extent of VFD against distance of tip of Meyer's loop to temporal pole (ML_TP), showing inverse correlation $r^2 = -0.80$.

7.5 Discussion

This study demonstrates the parcellation of the optic radiation and Meyer's loop using probabilistic tractography applied to diffusion tensor data acquired at 3 Tesla. The anatomy of the tracts that have been obtained using this technique is comparable to the results described in dissection based studies. In patients, the range of ML-TP was found to be 24mm to 43mm (mean 34mm), while the range of ML-TH was -15mm to 9mm (mean 0mm). While there was no statistically significant difference in the anterior extent of the right and left optic radiations across patients and controls, there was a trend toward the left optic radiation extending more anteriorly than the right optic radiation in both patients and controls. Because the optic radiation and its anterior extent could not previously be visualised with conventional, clinical MRI sequences, this information was not incorporated into studies investigating the relationship between MRI based volumetric assessment of resection size and VFDs. Using tractography we have now demonstrated that both the size of ATLR, and the anterior extent of the optic radiation are predictors of the occurrence and severity of post-operative VFDs.

7.5.1 Studies of Meyer's loop

Following the original description nearly one century ago by Meyer and Archambault, of the 'peculiar detour of the ventral portion of the geniculocalcarine path' (588,589), there has been considerable interest in the anatomy and pathology of the optic radiation. Initial studies were based on patients with tumours (590) or gunshot wounds to the temporal lobe (591). With the introduction of the anterior temporal lobe resection for refractory temporal lobe epilepsy and appreciation of the occurrence of post-operative VFDs, interest in the optic radiation and Meyer's loop has increased significantly. There has been considerable heterogeneity as to the incidence of VFDs following anterior temporal lobe resection. While some studies have reported a correlation between extent of resection and the presence/absence of a VFD (575,576,592,593), others have not found this to be the case (594–596). Even fewer studies have demonstrated a correlation between the severity of a resulting VFD and extent of resection (597). Moreover, in studies comparing selective with en bloc temporal lobe resections, there again appeared to be little correlation with either the frequency or extent of VFDs (580,598). While patient selection, and

the methods used for both surgery and VFD assessment have changed over time and differ between studies, the variability in the anterior extent of Meyer's loop is an additional confounding factor.

Studies assessing the anterior extent of Meyer's loop and its anatomical relationships can be broadly divided into three groups. The first and largest group of studies have used estimates of both resection size and the severity of post-operative VFDs, in order to deduce the anatomy of the OR (table 3). Penfield first stated over fifty years ago, that lesions that were less than 60mm from the temporal tip were not likely to produce a field deficit (599). Subsequent studies, however, have gradually reduced this estimate. Older studies which used intra-operative measurements are likely to have overestimated resection size (600), and therefore underestimated the anterior extent of Meyer's loop.

A smaller group of studies have used the Klingler dissection technique in the cadaveric brains of previously healthy subjects, in order to investigate the anatomical relationships of Meyer's loop. The largest of these studies reported an average distance of 27mm for ML-TP, but at the same time emphasised the variability between subjects (410). Other dissection-based studies demonstrated that Meyer's loop tends to cap the temporal horn, and all reported ML-TP distances which were smaller than those found in the first group of studies (table 4). In contrast to resection based assessments, however, these studies may be susceptible to overestimations of the anterior extent of Meyer's loop. It can be difficult to delineate accurately, the anterior extent of the optic radiation using micro-dissection techniques, particularly amongst a dense network of neighbouring fibres that includes the uncinate fasciculus, occipito-frontal fasciculus, anterior commissure and thalamic fibre tracts (601).

The final group of studies that have assessed the optic radiation have incorporated digital photography, and computer reconstructions of block images of cryosectioned brain (584,602). While these studies have tended not to derive measurements of the anatomical relationships of Meyer's loop, they do describe the anatomy of the optic radiation, and its relationship to the temporal horn. Burgel et al (584) studied 10 control brains, and found in all cases that Meyer's loop capped the temporal horn. On the other hand, Kier et al (602) studied the temporal stem of a single normal brain, and reported that Meyer's loop was posterior to the temporal horn.

Table 7.3 – Studies on temporal lobe surgery resection sizes, VFDs and inferred anatomy of the optic radiation

Reference	Numbers of Patients Undergoing Surgery	Method of Field Assessment	% VFD (magnitude)	Anatomical Inferences Regarding ML
Bjork et al (1957) (603)	26	Goldmann	96% (partial)	ML-TP = 30mm to 60mm ML caps TH
Falconer et al (1958) (575)	18 (right) 32 (left) *ATLR*	Bjerrum and tangent screen	64% (complete) 36% (incomplete)	ML-TP ≥ 45mm ML caps TH
Van Buren et al (1958) (604)	41 *ATLR*	Bjerrum and tangent screen	80% (severity not specified)	ML does not cap TH
Wendland et al (1960) (605)	24 *ATLR*	Kinetic perimetry (not specified)	29% (complete) 71% (partial)	ML-TP ≥ 50mm
Marino et al (1968) (594)	25 (right) 25 (left) *ATLR*	Haimark screen (form of static perimetry)	14% (complete) 52% (incomplete)	ML-TP ≥ 40mm ML does not cap TH
Hughes et al (1999) (593)	12 (left) 20 (right) *ATLR*	Humphreys	97% (not specified)	ML-TP ≥ 42mm
Krolak-Salmon et al (2000) (597)	11 (left) 7 (right) *ATLR*	Humphreys	28% (mild) 28% (moderate) 28% (total)	ML-TP = 20mm to 30mm ML cap TH and run lateral to TH
Nilsson et al (2004) (598)	34 *ATLR and Modified ATLR*	Goldmann	74% across both groups (no difference between groups) (40% partial, 34% complete)	ML-TP = 18mm to 36mm (note resection measured from TP-STG)
Barton et al (2005) (577)	16 (left) 13 (right) *ATLR*	Goldmann	100% (average loss of 63% of a quadrant)	ML-TP ≥ 24mm ML-TH = 4mm to 8mm

Table 7.4 – Dissection based studies of the optic radiation

Reference	No of Cadaveric Hemispheres Studied	Anatomical Inferences
Ebeling et al 1988 (410)	50 (controls)	ML-TP = 22mm to 37 mm (mean = 27mm) ML-TH = - 5 mm to 10mm (mean = 5mm)
Sincoff et al 2004 (606)	20 (controls)	ML caps TH
Rubino et al 2005 (607)	40 (controls)	ML-TP = 22mm to 30mm (mean = 25mm) ML-TH = 1mm to 3mm (mean = 2mm)
Choi et al 2006 (608)	10 (controls)	ML-TP = 28mm to 34mm (mean = 31.4mm) ML caps TH
Peltier et al 2006 (609)	20 (controls)	ML-TP = 15-30 mm ML ≤ 5mm anterior to TH

7.5.2 Tractography and Meyer's loop

The most recent development in the study of the optic radiation has been the application of diffusion based tractography. This technique has the advantage over post-mortem studies of allowing the study of the optic radiation and its anatomical relationships in vivo. All studies prior to the publication of this study incorporated small numbers of subjects and patients, and most used deterministic algorithms on diffusion data acquired at 1.5T. Yamamoto et al (411) assessed 5 healthy controls, and reported an ML-TP range of 33mm to 40mm (mean 37mm), and that Meyer's loop capped the temporal horn (range 3.7mm to 4.3mm, mean 4mm). Nilsson et al (583) studied 2 patients undergoing temporal lobe surgery and 7 controls. They reported that the ML-TP range was 34mm to 51mm (mean 44mm) in controls and 40mm to 51mm (mean 45.5mm) in patients. They also reported that Meyer's loop did not reach the temporal horn in any of the subjects studied. Both these studies placed Meyer's loop more posteriorly than reported in the current investigation. Deterministic tractography, however, can have difficulty in areas of crossing/kissing fibres such as Meyer's loop, and may therefore underestimate the anterior extent of Meyer's loop. For this reason, a modified approach was adopted by Taoka et al (610) in a study of 14 patients undergoing temporal lobe surgery. Although a deterministic method was used, the uncinate fasciculus (UF) was initially tracked, and used to define the anterior extent of ML. The ML-TP distances reported were less (mean 36.6 mm, range 30mm – 43.2mm) than the previous studies, but again smaller than those reported in this study and the other groups of studies described above. Taoka et al also reported a distance of 0mm between the UF and ML in at least 7 cases. It is therefore likely that despite the use of an anterior marker, the deterministic approach may have had difficulty in resolving neighbouring white matter bundles. A more recent study assessing the reconstruction of the entire human visual pathway using deterministic methods conceded that Meyer's loop was only fully reconstructed in half of the healthy control (611). And furthermore, a direct comparison of deterministic and probabilistic algorithms in 18 subjects showed a TP-ML distance of 32 to 51mm (mean, 41mm) using a deterministic algorithm and 17 to 42mm (mean, 30mm) with a probabilistic algorithm (612).

Probabilistic multi-fibre tractography applied to diffusion MRI data acquired at 3T is likely to cope

better with crossing and kissing fibres than deterministic methods. Consequently, it is therefore less likely to underestimate the anterior extent of Meyer's loop. This has been eloquently demonstrated by Sherbondy et al. who used a probabilistic multitensor approach with the use of priors, in a study of the optic radiation in 8 healthy volunteers (613). They found that the most anterior extent of Meyer's loop was 28+/-3mm posterior to the temporal pole, with a population range of 10mm. The results reported in the current study are similar to this, and another recently published tractography study by Chen et al. (614) who found that the mean distance of ML–TP was 32mm with a range of 21–52mm. The results reported in this study are also concordant with the largest reported dissection based study by Ebeling et al. (410) (ML-TP = 22mm to 37mm, mean = 27 mm and ML-TH = -5mm to 10mm, mean = 5mm), and the most recent resection-VFD based study by Barton et al (577) (ML-TP ≥ 24mm, ML-TH 4mm to 8mm). By measuring the resection size, as well as the anterior extent of Meyer's loop, we have also demonstrated that VFDs following ATLR are directly proportional to both variables, although the latter variable appears to be the more important factor. The upper limit of ML-TP that was associated with a VFD, regardless of resection size, was 32mm, and the categorical analysis demonstrates that patients with an ML–TP distance of <35 mm from the temporal pole are at greater risk of VFDs than those with ML–TP distances >35mm from the pole, regardless of resection size. The distance from the temporal pole to the temporal horn was relatively constant in this study (mean=34mm) and in agreement with other studies (410,583). The cut-off of 35mm may therefore represent the point at which a lateral or superior surgical approach causes large enough disruption of fibres covering the roof of the temporal horn so as to cause a significant VFD. Taoka et al (610) reported similar findings, but used an ANOVA analysis to compare the mean distance from the anterior limit of Meyer's loop to the posterior limit of resection, between categories of patients with varying severity of VFDs. The mean distance was calculated by subtracting the distance from the temporal tip to the posterior resection margin as measured on a post-operative T1 image, from the anterior limit of Meyer's loop as measured on a pre-operative b = 0 image. Patients with the most severe VFDs, typically had larger values suggesting greater overlap between Meyer's loop and the area of resection. This approach, however, does not lend itself to pre-surgical risk assessment, and may be problematic because the measurements used are susceptible to distortion artefact differences between the differing MRI sequences. By using a linear regression analysis incorporating the resection size and

the anterior extent of Meyer's loop, based on the T1 and b = 0 images respectively, the distortion errors should be similar in each subject in the current study.

The discovery of a trend towards the left optic radiation extending more anteriorly compared to the right optic radiation across all groups, is a novel finding. This may partly explain the higher incidence of visual field deficits in left compared to right ATLRs, despite the fact that larger resections typically occurred on the non-dominant, right side. A recent study in this centre of 105 patients who underwent ATLR has demonstrated similar findings (615). After accounting for the extent of tissue resections, left sided resections were found to be at significantly greater risk of VFDs compared with right sided resections (Odds Ratio 4.43, p = 0.01). The authors concluded that the geniculocalcarine tract extended further anteriorly on the left compared to the right sided tract. Histological based studies have also reported leftward asymmetry in the optic radiation (584), supporting to the findings reported here.

7.5.3 Limitations

The retrospective nature, lack of full blinding and significant operator input in placing a seed region are shortcomings of this study. To compensate for this, we used strict anatomical rules for the placement of start regions, as well as graphical displays to interpret the appropriate placement of fronto-temporal exclusion masks. Furthermore, we demonstrated that the intra-observer variability in the assessment of ML-TP was minimal which lends confidence to the reproducibility of our findings. Since the publication of the results reported in this chapter, other studies have proposed newer, and more automated methods of parcellation of the optic radiation and Meyer's loop (616,617). The study by Clatworthy et al (616) proposed complete automation of probabilistic tractography of the optic radiation, but no measurements of the location of Meyer's loop to confirm its validity were given, and the study only assessed healthy controls. The study by Winston et al (617) directly compared the method described in this chapter with another method using the same datasets in both patients and controls, in order to control for several parameters that might potentially bias the results. The aim of the newer method was to address some of the limitations of the method described in this chapter, by using a more automated technique to reduce operator time, and to depict the entire optic radiation by placing seed voxels within the lateral geniculate

nucleus and not anterior to it. The authors reported that whilst the core of the tract was common to both methods, there was significant variability between the methods. The earlier method, as described in this chapter, gave a more consistent and reproducible depiction of Meyer's loop with fewer spurious tracts. This is reassuring as this was the primary aim of the development of this method. The newer method gave a better depiction of the entire optic radiation, particularly in more posterior portions, but did not identify Meyer's loop in one patient. These findings are not surprising. The method described in this chapter better delineated the inferior portion of the optic radiation, presumably as the seed region was located within Meyer's loop, which conveys fibres to the inferior optic radiation, whilst the newer method used the LGN as a seed region. Tractography from this region would be expected to better delineate fibres passing directly posteriorly, and thus in the more superior part of the optic radiation than those subject to the high curvature of Meyer's loop which was depicted with less consistency and reliability. Our group has subsequently shown that by combining both methods, and seeding from both the LGN and Meyer's loop, the complete optic radiation can be visualised in patients. This is particularly important in patients in whom one wants to assess the relationship between structural lesions, and the optic radiation. It has been demonstrated to be of utility in informing the patient of the risks of surgery, and in planning the surgical procedure and approach in patients (618).

Although patients did not have pre-operative perimetry, all had normal visual fields to confrontation testing, and none had symptoms to suggest field deficits prior to surgery. The two patients with cavernomas had normal visual fields post-operatively. Furthermore, visual fields are typically normal in patients with non-expanding lesions of the temporal lobe, as reported in other studies (593,597). Although the methods used for resection estimation were based on previously validated studies (Barton *et al.* 2005), more sophisticated methods that take into account post-operative gliosis (600), may enable better modelling of the relationship between the anterior extent of Meyer's loop and VFDs. Similarly, development of more refined perimetric analysis methods should enable better understanding of this relationship. In this study we have used a relatively simple model that considers damage to the optic radiation in only the coronal plane. Because the anterior tip of Meyer's loop is the area that will typically incur the most damage after ATLR, damage in this plane should broadly correlate with postoperative VFDs. However, as

resection is typically at an oblique angle to the temporal pole, and can sometimes involve the removal of parts of the parahippocampal and fusiform gyri, in future studies it will be important to assess any damage to the optic radiation in other planes.

The remaining limitations of this study are common to most tractography based investigations. The resolution of tractography images is several orders of magnitude greater than the nerve bundles under examination. A single voxel contains numerous fibre populations, some of which may be kissing or crossing. The multiple fibre population model, and probabilistic tractography approach employed in this study, may be able to cope with this better than deterministic approaches. As methodological developments occur in spatial resolution, diffusion modelling and tractography algorithms, these limitations should prove less of a problem. In the interim, validation of the derived white matter tracts is crucial, particularly as tractography is a subjective process, dependent on user defined parameters. Though this technique is able to demonstrate the relationship between the anatomy of Meyer's loop and VFDs, the tracts themselves are 'virtual' representations of the underlying white matter. Kamada et al demonstrated that real-time, peri-operative visual evoked potentials confirmed the accuracy of tractography of the optic radiation (415). This, together with the qualitative similarity of the tracts in this study to those described in dissection studies, lends support to the anatomical validity of tractography derived images of the optic radiation. In the future, validation of the tractography derived anatomy of the visual pathway may also be aided by the implementation of a combination of manganese enhanced MRI and diffusion tensor tractography in animal models (619).

7.5.4 Conclusion and validation

In this study we have demonstrated the feasibility of tractography of the optic radiation in patients undergoing temporal lobe resections. By measuring the anatomical relationships of Meyer's loop we have shown that it is possible to predict the occurrence and extent of post-operative visual field deficits for a given resection size. This information could prove useful in the pre-operative advice given to patients regarding the risk of VFD. By using the information derived from the categorical analysis, it may be possible to stratify patients into groups at high or low risk for VFDs.

The definitive goal of tractography of the optic radiation is its integration into stereo-navigational systems together with T1 weighted anatomical images. However, differing geometric distortions between EPI and T1 based images makes accurate co-registration, particularly in areas such as the temporal lobe, difficult. Furthermore, peri-operative brain shift can complicate the nature of the anatomical relationships derived pre-operatively between the temporal pole and Meyer's loop. The use of alternative landmarks less prone to brainshift, such as the lateral geniculate body or brainstem, may prove more useful peri-operatively. Ultimately, the solution to both of these problems will encompass the use of real-time, peri-operative scanning. However, in view of the length of time needed in this study for the acquisition and tractography processing of diffusion tensor data, the feasibility of these advances depends on the development of robust and rapid diffusion acquisition schemes that may be co-registered with higher definition tractography that has been acquired preoperatively.

Daga et al. (620) have recently developed near real-time multichannel non-rigid image registration methods that use both anatomical and fractional anisotropy pre- and intra-operative images. The proposed workflow described by Daga et al incorporates the warping of the pre-operatively parcellated optic radiation to the intra-operative space in under 3 min making the proposed algorithm suitable for use under the stringent time constraints of neurosurgical procedures. Winston et al. (621) have demonstrated the feasibility of this method, and in turn validated the tractography techniques developed in this chapter. They studied 20 patients undergoing ATLR, and structural MRI scans, DTI, and visual fields were acquired before and 3 to 12 months following surgery. Tractography of the optic radiation using the techniques described and developed in this chapter were performed on preoperative images, and propagated onto postoperative images using novel and rapid registration methods (620). The anteroposterior extent of the damage to Meyer's loop was determined, and visual loss was quantified using Goldmann perimetry. Twelve patients (60%) suffered a VFD (10–92% of upper quadrant; median, 39%). Image registration took <3 minutes and predicted that Meyer's loop was 4.4 to 18.7mm anterior to the resection margin in these patients, but 0.0 to 17.6mm behind the resection margin in the 8 patients without VFD. The extent of damage to Meyer's loop significantly correlated with the degree of VFD and explained 65% of the variance in this measure. The technique was fast enough to propagate accurate preoperative tractography onto intraoperative scans acquired during neurosurgery, with the

potential to reduce the risk of VFD in real-time in patients undergoing anterior temporal lobe resections. Studies similar to this but incorporating peri-operatively acquired data are currently underway in order to assess whether the severity or incidence of visual field deficits can be reduced.

8 Overall Conclusions

8.1 Introduction

The aim of this thesis has been to explore the use of diffusion MRI to understand the causes and consequences of TLE, and to identify those patients at risk of language and visual impairment after surgery. I have compared two different methods of whole brain analysis of diffusion MRI data, and applied those methods to both pre- and post-operative TLE patients at two separate time points. In doing so I have identified a network of white matter connections that may be important in post-operative language function, and whose pre-operative quantification may aid prediction of post-operative language deficits. I have also developed methods of tractography to parcellate white matter tracts relevant to both memory and visual function. In the latter case, we have shown that this information is predictive of post-operative visual loss when the resection size is known. The techniques I developed have subsequently been validated, and are now in clinical use.

8.2 Summary of main findings

- In control subjects and patients, white matter connections were demonstrated between the anterior PHG and anterior temporal lobe, orbitofrontal cortex, posterior temporal and extrastriate occipital areas. Direct connections between hippocampus and parahippocampal gyrus were also visualised. These connections were reduced ipsilaterally in volume and FA in left TLE patients, and decreased FA was associated with poorer performance on both material specific memory measures.
- Unilateral TLE was associated with changes in an extensive white matter network. Extensive reduction of FA and increased MD was evident in the limbic system in the left, and to a lesser extent right, TLE patients group. Further DTI changes were evident in the ipsilateral temporal lobe and the AF. There were differences in the pattern of changes between the left and right TLE groups with more widespread changes in the left TLE group including the entire limbic system. In the right TLE group, contralateral findings in the temporal lobe and the inferior frontal gyrus were more prominent.
- While widespread decreases in FA occurred after left and right-sided anterior temporal lobe resections, only the left sided resections were followed by an increase of FA in an extensive area

at 4 months. The location of these changes and the results of tractography seeded from this area suggested that it is part of a parallel, ventro-medial language network. This was corroborated by a significant correlation between the diffusion parameters of this region and post-operative language function.

- Ipsilateral, white matter increases in FA were also apparent in right TLE patients in a similar distribution to that seen in left TLE patients, but took longer to develop after surgery, and appeared only at 12 months. Knowledge of preoperative FA in these areas, together with preoperative language function and lateralization, were predictive of language outcome after anterior temporal lobe resection across all TLE patients.
- Tractography of Meyer's loop, and knowledge of its distance from the temporal pole, and the size of temporal lobe resection size, is predictive of post-operative visual field deficits.

8.3 Neurobiological and clinical implications

8.3.1 Understanding the effects of TLE and ATLR on white matter

Previous studies have demonstrated that TLE is associated with widespread changes in grey matter (449,451). This thesis demonstrates that there are also widespread changes in white matter in patients with TLE that extend beyond the medial temporal lobes. These changes are associated with reduced performance in neuropsychological testing including memory as demonstrated in this thesis, and verbal fluency and task switching in other studies (454,460,463,622). This corroborates the concept that specific reductions in the integrity of the white matter network parallel the clinical picture of temporal lobe epilepsy. However, the challenge remains to differentiate between whether these white matter changes are a cause, or a consequence of TLE. Further studies incorporating for example patients with hippocampal atrophy but without epilepsy, or patients with refractory primary generalised epilepsy and longstanding seizures are necessary to address these issues.

The results reported in chapters 5 and 6 of this thesis constitute one of the first major assessments of quantitative changes in white matter after anterior temporal lobe resection. Widespread and dynamic changes were present in white matter parameters after temporal lobe surgery. Some of

these changes may represent direct and indirect Wallerian degeneration. Plasticity caused by the cessation of chronic seizures, and post-operative structural reorganisation may also be a critical factor, particularly in those areas with post-operative increases in FA.

8.3.2 Diffusion MRI and the prediction of postoperative deficits

As outlined in chapter 1, temporal lobe surgery has an increasingly important role in patients with medically refractory TLE, and leads to seizure freedom in at least 60% of patients. The most common complications of anterior temporal lobe resection are memory, language and visual field deficits. The purpose of the presurgical evaluation of such patients is the maximisation of the chance of seizure freedom, and the minimisation of post-operative complications. Preoperative neuropsychometry is used to assess preoperative language and memory function, and is used together with language lateralisation by fMRI or IAT to aid the prediction of post-operative language and memory outcome. There are currently no methods available to aid the prediction of post-operative visual field deficits. The establishment of non-invasive imaging techniques to provide information that aids the prediction of postoperative language and visual deficits in individual patients was a major aim of this thesis.

Mapping the connections of the medial temporal lobe provided results in keeping with evidence from invasive studies in animals. The connections demonstrated, to frontal and occipital lobes and to the cerebellum, along with direct hippocampal-parahippocampal connections, may play an important role, both in memory function as demonstrated in chapter 3, and in seizure propagation in patients with medial temporal lobe epilepsy. We think that further analysis of these connections in patients undergoing ATLR may be useful for predicting both seizure outcome and memory change following surgery. These studies are under way by our group.

Prior to the results reported in chapter 7 there were no accurate methods of predicting which patients are most at risk of visual field deficits following ATLR, due to the variability in the anterior extent of Meyer's loop, and difficulty in visualising this structure. In chapter 7 we developed tractography based techniques that can be used to parcellate this structure, and demonstrated that they are predictive of visual field deficits in patients undergoing ATLR. These techniques and results have subsequently been validated in,

and extended for use peri-operatively (617,620). Ultimately the use of these techniques peri-operatively will prevent the occurrence of visual field deficits.

Finally, the identification in chapters 5 and 6, of white matter networks, which increase in FA after anterior temporal lobe resection and appear to be related to language function, suggests that diffusion MRI may contribute significantly to predictive models of post-operative language function. Further, prospective studies are needed to validate these findings, and these are under way by our group.

8.4 Limitations of studies

The study reporting the connections of medial temporal lobe in chapter 3 was carried out on data acquired at 1.5T, while the remainder of the results reported in this thesis were based on data acquired at 3T. The reason for this was that that the start of this thesis coincided with the replacement of the old 1.5T scanner with a new 3T scanner, which resulted in a considerable time lag to the acquisition of newer data. However, given that the work in this thesis builds on previous similar work by our group, and the fact that the MRI acquisition parameters, and tractography algorithms used in the 1.5T study are similar to those used in the remainder of this thesis, we are confident of the robustness of our findings in chapter 3, and their generalizability.

The longitudinal studies reported in chapters 5 and 6 of this thesis are limited by the lack of repeat scans in a control group. Despite this limitation, we are confident of the robustness of our findings. Inter- and intra-site reproducibility studies using our scanner have demonstrated that any variability in longitudinal scans is many times smaller than the changes identified in our results (520).

The patients used in this thesis all had temporal lobe epilepsy, and most, though not all, had hippocampal sclerosis. While this may necessitate caution in drawing group level inferences, I would argue that it is clinically more valuable to have heterogeneous groups, particularly if these techniques are to be adopted as routine pre-surgical investigations. Typically, the types of patients that are encountered in an epilepsy surgical programme have heterogeneous pathology.

The remaining limitations of the studies reported in this thesis relate to the technical limitations of diffusion MRI and tractography. These have been explored in chapter 1, and the individual results chapters. The most pressing of these is the lack of in vivo, or in vitro 'gold standard' methods of validation of both tractography data, and the biological ramifications of diffusion data. Though studies have shown that the tractography can reconstruct white matter bundles that are consistent with major fibre tract trajectories, there is a paucity of robust standardized tests with which to assess the different algorithms and data acquisition techniques. In some ways epilepsy surgery may be in a prime position to rectify this by way of validation of the technique against electroclinical correlations, post-operative outcome, and correlation with the pathology of resected tissue. For this reason, the correlations described in the results chapters between diffusion and tractography data and independent neuropsychology and visual field data, lends confidence to the robustness of our findings. Finally, one major limitation of DTI, compared to traditional histopathology, is the spatial resolution of the information available. Many structures of interest are small compared to the scale of the imaging voxel, with a single $2mm^3$ voxel containing many hundred of axons. Increased signal-to-noise ratio (SNR) can now allow improved spatial resolution to be achieved (that is, smaller voxels). However as described in chapter 1, there are technical limits to the size of voxels that can be obtained due to the smaller signal acquired. This can be circumvented by the acquisition of data at higher field strengths. Alternatively, there are now methods that use post-processing techniques, to reveal structures beyond the resolution of the acquired imaging voxel by using additional information obtained from outside that voxel (623). These techniques would prove useful in some of the applications described in this thesis, such as the use of tractography to prevent visual field deficits.

8.5 Future work

The first stage in further work based on this thesis is the validation in individual subjects, as opposed to groups, of the predictive tools described here. The methods developed to predict post-operative visual field deficits are already being incorporated into the decision making process for individual subjects, and will soon be incorporated into peri-operative techniques to actually prevent visual field loss (617,618,620). On the other hand, larger, prospective studies are needed to assess the validity of the use of the white matter network identified in chapter 7 as a predictor of post-operative language deficits. The application of parameters derived from these white matter

connections, together with pre-operative language fMRI and psychology, to a wholly, new group of patients is necessary in order to assess the utility of the linear regression equation developed in chapter 7 to individual subjects. This work is on-going. In addition, in the future it would be useful to apply tractography based techniques to parcellate out the ventro-medial language tracts in order to assess whether information derived from this tract increases sensitivity of the prediction of post-operative language deficits.

Development of network based analysis techniques, will aid the use of diffusion MRI and tractography in predicting seizure and memory outcome after surgery, particularly as memory is likely to be reliant of a more distributed network in the brain than language (624). However at this time further refinement of these techniques is needed before they can be appied to large datasets, and this work is ongoing. Ultimately, the most robust validation of diffusion MRI and tractography based results are correlation with other independent data sets such as cortical thickness, fMRI, EEG and clinical data (625,626), and the simultaneous acquisition of these other forms of data is on-going.

Finally, any future studies should also incorporate many of the technical advances in diffusion MRI acquisition and tractography that have been reported since the start of this thesis (627). These include advances in accelerated imaging, gradient non-linearities, diffusion modelling, distortion correction, fibre orientation and estimation and tractography algorithms. Improved diffusion acquisition and processing will enable more accurate pre- and post-operative biological inferences to be drawn from the data.

9 Bibliography

1. Fisher RS, van Emde Boas W, Blume W, Elger C, Genton P, Lee P, et al. Epileptic seizures and epilepsy: definitions proposed by the International League Against Epilepsy (ILAE) and the International Bureau for Epilepsy (IBE). Epilepsia. 2005 Apr;46(4):470–2.

2. Guidelines for epidemiologic studies on epilepsy. Commission on Epidemiology and Prognosis, International League Against Epilepsy. Epilepsia. 1993 Aug;34(4):592–6.

3. Leonardi M, Ustun TB. The global burden of epilepsy. Epilepsia. 2002;43 Suppl 6:21–5.

4. Shorvon SD, Farmer PJ. Epilepsy in developing countries: a review of epidemiological, sociocultural, and treatment aspects. Epilepsia. 1988;29 Suppl 1:S36–54.

5. Sander JW, Shorvon SD. Epidemiology of the epilepsies. J Neurol Neurosurg Psychiatr. 1996 Nov;61(5):433–43.

6. Bell GS, Sander JW. The epidemiology of epilepsy: the size of the problem. Seizure. 2001 Jun;10(4):306–314; quiz 315–316.

7. Zarrelli MM, Beghi E, Rocca WA, Hauser WA. Incidence of epileptic syndromes in Rochester, Minnesota: 1980-1984. Epilepsia. 1999 Dec;40(12):1708–14.

8. MacDonald BK, Cockerell OC, Sander JW, Shorvon SD. The incidence and lifetime prevalence of neurological disorders in a prospective community-based study in the UK. Brain. 2000 Apr;123 (Pt 4):665–76.

9. Heaney DC, MacDonald BK, Everitt A, Stevenson S, Leonardi GS, Wilkinson P, et al. Socioeconomic variation in incidence of epilepsy: prospective community based study in south east England. BMJ. 2002 Nov 2;325(7371):1013–6.

10. Gaitatzis A, Purcell B, Carroll K, Sander JWAS, Majeed A. Differences in the use of health services among people with and without epilepsy in the United Kingdom: socio-economic and disease-specific determinants. Epilepsy Res. 2002 Aug;50(3):233–41.

11. Lindsten H, Stenlund H, Edlund C, Forsgren L. Socioeconomic prognosis after a newly diagnosed unprovoked epileptic seizure in adults: a population-based case-control study. Epilepsia. 2002 Oct;43(10):1239–50.

12. De Graaf AS. Epidemiological aspects of epilepsy in northern Norway. Epilepsia. 1974 Sep;15(3):291–9.

13. Benn EKT, Hauser WA, Shih T, Leary L, Bagiella E, Dayan P, et al. Estimating the incidence of first unprovoked seizure and newly diagnosed epilepsy in the low-income urban community of Northern Manhattan, New York City. Epilepsia. 2008 Aug;49(8):1431–9.

14. Hauser WA, Annegers JF, Kurland LT. Incidence of epilepsy and unprovoked seizures in Rochester, Minnesota: 1935-1984. Epilepsia. 1993 Jun;34(3):453–68.

15. Everitt AD, Sander JW. Incidence of epilepsy is now higher in elderly people than children. BMJ. 1998 Mar 7;316(7133):780.

16. Sander JW. The epidemiology of epilepsy revisited. Curr Opin Neurol. 2003 Apr;16(2):165–70.

17. Banerjee PN, Filippi D, Allen Hauser W. The descriptive epidemiology of epilepsy-a review. Epilepsy Res. 2009 Jul;85(1):31–45.

18. Sander JW. Some aspects of prognosis in the epilepsies: a review. Epilepsia. 1993 Dec;34(6):1007–16.

19. Gaitatzis A, Sander JW. The mortality of epilepsy revisited. Epileptic Disord. 2004 Mar;6(1):3–13.

20. O'Callaghan FJK, Osborne JP, Martyn CN. Epilepsy related mortality. Arch Dis Child. 2004 Aug;89(8):705–7.

21. Lhatoo SD, Johnson AL, Goodridge DM, MacDonald BK, Sander JW, Shorvon SD. Mortality in epilepsy in the first 11 to 14 years after diagnosis: multivariate analysis of a long-term, prospective, population-based cohort. Ann Neurol. 2001 Mar;49(3):336–44.

22. Lindsten H, Nyström L, Forsgren L. Mortality risk in an adult cohort with a newly diagnosed unprovoked epileptic seizure: a population-based study. Epilepsia. 2000 Nov;41(11):1469–73.

23. Nilsson L, Tomson T, Farahmand BY, Diwan V, Persson PG. Cause-specific mortality in epilepsy: a cohort study of more than 9,000 patients once hospitalized for epilepsy. Epilepsia. 1997 Oct;38(10):1062–8.

24. Shackleton DP, Westendorp RG, Trenité DG, Vandenbroucke JP. Mortality in patients with epilepsy: 40 years of follow up in a Dutch cohort study. J Neurol Neurosurg Psychiatr. 1999 May;66(5):636–40.

25. Nashef L, Fish DR, Sander JW, Shorvon SD. Incidence of sudden unexpected death in an adult outpatient cohort with epilepsy at a tertiary referral centre. J Neurol Neurosurg Psychiatr. 1995 Apr;58(4):462–4.

26. Sillanpää M, Jalava M, Kaleva O, Shinnar S. Long-term prognosis of seizures with onset in childhood. N Engl J Med. 1998 Jun 11;338(24):1715–22.

27. Kurtz Z, Tookey P, Ross E. Epilepsy in young people: 23 year follow up of the British national child development study. BMJ. 1998 Jan 31;316(7128):339–42.

28. Harvey AS, Nolan T, Carlin JB. Community-based study of mortality in children with epilepsy. Epilepsia. 1993 Aug;34(4):597–603.

29. Camfield CS, Camfield PR, Veugelers PJ. Death in children with epilepsy: a population-based study. Lancet. 2002 Jun 1;359(9321):1891–5.

30. Logroscino G, Hesdorffer DC, Cascino GD, Annegers JF, Bagiella E, Hauser WA. Long-term mortality after a first episode of status epilepticus. Neurology. 2002 Feb 26;58(4):537–41.

31. Nashef L. Sudden unexpected death in epilepsy: terminology and definitions. Epilepsia. 1997 Nov;38(11 Suppl):S6–8.

32. Jehi L, Najm IM. Sudden unexpected death in epilepsy: impact, mechanisms, and prevention. Cleve Clin J Med. 2008 Mar;75 Suppl 2:S66–70.

33. Nashef L, Shorvon SD. Mortality in epilepsy. Epilepsia. 1997 Oct;38(10):1059–61.

34. Kwan P, Sander JW. The natural history of epilepsy: an epidemiological view. J Neurol Neurosurg Psychiatr. 2004 Oct;75(10):1376–81.

35. Nicoletti A, Sofia V, Vitale G, Bonelli SI, Bejarano V, Bartalesi F, et al. Natural history and mortality of chronic epilepsy in an untreated population of rural Bolivia: a follow-up after 10 years. Epilepsia. 2009 Oct;50(10):2199–206.

36. Kwan P, Brodie MJ. Early identification of refractory epilepsy. N Engl J Med. 2000 Feb 3;342(5):314–9.

37. Kwan P, Arzimanoglou A, Berg AT, Brodie MJ, Allen Hauser W, Mathern G, et al. Definition of drug resistant epilepsy: consensus proposal by the ad hoc Task Force of the ILAE Commission on Therapeutic Strategies. Epilepsia. 2010 Jun;51(6):1069–77.

38. Luciano AL, Shorvon SD. Results of treatment changes in patients with apparently drug-resistant chronic epilepsy. Ann Neurol. 2007 Oct;62(4):375–81.

39. Proposal for revised clinical and electroencephalographic classification of epileptic seizures. From the Commission on Classification and Terminology of the International League Against Epilepsy. Epilepsia. 1981 Aug;22(4):489–501.

40. Proposal for revised classification of epilepsies and epileptic syndromes. Commission on Classification and Terminology of the International League Against Epilepsy. Epilepsia. 1989 Aug;30(4):389–99.

41. Lüders H, Acharya J, Baumgartner C, Benbadis S, Bleasel A, Burgess R, et al. Semiological seizure classification. Epilepsia. 1998 Sep;39(9):1006–13.

42. Engel J Jr. A proposed diagnostic scheme for people with epileptic seizures and with epilepsy: report of the ILAE Task Force on Classification and Terminology. Epilepsia. 2001 Jun;42(6):796–803.

43. Engel J. Report of the ILAE classification core group. Epilepsia. 2006 Sep;47(0013-9580 (Print)):1558–68.

44. Berg AT, Berkovic SF, Brodie MJ, Buchhalter J, Cross JH, van Emde Boas W, et al. Revised terminology and concepts for organization of seizures and epilepsies: report of the ILAE Commission on Classification and Terminology, 2005-2009. Epilepsia. 2010 Apr;51(4):676–85.

45. Guerrini R. Classification concepts and terminology: is clinical description assertive and laboratory testing objective? Epilepsia. 2010 Apr;51(4):718–20.

46. Shorvon S, Andermann F, Guerrini R. The Causes of Epilepsy. Common and Uncommon Causes in Adults and Children. 1st ed. Cambridge University Press; 2011.

47. Goodridge DM, Shorvon SD. Epileptic seizures in a population of 6000. II: Treatment and prognosis. British Medical Journal. 1983;287(6393):645.

48. Goodridge DM, Shorvon SD. Epileptic seizures in a population of 6000. I: Demography, diagnosis and classification, and role of the hospital services. British Medical Journal (Clinical research ed). 1983;287(6393):641.

49. Theodore WH. Distinguishing Lateral Temporal Neocortical and Mesial Temporal Lobe Epilepsy. Epilepsy Curr. 2004;4(2):55–6.

50. Barbosa-Coutinho LM, Hilbig A, Calcagnotto ME, Paglioli E, Paglioli Neto E, Da Costa JC, et al. [Neuropathology of hard to control epilepsy. Study of 300 consecutive cases]. Arq Neuropsiquiatr. 1999 Jun;57(2B):405–14.

51. Blumenfeld H. Neuroanatomy through clinical cases. Sunderland, Mass: Sinauer; 2002.

52. Duvernoy HM. The human hippocampus: functional anatomy, vascularization, and serial sections with MRI. 3rd ed. Berlin ; New York: Springer; 2005.

53. Blümcke I. Neuropathology of focal epilepsies: a critical review. Epilepsy Behav. 2009 May;15(1):34–9.

54. Blümcke I, Thom M, Wiestler OD. Ammon's horn sclerosis: a maldevelopmental disorder associated with temporal lobe epilepsy. Brain Pathol. 2002 Apr;12(2):199–211.

55. Quigg M, Bertram EH, Jackson T. Longitudinal distribution of hippocampal atrophy in mesial temporal lobe epilepsy. Epilepsy Res. 1997 May;27(2):101–10.

56. Briellmann RS, Jackson GD, Mitchell LA, Fitt GJ, Kim SE, Berkovic SF. Occurrence of hippocampal sclerosis: is one hemisphere or gender more vulnerable? Epilepsia. 1999 Dec;40(12):1816–20.

57. Babb TL. Bilateral pathological damage in temporal lobe epilepsy. Can J Neurol Sci. 1991 Nov;18(4 Suppl):645–8.

58. Margerison JH, Corsellis JA. Epilepsy and the temporal lobes. A clinical, electroencephalographic and neuropathological study of the brain in epilepsy, with particular reference to the temporal lobes. Brain. 1966 Sep;89(3):499–530.

59. SANO K, MALAMUD N. Clinical significance of sclerosis of the cornu ammonis: ictal psychic phenomena. AMA Arch Neurol Psychiatry. 1953 Jul;70(1):40–53.

60. Scott RC, Cross JH, Gadian DG, Jackson GD, Neville BGR, Connelly A. Abnormalities in hippocampi remote from the seizure focus: a T2 relaxometry study. Brain. 2003 Sep;126(Pt 9):1968–74.

61. Sommer W. Erkrankung des ammonshorns als aetiologisches moment der epilepsie. Arch Psychiatr Nervenkr. 1880;10:631–75.

62. Bratz E. Ammonshornbefunde bei epileptikern. Arch Psychiatr Nervenkr. 1899;32:820–35.

63. Stauder K. Epilepsie und schlafenlappen. Arch Psychiatr Nervenkr. 1936;104:181–211.

64. Wieser H-G. ILAE Commission Report. Mesial temporal lobe epilepsy with hippocampal sclerosis. Epilepsia. 2004 Jun;45(6):695–714.

65. De Lanerolle NC, Kim JH, Williamson A, Spencer SS, Zaveri HP, Eid T, et al. A retrospective analysis of hippocampal pathology in human temporal lobe epilepsy: evidence for distinctive patient subcategories. Epilepsia. 2003 May;44(5):677–87.

66. Blümcke I, Pauli E, Clusmann H, Schramm J, Becker A, Elger C, et al. A new clinico-pathological classification system for mesial temporal sclerosis. Acta Neuropathol. 2007 Mar;113(3):235–44.

67. Thom M, Liagkouras I, Elliot KJ, Martinian L, Harkness W, McEvoy A, et al. Reliability of patterns of hippocampal sclerosis as predictors of postsurgical outcome. Epilepsia. 2010 Sep;51(9):1801–8.

68. Malmgren K, Thom M. Hippocampal sclerosis-Origins and imaging. Epilepsia. 2012 Sep;53:19–33.

69. Wittner L, Eross L, Czirják S, Halász P, Freund TF, Maglóczky Z. Surviving CA1 pyramidal cells receive intact perisomatic inhibitory input in the human epileptic hippocampus. Brain. 2005 Jan;128(Pt 1):138–52.

70. Wittner L, Eross L, Szabó Z, Tóth S, Czirják S, Halász P, et al. Synaptic reorganization of calbindin-positive neurons in the human hippocampal CA1 region in temporal lobe epilepsy. Neuroscience. 2002;115(3):961–78.

71. O'Connor ER, Sontheimer H, Spencer DD, de Lanerolle NC. Astrocytes from human hippocampal epileptogenic foci exhibit action potential-like responses. Epilepsia. 1998 Apr;39(4):347–54.

72. Blümcke I, Kistner I, Clusmann H, Schramm J, Becker AJ, Elger CE, et al. Towards a clinico-pathological classification of granule cell dispersion in human mesial temporal lobe epilepsies. Acta Neuropathol. 2009 May;117(5):535–44.

73. Lurton D, El Bahh B, Sundstrom L, Rougier A. Granule cell dispersion is correlated with early epileptic events in human temporal lobe epilepsy. J Neurol Sci. 1998 Feb 5;154(2):133–6.

74. Heinrich C, Nitta N, Flubacher A, Müller M, Fahrner A, Kirsch M, et al. Reelin deficiency and displacement of mature neurons, but not neurogenesis, underlie the formation of granule cell dispersion in the epileptic hippocampus. J Neurosci. 2006 Apr 26;26(17):4701–13.

75. Longo BM, Mello LE. Blockade of pilocarpine- or kainate-induced mossy fiber sprouting by cycloheximide does not prevent subsequent epileptogenesis in rats. Neurosci Lett. 1997 May 2;226(3):163–6.

76. Nissinen J, Lukasiuk K, Pitkänen A. Is mossy fiber sprouting present at the time of the first spontaneous seizures in rat experimental temporal lobe epilepsy? Hippocampus. 2001;11(3):299–310.

77. Masukawa LM, Higashima M, Kim JH, Spencer DD. Epileptiform discharges evoked in hippocampal brain slices from epileptic patients. Brain Res. 1989 Jul 24;493(1):168–74.

78. Von Campe G, Spencer DD, de Lanerolle NC. Morphology of dentate granule cells in the human epileptogenic hippocampus. Hippocampus. 1997;7(5):472–88.

79. Eid T, Kovacs I, Spencer DD, de Lanerolle NC. Novel expression of AMPA-receptor subunit GluR1 on mossy cells and CA3 pyramidal neurons in the human epileptogenic hippocampus. Eur J Neurosci. 2002 Feb;15(3):517–27.

80. Maglóczky Z. Sprouting in human temporal lobe epilepsy: excitatory pathways and axons of interneurons. Epilepsy Res. 2010 Mar;89(1):52–9.

81. Pitkänen A, Tuunanen J, Kälviäinen R, Partanen K, Salmenperä T. Amygdala damage in experimental and human temporal lobe epilepsy. Epilepsy Res. 1998 Sep;32(1-2):233–53.

82. Yilmazer-Hanke DM, Wolf HK, Schramm J, Elger CE, Wiestler OD, Blümcke I. Subregional pathology of the amygdala complex and entorhinal region in surgical specimens from patients with pharmacoresistant temporal lobe epilepsy. J Neuropathol Exp Neurol. 2000 Oct;59(10):907–20.

83. Dawodu S, Thom M. Quantitative neuropathology of the entorhinal cortex region in patients with hippocampal sclerosis and temporal lobe epilepsy. Epilepsia. 2005 Jan;46(1):23–30.

84. Bartolomei F, Khalil M, Wendling F, Sontheimer A, Régis J, Ranjeva J-P, et al. Entorhinal cortex involvement in human mesial temporal lobe epilepsy: an electrophysiologic and volumetric study. Epilepsia. 2005 May;46(5):677–87.

85. Graebenitz S, Kedo O, Speckmann E-J, Gorji A, Panneck H, Hans V, et al. Interictal-like network activity and receptor expression in the epileptic human lateral amygdala. Brain. 2011 Oct;134(Pt 10):2929–47.

86. Moran NF, Lemieux L, Kitchen ND, Fish DR, Shorvon SD. Extrahippocampal temporal lobe atrophy in temporal lobe epilepsy and mesial temporal sclerosis. Brain. 2001 Jan;124(Pt 1):167–75.

87. Bonilha L, Rorden C, Halford JJ, Eckert M, Appenzeller S, Cendes F, et al. Asymmetrical extra-hippocampal grey matter loss related to hippocampal atrophy in patients with medial temporal lobe epilepsy. J Neurol Neurosurg Psychiatr. 2007 Mar;78(3):286–94.

88. Keller SS, Roberts N. Voxel-based morphometry of temporal lobe epilepsy: an introduction and review of the literature. Epilepsia. 2008 May;49(5):741–57.

89. McDonald CR, Hagler DJ Jr, Ahmadi ME, Tecoma E, Iragui V, Gharapetian L, et al. Regional neocortical thinning in mesial temporal lobe epilepsy. Epilepsia. 2008 May;49(5):794–803.

90. Blanc F, Martinian L, Liagkouras I, Catarino C, Sisodiya SM, Thom M. Investigation of widespread neocortical pathology associated with hippocampal sclerosis in epilepsy: a postmortem study. Epilepsia. 2011 Jan;52(1):10–21.

91. Blümcke I, Thom M, Aronica E, Armstrong DD, Vinters HV, Palmini A, et al. The clinicopathologic spectrum of focal cortical dysplasias: a consensus classification proposed by an ad hoc Task Force of the ILAE Diagnostic Methods Commission. Epilepsia. 2011 Jan;52(1):158–74.

92. Thom M, Eriksson S, Martinian L, Caboclo LO, McEvoy AW, Duncan JS, et al. Temporal lobe sclerosis associated with hippocampal sclerosis in temporal lobe epilepsy: neuropathological features. J Neuropathol Exp Neurol. 2009 Aug;68(8):928–38.

93. Blümcke I, Vinters HV, Armstrong D, Aronica E, Thom M, Spreafico R. Malformations of cortical development and epilepsies: neuropathological findings with emphasis on focal cortical dysplasia. Epileptic Disord. 2009 Sep;11(3):181–93.

94. Lévesque MF, Nakasato N, Vinters HV, Babb TL. Surgical treatment of limbic epilepsy associated with extrahippocampal lesions: the problem of dual pathology. J Neurosurg. 1991 Sep;75(3):364–70.

95. Thom M, Sisodiya S, Harkness W, Scaravilli F. Microdysgenesis in temporal lobe epilepsy. A quantitative and immunohistochemical study of white matter neurones. Brain. 2001 Nov;124(Pt 11):2299–309.

96. Thom M, Toma A, An S, Martinian L, Hadjivassiliou G, Ratilal B, et al. One hundred and one dysembryoplastic neuroepithelial tumors: an adult epilepsy series with immunohistochemical, molecular genetic, and clinical correlations and a review of the literature. J Neuropathol Exp Neurol. 2011 Oct;70(10):859–78.

97. Thom M, Zhou J, Martinian L, Sisodiya S. Quantitative post-mortem study of the hippocampus in chronic epilepsy: seizures do not inevitably cause neuronal loss. Brain. 2005 Jun;128(Pt 6):1344–57.

98. Mathern GW, Babb TL, Leite JP, Pretorius K, Yeoman KM, Kuhlman PA. The pathogenic and progressive features of chronic human hippocampal epilepsy. Epilepsy Res. 1996 Dec;26(1):151–61.

99. Blümcke I, Beck H, Suter B, Hoffmann D, Födisch HJ, Wolf HK, et al. An increase of hippocampal calretinin-immunoreactive neurons correlates with early febrile seizures in temporal lobe epilepsy. Acta Neuropathol. 1999 Jan;97(1):31–9.

100. Blümcke I, Schewe JC, Normann S, Brüstle O, Schramm J, Elger CE, et al. Increase of nestin-immunoreactive neural precursor cells in the dentate gyrus of pediatric patients with early-onset temporal lobe epilepsy. Hippocampus. 2001;11(3):311–21.

101. Brooks-Kayal AR, Shumate MD, Jin H, Rikhter TY, Coulter DA. Selective changes in single cell GABA(A) receptor subunit expression and function in temporal lobe epilepsy. Nat Med. 1998 Oct;4(10):1166–72.

102. Shumate MD, Lin DD, Gibbs JW 3rd, Holloway KL, Coulter DA. GABA(A) receptor function in epileptic human dentate granule cells: comparison to epileptic and control rat. Epilepsy Res. 1998 Sep;32(1-2):114–28.

103. Becker AJ, Chen J, Zien A, Sochivko D, Normann S, Schramm J, et al. Correlated stage- and subfield-associated hippocampal gene expression patterns in experimental and human temporal lobe epilepsy. Eur J Neurosci. 2003 Nov;18(10):2792–802.

104. Mathern GW, Babb TL, Vickrey BG, Melendez M, Pretorius JK. The clinical-pathogenic mechanisms of hippocampal neuron loss and surgical outcomes in temporal lobe epilepsy. Brain. 1995 Feb;118 (Pt 1):105–18.

105. Mathern GW, Pretorius JK, Babb TL. Influence of the type of initial precipitating injury and at what age it occurs on course and outcome in patients with temporal lobe seizures. J Neurosurg. 1995 Feb;82(2):220–7.

106. French JA, Williamson PD, Thadani VM, Darcey TM, Mattson RH, Spencer SS, et al. Characteristics of medial temporal lobe epilepsy: I. Results of history and physical examination. Ann Neurol. 1993 Dec;34(6):774–80.

107. Sutula T, Pitkänen A. Do seizures damage the brain. Amsterdam; New York: Elsevier; 2002.

108. Sisodiya SM. Surgery for malformations of cortical development causing epilepsy. Brain. 2000 Jun;123 (Pt 6):1075–91.

109. Duncan JS, Sagar HJ. Seizure characteristics, pathology, and outcome after temporal lobectomy. Neurology. 1987 Mar;37(3):405–9.

110. Kotagal P, Lüders H, Morris HH, Dinner DS, Wyllie E, Godoy J, et al. Dystonic posturing in complex partial seizures of temporal lobe onset: a new lateralizing sign. Neurology. 1989 Feb;39(2 Pt 1):196–201.

111. Fakhoury T, Abou-Khalil B, Peguero E. Differentiating clinical features of right and left temporal lobe seizures. Epilepsia. 1994 Oct;35(5):1038–44.

112. Geyer JD, Payne TA, Faught E, Drury I. Postictal nose-rubbing in the diagnosis, lateralization, and localization of seizures. Neurology. 1999 Mar 10;52(4):743–5.

113. Rayner G, Wrench JM, Wilson SJ. Differential contributions of objective memory and mood to subjective memory complaints in refractory focal epilepsy. Epilepsy Behav. 2010 Nov;19(3):359–64.

114. Hall KE, Isaac CL, Harris P. Memory complaints in epilepsy: an accurate reflection of memory impairment or an indicator of poor adjustment? A review of the literature. Clin Psychol Rev. 2009 Jun;29(4):354–67.

115. Baxendale S, Thompson P. Beyond localization: The role of traditional neuropsychological tests in an age of imaging. Epilepsia. 2010;51(11):2225–30.

116. Squire LR, Zola-Morgan S. The medial temporal lobe memory system. Science. 1991 Sep 20;253(5026):1380–6.

117. Baxendale SA. The hippocampus: functional and structural correlations. Seizure. 1995;4(2):105–17.

118. Saling MM. Verbal memory in mesial temporal lobe epilepsy: beyond material specificity. Brain. 2009 Mar;132(Pt 3):570–82.

119. Jokeit H, Schacher M. Neuropsychological aspects of type of epilepsy and etiological factors in adults. Epilepsy Behav. 2004 Feb;5 Suppl 1:S14–20.

120. Hamberger MJ, Seidel WT. Auditory and visual naming tests: normative and patient data for accuracy, response time, and tip-of-the-tongue. J Int Neuropsychol Soc. 2003 Mar;9(3):479–89.

121. Baxendale S, Heaney D, Thompson PJ, Duncan JS. Cognitive consequences of childhood-onset temporal lobe epilepsy across the adult lifespan. Neurology. 2010 Aug 24;75(8):705–11.

122. Hermann B, Seidenberg M, Lee E-J, Chan F, Rutecki P. Cognitive phenotypes in temporal lobe epilepsy. J Int Neuropsychol Soc. 2007 Jan;13(1):12–20.

123. Dabbs K, Jones J, Seidenberg M, Hermann B. Neuroanatomical correlates of cognitive phenotypes in temporal lobe epilepsy. Epilepsy Behav. 2009 Aug;15(4):445–51.

124. Helmstaedter C, Kurthen M. Memory and epilepsy: characteristics, course, and influence of drugs and surgery. Curr Opin Neurol. 2001 Apr;14(2):211–6.

125. Bengner T, Fortmeier C, Malina T, Lindenau M, Voges B, Goebell E, et al. Sex differences in face recognition memory in patients with temporal lobe epilepsy, patients with generalized epilepsy, and healthy controls. Epilepsy Behav. 2006 Dec;9(4):593–600.

126. Elger CE, Helmstaedter C, Kurthen M. Chronic epilepsy and cognition. The Lancet Neurology. 2004;3(11):663–72.

127. Kwan P, Brodie MJ. Neuropsychological effects of epilepsy and antiepileptic drugs. Lancet. 2001 Jan 20;357(9251):216–22.

128. Salas-Puig J, Gil-Nagel A, Serratosa JM, Sánchez-Alvarez JC, Elices E, Villanueva V, et al. Self-reported memory problems in everyday activities in patients with epilepsy treated with antiepileptic drugs. Epilepsy Behav. 2009 Apr;14(4):622–7.

129. Davies R, Baxendale S, Thompson P, Duncan JS. Epilepsy surgery for people with a low IQ. Seizure. 2009 Mar;18(2):150–2.

130. Aikiä M, Salmenperä T, Partanen K, Kälviäinen R. Verbal Memory in Newly Diagnosed Patients and Patients with Chronic Left Temporal Lobe Epilepsy. Epilepsy Behav. 2001 Feb;2(1):20–7.

131. Thompson PJ, Duncan JS. Cognitive decline in severe intractable epilepsy. Epilepsia. 2005 Nov;46(11):1780–7.

132. Helmstaedter C, Elger CE. Chronic temporal lobe epilepsy: a neurodevelopmental or progressively dementing disease? Brain. 2009 Oct;132(Pt 10):2822–30.

133. Jokeit H, Ebner A. Effects of chronic epilepsy on intellectual functions. Prog Brain Res. 2002;135:455–63.

134. Dodrill CB. Correlates of generalized tonic-clonic seizures with intellectual, neuropsychological, emotional, and social function in patients with epilepsy. Epilepsia. 1986 Aug;27(4):399–411.

135. Baxendale S, Thompson PJ, Duncan JS. Improvements in memory function following anterior temporal lobe resection for epilepsy. Neurology. 2008 Oct;71(17):1319–25.

136. Alpherts WCJ, Vermeulen J, van Rijen PC, da Silva FHL, van Veelen CWM. Verbal memory decline after temporal epilepsy surgery?: A 6-year multiple assessments follow-up study. Neurology. 2006 Aug 22;67(4):626–31.

137. Alpherts WCJ, Vermeulen J, Hendriks MPH, Franken MLO, van Rijen PC, Lopes da Silva FH, et al. Long-term effects of temporal lobectomy on intelligence. Neurology. 2004 Feb 24;62(4):607–11.

138. Andersson-Roswall L, Engman E, Samuelsson H, Malmgren K. Cognitive outcome 10 years after temporal lobe epilepsy surgery: a prospective controlled study. Neurology. 2010 Jun 15;74(24):1977–85.

139. Helmstaedter C, Kurthen M, Lux S, Reuber M, Elger CE. Chronic epilepsy and cognition: a longitudinal study in temporal lobe epilepsy. Annals of neurology. 2003;54(4):425–32.

140. Baxendale S, Heaney D. Socioeconomic status, cognition, and hippocampal sclerosis. Epilepsy Behav. 2011 Jan;20(1):64–7.

141. Ponds RWHM, Hendriks M. Cognitive rehabilitation of memory problems in patients with epilepsy. Seizure. 2006 Jun;15(4):267–73.

142. Gaitatzis A, Trimble MR, Sander JW. The psychiatric comorbidity of epilepsy. Acta Neurol Scand. 2004 Oct;110(4):207–20.

143. Marsh L, Rao V. Psychiatric complications in patients with epilepsy: a review. Epilepsy Res. 2002 Mar;49(1):11–33.

144. Ettinger AB. Psychotropic effects of antiepileptic drugs. Neurology. 2006 Dec 12;67(11):1916–25.

145. Mula M, Monaco F. Antiepileptic drugs and psychopathology of epilepsy: an update. Epileptic Disord. 2009 Mar;11(1):1–9.

146. Kanner AM, Balabanov A. Depression and epilepsy: how closely related are they? Neurology. 2002 Apr 23;58(8 Suppl 5):S27–39.

147. Quiske A, Helmstaedter C, Lux S, Elger CE. Depression in patients with temporal lobe epilepsy is related to mesial temporal sclerosis. Epilepsy Res. 2000 Apr;39(2):121–5.

148. Mula M, Sander JW. Negative effects of antiepileptic drugs on mood in patients with epilepsy. Drug Saf. 2007;30(7):555–67.

149. Boylan LS, Flint LA, Labovitz DL, Jackson SC, Starner K, Devinsky O. Depression but not seizure frequency predicts quality of life in treatment-resistant epilepsy. Neurology. 2004 Jan 27;62(2):258–61.

150. Cramer JA, Blum D, Reed M, Fanning K. The influence of comorbid depression on seizure severity. Epilepsia. 2003 Dec;44(12):1578–84.

151. Kanner AM. Depression in epilepsy: a complex relation with unexpected consequences. Curr Opin Neurol. 2008 Apr;21(2):190–4.

152. Hitiris N, Mohanraj R, Norrie J, Brodie MJ. Mortality in epilepsy. Epilepsy Behav. 2007 May;10(3):363–76.

153. Blanchet P, Frommer GP. Mood change preceding epileptic seizures. J Nerv Ment Dis. 1986 Aug;174(8):471–6.

154. Guimond A, Braun CMJ, Bélanger E, Rouleau I. Ictal fear depends on the cerebral laterality of the epileptic activity. Epileptic Disord. 2008 Jun;10(2):101–12.

155. Feichtinger M, Pauli E, Schäfer I, Eberhardt KW, Tomandl B, Huk J, et al. Ictal fear in temporal lobe epilepsy: surgical outcome and focal hippocampal changes revealed by proton magnetic resonance spectroscopy imaging. Arch Neurol. 2001 May;58(5):771–7.

156. Kanner AM, Soto A, Gross-Kanner H. Prevalence and clinical characteristics of postictal psychiatric symptoms in partial epilepsy. Neurology. 2004 Mar 9;62(5):708–13.

157. Tellez-Zenteno JF, Patten SB, Jetté N, Williams J, Wiebe S. Psychiatric comorbidity in epilepsy: a population-based analysis. Epilepsia. 2007 Dec;48(12):2336–44.

158. Ring HA, Moriarty J, Trimble MR. A prospective study of the early postsurgical psychiatric associations of epilepsy surgery. J Neurol Neurosurg Psychiatr. 1998 May;64(5):601–4.

159. Hesdorffer DC, Hauser WA, Annegers JF, Cascino G. Major depression is a risk factor for seizures in older adults. Ann Neurol. 2000 Feb;47(2):246–9.

160. Blumer D. Dysphoric disorders and paroxysmal affects: recognition and treatment of epilepsy-related psychiatric disorders. Harv Rev Psychiatry. 2000 Jun;8(1):8–17.

161. Jones JE, Hermann BP, Barry JJ, Gilliam F, Kanner AM, Meador KJ. Clinical assessment of Axis I psychiatric morbidity in chronic epilepsy: a multicenter investigation. J Neuropsychiatry Clin Neurosci. 2005;17(2):172–9.

162. Mula M, Schmitz B, Sander JW. The pharmacological treatment of depression in adults with epilepsy. Expert Opin Pharmacother. 2008 Dec;9(18):3159–68.

163. Aksoy-Poyraz C, Ozdemir A, Ozmen M, Arikan K, Ozkara C. Electroconvulsive therapy for bipolar depressive and mixed episode with high suicide risk after epilepsy surgery. Epilepsy Behav. 2008 Nov;13(4):707–9.

164. Bredkjaer SR, Mortensen PB, Parnas J. Epilepsy and non-organic non-affective psychosis. National epidemiologic study. Br J Psychiatry. 1998 Mar;172:235–8.

165. Qin P, Xu H, Laursen TM, Vestergaard M, Mortensen PB. Risk for schizophrenia and schizophrenia-like psychosis among patients with epilepsy: population based cohort study. BMJ. 2005 Jul 2;331(7507):23.

166. Logsdail SJ, Toone BK. Post-ictal psychoses. A clinical and phenomenological description. Br J Psychiatry. 1988 Feb;152:246–52.

167. Kanemoto K, Kawasaki J, Kawai I. Postictal psychosis: a comparison with acute interictal and chronic psychoses. Epilepsia. 1996 Jun;37(6):551–6.

168. Kanemoto K, Takeuchi J, Kawasaki J, Kawai I. Characteristics of temporal lobe epilepsy with mesial temporal sclerosis, with special reference to psychotic episodes. Neurology. 1996 Nov;47(5):1199–203.

169. Kanemoto K, Kawasaki J, Mori E. Violence and epilepsy: a close relation between violence and postictal psychosis. Epilepsia. 1999 Jan;40(1):107–9.

170. Falip M, Carreño M, Donaire A, Maestro I, Pintor L, Bargalló N, et al. Postictal psychosis: a retrospective study in patients with refractory temporal lobe epilepsy. Seizure. 2009 Mar;18(2):145–9.

171. Adachi N, Matsuura M, Okubo Y, Oana Y, Takei N, Kato M, et al. Predictive variables of interictal psychosis in epilepsy. Neurology. 2000 Nov 14;55(9):1310–4.

172. Flor-Henry P. Determinants of psychosis in epilepsy: laterality and forced normalization. Biol Psychiatry. 1983 Sep;18(9):1045–57.

173. Bruton CJ, Stevens JR, Frith CD. Epilepsy, psychosis, and schizophrenia: clinical and neuropathologic correlations. Neurology. 1994 Jan;44(1):34–42.

174. Tebartz Van Elst L, Baeumer D, Lemieux L, Woermann FG, Koepp M, Krishnamoorthy S, et al. Amygdala pathology in psychosis of epilepsy: A magnetic resonance imaging study in patients with temporal lobe epilepsy. Brain. 2002 Jan;125(Pt 1):140–9.

175. Getz K, Hermann B, Seidenberg M, Bell B, Dow C, Jones J, et al. Negative symptoms in temporal lobe epilepsy. Am J Psychiatry. 2002 Apr;159(4):644–51.

176. Bell GS, Gaitatzis A, Bell CL, Johnson AL, Sander JW. Suicide in people with epilepsy: how great is the risk? Epilepsia. 2009 Aug;50(8):1933–42.

177. Krishnamoorthy ES, Trimble MR. Forced normalization: clinical and therapeutic relevance. Epilepsia. 1999;40 Suppl 10:S57–64.

178. Schuele S, Bermeo A, Lhatoo S. Chapter 9 - The electroencehalogram in the investigation of epilepsy. In: Shorvon S, editor. Oxford Textbook of Epilepsy and Epileptic Seizures. Oxford Univ Pr; 2013.

179. Williamson PD, French JA, Thadani VM, Kim JH, Novelly RA, Spencer SS, et al. Characteristics of medial temporal lobe epilepsy: II. Interictal and ictal scalp electroencephalography, neuropsychological testing, neuroimaging, surgical results, and pathology. Ann Neurol. 1993 Dec;34(6):781–7.

180. Foldvary N, Klem G, Hammel J, Bingaman W, Najm I, Lüders H. The localizing value of ictal EEG in focal epilepsy. Neurology. 2001 Dec 11;57(11):2022–8.

181. Risinger MW, Engel J Jr, Van Ness PC, Henry TR, Crandall PH. Ictal localization of temporal lobe seizures with scalp/sphenoidal recordings. Neurology. 1989 Oct;39(10):1288–93.

182. Mintzer S, Cendes F, Soss J, Andermann F, Engel J Jr, Dubeau F, et al. Unilateral hippocampal sclerosis with contralateral temporal scalp ictal onset. Epilepsia. 2004 Jul;45(7):792–802.

183. Ebersole JS, Pacia SV. Localization of temporal lobe foci by ictal EEG patterns. Epilepsia. 1996 Apr;37(4):386–99.

184. Sperling MR, O'Connor MJ. Auras and subclinical seizures: characteristics and prognostic significance. Ann Neurol. 1990 Sep;28(3):320–8.

185. Duncan JS. Imaging and epilepsy. Brain. 1997 Feb;120 (Pt 2):339–77.

186. Von Oertzen J, Urbach H, Jungbluth S, Kurthen M, Reuber M, Fernandez G, et al. Standard magnetic resonance imaging is inadequate for patients with refractory focal epilepsy. Journal of Neurology, Neurosurgery & Psychiatry. 2002;73(6):643.

187. Jackson GD, Berkovic SF, Tress BM, Kalnins RM, Fabinyi GC, Bladin PF. Hippocampal sclerosis can be reliably detected by magnetic resonance imaging. Neurology. 1990 Dec;40(12):1869–75.

188. Von Oertzen J, Urbach H, Blümcke I, Reuber M, Träber F, Peveling T, et al. Time-efficient T2 relaxometry of the entire hippocampus is feasible in temporal lobe epilepsy. Neurology. 2002 Jan 22;58(2):257–64.

189. Van Paesschen W, Revesz T, Duncan JS, King MD, Connelly A. Quantitative neuropathology and quantitative magnetic resonance imaging of the hippocampus in temporal lobe epilepsy. Ann Neurol. 1997 Nov;42(5):756–66.

190. Jackson GD, Connelly A, Duncan JS, Grünewald RA, Gadian DG. Detection of hippocampal pathology in intractable partial epilepsy: increased sensitivity with quantitative magnetic resonance T2 relaxometry. Neurology. 1993 Sep;43(9):1793–9.

191. Cambier DM, Cascino GD, So EL, Marsh WR. Video-EEG monitoring in patients with hippocampal atrophy. Acta Neurol Scand. 2001 Apr;103(4):231–7.

192. Trenerry MR, Jack CR Jr, Ivnik RJ, Sharbrough FW, Cascino GD, Hirschorn KA, et al. MRI hippocampal volumes and memory function before and after temporal lobectomy. Neurology. 1993 Sep;43(9):1800–5.

193. Liu RSN, Lemieux L, Bell GS, Hammers A, Sisodiya SM, Bartlett PA, et al. Progressive neocortical damage in epilepsy. Ann Neurol. 2003 Mar;53(3):312–24.

194. Briellmann RS, Berkovic SF, Syngeniotis A, King MA, Jackson GD. Seizure-associated hippocampal volume loss: a longitudinal magnetic resonance study of temporal lobe epilepsy. Ann Neurol. 2002 May;51(5):641–4.

195. Fuerst D, Shah J, Shah A, Watson C. Hippocampal sclerosis is a progressive disorder: a longitudinal volumetric MRI study. Ann Neurol. 2003 Mar;53(3):413–6.

196. Cascino GD. Advances in neuroimaging: surgical localization. Epilepsia. 2001 Jan;42(1):3–12.

197. Rugg-Gunn FJ, Boulby PA, Symms MR, Barker GJ, Duncan JS. Whole-brain T2 mapping demonstrates occult abnormalities in focal epilepsy. Neurology. 2005 Jan 25;64(2):318–25.

198. Rugg-Gunn FJ, Eriksson SH, Symms MR, Barker GJ, Duncan JS. Diffusion tensor imaging of cryptogenic and acquired partial epilepsies. Brain. 2001 Mar;124(Pt 3):627–36.

199. Rugg-Gunn FJ, Eriksson SH, Boulby PA, Symms MR, Barker GJ, Duncan JS. Magnetization transfer imaging in focal epilepsy. Neurology. 2003 May 27;60(10):1638–45.

200. Rugg-Gunn FJ, Boulby PA, Symms MR, Barker GJ, Duncan JS. Imaging the neocortex in epilepsy with double inversion recovery imaging. Neuroimage. 2006 May 15;31(1):39–50.

201. Devinsky O. Patients with refractory seizures. N Engl J Med. 1999 May 20;340(20):1565–70.

202. Dlugos DJ. The early identification of candidates for epilepsy surgery. Arch Neurol. 2001 Oct;58(10):1543–6.

203. Semah F, Picot MC, Adam C, Broglin D, Arzimanoglou A, Bazin B, et al. Is the underlying cause of epilepsy a major prognostic factor for recurrence? Neurology. 1998 Nov;51(5):1256–62.

204. Baker GA, Nashef L, van Hout BA. Current issues in the management of epilepsy: the impact of frequent seizures on cost of illness, quality of life, and mortality. Epilepsia. 1997;38 Suppl 1:S1–8.

205. Wiebe S, Blume WT, Girvin JP, Eliasziw M. A randomized, controlled trial of surgery for temporal-lobe epilepsy. N Engl J Med. 2001 Aug 2;345(5):311–8.

206. Falconer MA, Taylor DC. Surgical treatment of drug-resistant epilepsy due to mesial temporal sclerosis. Etiology and significance. Arch Neurol. 1968 Oct;19(4):353–61.

207. Yaşargil MG, Krayenbühl N, Roth P, Hsu SPC, Yaşargil DCH. The selective amygdalohippocampectomy for intractable temporal limbic seizures. J Neurosurg. 2010 Jan;112(1):168–85.

208. Rosenow F, Lüders H. Presurgical evaluation of epilepsy. Brain. 2001 Sep;124(Pt 9):1683–700.

209. Duncan JS. Selecting patients for epilepsy surgery: synthesis of data. Epilepsy Behav. 2011 Feb;20(2):230–2.

210. O'Brien TJ, Miles K, Ware R, Cook MJ, Binns DS, Hicks RJ. The cost-effective use of 18F-FDG PET in the presurgical evaluation of medically refractory focal epilepsy. J Nucl Med. 2008 Jun;49(6):931–7.

211. Won HJ, Chang KH, Cheon JE, Kim HD, Lee DS, Han MH, et al. Comparison of MR imaging with PET and ictal SPECT in 118 patients with intractable epilepsy. AJNR Am J Neuroradiol. 1999 Apr;20(4):593–9.

212. Knowlton RC. The role of FDG-PET, ictal SPECT, and MEG in the epilepsy surgery evaluation. Epilepsy Behav. 2006 Feb;8(1):91–101.

213. Vinton AB, Carne R, Hicks RJ, Desmond PM, Kilpatrick C, Kaye AH, et al. The extent of resection of FDG-PET hypometabolism relates to outcome of temporal lobectomy. Brain. 2007 Feb;130(Pt 2):548–60.

214. Willmann O, Wennberg R, May T, Woermann FG, Pohlmann-Eden B. The contribution of 18F-FDG PET in preoperative epilepsy surgery evaluation for patients with temporal lobe epilepsy A meta-analysis. Seizure. 2007 Sep;16(6):509–20.

215. La Fougère C, Rominger A, Förster S, Geisler J, Bartenstein P. PET and SPECT in epilepsy: a critical review. Epilepsy Behav. 2009 May;15(1):50–5.

216. Castro LH, Serpa MH, Valério RM, Jorge CL, Ono CR, Arantes PR, et al. Good surgical outcome in discordant ictal EEG-MRI unilateral mesial temporal sclerosis patients. Epilepsia. 2008 Aug;49(8):1324–32.

217. Son YJ, Chung CK, Lee SK, Chang KH, Lee DS, Yi YN, et al. Comparison of localizing values of various diagnostic tests in non-lesional medial temporal lobe epilepsy. Seizure. 1999 Dec;8(8):465–70.

218. Ho SS, Newton MR, McIntosh AM, Kalnins RM, Fabinyi GC, Brazenor GA, et al. Perfusion patterns during temporal lobe seizures: relationship to surgical outcome. Brain. 1997 Nov;120 (Pt 11):1921–8.

219. Salanova V, Andermann F, Rasmussen T, Olivier A, Quesney L. The running down phenomenon in temporal lobe epilepsy. Brain. 1996 Jun;119 (Pt 3):989–96.

220. Hennessy MJ, Elwes RD, Rabe-Hesketh S, Binnie CD, Polkey CE. Prognostic factors in the surgical treatment of medically intractable epilepsy associated with mesial temporal sclerosis. Acta Neurol Scand. 2001 Jun;103(6):344–50.

221. Holmes MD, Miles AN, Dodrill CB, Ojemann GA, Wilensky AJ. Identifying potential surgical candidates in patients with evidence of bitemporal epilepsy. Epilepsia. 2003 Aug;44(8):1075–9.

222. Stefan H, Hummel C, Scheler G, Genow A, Druschky K, Tilz C, et al. Magnetic brain source imaging of focal epileptic activity: a synopsis of 455 cases. Brain. 2003 Nov;126(Pt 11):2396–405.

223. Pataraia E, Simos PG, Castillo EM, Billingsley RL, Sarkari S, Wheless JW, et al. Does magnetoencephalography add to scalp video-EEG as a diagnostic tool in epilepsy surgery? Neurology. 2004 Mar 23;62(6):943–8.

224. Fountas KN, Smith JR. Subdural electrode-associated complications: a 20-year experience. Stereotact Funct Neurosurg. 2007;85(6):264–72.

225. Widdess-Walsh P, Jeha L, Nair D, Kotagal P, Bingaman W, Najm I. Subdural electrode analysis in focal cortical dysplasia: predictors of surgical outcome. Neurology. 2007 Aug 14;69(7):660–7.

226. Weber JP, Silbergeld DL, Winn HR. Surgical resection of epileptogenic cortex associated with structural lesions. Neurosurg Clin N Am. 1993 Apr;4(2):327–36.

227. Wieser HG, Blume WT, Fish D, Goldensohn E, Hufnagel A, King D, et al. ILAE Commission Report. Proposal for a new classification of outcome with respect to epileptic seizures following epilepsy surgery. Epilepsia. 2001 Feb;42(2):282–6.

228. Malla BR, O'Brien TJ, Cascino GD, So EL, Radhakrishnan K, Silbert P, et al. Acute postoperative seizures following anterior temporal lobectomy for intractable partial epilepsy. J Neurosurg. 1998 Aug;89(2):177–82.

229. McIntosh AM, Kalnins RM, Mitchell LA, Berkovic SF. Early seizures after temporal lobectomy predict subsequent seizure recurrence. Ann Neurol. 2005 Feb;57(2):283–8.

230. Keogan M, McMackin D, Peng S, Phillips J, Burke T, Murphy S, et al. Temporal neocorticectomy in management of intractable epilepsy: long-term outcome and predictive factors. Epilepsia. 1992 Oct;33(5):852–61.

231. Téllez-Zenteno JF, Dhar R, Wiebe S. Long-term seizure outcomes following epilepsy surgery: a systematic review and meta-analysis. Brain. 2005 May;128(Pt 5):1188–98.

232. Téllez-Zenteno JF, Dhar R, Hernandez-Ronquillo L, Wiebe S. Long-term outcomes in epilepsy surgery: antiepileptic drugs, mortality, cognitive and psychosocial aspects. Brain. 2007 Feb;130(Pt 2):334–45.

233. Tonini C, Beghi E, Berg AT, Bogliun G, Giordano L, Newton RW, et al. Predictors of epilepsy surgery outcome: a meta-analysis. Epilepsy Res. 2004 Nov;62(1):75–87.

234. McIntosh AM, Kalnins RM, Mitchell LA, Fabinyi GCA, Briellmann RS, Berkovic SF. Temporal lobectomy: long-term seizure outcome, late recurrence and risks for seizure recurrence. Brain. 2004 Sep;127(Pt 9):2018–30.

235. Lowe AJ, David E, Kilpatrick CJ, Matkovic Z, Cook MJ, Kaye A, et al. Epilepsy surgery for pathologically proven hippocampal sclerosis provides long-term seizure control and improved quality of life. Epilepsia. 2004 Mar;45(3):237–42.

236. Paolicchi JM, Jayakar P, Dean P, Yaylali I, Morrison G, Prats A, et al. Predictors of outcome in pediatric epilepsy surgery. Neurology. 2000 Feb 8;54(3):642–7.

237. Carne RP, O'Brien TJ, Kilpatrick CJ, MacGregor LR, Hicks RJ, Murphy MA, et al. MRI-negative PET-positive temporal lobe epilepsy: a distinct surgically remediable syndrome. Brain. 2004 Oct;127(Pt 10):2276–85.

238. Alarcón G, Valentín A, Watt C, Selway RP, Lacruz ME, Elwes RDC, et al. Is it worth pursuing surgery for epilepsy in patients with normal neuroimaging? J Neurol Neurosurg Psychiatr. 2006 Apr;77(4):474–80.

239. Jeha LE, Najm IM, Bingaman WE, Khandwala F, Widdess-Walsh P, Morris HH, et al. Predictors of outcome after temporal lobectomy for the treatment of intractable epilepsy. Neurology. 2006 Jun 27;66(12):1938–40.

240. De Tisi J, Bell GS, Peacock JL, McEvoy AW, Harkness WFJ, Sander JW, et al. The long-term outcome of adult epilepsy surgery, patterns of seizure remission, and relapse: a cohort study. Lancet. 2011 Oct 15;378(9800):1388–95.

241. Cunha I, Oliveira J. Quality of life after surgery for temporal lobe epilepsy: a 5-year follow-up. Epilepsy Behav. 2010 Apr;17(4):506–10.

242. Wrench J, Wilson SJ, Bladin PF. Mood disturbance before and after seizure surgery: a comparison of temporal and extratemporal resections. Epilepsia. 2004 May;45(5):534–43.

243. Altshuler L, Rausch R, Delrahim S, Kay J, Crandall P. Temporal lobe epilepsy, temporal lobectomy, and major depression. J Neuropsychiatry Clin Neurosci. 1999;11(4):436–43.

244. Anhoury S, Brown RJ, Krishnamoorthy ES, Trimble MR. Psychiatric outcome after temporal lobectomy: a predictive study. Epilepsia. 2000 Dec;41(12):1608–15.

245. Kanner AM, Stagno S, Kotagal P, Morris HH. Postictal psychiatric events during prolonged video-electroencephalographic monitoring studies. Arch Neurol. 1996 Mar;53(3):258–63.

246. Reutens DC, Savard G, Andermann F, Dubeau F, Olivier A. Results of surgical treatment in temporal lobe epilepsy with chronic psychosis. Brain. 1997 Nov;120 (Pt 11):1929–36.

247. Helmstaedter C. Neuropsychological aspects of epilepsy surgery. Epilepsy Behav. 2004 Feb;5 Suppl 1:S45–55.

248. Lee TMC, Yip JTH, Jones-Gotman M. Memory deficits after resection from left or right anterior temporal lobe in humans: a meta-analytic review. Epilepsia. 2002 Mar;43(3):283–91.

249. Bell BD, Davies KG, Haltiner AM, Walters GL. Intracarotid amobarbital procedure and prediction of postoperative memory in patients with left temporal lobe epilepsy and hippocampal sclerosis. Epilepsia. 2000 Aug;41(8):992–7.

250. Helmstaedter C, Elger CE. Cognitive consequences of two-thirds anterior temporal lobectomy on verbal memory in 144 patients: a three-month follow-up study. Epilepsia. 1996 Feb;37(2):171–80.

251. Loring DW, Meador KJ, Lee GP. Effects of temporal lobectomy on generative fluency and other language functions. Arch Clin Neuropsychol. 1994 May;9(3):229–38.

252. Saykin AJ, Stafiniak P, Robinson LJ, Flannery KA, Gur RC, O'Connor MJ, et al. Language before and after temporal lobectomy: specificity of acute changes and relation to early risk factors. Epilepsia. 1995 Nov;36(11):1071–7.

253. Davies KG, Maxwell RE, Beniak TE, Destafney E, Fiol ME. Language function after temporal lobectomy without stimulation mapping of cortical function. Epilepsia. 1995 Feb;36(2):130–6.

254. Langfitt JT, Rausch R. Word-finding deficits persist after left anterotemporal lobectomy. Arch Neurol. 1996 Jan;53(1):72–6.

255. Chelune GJ, Naugle RI, Lüders H, Awad IA. Prediction of cognitive change as a function of preoperative ability status among temporal lobectomy patients seen at 6-month follow-up. Neurology. 1991 Mar;41(3):399–404.

256. Seidenberg M, Hermann B, Wyler AR, Davies K, Dohan FC Jr, Leveroni C. Neuropsychological outcome following anterior temporal lobectomy in patients with and without the syndrome of mesial temporal lobe epilepsy. Neuropsychology. 1998 Apr;12(2):303–16.

257. Rabin ML, Narayan VM, Kimberg DY, Casasanto DJ, Glosser G, Tracy JI, et al. Functional MRI predicts post-surgical memory following temporal lobectomy. Brain. 2004 Oct;127(Pt 10):2286–98.

258. Richardson MP, Strange BA, Thompson PJ, Baxendale SA, Duncan JS, Dolan RJ. Pre-operative verbal memory fMRI predicts post-operative memory decline after left temporal lobe resection. Brain. 2004 Nov;127(Pt 11):2419–26.

259. Janszky J, Jokeit H, Kontopoulou K, Mertens M, Ebner A, Pohlmann-Eden B, et al. Functional MRI predicts memory performance after right mesiotemporal epilepsy surgery. Epilepsia. 2005 Feb;46(2):244–50.

260. Sabsevitz DS, Swanson SJ, Hammeke TA, Spanaki MV, Possing ET, Morris III GL, et al. Use of preoperative functional neuroimaging to predict language deficits from epilepsy surgery. Neurology. 2003;60(11):1788.

261. Bonelli SB, Thompson PJ, Yogarajah M, Vollmar C, Powell RHW, Symms MR, et al. Imaging language networks before and after anterior temporal lobe resection: results of a longitudinal fMRI study. Epilepsia. 2012 Apr;53(4):639–50.

262. Griffith HR, Perlman SB, Woodard AR, Rutecki PA, Jones JC, Ramirez LF, et al. Preoperative FDG-PET temporal lobe hypometabolism and verbal memory after temporal lobectomy. Neurology. 2000 Mar 14;54(5):1161–5.

263. Kneebone AC, Chelune GJ, Dinner DS, Naugle RI, Awad IA. Intracarotid amobarbital procedure as a predictor of material-specific memory change after anterior temporal lobectomy. Epilepsia. 1995 Sep;36(9):857–65.

264. Chiaravalloti ND, Glosser G. Material-specific memory changes after anterior temporal lobectomy as predicted by the intracarotid amobarbital test. Epilepsia. 2001 Jul;42(7):902–11.

265. Loring DW, Meador KJ, Lee GP, King DW, Nichols ME, Park YD, et al. Wada memory asymmetries predict verbal memory decline after anterior temporal lobectomy. Neurology. 1995 Jul;45(7):1329–33.

266. Pauli E, Pickel S, Schulemann H, Buchfelder M, Stefan H. Neuropsychologic findings depending on the type of the resection in temporal lobe epilepsy. Adv Neurol. 1999;81:371–7.

267. Chelune GJ. Hippocampal adequacy versus functional reserve: predicting memory functions following temporal lobectomy. Arch Clin Neuropsychol. 1995 Oct;10(5):413–32.

268. Hermann BP, Seidenberg M, Haltiner A, Wyler AR. Relationship of age at onset, chronologic age, and adequacy of preoperative performance to verbal memory change after anterior temporal lobectomy. Epilepsia. 1995 Feb;36(2):137–45.

269. Bonelli SB, Powell RHW, Yogarajah M, Samson RS, Symms MR, Thompson PJ, et al. Imaging memory in temporal lobe epilepsy: predicting the effects of temporal lobe resection. Brain. 2010 Apr;133(Pt 4):1186–99.

270. Bonelli SB, Thompson PJ, Yogarajah M, Powell RHW, Samson RS, McEvoy AW, et al. Memory reorganization following anterior temporal lobe resection: a longitudinal functional MRI study. Brain. 2013 Jun;136(Pt 6):1889–900.

271. Sidhu MK, Stretton J, Winston GP, Bonelli S, Centeno M, Vollmar C, et al. A functional magnetic resonance imaging study mapping the episodic memory encoding network in temporal lobe epilepsy. Brain. 2013 May 14;136(6):1868–88.

272. Westbrook C. MRI at a glance. Chichester, U.K.; Malden, MA: Wiley-Blackwell; 2010.

273. Pooley RA. AAPM/RSNA Physics Tutorial for Residents: Fundamental Physics of MR Imaging. Radiographics. 2005 Jul 1;25(4):1087–99.

274. Westbrook C, Roth CK, Talbot J. MRI in practice. Chichester, West Sussex; Malden, MA: Wiley-Blackwell; 2011.

275. Poustchi-Amin M, Mirowitz SA, Brown JJ, McKinstry RC, Li T. Principles and Applications of Echo-planar Imaging: A Review for the General Radiologist1. Radiographics. 2001;21(3):767–79.

276. Brown R. A brief account of microscopical observations made in the months of June, July, and August, 1827, on the particles contained in the pollen of plants; and on the general existence of active molecules in organic and inorganic bodies. Phil Mag. 1828;4:161–73.

277. Fick A. Concerns diffusion and concentration gradient. Ann Phys Lpz. 1855;170:59.

278. Einstein A. Über die von der molekularkinetischen Theorie der wärme gefordete Bewegung von in ruhenden Flüssigkeiten suspendierten Teilchen. Ann Physik. 1905;4:549–60.

279. Stejskal EO, Tanner JE. Spin Diffusion Measurements: Spin Echoes in the Presence of a Time-Dependent Field Gradient. The Journal of Chemical Physics. 1965;42(1):288.

280. Le Bihan D, Breton E, Lallemand D, Grenier P, Cabanis E, Laval-Jeantet M. MR imaging of intravoxel incoherent motions: application to diffusion and perfusion in neurologic disorders. Radiology. 1986 Nov;161(2):401–7.

281. Moseley ME, Cohen Y, Mintorovitch J, Chileuitt L, Shimizu H, Kucharczyk J, et al. Early detection of regional cerebral ischemia in cats: comparison of diffusion- and T2-weighted MRI and spectroscopy. Magn Reson Med. 1990 May;14(2):330–46.

282. Moseley ME, Cohen Y, Kucharczyk J, Mintorovitch J, Asgari HS, Wendland MF, et al. Diffusion-weighted MR imaging of anisotropic water diffusion in cat central nervous system. Radiology. 1990 Aug;176(2):439–45.

283. Seunarine K, Alexander DC. Multiple Fibers: Beyond the Diffusion Tensor. Diffusion MRI from quantitative measurement to in-vivo neuroanatomy. Amsterdam; Boston: Academic Press; 2009. p. 55–72.

284. Basser PJ, Mattiello J, LeBihan D. MR diffusion tensor spectroscopy and imaging. Biophys J. 1994 Jan;66(1):259–67.

285. Basser PJ, Mattiello J, LeBihan D. Estimation of the effective self-diffusion tensor from the NMR spin echo. J Magn Reson B. 1994 Mar;103(3):247–54.

286. Pierpaoli C, Jezzard P, Basser PJ, Barnett A, Di Chiro G. Diffusion tensor MR imaging of the human brain. Radiology. 1996 Dec;201(3):637–48.

287. Lythgoe MF, Busza AL, Calamante F, Sotak CH, King MD, Bingham AC, et al. Effects of diffusion anisotropy on lesion delineation in a rat model of cerebral ischemia. Magn Reson Med. 1997 Oct;38(4):662–8.

288. Yoshiura T, Wu O, Zaheer A, Reese TG, Sorensen AG. Highly diffusion-sensitized MRI of brain: dissociation of gray and white matter. Magn Reson Med. 2001 May;45(5):734–40.

289. Basser PJ, Pierpaoli C. Microstructural and physiological features of tissues elucidated by quantitative-diffusion-tensor MRI. J Magn Reson B. 1996 Jun;111(3):209–19.

290. Pierpaoli C, Basser PJ. Toward a quantitative assessment of diffusion anisotropy. Magn Reson Med. 1996 Dec;36(6):893–906.

291. Basser PJ. New histological and physiological stains derived from diffusion-tensor MR images. Ann N Y Acad Sci. 1997 May 30;820:123–38.

292. Westin CF, Peled S, Gudbjartsson H, Kikinis R, Jolesz FA. Geometrical diffusion measures for MRI from tensor basis analysis. Proceedings of the 5th Annual Meeting of ISMRM. Vancouver, Canada; 1997. p. 1742.

293. Alexander DC, Barker GJ, Arridge SR. Detection and modeling of non-Gaussian apparent diffusion coefficient profiles in human brain data. Magn Reson Med. 2002 Aug;48(2):331–40.

294. Alexander DC, Barker GJ. Optimal imaging parameters for fiber-orientation estimation in diffusion MRI. NeuroImage. 2005;27(2):357–67.

295. Behrens TEJ, Woolrich MW, Jenkinson M, Johansen-Berg H, Nunes RG, Clare S, et al. Characterization and propagation of uncertainty in diffusion-weighted MR imaging. Magn Reson Med. 2003 Nov;50(5):1077–88.

296. Kaden E, Knösche TR, Anwander A. Parametric spherical deconvolution: inferring anatomical connectivity using diffusion MR imaging. Neuroimage. 2007 Aug 15;37(2):474–88.

297. Assaf Y, Freidlin RZ, Rohde GK, Basser PJ. New modeling and experimental framework to characterize hindered and restricted water diffusion in brain white matter. Magn Reson Med. 2004 Nov;52(5):965–78.

298. Parker GJM, Alexander DC. Probabilistic Monte-Carlo based mapping of cerebral connections utilizing whole-brain crossing fibre information. Lecture Notes in Computer Science (Taylor CJ, Noble JA eds): Image Processing in Medical Imaging. 2003. p. 684–95.

299. Behrens TEJ, Berg HJ, Jbabdi S, Rushworth MFS, Woolrich MW. Probabilistic diffusion tractography with multiple fibre orientations: What can we gain? Neuroimage. 2007 Jan 1;34(1):144–55.

300. Reese TG, Heid O, Weisskoff RM, Wedeen VJ. Reduction of eddy-current-induced distortion in diffusion MRI using a twice-refocused spin echo. Magn Reson Med. 2003 Jan;49(1):177–82.

301. Bastin ME. Correction of eddy current-induced artefacts in diffusion tensor imaging using iterative cross-correlation. Magn Reson Imaging. 1999 Sep;17(7):1011–24.

302. Jezzard P, Barnett AS, Pierpaoli C. Characterization of and correction for eddy current artifacts in echo planar diffusion imaging. Magn Reson Med. 1998 May;39(5):801–12.

303. Bastin ME, Armitage PA. On the use of water phantom images to calibrate and correct eddy current induced artefacts in MR diffusion tensor imaging. Magn Reson Imaging. 2000 Jul;18(6):681–7.

304. Jenkinson M, Smith S. A global optimisation method for robust affine registration of brain images. Med Image Anal. 2001 Jun;5(2):143–56.

305. Rohde GK, Barnett AS, Basser PJ, Marenco S, Pierpaoli C. Comprehensive approach for correction of motion and distortion in diffusion-weighted MRI. Magn Reson Med. 2004 Jan;51(1):103–14.

306. Jezzard P, Clare S. Sources of distortion in functional MRI data. Hum Brain Mapp. 1999;8(2-3):80–5.

307. Bammer R, Auer M, Keeling SL, Augustin M, Stables LA, Prokesch RW, et al. Diffusion tensor imaging using single-shot SENSE-EPI. Magn Reson Med. 2002 Jul;48(1):128–36.

308. Chang H, Fitzpatrick JM. A technique for accurate magnetic resonance imaging in the presence of field inhomogeneities. IEEE Trans Med Imaging. 1992;11(3):319–29.

309. Jezzard P, Balaban RS. Correction for geometric distortion in echo planar images from B0 field variations. Magn Reson Med. 1995 Jul;34(1):65–73.

310. Anderson AW, Gore JC. Analysis and correction of motion artifacts in diffusion weighted imaging. Magn Reson Med. 1994 Sep;32(3):379–87.

311. Skare S, Andersson JL. On the effects of gating in diffusion imaging of the brain using single shot EPI. Magn Reson Imaging. 2001 Oct;19(8):1125–8.

312. Nunes RG, Jezzard P, Clare S. Investigations on the efficiency of cardiac-gated methods for the acquisition of diffusion-weighted images. J Magn Reson. 2005 Nov;177(1):102–10.

313. Chang L-C, Jones DK, Pierpaoli C. RESTORE: robust estimation of tensors by outlier rejection. Magn Reson Med. 2005 May;53(5):1088–95.

314. Jones DK, Basser PJ. 'Squashing peanuts and smashing pumpkins': how noise distorts diffusion-weighted MR data. Magn Reson Med. 2004 Nov;52(5):979–93.

315. Basser PJ, Pajevic S. Statistical artifacts in diffusion tensor MRI (DT-MRI) caused by background noise. Magn Reson Med. 2000 Jul;44(1):41–50.

316. Johnson GA, Maki JH. In vivo measurement of proton diffusion in the presence of coherent motion. Invest Radiol. 1991 Jun;26(6):540–5.

317. Butts K, de Crespigny A, Pauly JM, Moseley M. Diffusion-weighted interleaved echo-planar imaging with a pair of orthogonal navigator echoes. Magn Reson Med. 1996 May;35(5):763–70.

318. Ashburner J, Friston KJ. Voxel-based morphometry--the methods. Neuroimage. 2000 Jun;11(6 Pt 1):805–21.

319. Good CD, Johnsrude IS, Ashburner J, Henson RN, Friston KJ, Frackowiak RS. A voxel-based morphometric study of ageing in 465 normal adult human brains. Neuroimage. 2001 Jul;14(1 Pt 1):21–36.

320. Worsley KJ, Evans AC, Marrett S, Neelin P. A three-dimensional statistical analysis for CBF activation studies in human brain. J Cereb Blood Flow Metab. 1992 Nov;12(6):900–18.

321. Davatzikos C. Why voxel-based morphometric analysis should be used with great caution when characterizing group differences. Neuroimage. 2004 Sep;23(1):17–20.

322. Jones DK, Griffin LD, Alexander DC, Catani M, Horsfield MA, Howard R, et al. Spatial normalization and averaging of diffusion tensor MRI data sets. Neuroimage. 2002 Oct;17(2):592–617.

323. Jones DK, Symms MR, Cercignani M, Howard RJ. The effect of filter size on VBM analyses of DT-MRI data. Neuroimage. 2005 Jun;26(2):546–54.

324. Smith SM, Jenkinson M, Johansen-Berg H, Rueckert D, Nichols TE, Mackay CE, et al. Tract-based spatial statistics: voxelwise analysis of multi-subject diffusion data. Neuroimage. 2006 Jul 15;31(4):1487–505.

325. Smith SM, Johansen-Berg H, Jenkinson M, Rueckert D, Nichols TE, Miller KL, et al. Acquisition and voxelwise analysis of multi-subject diffusion data with tract-based spatial statistics. Nat Protoc. 2007;2(3):499–503.

326. Smith SM, Nichols TE. Threshold-free cluster enhancement: addressing problems of smoothing, threshold dependence and localisation in cluster inference. Neuroimage. 2009;44(1):83–98.

327. Nichols TE, Holmes AP. Nonparametric permutation tests for functional neuroimaging: a primer with examples. Human Brain Mapping. 2002;15(1):1–25.

328. Basser PJ, Pajevic S, Pierpaoli C, Duda J, Aldroubi A. In vivo fiber tractography using DT-MRI data. Magn Reson Med. 2000 Oct;44(4):625–32.

329. Jones DK. Determining and visualizing uncertainty in estimates of fiber orientation from diffusion tensor MRI. Magn Reson Med. 2003 Jan;49(1):7–12.

330. Mori S, Crain BJ, Chacko VP, van Zijl PC. Three-dimensional tracking of axonal projections in the brain by magnetic resonance imaging. Ann Neurol. 1999 Feb;45(2):265–9.

331. Lazar M, Alexander AL. An error analysis of white matter tractography methods: synthetic diffusion tensor field simulations. Neuroimage. 2003 Oct;20(2):1140–53.

332. Jones DK. Tractography gone wild: probabilistic fibre tracking using the wild bootstrap with diffusion tensor MRI. IEEE Trans Med Imaging. 2008 Sep;27(9):1268–74.

333. Parker GJM, Alexander DC. Probabilistic Monte Carlo based mapping of cerebral connections utilising whole-brain crossing fibre information. Inf Process Med Imaging. 2003 Jul;18:684–95.

334. Parker GJM, Alexander DC. Probabilistic anatomical connectivity derived from the microscopic persistent angular structure of cerebral tissue. Philosophical Transactions of the Royal Society B: Biological Sciences. 2005 May;360(1457):893–902.

335. Parker GJM, Wheeler-Kingshott CAM, Barker GJ. Estimating distributed anatomical connectivity using fast marching methods and diffusion tensor imaging. IEEE Trans Med Imaging. 2002 May;21(5):505–12.

336. Jbabdi S, Bellec P, Toro R, Daunizeau J, Pélégrini-Issac M, Benali H. Accurate anisotropic fast marching for diffusion-based geodesic tractography. Int J Biomed Imaging. 2008;2008:320195.

337. Hansen JR. Pulsed NMR study of water mobility in muscle and brain tissue. Biochem Biophys Acta. 1971;230:482–6.

338. Le Bihan D. Looking into the functional architecture of the brain with diffusion MRI. Nat Rev Neurosci. 2003 Jun;4(6):469–80.

339. Beaulieu C. The basis of anisotropic water diffusion in the nervous system - a technical review. NMR Biomed. 2001;15:435–55.

340. Righini A, Pierpaoli C, Alger JR, Di Chiro G. Brain parenchyma apparent diffusion coefficient alterations associated with experimental complex partial status epilepticus. Magn Reson Imaging. 1994;12(0730-725X (Print)):865–71.

341. Zhong J, Petroff OA, Prichard JW, Gore JC. Changes in water diffusion and relaxation properties of rat cerebrum during status epilepticus. Magn Reson Med. 1993 Aug;30(0740-3194 (Print)):241–6.

342. Engelhorn T, Weise J, Hammen T, Bluemcke I, Hufnagel A, Doerfler A. Early diffusion-weighted MRI predicts regional neuronal damage in generalized status epilepticus in rats treated with diazepam. Neurosci Lett. 2007 May 7;417(3):275–80.

343. Jansen JFA, Lemmens EMP, Strijkers GJ, Prompers JJ, Schijns OEMG, Kooi ME, et al. Short- and long-term limbic abnormalities after experimental febrile seizures. Neurobiol Dis. 2008 Nov;32(2):293–301.

344. Szabo K, Poepel A, Pohlmann-Eden B, Hirsch J, Back T, Sedlaczek O, et al. Diffusion-weighted and perfusion MRI demonstrates parenchymal changes in complex partial status epilepticus. Brain. 2005 Jun;128(1460-2156 (Electronic)):1369–76.

345. Bruehl C, Hagemann G, Witte OW. Uncoupling of blood flow and metabolism in focal epilepsy. Epilepsia. 1998 Dec;39(0013-9580 (Print)):1235–42.

346. Wang Y, Majors A, Najm I, Xue M, Comair Y, Modic M, et al. Postictal alteration of sodium content and apparent diffusion coefficient in epileptic rat brain induced by kainic acid. Epilepsia. 1996 Oct;37(0013-9580 (Print)):1000–6.

347. Lux HD, Heinemann U, Dietzel I. Ionic changes and alterations in the size of the extracellular space during epileptic activity. AdvNeurol. 1986;44(0091-3952 (Print)):619–39.

348. van der Toorn A., Sykova E, Dijkhuizen RM, Vorisek I, Vargova L, Skobisova E, et al. Dynamic changes in water ADC, energy metabolism, extracellular space volume, and tortuosity in neonatal rat brain during global ischemia. Magn Reson Med. 1996 Jul;36(0740-3194 (Print)):52–60.

349. Tanaka T, Tanaka S, Fujita T, Takano K, Fukuda H, Sako K, et al. Experimental complex partial seizures induced by a microinjection of kainic acid into limbic structures. ProgNeurobiol. 1992;38(0301-0082 (Print)):317–34.

350. Nitsch C, Klatzo I. Regional patterns of blood-brain barrier breakdown during epileptiform seizures induced by various convulsive agents. J Neurol Sci. 1983 Jun;59(0022-510X (Print)):305–22.

351. Nedelcu J, Klein MA, Aguzzi A, Boesiger P, Martin E. Biphasic edema after hypoxic-ischemic brain injury in neonatal rats reflects early neuronal and late glial damage. PediatrRes. 1999 Sep;46(0031-3998 (Print)):297–304.

352. Wasterlain CG, Fujikawa DG, Penix L, Sankar R. Pathophysiological mechanisms of brain damage from status epilepticus. Epilepsia. 1993;34 Suppl 1(0013-9580 (Print)):S37–S53.

353. Hasegawa D, Orima H, Fujita M, Nakamura S, Takahashi K, Ohkubo S, et al. Diffusion-weighted imaging in kainic acid-induced complex partial status epilepticus in dogs. Brain Res. 2003 Sep 5;983(0006-8993 (Print)):115–27.

354. Pitkanen A, Nissinen J, Nairismagi J, Lukasiuk K, Grohn OH, Miettinen R, et al. Progression of neuronal damage after status epilepticus and during spontaneous seizures in a rat model of temporal lobe epilepsy. ProgBrain Res. 2002;135(0079-6123 (Print)):67–83.

355. Wieshmann UC, Symms MR, Shorvon SD. Diffusion changes in status epilepticus. Lancet. 1997 Aug 16;350(0140-6736 (Print)):493–4.

356. Hong KS, Cho YJ, Lee SK, Jeong SW, Kim WK, Oh EJ. Diffusion changes suggesting predominant vasogenic oedema during partial status epilepticus. Seizure. 2004 Jul;13(1059-1311 (Print)):317–21.

357. Kim JA, Chung JI, Yoon PH, Kim DI, Chung TS, Kim EJ, et al. Transient MR signal changes in patients with generalized tonicoclonic seizure or status epilepticus: periictal diffusion-weighted imaging. AJNR AmJ Neuroradiol. 2001 Jun;22(0195-6108 (Print)):1149–60.

358. Lansberg MG, O'Brien MW, Norbash AM, Moseley ME, Morrell M, Albers GW. MRI abnormalities associated with partial status epilepticus. Neurology. 1999 Mar 23;52(0028-3878 (Print)):1021–7.

359. Calistri V, Caramia F, Bianco F, Fattapposta F, Pauri F, Bozzao L. Visualization of evolving status epilepticus with diffusion and perfusion MR imaging. AJNR AmJ Neuroradiol. 2003 Apr;24(0195-6108 (Print)):671–3.

360. Diehl B, Najm I, Ruggieri P, Foldvary N, Mohamed A, Tkach J, et al. Periictal diffusion-weighted imaging in a case of lesional epilepsy. Epilepsia. 1999 Nov;40(0013-9580 (Print)):1667–71.

361. Flacke S, Wullner U, Keller E, Hamzei F, Urbach H. Reversible changes in echo planar perfusion- and diffusion-weighted MRI in status epilepticus. Neuroradiology. 2000 Feb;42(0028-3940 (Print)):92–5.

362. El Koussy M, Mathis J, Lovblad KO, Stepper F, Kiefer C, Schroth G. Focal status epilepticus: follow-up by perfusion- and diffusion MRI. EurRadiol. 2002 Mar;12(0938-7994 (Print)):568–74.

363. Diehl B, Najm I, Ruggieri P, Tkach J, Mohamed A, Morris H, et al. Postictal diffusion-weighted imaging for the localization of focal epileptic areas in temporal lobe epilepsy. Epilepsia. 2001 Jan;42(0013-9580 (Print)):21–8.

364. Salmenpera TM, Symms MR, Boulby PA, Barker GJ, Duncan JS. Postictal diffusion weighted imaging. Epilepsy Research. 2006 Aug;70(2-3):133–43.

365. Konermann S, Marks S, Ludwig T, Weber J, de Greiff A, Dorfler A, et al. Presurgical evaluation of epilepsy by brain diffusion: MR-detected effects of flumazenil on the epileptogenic focus. Epilepsia. 2003 Mar;44(0013-9580 (Print)):399–407.

366. Hufnagel A, Weber J, Marks S, Ludwig T, de Greiff A, Leonhardt G, et al. Brain diffusion after single seizures. Epilepsia. 2003 Jan;44(0013-9580 (Print)):54–63.

367. Oh JB, Lee SK, Kim KK, Song IC, Chang KH. Role of immediate postictal diffusion-weighted MRI in localizing epileptogenic foci of mesial temporal lobe epilepsy and non-lesional neocortical epilepsy. Seizure. 2004 Oct;13(1059-1311 (Print)):509–16.

368. Diehl B, Symms MR, Boulby PA, Salmenpera T, Wheeler-Kingshott CAM, Barker GJ, et al. Postictal diffusion tensor imaging. Epilepsy Research. 2005 Jul;65(3):137–46.

369. Hakyemez B, Erdogan C, Yildiz H, Ercan I, Parlak M. Apparent diffusion coefficient measurements in the hippocampus and amygdala of patients with temporal lobe seizures and in healthy volunteers. Epilepsy Behav. 2005 Mar;6(1525-5050 (Print)):250–6.

370. Hugg JW, Butterworth EJ, Kuzniecky RI. Diffusion mapping applied to mesial temporal lobe epilepsy: preliminary observations. Neurology. 1999 Jul 13;53(0028-3878 (Print)):173–6.

371. Kantarci K, Shin C, Britton JW, So EL, Cascino GD, Jack CR. Comparative diagnostic utility of 1H MRS and DWI in evaluation of temporal lobe epilepsy. Neurology. 2002 Jun 25;58(0028-3878 (Print)):1745–53.

372. Wieshmann UC, Clark CA, Symms MR, Barker GJ, Birnie KD, Shorvon SD. Water diffusion in the human hippocampus in epilepsy. Magn Reson Imaging. 1999 Jan;17(0730-725X (Print)):29–36.

373. Yoo SY, Chang KH, Song IC, Han MH, Kwon BJ, Lee SH, et al. Apparent diffusion coefficient value of the hippocampus in patients with hippocampal sclerosis and in healthy volunteers. AJNR AmJ Neuroradiol. 2002 May;23(0195-6108 (Print)):809–12.

374. Salmenpera TM, Simister RJ, Bartlett P, Symms MR, Boulby PA, Free SL, et al. High-resolution diffusion tensor imaging of the hippocampus in temporal lobe epilepsy. Epilepsy Res. 2006 Oct;71(0920-1211 (Print)):102–6.

375. Assaf BA, Mohamed FB, Abou-Khaled KJ, Williams JM, Yazeji MS, Haselgrove J, et al. Diffusion tensor imaging of the hippocampal formation in temporal lobe epilepsy. AJNR AmJ Neuroradiol. 2003 Oct;24(0195-6108 (Print)):1857–62.

376. Goncalves Pereira PM, Oliveira E, Rosado P. Apparent diffusion coefficient mapping of the hippocampus and the amygdala in pharmaco-resistant temporal lobe epilepsy. AJNR AmJ Neuroradiol. 2006 Mar;27(0195-6108 (Print)):671–83.

377. Wang R, Li S-Y, Chen M, Zhou C. Diagnostic value of interictal diffusion-weighted imaging in evaluation of intractable temporal lobe epilepsy. Chin Med Sci J. 2008 Jun;23(2):68–72.

378. Liacu D, de Marco G, Ducreux D, Bouilleret V, Masnou P, Idy-Peretti I. Diffusion tensor changes in epileptogenic hippocampus of TLE patients. Neurophysiol Clin. 2010 Jun;40(3):151–7.

379. Londono A, Castillo M, Lee YZ, Smith JK. Apparent diffusion coefficient measurements in the hippocampi in patients with temporal lobe seizures. AJNR AmJ Neuroradiol. 2003 Sep;24(0195-6108 (Print)):1582–6.

380. Wehner T, Lapresto E, Tkach J, Liu P, Bingaman W, Prayson RA, et al. The value of interictal diffusion-weighted imaging in lateralizing temporal lobe epilepsy. Neurology. 2007 Jan 9;68(1526-632X (Electronic)):122–7.

381. Lee JH, Chung CK, Song IC, Chang KH, Kim HJ. Limited utility of interictal apparent diffusion coefficient in the evaluation of hippocampal sclerosis. Acta Neurol Scand. 2004 Jul;110(0001-6314 (Print)):53–8.

382. Gupta RK, Saksena S, Agarwal A, Hasan KM, Husain M, Gupta V, et al. Diffusion tensor imaging in late posttraumatic epilepsy. Epilepsia. 2005 Sep;46(9):1465–71.

383. Eriksson SH, Rugg-Gunn FJ, Symms MR, Barker GJ, Duncan JS. Diffusion tensor imaging in patients with epilepsy and malformations of cortical development. Brain. 2001 Mar;124(0006-8950 (Print)):617–26.

384. Dumas de la R, Oppenheim C, Chassoux F, Rodrigo S, Beuvon F, Daumas-Duport C, et al. Diffusion tensor imaging of partial intractable epilepsy. EurRadiol. 2005 Feb;15(0938-7994 (Print)):279–85.

385. Widjaja E, Geibprasert S, Otsubo H, Snead OC, Mahmoodabadi SZ. Diffusion Tensor Imaging Assessment of the Epileptogenic Zone in Children with Localization-Related Epilepsy. American Journal of Neuroradiology. 2011 Oct 13;32(10):1789–94.

386. Lippé S, Poupon C, Cachia A, Archambaud F, Rodrigo S, Dorfmuller G, et al. White matter abnormalities revealed by DTI correlate with interictal grey matter FDG-PET metabolism in focal childhood epilepsies. Epileptic Disord. 2012 Dec;14(4):404–13.

387. Rugg-Gunn FJ, Eriksson SH, Symms MR, Barker GJ, Thom M, Harkness W, et al. Diffusion tensor imaging in refractory epilepsy. Lancet. 2002 May 18;359(0140-6736 (Print)):1748–51.

388. Guye M, Ranjeva JP, Bartolomei F, Confort-Gouny S, McGonigal A, Regis J, et al. What is the significance of interictal water diffusion changes in frontal lobe epilepsies? Neuroimage. 2007 Mar;35(1053-8119 (Print)):28–37.

389. Thivard L, Adam C, Hasboun D, Clemenceau S, Dezamis E, Lehericy S, et al. Interictal diffusion MRI in partial epilepsies explored with intracerebral electrodes. Brain. 2006 Feb;129(1460-2156 (Electronic)):375–85.

390. Thivard L, Bouilleret V, Chassoux F, Adam C, Dormont D, Baulac M, et al. Diffusion tensor imaging can localize the epileptogenic zone in nonlesional extra-temporal refractory epilepsies when [18F]FDG-PET is not contributive. Epilepsy Research. 2011 Nov;97(1-2):170–82.

391. Stefan H, Feichtinger M, Pauli E, Schäfer I, Eberhardt KW, Kasper BS, et al. Magnetic resonance spectroscopy and histopathological findings in temporal lobe epilepsy. Epilepsia. 2001 Jan;42(1):41–6.

392. Keller S. Voxel-Based Morphometric Comparison of Hippocampal and Extrahippocampal Abnormalities in Patients with Left and Right Hippocampal Atrophy. NeuroImage. 2002 May;16(1):23–31.

393. Concha L, Beaulieu C, Gross DW. Bilateral limbic diffusion abnormalities in unilateral temporal lobe epilepsy. Ann Neurol. 2005 Feb;57(2):188–96.

394. Concha L, Beaulieu C, Collins DL, Gross DW. White-matter diffusion abnormalities in temporal-lobe epilepsy with and without mesial temporal sclerosis. Journal of Neurology, Neurosurgery & Psychiatry. 2009 Mar;80(3):312–9.

395. Kim H, Piao Z, Liu P, Bingaman W, Diehl B. Secondary white matter degeneration of the corpus callosum in patients with intractable temporal lobe epilepsy: A diffusion tensor imaging study. Epilepsy Research. 2008 Oct;81(2-3):136–42.

396. Govindan R, Makki M, Sundaram S, Juhasz C, Chugani H. Diffusion tensor analysis of temporal and extra-temporal lobe tracts in temporal lobe epilepsy. Epilepsy Research. 2008 Jul;80(1):30–41.

397. Lin J, Riley J, Juranek J, Cramer S. Vulnerability of the frontal-temporal connections in temporal lobe epilepsy. Epilepsy Research. 2008 Dec;82(2-3):162–70.

398. Arfanakis K, Hermann BP, Rogers BP, Carew JD, Seidenberg M, Meyerand ME. Diffusion tensor MRI in temporal lobe epilepsy. Magnetic resonance imaging. 2002;20(7):511–9.

399. Thivard L, Lehericy S, Krainik A, Adam C, Dormont D, Chiras J, et al. Diffusion tensor imaging in medial temporal lobe epilepsy with hippocampal sclerosis. Neuroimage. 2005 Nov 15;28(1053-8119 (Print)):682–90.

400. Gross DW, Concha L, Beaulieu C. Extratemporal white matter abnormalities in mesial temporal lobe epilepsy demonstrated with diffusion tensor imaging. Epilepsia. 2006 Aug;47(0013-9580 (Print)):1360–3.

401. Concha L, Beaulieu C, Wheatley BM, Gross DW. Bilateral White Matter Diffusion Changes Persist after Epilepsy Surgery. Epilepsia. 2007 May;48(5):931–40.

402. Pujol J, Deus J, Losilla JM, Capdevila A. Cerebral lateralization of language in normal left-handed people studied by functional MRI. Neurology. 1999 Mar 23;52(5):1038–43.

403. Adcock JE, Wise RG, Oxbury JM, Oxbury SM, Matthews PM. Quantitative fMRI assessment of the differences in lateralization of language-related brain activation in patients with temporal lobe epilepsy. Neuroimage. 2003 Feb;18(2):423–38.

404. Powell HWR, Parker GJM, Alexander DC, Symms MR, Boulby PA, Wheeler-Kingshott CAM, et al. Hemispheric asymmetries in language-related pathways: A combined functional MRI and tractography study. NeuroImage. 2006 Aug;32(1):388–99.

405. Powell HWR, Parker GJM, Alexander DC, Symms MR, Boulby PA, Wheeler-Kingshott CAM, et al. Abnormalities of language networks in temporal lobe epilepsy. NeuroImage. 2007 May;36(1):209–21.

406. Rodrigo S, Oppenheim C, Chassoux F, Hodel J, de Vanssay A, Baudoin-Chial S, et al. Language lateralization in temporal lobe epilepsy using functional MRI and probabilistic tractography. Epilepsia. 2008 Aug;49(8):1367–76.

407. Ellmore TM, Beauchamp MS, Breier JI, Slater JD, Kalamangalam GP, O'Neill TJ. Temporal lobe white matter asymmetry and language laterality in epilepsy patients. NeuroImage. 2010;49(3):2033–44.

408. Powell HWR, Parker GJM, Alexander DC, Symms MR, Boulby PA, Barker GJ, et al. Imaging language pathways predicts postoperative naming deficits. Journal of Neurology, Neurosurgery & Psychiatry. 2008 Mar;79(3):327–30.

409. Manji H, Plant GT. Epilepsy surgery, visual fields, and driving: a study of the visual field criteria for driving in patients after temporal lobe epilepsy surgery with a comparison of Goldmann and Esterman perimetry. J Neurol Neurosurg Psychiatry. 2000 Jan;68(0022-3050 (Print)):80–2.

410. Ebeling U, Reulen HJ. Neurosurgical topography of the optic radiation in the temporal lobe. Acta neurochirurgica. 1988;92(1):29–36.

411. Yamamoto T, Yamada K, Nishimura T, Kinoshita S. Tractography to Depict Three Layers of Visual Field Trajectories to the Calcarine Gyri. American Journal of Ophthalmology. 2005 Nov;140(5):781–781.

412. Kikuta K, Takagi Y, Nozaki K, Hanakawa T, Okada T, Miki Y, et al. Early experience with 3-T magnetic resonance tractography in the surgery of cerebral arteriovenous malformations in and around the visual pathway. Neurosurgery. 2006;58(2):331.

413. Powell HWR, Parker GJM, Alexander DC, Symms MR, Boulby PA, Wheeler-Kingshott CAM, et al. MR tractography predicts visual field defects following temporal lobe resection. Neurology. 2005 Aug 23;65(4):596–9.

414. Yu CS, Li KC, Xuan Y, Ji XM, Qin W. Diffusion tensor tractography in patients with cerebral tumors: a helpful technique for neurosurgical planning and postoperative assessment. EurJ Radiol. 2005 Nov;56(0720-048X (Print)):197–204.

415. Kamada K, Todo T, Morita A, Masutani Y, Aoki S, Ino K, et al. Functional monitoring for visual pathway using real-time visual evoked potentials and optic-radiation tractography. Neurosurgery. 2005;57(1):121.

416. Oldfield RC. The assessment and analysis of handedness: the Edinburgh inventory. Neuropsychologica. 1971;9:97–113.

417. Coughlan AK, Hollows SE. The Adult Memory and Information Processing Battery. Psychology Department, St James' Hospital Leeds; 1985.

418. Cook PA, Symms M, Boulby PA, Alexander DC. Optimal acquisition orders of diffusion-weighted MRI measurements. J Magn Reson Imaging. 2007 May;25(5):1051–8.

419. Boulby PA, Symms M, Barker GJ. Distortion matching echo planar images at different field strengths. ISMRM. 2005;13th Scientific Meeting & Exhibition, Miami, Fla, USA, 2276.

420. Parker GJM, Haroon HA, Wheeler-Kingshott CAM. A framework for a streamline-based probabilistic index of connectivity (PICo) using a structural interpretation of MRI diffusion measurements. J Magn Reson Imaging. 2003 Aug;18(2):242–54.

421. Cook PA, Alexander DC, Parker GJ. Modelling noise-induced fibre-orientation error in diffusion-tensor MRI. IEEE International Symposium on Biomedical Imaging. 2004;332–5.

422. Smith SM, Jenkinson M, Woolrich MW, Beckmann CF, Behrens TE, Johansen-Berg H, et al. Advances in functional and structural MR image analysis and implementation as FSL. Neuroimage. 2004;23 Suppl 1(1053-8119 (Print)):S208–S219.

423. Rutecki PA, Grossman R, Armstrong D, Irish-Loewen S. Electrophysiological connections between the hippocampus and entorhinal cortex in patients with complex partial seizures. JNeurosurg. 1989;70:667–75.

424. Spencer SS, Spencer DD. Entorhinal-hippocampal interactions in medial temporal lobe epilepsy. Epilepsia. 1994;35:721–7.

425. Eichenbaum H. A cortical-hippocampal system for declarative memory. Nat Rev Neurosci. 2000 Oct;1(1):41–50.

426. Powell HW, Koepp MJ, Symms MR, Boulby PA, Salek-Haddadi A, Thompson PJ, et al. Material-specific lateralization of memory encoding in the medial temporal lobe: blocked versus event-related design. Neuroimage. 2005;27:231–9.

427. Powell HW, Richardson MP, Symms MR, Boulby PA, Thompson PJ, Duncan JS, et al. Reorganization of verbal and non-verbal memory in temporal lobe epilepsy. Epilepsia. 2006;Epub ahead of print.

428. Frisk V, Milner B. The role of the left hippocampal region in the acquisition and retention of story content. Neuropsychologica. 1990;28:349–59.

429. Smith ML, Milner B. The role of the right hippocampus in the recall of spatial location. Neuropsychologica. 1981;19:781–93.

430. Rolls ET. Hippocampo-cortical and cortico-cortical backprojections. Hippocampus. 2000;10(4):380–8.

431. Powell HW, Guye M, Parker GJ, Symms MR, Boulby PA, Koepp MJ, et al. Noninvasive demonstration of the connections of the human parahippocampal gyrus. Neuroimage. 2004;22:740–7.

432. Pandya DN, Kuypers HG. Cortico-cortical connections in the rhesus monkey. Brain Res. 1969 Mar;13(1):13–36.

433. Van Hoesen GW, Pandya DN, Butters N. Cortical afferents to the entorhinal cortex of the Rhesus monkey. Science. 1972 Mar 31;175(4029):1471–3.

434. Martin-Elkins CL, Horel JA. Cortical afferents to behaviorally defined regions of the inferior temporal and parahippocampal gyri as demonstrated by WGA-HRP. J Comp Neurol. 1992 Jul 8;321(0021-9967 (Print)):177–92.

435. Woermann FG, Barker GJ, Birnie KD, Meencke HJ, Duncan JS. Regional changes in hippocampal T2 relaxation and volume: a quantitative magnetic resonance imaging study of hippocampal sclerosis. J Neurol Neurosurg Psychiatry. 1998 Nov;65(0022-3050 (Print)):656–64.

436. Baxendale SA, Van Paesschen W, Thompson PJ, Connelly A, Duncan JS, Harkness WF, et al. The relationship between quantitative MRI and neuropsychological functioning in temporal lobe epilepsy. Epilepsia. 1998 Feb;39(0013-9580 (Print)):158–66.

437. Wieser HG, Blume WT, Fish D, et al. Proposal for a new classification of outcome with respect to epileptic seizures following epilepsy surgery. Epilepsia. 2001;42_ _:282–6.

438. Moran NF, Lemieux L, Maudgil D, Kitchen ND, Fish DR, Shorvon SD. Analysis of temporal lobe resections in MR images. Epilepsia. 1999 Aug;40(0013-9580 (Print)):1077–84.

439. Wheeler-Kingshott CA, Hickman SJ, Parker GJ, Ciccarelli O, Symms MR, Miller DH, et al. Investigating cervical spinal cord structure using axial diffusion tensor imaging. Neuroimage. 2002;16:93–102.

440. Tuch DS, Reese TG, Wiegell MR, Makris N, Belliveau JW, Wedeen VJ. High angular resolution diffusion imaging reveals intravoxel white matter heterogeneity. Magn Reson Med. 2002;48:577–82.

441. Parker GJ, Luzzi S, Alexander DC, Wheeler-Kingshott CA, Ciccarelli O, Lambon Ralph MA. Lateralization of ventral and dorsal auditory-langauge pathways in the human brain. Neuroimage. 2005;24:656–66.

442. Toosy AT, Ciccarelli O, Parker GJ., Wheeler-Kingshott CA., Miller DH, Thompson AJ. Characterizing function-structure relationships in the human visual system with functional MRI and diffusion tensor imaging. Neuroimage. 2004;21(4):1452–63.

443. Jutila L, Ylinen A, Partanen K, Alafuzoff I, Mervaala E, Partanen J, et al. MR volumetry of the entorhinal, perirhinal, and temporopolar cortices in drug-refractory temporal lobe epilepsy. AJNR Am J Neuroradiol. 2001 Sep;22(8):1490–501.

444. Shin WC, Hong SB, Tae WS, Seo DW, Kim SE. Ictal hyperperfusion of cerebellum and basal ganglia in temporal lobe epilepsy: SPECT subtraction with MRI coregistration. J NuclMed. 2001 Jun;42(0161-5505 (Print)):853–8.

445. Van Paesschen W, Dupont P, Van Driel G, Van Billoen H, Maes A. SPECT perfusion changes during complex partial seizures in patients with hippocampal sclerosis. Brain. 2003 May;126(0006-8950 (Print)):1103–11.

446. Hamandi K, Powell HWR, Laufs H, Symms MR, Barker GJ, Parker GJM, et al. Combined EEG-fMRI and tractography to visualise propagation of epileptic activity. J Neurol Neurosurg Psychiatr. 2008 May;79(5):594–7.

447. Bernasconi N, Bernasconi A, Caramanos Z, Antel SB, Andermann F, Arnold DL. Mesial temporal damage in temporal lobe epilepsy: a volumetric MRI study of the hippocampus, amygdala and parahippocampal region. Brain. 2003 Feb;126(0006-8950 (Print)):462–9.

448. Bonilha L, Kobayashi E, Rorden C, Cendes F, Li LM. Medial temporal lobe atrophy in patients with refractory temporal lobe epilepsy. J NeurolNeurosurg Psychiatry. 2003 Dec;74(0022-3050 (Print)):1627–30.

449. Bernasconi N, Duchesne S, Janke A, Lerch J, Collins DL, Bernasconi A. Whole-brain voxel-based statistical analysis of gray matter and white matter in temporal lobe epilepsy. Neuroimage. 2004 Oct;23(1053-8119 (Print)):717–23.

450. Bonilha L, Rorden C, Castellano G, Pereira F, Rio PA, Cendes F, et al. Voxel-based morphometry reveals gray matter network atrophy in refractory medial temporal lobe epilepsy. ArchNeurol. 2004 Sep;61(0003-9942 (Print)):1379–84.

451. Keller SS, Wieshmann UC, Mackay CE, Denby CE, Webb J, Roberts N. Voxel based morphometry of grey matter abnormalities in patients with medically intractable temporal lobe epilepsy: effects of side of seizure onset and epilepsy duration. J NeurolNeurosurg Psychiatry. 2002 Dec;73(0022-3050 (Print)):648–55.

452. Bonilha L, Rorden C, Halford JJ, Eckert M, Appenzeller S, Cendes F, et al. Asymmetrical extra-hippocampal gray matter loss related to hippocampal atrophy in patients with medial

temporal lobe epilepsy. J NeurolNeurosurg Psychiatry [Internet]. 2006 Sep 29;(1468-330X (Electronic)). Available from: PM:17012334

453. Lui YW, Nusbaum AO, Barr WB, Johnson G, Babb JS, Orbach D, et al. Correlation of apparent diffusion coefficient with neuropsychological testing in temporal lobe epilepsy. AJNR AmJ Neuroradiol. 2005 Aug;26(0195-6108 (Print)):1832–9.

454. McDonald CR, Ahmadi ME, Hagler DJ, Tecoma ES, Iragui VJ, Gharapetian L, et al. Diffusion tensor imaging correlates of memory and language impairments in temporal lobe epilepsy. Neurology. 2008 Dec;71(23):1869–76.

455. Ahmadi ME, Hagler Jr DJ, McDonald CR, Tecoma ES, Iragui VJ, Dale AM, et al. Side matters: diffusion tensor imaging tractography in left and right temporal lobe epilepsy. American Journal of Neuroradiology. 2009;30(9):1740.

456. Knake S, Salat DH, Halgren E, Halko MA, Greve DN, Grant PE. Changes in white matter microstructure in patients with TLE and hippocampal sclerosis. Epileptic Disord. 2009;11(3):244–50.

457. Kemmotsu N, Girard HM, Bernhardt BC, Bonilha L, Lin JJ, Tecoma ES, et al. MRI analysis in temporal lobe epilepsy: cortical thinning and white matter disruptions are related to side of seizure onset. Epilepsia. 2011 Dec;52(12):2257–66.

458. Otte WM, van Eijsden P, Sander JW, Duncan JS, Dijkhuizen RM, Braun KPJ. A meta-analysis of white matter changes in temporal lobe epilepsy as studied with diffusion tensor imaging. Epilepsia. 2012 Apr;53(4):659–67.

459. Rodrigo S, Oppenheim C, Chassoux F, Golestani N, Cointepas Y, Poupon C, et al. Uncinate fasciculus fiber tracking in mesial temporal lobe epilepsy. Initial findings. European Radiology. 2007 Jan 12;17(7):1663–8.

460. Diehl B, Lapresto E, Liu P, Bingaman W, Busch R. Diffusion tensor imaging characteristics of the uncinate fasiculus in temporal lobe epilepsy and correlates with memory scores. 2006.

461. Wang X-Q, Lang S-Y, Hong LU, Lin MA, Yan-Ling MAO, Yang F. Changes in extratemporal integrity and cognition in temporal lobe epilepsy: A diffusion tensor imaging study. Neurol India. 2010 Dec;58(6):891–9.

462. Kim CH, Chung CK, Koo B-B, Lee J-M, Kim JS, Lee SK. Changes in language pathways in patients with temporal lobe epilepsy: diffusion tensor imaging analysis of the uncinate and arcuate fasciculi. World Neurosurg. 2011 Apr;75(3-4):509–16.

463. Kucukboyaci NE, Girard HM, Hagler DJ, Kuperman J, Tecoma ES, Iragui VJ, et al. Role of Frontotemporal Fiber Tract Integrity in Task-Switching Performance of Healthy Controls and Patients with Temporal Lobe Epilepsy. Journal of the International Neuropsychological Society. 2011 Oct 12;18(01):57–67.

464. Liacu D, Idy-Peretti I, Ducreux D, Bouilleret V, de Marco G. Diffusion tensor imaging tractography parameters of limbic system bundles in temporal lobe epilepsy patients. Journal of Magnetic Resonance Imaging. 2012 Sep;36(3):561–8.

465. Keller SS, Schoene-Bake J-C, Gerdes JS, Weber B, Deppe M. Concomitant Fractional Anisotropy and Volumetric Abnormalities in Temporal Lobe Epilepsy: Cross-Sectional Evidence for Progressive Neurologic Injury. Zhan W, editor. PLoS ONE. 2012 Oct 11;7(10):e46791.

466. Brown MW, Aggleton JP. Recognition memory: what are the roles of the perirhinal cortex and hippocampus? NatRevNeurosci. 2001 Jan;2(1471-003X (Print)):51–61.

467. Suzuki WA, Zola-Morgan S, Squire LR, Amaral DG. Lesions of the perirhinal and parahippocampal cortices in the monkey produce long-lasting memory impairment in the visual and tactual modalities. J Neurosci. 1993 Jun;13(0270-6474 (Print)):2430–51.

468. Hermann BP, Seidenberg M, Schoenfeld J, Davies K. Neuropsychological charactertistics of the syndrome of mesial temporal lobe epilepsy. Arch Neurol. 1997;54:369–76.

469. Alessio A, Damasceno BP, Carmago CH, et al. Differences in memory performance and other clinical characteristics in patients with mesial temporal lobe epilepsy with and without hippocampal atrophy. Epilepsy Behav. 2004;5:22–7.

470. Suzuki WA, Amaral DG. Perirhinal and parahippocampal cortices of the macaque monkey: cortical afferents. J Comp Neurol. 1994 Dec 22;350(0021-9967 (Print)):497–533.

471. Charlton RA, Barrick TR, McIntyre DJ, Shen Y, O'Sullivan M, Howe FA, et al. White matter damage on diffusion tensor imaging correlates with age-related cognitive decline. Neurology. 2006 Jan 24;66(1526-632X (Electronic)):217–22.

472. Heiervang E, Behrens TEJ, Mackay CE, Robson MD, Johansen-Berg H. Between session reproducibility and between subject variability of diffusion MR and tractography measures. Neuroimage. 2006;33(3):867–77.

473. Alexander AL, Lee JE, Lazar M, Field AS. Diffusion tensor imaging of the brain. Neurotherapeutics. 2007 Jul;4(1933-7213 (Print)):316–29.

474. Wieshmann UC, Clark CA, Symms MR, Franconi F, Barker GJ, Shorvon SD. Reduced anisotropy of water diffusion in structural cerebral abnormalities demonstrated with diffusion tensor imaging. Magn Reson Imaging. 1999 Nov;17(0730-725X (Print)):1269–74.

475. Kalviainen R, Partanen K, Aikia M, Mervaala E, Vainio P, Riekkinen PJ, et al. MRI-based hippocampal volumetry and T2 relaxometry: correlation to verbal memory performance in newly diagnosed epilepsy patients with left-sided temporal lobe focus. Neurology. 1997 Jan;48(0028-3878 (Print)):286–7.

476. Lencz T, McCarthy G, Bronen RA, Scott TM, Inserni JA, Sass KJ, et al. Quantitative magnetic resonance imaging in temporal lobe epilepsy: relationship to neuropathology and neuropsychological function. AnnNeurol. 1992 Jun;31(0364-5134 (Print)):629–37.

477. Gadian DG, Isaacs EB, Cross JH, Connelly A, Jackson GD, King MD, et al. Lateralization of brain function in childhood revealed by magnetic resonance spectroscopy. Neurology. 1996 Apr;46(0028-3878 (Print)):974–7.

478. Wendel JD, Trenerry MR, Xu YC, Sencakova D, Cascino GD, Britton JW, et al. The relationship between quantitative T2 relaxometry and memory in nonlesional temporal lobe epilepsy. Epilepsia. 2001 Jul;42(0013-9580 (Print)):863–8.

479. Riley JD, Franklin DL, Choi V, Kim RC, Binder DK, Cramer SC, et al. Altered white matter integrity in temporal lobe epilepsy: Association with cognitive and clinical profiles. Epilepsia. 2010 Apr;51(4):536–45.

480. Winston GP, Stretton J, Sidhu MK, Symms MR, Thompson PJ, Duncan JS. Structural correlates of impaired working memory in hippocampal sclerosis. Epilepsia. 2013 Apr;n/a–n/a.

481. Voets NL, Adcock JE, Stacey R, Hart Y, Carpenter K, Matthews PM, et al. Functional and structural changes in the memory network associated with left temporal lobe epilepsy. Hum Brain Mapp. 2009 Dec;30(12):4070–81.

482. Ashburner J, Friston KJ. Nonlinear spatial normalization using basis functions. Hum Brain Mapp. 1999;7(4):254–66.

483. Schwamm LH, Koroshetz WJ, Sorensen AG, Wang B, Copen WA, Budzik R, et al. Time course of lesion development in patients with acute stroke: serial diffusion- and hemodynamic-weighted magnetic resonance imaging. Stroke. 1998 Nov;29(11):2268–76.

484. Mueller SG, Laxer KD, Cashdollar N, Buckley S, Paul C, Weiner MW. Voxel-based optimized morphometry (VBM) of gray and white matter in temporal lobe epilepsy (TLE) with and without mesial temporal sclerosis. Epilepsia. 2006 May;47(0013-9580 (Print)):900–7.

485. Townsend TN, Bernasconi N, Pike GB, Bernasconi A. Quantitative analysis of temporal lobe white matter T2 relaxation time in temporal lobe epilepsy. Neuroimage. 2004 Sep;23(1):318–24.

486. DeCarli C, Hatta J, Fazilat S, Fazilat S, Gaillard WD, Theodore WH. Extratemporal atrophy in patients with complex partial seizures of left temporal origin. Ann Neurol. 1998 Jan;43(1):41–5.

487. Natsume J, Bernasconi N, Andermann F, Bernasconi A. MRI volumetry of the thalamus in temporal, extratemporal, and idiopathic generalized epilepsy. Neurology. 2003 Apr 22;60(8):1296–300.

488. Kimiwada T, Juhász C, Makki M, Muzik O, Chugani DC, Asano E, et al. Hippocampal and thalamic diffusion abnormalities in children with temporal lobe epilepsy. Epilepsia. 2006 Jan;47(1):167–75.

489. Van Paesschen W, Sisodiya S, Connelly A, Duncan JS, Free SL, Raymond AA, et al. Quantitative hippocampal MRI and intractable temporal lobe epilepsy. Neurology. 1995;45:2233–40.

490. Vernooij MW, Smits M, Wielopolski PA, Houston GC, Krestin GP, van der Lugt A. Fiber density asymmetry of the arcuate fasciculus in relation to functional hemispheric language lateralization in both right- and left-handed healthy subjects: a combined fMRI and DTI study. Neuroimage. 2007 Apr 15;35(3):1064–76.

491. Hofer S, Frahm J. Topography of the human corpus callosum revisited--comprehensive fiber tractography using diffusion tensor magnetic resonance imaging. Neuroimage. 2006 Sep;32(3):989–94.

492. Afzali M, Soltanian-Zadeh H, Elisevich KV. Tract based spatial statistical analysis and voxel based morphometry of diffusion indices in temporal lobe epilepsy. Comput Biol Med [Internet]. 2011 May 24 [cited 2011 Jun 6]; Available from: http://www.ncbi.nlm.nih.gov/pubmed/21616484

493. Shon Y-M, Kim Y-I, Koo B-B, Lee J-M, Kim HJ, Kim WJ, et al. Group-specific regional white matter abnormality revealed in diffusion tensor imaging of medial temporal lobe epilepsy without hippocampal sclerosis. Epilepsia. 2010 Apr;51(4):529–35.

494. Concha L, Livy DJ, Beaulieu C, Wheatley BM, Gross DW. In Vivo Diffusion Tensor Imaging and Histopathology of the Fimbria-Fornix in Temporal Lobe Epilepsy. Journal of Neuroscience. 2010 Jan 20;30(3):996–1002.

495. Van Eijsden P, Otte WM, van der Hel WS, van Nieuwenhuizen O, Dijkhuizen RM, de Graaf RA, et al. In vivo diffusion tensor imaging and ex vivo histologic characterization of white matter pathology in a post-status epilepticus model of temporal lobe epilepsy. Epilepsia. 2011 Apr;52(4):841–5.

496. Concha L, Kim H, Bernasconi A, Bernhardt BC, Bernasconi N. Spatial patterns of water diffusion along white matter tracts in temporal lobe epilepsy. Neurology. 2012 Jul 18;79(5):455–62.

497. Bonilha L, Edwards JC, Kinsman SL, Morgan PS, Fridriksson J, Rorden C, et al. Extrahippocampal gray matter loss and hippocampal deafferentation in patients with temporal lobe epilepsy. Epilepsia. 2010 Apr;51(4):519–28.

498. Backes WH, Deblaere K, Vonck K, Kessels AG, Boon P, Hofman P, et al. Language activation distributions revealed by fMRI in post-operative epilepsy patients: Differences between left- and right-sided resections. Epilepsy research. 2005;66(1-3):1–12.

499. Noppeney U, Price CJ, Duncan JS, Koepp MJ. Reading skills after left anterior temporal lobe resection: an fMRI study. Brain. 2005 Jun;128(1460-2156 (Electronic)):1377–85.

500. Pataraia E, Billingsley-Marshall RL, Castillo EM, Breier JI, Simos PG, Sarkari S, et al. Organization of receptive language-specific cortex before and after left temporal lobectomy. Neurology. 2005 Feb 8;64(1526-632X (Electronic)):481–7.

501. Maccotta L, Buckner RL, Gilliam FG, Ojemann JG. Changing frontal contributions to memory before and after medial temporal lobectomy. CerebCortex. 2007 Feb;17(1047-3211 (Print)):443–56.

502. Cheung MC, Chan AS, Lam JM, Chan YL. Pre- and postoperative fMRI and clinical memory performance in temporal lobe epilepsy. J Neurol Neurosurg Psychiatry. 2009 Oct;80(1468-330X (Electronic)):1099–106.

503. Wong SWH, Jong L, Bandur D, Bihari F, Yen Y-F, Takahashi AM, et al. Cortical reorganization following anterior temporal lobectomy in patients with temporal lobe epilepsy. Neurology. 2009 Aug;73(7):518–25.

504. Concha L, Gross DW, Wheatley BM, Beaulieu C. Diffusion tensor imaging of time-dependent axonal and myelin degradation after corpus callosotomy in epilepsy patients. Neuroimage. 2006 Sep;32(1053-8119 (Print)):1090–9.

505. Schoene-Bake JC, Faber J, Trautner P, Kaaden S, Tittgemeyer M, Elger CE, et al. Widespread affections of large fiber tracts in postoperative temporal lobe epilepsy. Neuroimage. 2009 Jul 1;46(1095-9572 (Electronic)):569–76.

506. Yasuda CL, Valise C, others. Dynamic changes in white and gray matter volume are associated with outcome of surgical treatment in temporal lobe epilepsy. NeuroImage. 2010;49(1):71–9.

507. Wilke M, Lidzba K. LI-tool: a new toolbox to assess lateralization in functional MR-data. JNeurosciMethods. 2007 Jun 15;163(0165-0270 (Print)):128–36.

508. Briellmann RS, Mitchell LA, Waites AB, Abbott DF, Pell GS, Saling MM, et al. Correlation between language organization and diffusion tensor abnormalities in refractory partial epilepsy. Epilepsia. 2003 Dec;44(0013-9580 (Print)):1541–5.

509. McKenna P, Warrington EK. Graded naming test manual. NFER Nelson; 1983.

510. Spreen O, Strauss E. A Compendium of Neuropsychological Tests. New York: Oxford University Press; 1998.

511. Song SK, Sun SW, Ramsbottom MJ, Chang C, Russell J, Cross AH. Dysmyelination revealed through MRI as increased radial (but unchanged axial) diffusion of water. Neuroimage. 2002 Nov;17(1053-8119 (Print)):1429–36.

512. Andersson JLR, Jenkinson M, Smith S. Non-linear optimisation. [Internet]. 2007. Available from: FMRIB technical report TR07JA1 from _www.fmrib.ox.ac.uk/analysis/techrep___ __

513. Andersson JLR, Jenkinson M, Smith S. Non-linear registration, aka Spatial normalisation [Internet]. 2007. Available from: FMRIB technical report TR07JA2 from _www.fmrib.ox.ac.uk/analysis/techrep___ __

514. Rueckert D, Sonoda LI, Hayes C, Hill DL, Leach MO, Hawkes DJ. Nonrigid registration using free-form deformations: application to breast MR images. IEEE TransMed Imaging. 1999 Aug;18(0278-0062 (Print)):712–21.

515. Jenkinson M, Bannister P, Brady M, Smith S. Improved optimization for the robust and accurate linear registration and motion correction of brain images. Neuroimage. 2002 Oct;17(1053-8119 (Print)):825–41.

516. Brett M, Leff AP, Rorden C, Ashburner J. Spatial normalization of brain images with focal lesions using cost function masking. Neuroimage. 2001 Aug;14(1053-8119 (Print)):486–500.

517. Crinion J, Ashburner J, Leff A, Brett M, Price C, Friston K. Spatial normalization of lesioned brains: performance evaluation and impact on fMRI analyses. Neuroimage. 2007 Sep 1;37(1053-8119 (Print)):866–75.

518. Jackson GD, Duncan JS. MRI Atlas of the Brain. Churchill Livingston; 1996.

519. Mori S, Wakana S, Nagae-Poetscher LM, van Zijl PC. MRI Atlas of Human White Matter. Elsevier; 2005.

520. Vollmar C, O'Muircheartaigh J, Barker GJ, Symms MR, Thompson P, Kumari V, et al. Identical, but not the same: intra-site and inter-site reproducibility of fractional anisotropy measures on two 3.0T scanners. Neuroimage. 2010 Jul 15;51(1095-9572 (Electronic)):1384–94.

521. Hoeft F, Barnea-Goraly N, Haas BW, Golarai G, Ng D, Mills D, et al. More is not always better: increased fractional anisotropy of superior longitudinal fasciculus associated with poor visuospatial abilities in Williams syndrome. J Neurosci. 2007 Oct 31;27(1529-2401 (Electronic)):11960–5.

522. Saur D, Kreher BW, Schnell S, Kümmerer D, Kellmeyer P, Vry M-S, et al. Ventral and dorsal pathways for language. Proc Natl Acad Sci USA. 2008 Nov 18;105(46):18035–40.

523. Chahboune H, Mishra AM, DeSalvo MN, Staib LH, Purcaro M, Scheinost D, et al. DTI abnormalities in anterior corpus callosum of rats with spike-wave epilepsy. Neuroimage. 2009 Aug 15;47(1095-9572 (Electronic)):459–66.

524. Hui ES, Fu QL, So KF, Wu EX. Diffusion tensor MR study of optic nerve degeneration in glaucoma. ConfProcIEEE Eng Med BiolSoc. 2007;2007(1557-170X (Print)):4312–5.

525. Concha L, Livy D, Gross DW, Wheatley BM, Beaulieu C. Direct correlation between diffusion tensor imaging and electron microscopy of the fornix in humans with temporal lobe epilepsy. ProcIntlSocMagResonMed(ISMRM). 2008;

526. Gulani V, Webb AG, Duncan ID, Lauterbur PC. Apparent diffusion tensor measurements in myelin-deficient rat spinal cords. Magn Reson Med. 2001 Feb;45(0740-3194 (Print)):191–5.

527. Harsan LA, Poulet P, Guignard B, Steibel J, Parizel N, de Sousa PL, et al. Brain dysmyelination and recovery assessment by noninvasive in vivo diffusion tensor magnetic resonance imaging. J NeurosciRes. 2006 Feb 15;83(0360-4012 (Print)):392–402.

528. Kinoshita Y, Ohnishi A, Kohshi K, Yokota A. Apparent diffusion coefficient on rat brain and nerves intoxicated with methylmercury. EnvironRes. 1999 May;80(0013-9351 (Print)):348–54.

529. Liu M, Gross DW, Wheatley BM, Concha L, Beaulieu C. The acute phase of Wallerian degeneration: longitudinal diffusion tensor imaging of the fornix following temporal lobe surgery. Neuroimage. 2013 Jul 1;74:128–39.

530. Faber J, Schoene-Bake J-C, Trautner P, von Lehe M, Elger CE, Weber B. Progressive fiber tract affections after temporal lobe surgery. Epilepsia. 2013 Apr;54(4):e53–e57.

531. Nguyen D, Vargas MI, Khaw N, Seeck M, Delavelle J, Lovblad KO, et al. Diffusion tensor imaging analysis with tract-based spatial statistics of the white matter abnormalities after epilepsy surgery. Epilepsy Research [Internet]. 2011 Mar; Available from: http://linkinghub.elsevier.com/retrieve/pii/S0920121111000386

532. McDonald CR, Hagler DJ Jr, Girard HM, Pung C, Ahmadi ME, Holland D, et al. Changes in fiber tract integrity and visual fields after anterior temporal lobectomy. Neurology. 2010 Nov 2;75(18):1631–8.

533. Govindan RM, Chugani HT, Altinok D, Sood S. Postsurgical white matter changes identified using diffusion tensor imaging in children following hemispherectomy. Epilepsia. 2009;Abstracts from the 2009 Annual Meeting of the American Epilepsy Society(Epub ahead of print).

534. Wu Q, Butzkueven H, Gresle M, Kirchhoff F, Friedhuber A, Yang Q, et al. MR diffusion changes correlate with ultra-structurally defined axonal degeneration in murine optic nerve. Neuroimage. 2007 Oct 1;37(1053-8119 (Print)):1138–47.

535. Hugg JW, Kuzniecky RI, Gilliam FG, Morawetz RB, Fraught RE, Hetherington HP. Normalization of contralateral metabolic function following temporal lobectomy demonstrated by 1H magnetic resonance spectroscopic imaging. AnnNeurol. 1996 Aug;40(0364-5134 (Print)):236–9.

536. Cendes F, Andermann F, Dubeau F, Matthews PM, Arnold DL. Normalization of neuronal metabolic dysfunction after surgery for temporal lobe epilepsy. Evidence from proton MR spectroscopic imaging. Neurology. 1997 Dec;49(0028-3878 (Print)):1525–33.

537. Spanaki MV, Kopylev L, DeCarli C, Gaillard WD, Liow K, Fazilat S, et al. Postoperative changes in cerebral metabolism in temporal lobe epilepsy. ArchNeurol. 2000 Oct;57(0003-9942 (Print)):1447–52.

538. Joo EY, Hong SB, Han HJ, Tae WS, Kim JH, Han SJ, et al. Postoperative alteration of cerebral glucose metabolism in mesial temporal lobe epilepsy. Brain. 2005;128(8):1802.

539. Blumenfeld H, Varghese GI, Purcaro MJ, Motelow JE, Enev M, McNally KA, et al. Cortical and subcortical networks in human secondarily generalized tonic-clonic seizures. Brain. 2009 Apr;132(1460-2156 (Electronic)):999–1012.

540. Schmahmann JD, Pandya DN. Disconnection syndromes of basal ganglia, thalamus, and cerebrocerebellar systems. Cortex. 2008 Sep;44(0010-9452 (Print)):1037–66.

541. May A, Gaser C. Magnetic resonance-based morphometry: a window into structural plasticity of the brain. Curr Opin Neurol. 2006 Aug;19(4):407–11.

542. Johansen-Berg H. Structural plasticity: rewiring the brain. CurrBiol. 2007 Feb 20;17(0960-9822 (Print)):R141–R144.

543. Gould E. How widespread is adult neurogenesis in mammals? NatRev Neurosci. 2007 Jun;8(1471-003X (Print)):481–8.

544. Draganski B, May A. Training-induced structural changes in the adult human brain. Behav Brain Res. 2008 Sep 1;192(0166-4328 (Print)):137–42.

545. Kaas JH, Florence SL, Jain N. Subcortical contributions to massive cortical reorganizations. Neuron. 1999 Apr;22(0896-6273 (Print)):657–60.

546. Jain N, Florence SL, Qi HX, Kaas JH. Growth of new brainstem connections in adult monkeys with massive sensory loss. ProcNatlAcadSci USA. 2000 May 9;97(0027-8424 (Print)):5546–50.

547. Dancause N, Barbay S, Frost SB, Plautz EJ, Chen D, Zoubina EV, et al. Extensive cortical rewiring after brain injury. J Neurosci. 2005 Nov 2;25(1529-2401 (Electronic)):10167–79.

548. Leh SE, Johansen-Berg H, Ptito A. Unconscious vision: new insights into the neuronal correlate of blindsight using diffusion tractography. Brain. 2006 Jul;129(1460-2156 (Electronic)):1822–32.

549. Bridge H, Thomas O, Jbabdi S, Cowey A. Changes in connectivity after visual cortical brain damage underlie altered visual function. Brain. 2008 Jun;131(1460-2156 (Electronic)):1433–44.

550. Ramu J, Herrera J, Grill R, Bockhorst T, Narayana P. Brain fiber tract plasticity in experimental spinal cord injury: diffusion tensor imaging. Exp Neurol. 2008 Jul;212(1090-2430 (Electronic)):100–7.

551. Grodzinsky Y, Amunts K. Broca's region. New York_ _: Oxford University Press; 2006.

552. Geschwind N. The organization of language and the brain. Science. 1970 Nov 27;170(0036-8075 (Print)):940–4.

553. Catani M, Jones DK, others. Perisylvian language networks of the human brain. Annals of neurology. 2005;57(1):8–16.

554. Glasser MF, Rilling JK. DTI tractography of the human brain's language pathways. Cerebral Cortex. 2008;18(11):2471.

555. Frey S, Campbell JS., Pike GB, Petrides M. Dissociating the human language pathways with high angular resolution diffusion fiber tractography. Journal of Neuroscience. 2008;28(45):11435.

556. Bernal B, Altman N. The connectivity of the superior longitudinal fasciculus: a tractography DTI study. Magn Reson Imaging [Internet]. 2009 Aug 18;(1873-5894 (Electronic)). Available from: PM:19695825

557. Schmahmann JD, Pandya DN. Fibre Pathways of the Brain. New York: Oxford University Press; 2006.

558. Makris N, Kennedy DN, McInerney S, Sorensen AG, Wang R, Caviness VS, et al. Segmentation of subcomponents within the superior longitudinal fascicle in humans: a quantitative, in vivo, DT-MRI study. CerebCortex. 2005 Jun;15(1047-3211 (Print)):854–69.

559. Schmahmann JD, Pandya DN, Wang R, Dai G, D'Arceuil HE, de Crespigny AJ, et al. Association fibre pathways of the brain: parallel observations from diffusion spectrum imaging and autoradiography. Brain. 2007 Mar;130(1460-2156 (Electronic)):630–53.

560. Makris N, Pandya DN. The extreme capsule in humans and rethinking of the language circuitry. Brain Struct Funct. 2008 Dec;213(3):343–58.

561. Petrides M, Pandya DN. Projections to the frontal cortex from the posterior parietal region in the rhesus monkey. J Comp Neurol. 1984 Sep 1;228(0021-9967 (Print)):105–16.

562. Petrides M, Pandya DN. Association fiber pathways to the frontal cortex from the superior temporal region in the rhesus monkey. J Comp Neurol. 1988 Jul 1;273(0021-9967 (Print)):52–66.

563. Petrides M, Pandya DN. Efferent association pathways originating in the caudal prefrontal cortex in the macaque monkey. J Comp Neurol. 2006 Sep 10;498(0021-9967 (Print)):227–51.

564. Petrides M, Pandya DN. Efferent association pathways from the rostral prefrontal cortex in the macaque monkey. J Neurosci. 2007 Oct 24;27(1529-2401 (Electronic)):11573–86.

565. Duffau H. The anatomo-functional connectivity of language revisited:: New insights provided by electrostimulation and tractography. Neuropsychologia. 2008;46(4):927–34.

566. Friederici AD. Pathways to language: fiber tracts in the human brain. Trends Cogn Sci. 2009 Apr;13(1364-6613 (Print)):175–81.

567. DeBoy CA, Zhang J, Dike S, Shats I, Jones M, Reich DS, et al. High resolution diffusion tensor imaging of axonal damage in focal inflammatory and demyelinating lesions in rat spinal cord. Brain. 2007 Aug;130(1460-2156 (Electronic)):2199–210.

568. Sun SW, Liang HF, Cross AH, Song SK. Evolving Wallerian degeneration after transient retinal ischemia in mice characterized by diffusion tensor imaging. Neuroimage. 2008 Mar 1;40(1053-8119 (Print)):1–10.

569. Helmstaedter C, Fritz NE, Gonzalez Perez PA, Elger CE, Weber B. Shift-back of right into left hemisphere language dominance after control of epileptic seizures: evidence for epilepsy driven functional cerebral organization. Epilepsy Res. 2006 Aug;70(0920-1211 (Print)):257–62.

570. Saur D, Lange R, Baumgaertner A, Schraknepper V, Willmes K, Rijntjes M, et al. Dynamics of language reorganization after stroke. Brain. 2006 Jun;129(1460-2156 (Electronic)):1371–84.

571. Catani M. From hodology to function. Brain. 2007 Mar;130(1460-2156 (Electronic)):602–5.

572. Barr WB. Neuropsychological Outcome. In: Luders H, editor. Textbook of Epilepsy Surgery. London: Informa Healthcare; 2009. p. 1277–99.

573. Lindell AK. In your right mind: right hemisphere contributions to language processing and production. Neuropsychol Rev. 2006 Sep;16(3):131–48.

574. Szaflarski JP, Allendorfer JB, Banks C, Vannest J, Holland SK. Recovered vs. not-recovered from post-stroke aphasia: The contributions from the dominant and non-dominant hemispheres. Restor Neurol Neurosci. 2013 Mar 12;

575. Falconer MA, Wilson JL. Visual field changes following anterior temporal lobectomy: their significance in relation to Meyer's loop of the optic radiation. Brain. 1958;81(1):1–14.

576. Jensen I, Seedorff HH. Temporal lobe epilepsy and neuro-ophthalmology. Ophthalmological findings in 74 temporal lobe resected patients. Acta Ophthalmol(Copenh). 1976 Dec;54(0001-639X (Print)):827–41.

577. Barton JJ., Hefter R, Chang B, Schomer D, Drislane F. The field defects of anterior temporal lobectomy: a quantitative reassessment of Meyer's loop. Brain. 2005;128(9):2123.

578. Ray A, Pathak-Ray V, Walters R, Hatfield R. Driving after epilepsy surgery: effects of visual field defects and epilepsy control. Br J Neurosurg. 2002 Jan;16(5):456–60.

579. Taylor DC, McMacKin D, Staunton H, Delanty N, Phillips J. Patients' aims for epilepsy surgery: desires beyond seizure freedom. Epilepsia. 2001 May;42(0013-9580 (Print)):629–33.

580. Egan RA, Shults WT, So N, Burchiel K, Kellogg JX, Salinsky M. Visual field deficits in conventional anterior temporal lobectomy versus amygdalohippocampectomy. Neurology. 2000;55(12):1818.

581. Cook PA, Bai Y, Nedjati-Gilani S, Seunarine KK, Hall MG, Parker GJ, et al. Camino: Open-source diffusion-MRI reconstruction and processing. 14th Scientific Meeting of the International Society for Magentic Resonance in Medicine, Seattle, WA, USA. 2006;2759.

582. Ciccarelli O, Toosy AT, Hickman SJ, Parker GJM, Wheeler-Kingshott CAM, Miller DH, et al. Optic radiation changes after optic neuritis detected by tractography-based group mapping. Hum Brain Mapp. 2005 Jul;25(3):308–16.

583. Nilsson D, Starck G, Ljungberg M, Ribbelin S, Jonsson L, Malmgren K, et al. Intersubject variability in the anterior extent of the optic radiation assessed by tractography. Epilepsy Research. 2007 Oct;77(1):11–6.

584. B\ürgel U, Schormann T, Schleicher A, Zilles K. Mapping of histologically identified long fiber tracts in human cerebral hemispheres to the MRI volume of a reference brain: position and spatial variability of the optic radiation. NeuroImage. 1999;10(5):489–99.

585. Frisen L. The cartographic deformations of the visual field. Ophthalmologica. 1970;161(0030-3755 (Print)):38–54.

586. Kirkham TH, Meyer E. Visual field area on the Goldmann hemispheric perimeter surface. Correction of cartographic errors inherent in perimetry. CurrEye Res. 1981;1(0271-3683 (Print)):93–9.

587. Curcio CA, Allen KA. Topography of ganglion cells in human retina. J Comp Neurol. 1990 Oct 1;300(0021-9967 (Print)):5–25.

588. Archambault L. Le faisceau longitudinal inferieur et le faisceau optique central: Quelques considerations sur les fibers d'association du cerveau. Rev Neurol. 1906;4:1206.

589. Meyer A. The connections of the occpital lobes and the present status of the cerebral visual affections. TransAssAmerPhycns. 1907;22:7–30.

590. Cushing H. Distortions of visual fields in cases of brain tumour. Brain. 1922;44:341.

591. Spalding JM. Wounds of the visual pathway. I. The visual radiation. J Neurol Neurosurg Psychiatry. 1952 May;15(0022-3050 (Print)):99–109.

592. Katz A, Awad IA, Kongy AK, Chelune GJ, Naugle RI, Wyllie E, et al. Extent of resection in temporal lobectomy for epilepsy. II. Memory changes and neurologic complications. Epilepsia. 1989;30(6):763–71.

593. Hughes TS, Abou-Khalil B, Lavin PJM, Fakhoury T, Blumenkopf B, Donahue SP. Visual field defects after temporal lobe resection: a prospective quantitative analysis. Neurology. 1999;53(1):167.

594. Marino R, Rasmussen T. Visual field changes after temporal lobectomy in man. Neurology. 1968 Sep;18(0028-3878 (Print)):825–35.

595. Tecoma ES, Laxer KD, Barbaro NM, Plant GT. Frequency and characteristics of visual field deficits after surgery for mesial temporal sclerosis. Neurology. 1993 Jun;43(0028-3878 (Print)):1235–8.

596. Babb TL, Wilson CL, Crandall PH. Asymmetry and ventral course of the human geniculostriate pathway as determined by hippocampal visual evoked potentials and subsequent visual field defects after temporal lobectomy. Exp Brain Res. 1982;47(0014-4819 (Print)):317–28.

597. Krolak-Salmon P, Guenot M, Tiliket C, Isnard J, Sindou M, Mauguiere F, et al. Anatomy of optic nerve radiations as assessed by static perimetry and MRI after tailored temporal lobectomy. British Journal of Ophthalmology. 2000;84(8):884.

598. Nilsson D, Malmgren K, Rydenhag B, Frisen L. Visual field defects after temporal lobectomy -- comparing methods and analysing resection size. Acta Neurol Scand. 2004 Nov;110(0001-6314 (Print)):301–7.

599. Penfield W. Temporal lobe epilepsy. Br J Surg. 1954 Jan;41(0007-1323 (Print)):337–43.

600. Awad IA, Katz A, Hahn JF, Katz AKK., Ahl J, L\üders H. Extent of resection in temporal lobectomy for epilepsy. I. Interobserver analysis and correlation with seizure outcome. Epilepsia. 1989;30(6):756–62.

601. Yaşargil MG, T\üre U, Yaşargil DC. Impact of temporal lobe surgery. Journal of Neurosurgery: Pediatrics. 2004;101(5).

602. Kier EL, Staib LH, Davis LM, Bronen RA. MR imaging of the temporal stem: anatomic dissection tractography of the uncinate fasciculus, inferior occipitofrontal fasciculus, and Meyer's loop of the optic radiation. American Journal of Neuroradiology. 2004;25(5):677.

603. Bjork A, Kugelberg E. Visual field deficits after temporal lobectomy. ArchOphthalmol. 1957;35:211–6.

604. Van Buren JM, Baldwin M. The architecture of the optic radiation in the temporal lobe of man. Brain. 1958 Mar;81(0006-8950 (Print)):15–40.

605. Wendlland JP, Nerenberg S. Visual field studies after temporal lobectomy for epilepsy. ArchOphthalmol. 1960 Aug;64(0003-9950 (Print)):195–200.

606. Sincoff EH, Tan Y, Abdulrauf SI. White matter fiber dissection of the optic radiations of the temporal lobe and implications for surgical approaches to the temporal horn. J Neurosurg. 2004 Nov;101(5):739–46.

607. Rubino PA, Rhoton AL, Tong X, Oliveira E de. Three-dimensional relationships of the optic radiation. Neurosurgery. 2005 Oct;57(4 Suppl):219–227; discussion 219–227.

608. Choi C, Rubino PA, Fernandez-Miranda JC, Abe H, Rhoton Jr AL. Meyer's loop and the optic radiations in the transsylvian approach to the mediobasal temporal lobe. Neurosurgery. 2006;59(4).

609. Peltier J, Travers N, Destrieux C, Velut S. Optic radiations: a microsurgical anatomical study. J Neurosurg. 2006 Aug;105(2):294–300.

610. Taoka T, Sakamoto M, Nakagawa H, Nakase H, Iwasaki S, Takayama K, et al. Diffusion Tensor Tractography of the Meyer Loop in Cases of Temporal Lobe Resection for Temporal Lobe Epilepsy: Correlation between Postsurgical Visual Field Defect and Anterior Limit of Meyer Loop on Tractography. American Journal of Neuroradiology. 2008 Jan;29(7):1329–34.

611. Hofer S, Karaus A, Frahm J. Reconstruction and dissection of the entire human visual pathway using diffusion tensor MRI. Frontiers in Neuroanatomy. 2010;4.

612. Nilsson DT, B R, Malmgren K, Starck G, Ljungberg M. Anatomical accuracy and feasibility of probabilistic and deterministic tractography of the optic radiation. Epilepsia [Internet].

Rhodes, Greece; 2010 [cited 2013 Jul 2]. p. 91. Available from: http://doi.wiley.com/10.1111/j.1528-1167.2010.02658.x

613. Sherbondy AJ, Dougherty RF, Napel S, Wandell BA. Identifying the human optic radiation using diffusion imaging and fibre tractography. Journal of Vision. 2008;8(10)_ _(12):1–11.

614. Chen X, Weigel D, Ganslandt O, Buchfelder M, Nimsky C. Prediction of visual field deficits by diffusion tensor imaging in temporal lobe epilepsy surgery. NeuroImage. 2009 Apr;45(2):286–97.

615. Jeelani N u. O, Jindahra P, Tamber MS, Poon TL, Kabasele P, James-Galton M, et al. 'Hemispherical asymmetry in the Meyer's Loop': a prospective study of visual-field deficits in 105 cases undergoing anterior temporal lobe resection for epilepsy. Journal of Neurology, Neurosurgery & Psychiatry. 2010 Jun;81(9):985–91.

616. Clatworthy PL, Williams GB, Acosta-Cabronero J, Jones SP, Harding SG, Johansen-Berg H, et al. Probabilistic tractography of the optic radiations--an automated method and anatomical validation. Neuroimage. 2010 Feb 1;49(3):2001–12.

617. Winston GP, Mancini L, Stretton J, Ashmore J, Symms MR, Duncan JS, et al. Diffusion tensor imaging tractography of the optic radiation for epilepsy surgical planning: a comparison of two methods. Epilepsy Res. 2011 Nov;97(1-2):124–32.

618. Winston GP, Yogarajah M, Symms MR, McEvoy AW, Micallef C, Duncan JS. Diffusion tensor imaging tractography to visualize the relationship of the optic radiation to epileptogenic lesions prior to neurosurgery. Epilepsia [Internet]. 2011 May 13 [cited 2011 Jun 6]; Available from: http://www.ncbi.nlm.nih.gov/pubmed/21569018

619. Yamada M, Momoshima S, Masutani Y, Fujiyoshi K, Abe O, Nakamura M, et al. Diffusion-tensor neuronal fiber tractography and manganese-enhanced MR imaging of primate visual pathway in the common marmoset: preliminary results. Radiology. 2008 Dec;249(1527-1315 (Electronic)):855–64.

620. Daga P, Winston G, Modat M, White M, Mancini L, Cardoso MJ, et al. Accurate localization of optic radiation during neurosurgery in an interventional MRI suite. IEEE Trans Med Imaging. 2012 Apr;31(4):882–91.

621. Winston GP, Daga P, Stretton J, Modat M, Symms MR, McEvoy AW, et al. Optic radiation tractography and vision in anterior temporal lobe resection. Ann Neurol. 2012 Mar;71(3):334–41.

622. Yogarajah M, Powell HWR, Parker GJ., Alexander DC, Thompson PJ, Symms MR, et al. Tractography of the parahippocampal gyrus and material specific memory impairment in unilateral temporal lobe epilepsy. NeuroImage. 2008 May;40(4):1755–64.

623. Calamante F, Tournier J-D, Jackson GD, Connelly A. Track-density imaging (TDI): Super-resolution white matter imaging using whole-brain track-density mapping. NeuroImage. 2010 Dec;53(4):1233–43.

624. Vaessen MJ, Jansen JFA, Vlooswijk MCG, Hofman PAM, Majoie HJM, Aldenkamp AP, et al. White matter network abnormalities are associated with cognitive decline in chronic epilepsy. Cereb Cortex. 2012 Sep;22(9):2139–47.

625. Liao W, Zhang Z, Pan Z, Mantini D, Ding J, Duan X, et al. Default mode network abnormalities in mesial temporal lobe epilepsy: A study combining fMRI and DTI. Hum Brain Mapp. 2010 Jun;n/a–n/a.

626. Voets NL, Beckmann CF, Cole DM, Hong S, Bernasconi A, Bernasconi N. Structural substrates for resting network disruption in temporal lobe epilepsy. Brain. 2012 Aug;135(Pt 8):2350–7.

627. Sotiropoulos SN, Jbabdi S, Xu J, Andersson JL, Moeller S, Auerbach EJ, et al. Advances in diffusion MRI acquisition and processing in the Human Connectome Project. NeuroImage. 2013 Oct;80:125–43.